Dissertation

submitted to the

Combined Faculty of Natural Sciences and Mathematics

of the Ruperto Carola University Heidelberg, Germany

for the degree of

Doctor of Natural Sciences

presented by

M.Sc. Sebastian Hauke

Born in Schweinfurt (Mainfranken), Germany

Oral examination: February 6th, 2019

Investigations of Trace Amines and Fatty Acids as Essential Endogenous Signaling Factors for β-Cell Activity and Insulin Secretion

Referees: Dr. Anne-Claude Gavin

Prof. Dr. Andres Jäschke

Meinen Eltern

This study was carried out in the Cell Biology and Biophysics Unit (CBB) at the European Molecular Biology Laboratory (EMBL) Heidelberg from May 2015 to September 2018, supervised by Carsten Schultz.

'Es wird ja fleißig gearbeitet und viel mikroskopiert, aber es müsste mal wieder einer einen gescheiten Gedanken haben.'

Rudolf Virchow (1821 - 1902)
German physiologist, founder of cellular pathology

Summary

Secretion of insulin in response to extracellular stimuli, such as elevated glucose levels and small molecules that act on G-protein coupled receptors (GPCRs), is the hallmark of β-cell physiology. Sufficiently high blood insulin levels are ensured by the coupling of the secretory activity within pancreatic islets. Intercellular and inter-islet coordination are partly mediated by small diffusible ligands of GPCRs within the extracellular space of pancreatic islets. Therefore, insulin release is considered a synchronized multi-cellular process. We show herein that β-cell activity and insulin secretion essentially rely on the presence of extracellular endogenous (autocrine) signaling factors, exemplified by two classes of small cellular metabolites.

Trace amines (TAs) are small aromatic metabolites that were identified as low-abundant ligands of the trace amine-associated receptor 1 (TAAR1) in the central nervous system (CNS). In the presented work, we identify TAs as essential autocrine signaling factors that maintain and regulate oscillations of the intracellular Ca^{2+} concentration ($[Ca^{2+}]_i$ oscillations) along with insulin secretion from β-cells via TAAR1. We found that the modulation of endogenous TA levels by the selective inhibition of TA biosynthetic pathways directly translated into changes of $[Ca^{2+}]_i$ oscillations and insulin secretion. Application of aromatic amine-withdrawing β-cyclodextrin temporarily reduced $[Ca^{2+}]_i$ oscillations. This demonstrates the essential role of TAs for β-cell activity as well as their high metabolic turnover rates. Notably, herein applied inhibitors and synthetic TAAR1 (ant-)agonists are partly approved for the therapeutic modulation of biogenic amine levels within the CNS, and hence for the treatment of common neurological disorders. According to our findings, these drugs even affect β-cell activity and insulin secretion through pancreatic TAAR1.

With the discovery of the free fatty acid (FA) receptor GPR40 in β-cells, FAs have come into focus as exogenous insulin secretagogues. However, the role of FAs as endogenous (local) signaling factors of β-cells has not been considered so far. We show herein that lowering endogenous FA-levels in the presence of FA-free bovine serum albumin (FAF-BSA) immediately reduced $[Ca^{2+}]_i$ oscillations and insulin secretion. $[Ca^{2+}]_i$ oscillations resumed upon exchange of FAF-BSA by buffer or upon restoration of extracellular FA pools. The latter was accomplished by the photolysis of caged FAs on plasma membranes, by the addition of a recombinant lipase or of FA-loaded BSA. Our approach to subordinate β-cell activity and insulin secretion to the presence of autocrine signaling factors of the yet underestimated receptors TAAR1 and GPR40 in the pancreas contributes to a more detailed and complete understanding of the fundamental regulation of β-cell activity and insulin secretion.

Zusammenfassung

Ein Merkmal der Physiologie von *β*-Zellen besteht in der Sekretion von Insulin als Antwort auf extrazelluläre Stimuli, wie erhöhte Blutzuckerspiegel und niedermolekulare Liganden von G-Protein gekoppelten Rezeptoren (GPCRs). Angepasste Blutinsulinspiegel werden durch die gekoppelte sekretorische Aktivität zwischen pankreatischen Inseln ermöglicht. Die Koordination unter pankreatischen Zellen und Inseln wird teilweise durch niedermolekulare, diffusible Liganden von GPCRs im extrazellulären Bereich von pankreatischen Inseln vermittelt. Insulinausschüttung wird daher als ein synchronisierter multi-zellulärer Prozess angesehen. In dieser Arbeit zeigen wir, am Beispiel zweier Klassen niedermolekularer zellulärer Metabolite, dass *β*-Zellaktivität und Insulinsekretion vom Vorhandensein extrazellulärer, endogener (autokriner) Signalfaktoren abhängen.

‚Trace amines (TAs)' sind kleine, aromatische Metabolite, die als niederabundante Liganden des ‚trace amine-associated receptor 1 (TAAR1)' im zentralen Nervensystem (ZNS) entdeckt wurden. In dieser Arbeit identizifieren wir TAs als essentielle autokrine Signalfaktoren, die Oszillationen der intrazellulären Ca^{2+} Konzentration ($[Ca^{2+}]_i$ Oszillationen), sowie Insulinsekretion von *β*-Zellen durch Stimulation des TAAR1 aufrecht erhalten und modulieren. Wir stellten fest, dass sich die Modulation endogener TA Konzentrationen durch selektive Inhibition von TA Biosynthesewegen sofort in veränderten $[Ca^{2+}]_i$ Oszillationen und Insulinsekretion niederschlug. $[Ca^{2+}]_i$ Oszillationen wurden durch Verabreichung von *β*-Cyclodextrin zeitweise reduziert, das aromatische Amine von Zellen bindet und diese entzieht. Dies zeigt die essentielle Rolle von TAs für die *β*-Zellaktivität, sowie ihren hohen metabolischen Umsatz. Bemerkenswerterweise sind die hier verwendeteten Inhibitoren und synthetischen TAAR1 (Ant-)Agonisten teilweise für die therapeutische Modulation der Konzentrationen biogener Amine im ZNS und daher auch für die Behandlung von verbreiteten neurologischen Erkrankungen zugelassen. Unsere Beobachtungen zeigen, dass diese Therapeutika auch *β*-Zellaktivität und Insulinsekretion durch TAAR1 im Pankreas beeinflussen.

Durch die Entdeckung des freien Fettsäure- (FA-)rezeptors GPR40 in *β*-Zellen rückten FAs als exogene Stimuli für Insulinsekretion in den Fokus. Jedoch wurden FAs bisher nicht in der Rolle endogener (lokaler) Signalfaktoren von *β*-Zellen betrachtet. In dieser Arbeit zeigen wir, dass eine Verringerung endogener FA Konzentrationen in Gegenwart von FA-freiem bovinem Serumalbumin (FAF-BSA) mit einer unverzüglichen Reduktion von $[Ca^{2+}]_i$ Oszillationen und Insulinsekretion einhergeht. Der Austausch von FAF-BSA durch Puffer oder die Wiederherstellung von extrazellulären FA-Pools bewirkte die Wiederaufnahme von $[Ca^{2+}]_i$ Oszillationen. Letzteres wurde ermöglicht durch Photolyse von photogeschützten FAs an

Zusammenfassung

Plasmamembranen, durch Zugabe von rekombinanter Lipase oder FA-geladenem BSA. Der hier präsentierte Ansatz, β-Zellaktivität und Insulinsekretion dem Vorhandensein autokriner Signalfaktoren der bislang unterschätzten pankreatischen Rezeptoren TAAR1 und GPR40 unterzuordnen, trägt zu einem detailierterem und vollständigerem Verständnis fundamentaler Regulation von β-Zellaktivität und Insulinsekretion bei.

Table of contents

List of figures

List of figures

List of tables

List of abbreviations

AADC	Aromatic L-amino acid decarboxylase
ACh	Acetlycholine
β-PEA	β-Phenylethylamine
BSA	Bovine serum albumin
$[Ca^{2+}]_i$	Intracellular Ca^{2+} concentration
cAMP	Cyclic adenosine monophosphate
CLSM	Confocal laser scanning microscopy
CNS	Central nervous system
DAG	Diacylglycerol
DAT	Dopamine transporter
DBH	Dopamine β-hydroxylase
DR2	Dopamine receptor 2
EC_{50}	Half maximal effective concentration
ELISA	Enzyme-linked immunosorbent assay
ER	Endoplasmic reticulum
FAs	Fatty acids
FAF	Fatty acid-free
GABA	γ-Aminobutyric acid
GLP-1	Glucagon-like peptide 1
GIP	Gastric inhibitory polypeptide
GLUT	Glucose transporter
GPCR	G-protein coupled receptor
GPR40	Free fatty acid receptor
GSIS	Glucose-stimulated insulin secretion
HSA	Human serum albumin
HCl	Hydrochloric acid
hpβ-CD	Hydroxypropyl β-cyclodextrin
IBMX	3-Isobutyl-1-methylxanthine
IC_{50}	Half maximal inhibitory concentration
INS-1	Rat insulinoma cell line
IP_3	Inositoltriphosphate
LAMPA	Lysergic acid methylpropylamide
LSD	Lysergic acid diethylamide
MAO	Monoamine oxidase
MeOH	Methanol
MIN6	Mouse insulinoma cell line
NMT	*N*-methyltransferase
OA	Oleic acid
PA	Palmitic acid

PIPs	Phosphatidylinositolphosphates
PKA	Protein kinase A
PKC	Protein kinase C
PLA_2	Phospholipase A_2
PLC	Phospholipase C
PM	Plasma membrane
PNMT	Phenylethanolamine *N*-methyltransferase
PP	Pancreatic polypeptide
SA	Stearic acid
Scg-	Sulfo-caged
SN	Supernatant
TAs	Trace amines
TAAR1	Trace amine-associated receptor 1
T1AM	3-Iodothyronamine
T2D	Type-2-diabetes
VGCC	Voltage-gated calcium channel

1. Introduction

1.1. Pancreatic modulation of glucose homeostasis

1.1.1. Physiology of glucose homeostasis

The precise regulation of physiological blood glucose levels is essential for overall metabolism and energy homeostasis. For this, liver, intestine, adipose and muscle tissue as well as the brain are tightly intertwined by a sensitive network of various hormones and neuropeptides in mammals [1]. Encapsulated within the islets of Langerhans, pancreatic endocrine cells produce the hormones insulin, glucagon and ghrelin, which are secreted into the bloodstream [2,3] (Fig. 1 A). For adjusted secretory responses, pancreatic islets need to sense multiple physiological parameters in the body, *e.g.* blood glucose and nutrient levels after food intake or hormones from endocrine glands. The adult human pancreas comprises 0.5 - 1 x10^6 islets of Langerhans. Being 100 - 150 µm in diameter, pancreatic islets account for 2 - 3 % of the total pancreatic volume [4,5]. Pancreatic islets are considered as fully functional secretory units, as they contain all elements that are necessary for adequate responses to fluctuating nutrient levels. Human islets comprise different secretory cell types: β-cells (~75 - 80 %, insulin), α-cells (~18 %, glucagon), δ-cells (~6 %, somatostatin), ε-cells (~1 %, ghrelin) and γ-cells (~1 %, pancreatic peptide (PP)) (Fig. 1 B) [6,7]. The anabolic hormone insulin is secreted in response to elevated blood glucose levels to promote glucose uptake into adipose and muscle tissue [8–10], lipogenesis [11], glycogenesis [12–14] and protein biosynthesis [15]. The catabolic hormone glucagon increases blood glucose levels, promoting glycogenolysis and gluconeogenesis in liver and kidneys in between meals and during sleep [16]. The interplay between glucagon and insulin action keeps human blood glucose levels in a physiological range of 4 - 6 mM [17] and is generally referred to as 'glucose homeostasis'. Both glucagon and insulin release are inhibited by somatostatin [18]. The overall secretory activity of the pancreas is regulated by the PP [19]. Pancreatic islets are also composed of various other cell types, such as resident immune cells, neural and glial cells [3]. Relative proportions of islet cell types, and even more important, the cytoarchitecture within islets may vary significantly amongst islets, individuals and species. In rodent islets, α- and δ-cells are segregated to the periphery with a homogenous center formed by β-cells. Human islets are, however, more heterogeneous (Fig. 1 B and C) [3,6,20,21]. Apart from pancreatic endocrine cells, acinar (exocrine) cells secrete a cocktail of digestive enzymes, such as pancreatic lipase, trypsinogen and amylase via the pancreatic duct into the duodenum (Fig. 1 A) [1].

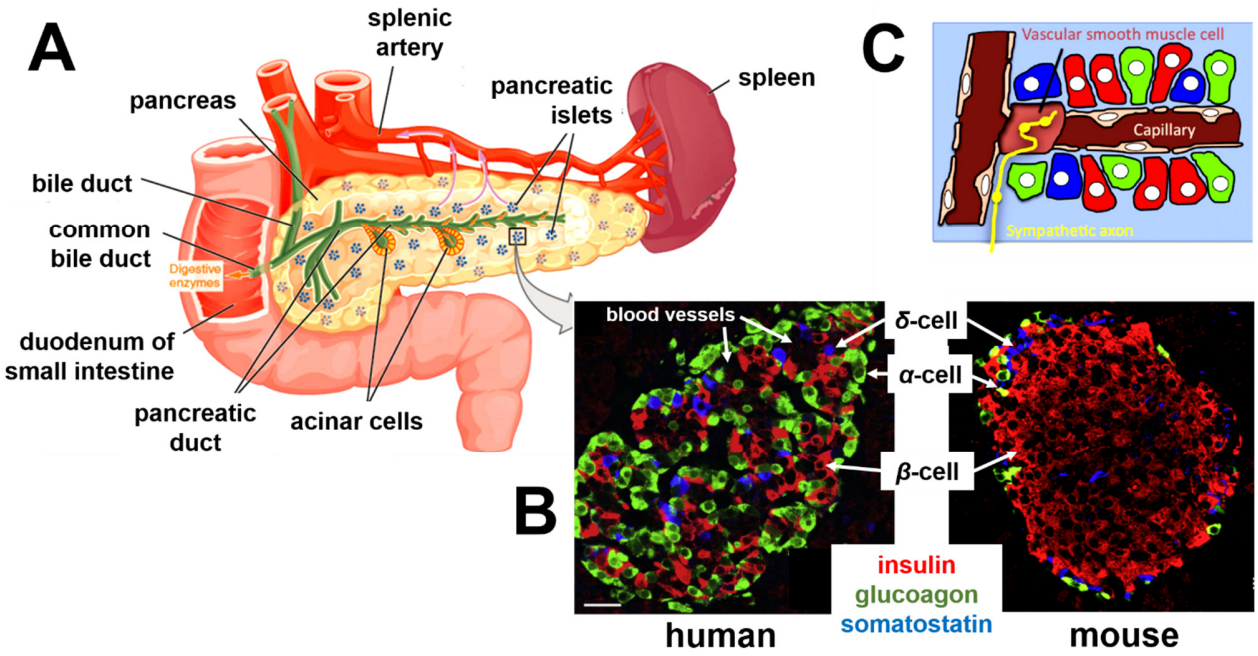

Figure 1. Anatomy of insulin secretion. (A) Hormone secreting islets of Langerhans constitute the endocrine part of the pancreas. A composite of different digestive enzymes is secreted from acinar cells together with bile into the upper small intestine via the pancreatic duct (*i.e.* the exocrine section of the pancreas). **(B)** Human (left) and mouse (right) islet sections, immuno-stained for insulin (red, β-cells), glucagon (green, α-cells) and somatostatin (blue, ε-cells). Scale bar, 50 µm. **(C)** Different types of pancreatic cells surround blood vessels inside human islets. Adapted and modified from [1,3,22].

1.1.2. β-Cell physiology in glucose-stimulated insulin secretion

Insulin is released from pancreatic β-cells in response to changes in blood glucose levels, which presents the main physiological stimulus. Glucose is shuffled into β-cells by glucose transporters (GLUTs), where a high-K_m isoform of glucokinase acts as a rate-limiting glucose sensor. Glucokinase determines the sigmoidal dose-response-relation of glucose-stimulated insulin secretion (GSIS). Glucose at 3 - 7 mM presents a (species-specific) stimulatory threshold for GSIS, followed by a steep increase to reach maximal levels of secretion at 15 - 30 mM [23,24].

GSIS involves glucose metabolism, along with increased cytosolic ATP / ADP ratios. Elevated ATP levels block ATP-sensitive K^+ (K_{ATP})-channels within the plasma membrane (PM), which leads to membrane depolarization (Fig. 2 A). Open K_{ATP}-channels under non-stimulatory conditions allow K^+-outflow, which presents the main originator of the PM resting potential [25]. PM depolarization mediates the opening of voltage-gated Ca^{2+}-channels (VGCC). Ca^{2+} influx,

sensed by synaptotagmins, SNARE and Sec1/Munc18-like proteins, triggers the fusion of insulin-filled secretory granules with the PM (Fig. 2 A) [26–28].

Notably, the mitochondrial membrane potential, along with cellular ATP levels and K_{ATP}-channel gating were found to oscillate in β-cells [29,30]. Rhythmic depolarization of the PM ensures regular transients of the cytosolic Ca^{2+} concentration ($[Ca^{2+}]_i$ oscillations) along with pulsatile insulin secretion [31–33]. In isolated β-cells, $[Ca^{2+}]_i$ oscillations occur with frequencies of 0.1 - 0.5 min^{-1}. Even faster or mixed $[Ca^{2+}]_i$ events are described with frequencies of 2 - 6 min^{-1} [34–36]. Also, other metabolic factors have been described to oscillate in β-cells, such as glucose-6-phosphate, NADH and ATP [37–40], phospholipase C (PLC) activity [41], diacylglycerol (DAG)-, phosphoinositide (PIP_n) levels within the PM [42,43] and the intracellular cyclic AMP (cAMP) concentration [44–46]. Therefore, β-cells are considered as biological oscillators [47].

Insulin secretion from β-cell populations or islets can be followed by traditional immunoassays, *e.g.* enzyme-linked immunosorbent assay (ELISA). However, these bulk techniques are mostly limited by insufficient sensitivity to monitor insulin secretion events from single cells or to resolve the fast kinetics of insulin secretion, especially when it comes to transient stimulation [48]. Cytosolic Ca^{2+} is a key second messenger of insulin exocytotic events. As $[Ca^{2+}]_i$ oscillations are directly coupled with pulsatile insulin secretion from β-cells and islets (Fig. 2 B, Fig. A1 (appendix) and [31,32,49–51]), monitoring $[Ca^{2+}]_i$ provides a sensitive readout of β-cell responses and insulin secretion. Cell-permeant, bright and photostable Ca^{2+} sensitive fluorescent indicators such as Fluo-4 allow for monitoring $[Ca^{2+}]_i$ oscillations in real time [52].

In the presence of glucose, insulin secretion can be potentiated or inhibited via G-protein coupled receptor (GPCR)-stimulation by neurotransmitters, hormones or small molecule metabolites [26]. Here, $G_{\alpha s}$-coupled receptors trigger cyclic AMP (cAMP) formation via adenylyl cyclase to amplify insulin secretion (Fig. 2 C). Next to Ca^{2+}, cAMP ranks amongst the most critical messengers for the regulation of insulin secretion [53–55]. Glucagon-like peptide 1 (GLP-1), glucagon or the gastric inhibitory polypeptide (GIP) are described to increase cellular cAMP levels in β-cells [56,57]. cAMP activates protein kinase A (PKA), which phosphorylates proteins of the insulin exocytosis machinery, thereby sensitizing insulin secretion to Ca^{2+} [58,59]. Further, PKA-mediated phosphorylation of K_{ATP} channels [60,61] and VGCC [62,63] directly modulates cellular $[Ca^{2+}]_i$. Also, gated intracellular Ca^{2+} mobilization from endoplasmatic reticulum (ER) stores might occur due to PKA-mediated phosphorylation and sensitization of 1,4,5-trisphosphate receptors (IP3Rs) [64,65]. Insulin release is additionally regulated by muscarinic GPCRs. Acetylcholine (ACh)- or

fatty acid (FA)-mediated stimulation of $G_{\alpha q}$-coupled receptors activates PLC at the inner leaflet of the PM, hydrolyzing phosphatidylinositol-4,5-bisphosphate (PIP_2) to DAG and IP_3. DAG activates protein kinase C (PKC), while IP_3 mobilizes Ca^{2+} from intracellular ER stores, which, in turn, triggers Ca^{2+}-influx from PM channels and exocytosis of insulin granules [66–68] (Fig. 2 A).

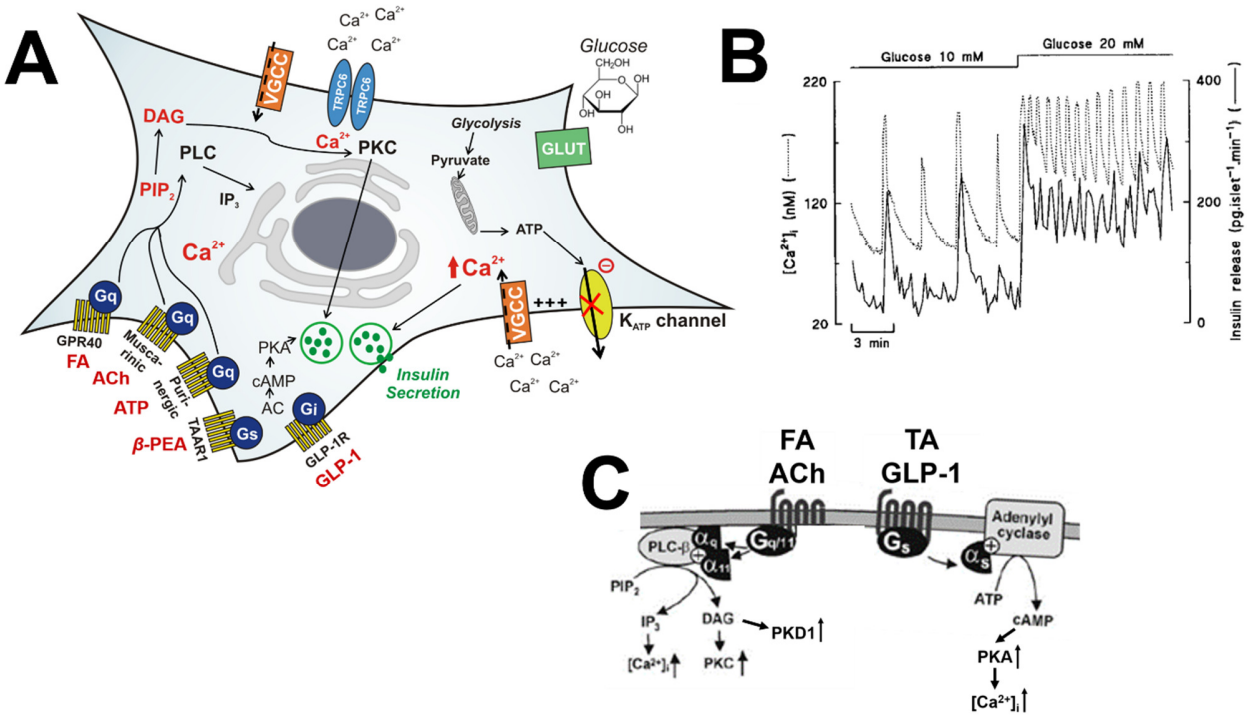

Figure 2. Mechanisms for the regulation of insulin secretion. (A) Glucose-stimulated insulin secretion (GSIS). Glucose is taken up into the *β*-cell by glucose transporters (GLUT) and metabolized. Increased cellular ATP levels block K_{ATP}-channels, followed by membrane depolarization. Voltage-gated Ca^{2+}-channels (VGCC) open to allow Ca^{2+}-influx, mediating the exocytosis of insulin-filled granules. **(B)** Temporal correlation of $[Ca^{2+}]_i$ oscillations (solid line) and insulin secretion (dashed line) was shown by simultaneous recordings in isolated mouse pancreatic islets at different glucose concentrations. Adapted from [51]. **(C)** GSIS is modulated by $G_{\alpha s}$- and $G_{\alpha q}$-coupled receptor signaling. Stimulation of $G_{\alpha s}$-coupled receptors by GLP-1 or trace amines (*β*-phenylethylamine, *β*-PEA) triggers cAMP formation by adenylyl cyclase (AC) action. cAMP activates protein kinase A (PKA) with direct effects on the insulin exocytotic machinery or ion channels. Stimulation of $G_{\alpha q}$-coupled receptors by fatty acids (FA) or acetylcholine (ACh) induces IP_3 and DAG formation via PLC-mediated hydrolysis of PIP_2, along with Ca^{2+} efflux from the ER, PKC and PKD1 activation. Adapted and modified from [69].

1.1.3. Cellular model systems for the investigation of the regulation of insulin secretion

Pancreatic cell lines or primary β-cells are well-established model systems that allow for the investigation of the cellular mechanisms that regulate insulin secretion. Mouse primary β-cells can be isolated from pancreatic tissue by mechanical or enzymatic fragmentation. The latter is achieved by injection of a collagenase solution into the pancreatic duct of the sacrificed animal, followed by the removal of the pre-digested pancreas, dispersion as well as separation of the islets from connective and fat tissue by density gradient centrifugation [70].

Compared to primary β-cells, pancreatic cell lines have the advantage of reproducibility and consistency, which is important for large-scale toxin or drug testing experiments [71]. Also, firmly attached to the cover slip, cultured cell lines easily stand buffer exchange and washing procedures. However, being of tumor origin, β-cell lines come with genetic (chromosomal) variability, along with abnormal metabolism and protein expression. This might lead to occasional differences in insulin secretory characteristics and glucose responsiveness between β-cell lines and primary β-cells. In addition, β-cell lines require β-mercaptoethanol as a culture medium supplement, which is likely to change the natural functionality of proteins [71]. Several pancreatic cell lines have been established as models that allow for the investigation of β-cell regulation and insulin secretion [71]. Insulin producing INS-1 (derived from rat insulinoma by X-ray treatment [72]) and MIN6 cells (generated from a transgenic mouse pancreatic tumor [73]) are amongst the pancreatic cell lines that are most commonly applied in the field. MIN6 cells grow as pseudo-islets and exhibit key characteristics of normal pancreatic islets [74]. Due to expression of glucokinase and GLUT-2, MIN6 and INS-1 cells show good responsiveness to glucose in the physiological range (Fig. A1 (appendix)) and high levels of insulin secretion in ranges similar to pancreatic islets [71,73,74]). Apart from insulin, secretion of glucagon, ghrelin and somatostatin from MIN6 cells was reported. This identifies MIN6 cells as a mixed cell line consisting of different pancreatic endocrine cells [75] and makes it ideally suited for the investigation of intercellular communication.

1.2. Intercellular signaling and β-cell synchronization inside the pancreas

Blood insulin levels are not maintained at constant levels, but rather oscillate at periodicities of ~5-15 min/oscillation in vertebrates, with variabilities due to species diversity, different sampling sites and methods of analysis (Fig. 3 A) [76–79]. However, hyperglycemic, hyperinsulinemic *ob/ob*

mice [80], diabetic rats [81] and type-2-diabetes mellitus (T2D) patients [82] as well as their close relatives [83,84] were diagnosed with disturbances in oscillatory insulin secretion. Loss of pulsatile insulin secretion was suggested to promote insulin resistance, which needs to be adjusted by insulin hypersecretion. This, in turn, might lead to the exhaustion of β-cells and to T2D [48].

In comparison to a constant insulin supply, clinical studies on diabetic patients indicate that oscillatory infusion of insulin lowers the insulin doses that are necessary to sustain normoglycemia [85–90]. The oscillatory nature of $[Ca^{2+}]_i$, along with pulsatile insulin secretion prevents β-cell overstimulation and cell death [91]. Oscillatory insulin levels *in vivo* are essential for avoiding the downregulation of systemic insulin receptor levels (*i.e.* obviating insulin resistance) and therefore enhance the physiological effects of secreted insulin [92]. Periodic secretory bursts of insulin secretion are ensured by both the integration of the β-cell population into a functional syncytium within pancreatic islets (intra-islet synchronization, Fig. 3 C) and the concerted secretory action of pancreatic islets (inter-islet synchronization, Fig. 3 B). In particular, pulsatile insulin secretion has been detected from isolated canine pancreata [93] and from individual rodent pancreatic islets [94,95] (Fig. 3 A). Even though patterns of $[Ca^{2+}]_i$ oscillations amongst individual β-cells can be quite variable, β-cells within pancreatic islets are well integrated into a common rhythm [32,76,96] (Fig. 3 C). Direct gap-junctional coupling of β-cells by intercellular channel proteins of the connexin family has been described as the pivotal mechanism for the synchronization of $[Ca^{2+}]_i$ oscillations within β-cells and thereby for pulsatile insulin release [48,97–99]. However, loss of functional gap junctions in mice was shown to compromise, but not to abolish the synchronization of $[Ca^{2+}]_i$ oscillations and pulsatile insulin secretion [100]. Notably, synchronized insulin release has also been observed within groups of dissociated islets, lacking physical contact [101]. Therefore, intra- and inter-islet synchronization have been suggested to also underlie para- and autocrine regulation, in addition to direct electrical coupling [3,48]. Autocrine signaling is based on the microcirculation of small diffusive extracellular messengers, mediating effects on either cells from which they were originally released or on neighboring cells of the same type [3]. Paracrine signaling is based on secreted messengers that affect different types of cells. Auto- and paracrine signaling present a means for information exchange about the functional state of neighboring cells as well as for the integration of β-cells and pancreatic islets into functional networks (Fig. 3 B). Prerequisite for efficient auto- and paracrine signaling are short distances between communicating cells, ensuring spatial restriction of the signaling. Therefore, the cellular arrangement and the confined extracellular space within human islets of Langerhans are perfectly

suited for auto- and paracrine signaling (Fig. 1 B and C) [3,5]. High local concentrations are reached by comparably small numbers of molecules that are also rapidly turned over by metabolizing enzymes [3]. More than two decades ago, coordinated $[Ca^{2+}]_i$ oscillations amongst dispersed isolated β-cells have been first described, assuming the presence of small diffusible factors, such as ATP and NO that mediate synchronization [102,103]. ATP was found co-released with insulin from secretory granules in a pulsatile fashion [65,104], stimulating P2 purinergic receptors of neighboring β-cells [105]. Thereby, ATP promotes intra- and inter-islet propagation of $[Ca^{2+}]_i$ oscillations, entrains pancreatic islets into a common rhythm, makes islets sensitive to fluctuating glucose levels [106] and ensures rapid adapted insulin responsiveness in a positive autocrine feedback mechanism [107–110]. Release of ATP from intra-pancreatic neurons was suggested as an ignition switch for the stimulation and coordination of pulses of insulin secretion [110,111].

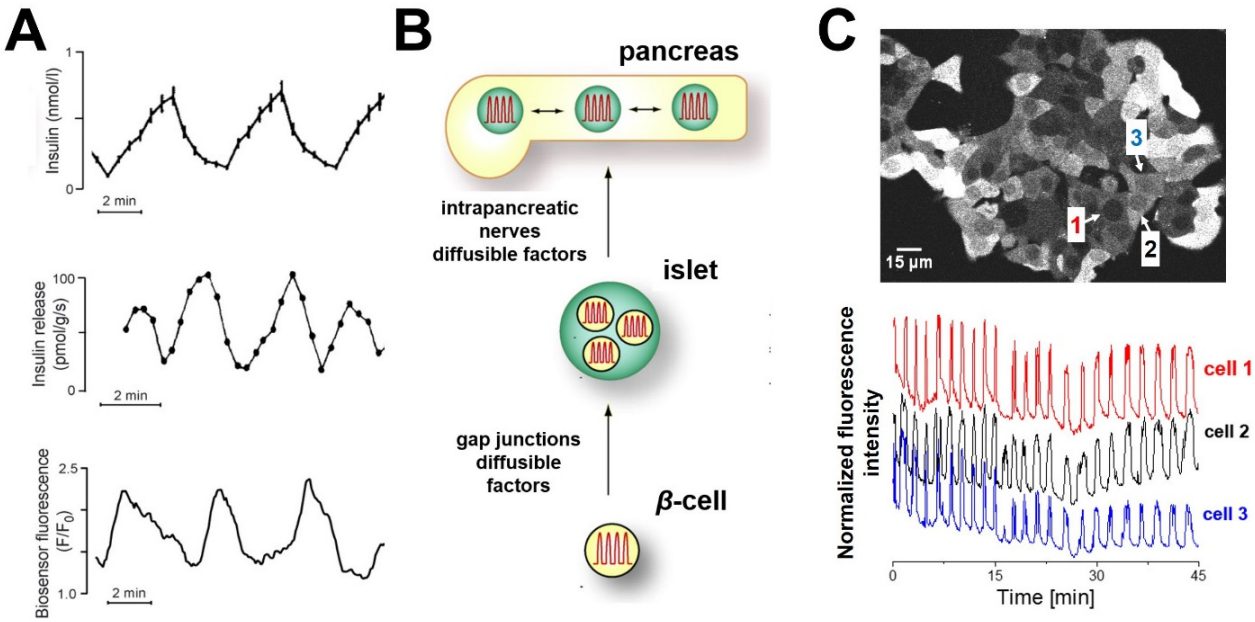

Figure 3. Intercellular and inter-islet synchronization within the pancreas constitute the basis for pulsatile insulin secretion. (A) Pulsatile insulin secretion, as recorded in the portal vein of a perfused rat pancreas (top, adapted from [112]), from an isolated pancreatic islet (middle, adapted from [32]) and from a single β-cell, recorded with a fluorescent sensor for the autocrine activation of insulin receptors [48,113]. **(B)** Hierarchy of pulsatile insulin secretion. β-Cells are synchronized via direct electrical coupling (gap junctions) and diffusible auto- and paracrine signaling factors. Thereby, pancreatic islets form synchronized syncytia that communicate via diffusible factors and nervous innervation within the pancreas. **(C)** Cultured MIN6 cells grow as pseudo-islets (top). Ca^{2+} traces, recorded from three adjacent MIN6 cells in the presence of glucose (bottom). The Ca^{2+} indicator Fluo-4 (5 µM) was applied for visualization of Ca^{2+} oscillations. Scale bar, 15 µm.

Other examples of pancreatic para- and autocrine signaling factors include small gaseous molecules, ions, hormones and neurotransmitters, such as NO [103,114], CO [115], Zn^{2+} [116,117], neuropeptide Y [118] or cellular metabolites, *e.g.* glutamate [119] and γ-aminobutyric acid (GABA) [120,121], but also insulin [122]. Taking into consideration ATP, GABA and Zn^{2+} concentrations in insulin secretory granules, the average volume and the amount of released insulin granules, as well as the volume of a *β*-cell and of the extracellular space, Braun *et al.* estimated extracellular concentrations of secreted autocrine signaling factors in the micromolar range. For this, however, degradation processes were neglected [123]. Considering the multitude of GPCRs that have been identified in *β*-cells [69], it is very likely that even more autocrine signaling factors participate in the regulation of *β*-cell activity, such as small aromatic amines and fatty acids.

1.3. Trace amines are small aromatic amines with implications for central nervous system function and glucose homeostasis

1.3.1. Trace amines act as neuromodulators via the trace amine-associated receptor 1

'Biogenic amines' is a generic term for a set of amines that show important biological effects as chemical messengers, *i.e.* neurotransmitters, neuromodulators and (local) hormones [124]. Catecholamines, including adrenaline, noradrenaline, dopamine and serotonin (Fig. 4 (6-9)) are amongst the first biogenic amines discovered [125]. In turn, the term 'trace amines' (TAs) describes a family of small endogenous aromatic amines that were detected at low concentrations (0.1 – 10 nM) in the central nervous system (CNS) [126,127]. Even though constituting only 0.1 % of the total amount of biogenic amines, TAs have been implicated in several neurological effects, including the fine-tuning of aminergic neurotransmission [127–129]. Common TAs are generated by the decarboxylation of amino acids. *β*-Phenylethylamine (*β*-PEA), *p*-tyramine, tryptamine, *p*-octopamine and synephrine are the most important representatives of TAs (Fig. 4 (1-5)) [124]. Unlike for neurotransmitters, no vesicular storage has been reported for TAs so far [127,130,131]. The discovery of the 'trace amine-associated receptor 1' (TAAR1) by two independent groups in 2001 provided the missing link for a molecular understanding of TA-mediated effects [132,133]. Whereas serotonin, dopamine and epinephrine show EC_{50}s in the micromolar range at TAAR1, EC_{50}s of TAs were reported at nanomolar levels [132,133]. TAAR1 was described to play a functional role for the fine-tuning of neuron excitability and neurotransmitter release [127].

Coupled to a $G_{\alpha s}$ protein, stimulation of TAAR1 triggers adenylyl cyclase-mediated generation of cAMP, along with modulation of PKA- and PKC-mediated signaling [132,133]. Further, TAAR1 enhances the opening of inwardly rectifying K^+ channels [134].

Monitoring intracellular cAMP levels in heterologous cell lines (*e.g.* HEK-293 or COS-7 cells) that overexpressed TAAR1 allowed for the pharmacological characterization of this receptor and for screening for endogenous and exogenous (artificial) agonists [132,133,135–138]. Thyronamines are endogenous amines with structural similarities to thyroid hormones that act as physiological TAAR1 agonists in addition to TAs [139]. Deiodination and decarboxylation of the thyroid hormone yield 3-iodothyronamine (T1AM) (Fig. 4 (10)), detected in human and rodent tissue as well as in blood [140,141]. T1AM is described as the most potent endogenous TAAR1 agonist [141]. Notably, addictive drugs, such as (meth-)amphetamine and 3,4-methylenedioxymethamphetamine (MDMA), sharing the same scaffold with *β*-PEA, were found to act as potent TAAR1 agonists (Fig. 4 (11-12)) [133].

Up until now, the subcellular localization of TAAR1 has been under debate. TAAR1 was reported to not only reside at internal membranes [128,142,143], but to translocate to the PM after heterodimerization [144,145]. Forming heterodimers with the D2 dopamine receptor (DR2) and dopamine transporter (DAT), TAAR1 activation was described to modulate dopaminergic signaling [134,146,147]. Interaction of TAAR1 with DAT was suggested to provide a mechanism for the regulated entry of TAs into the cytoplasm for TAAR1 binding. Variations of TA levels have been linked to common psychiatric disorders, such as major depression [148,149], schizophrenia [150], Parkinson's disease and anxiety states [151,152]. Therefore, selective agonists for the modulation of TAAR1 activity are high in demand.

Hoffmann-La Roche developed a series of potent synthetic full (*e.g.* RO5166017, RO5256390) and partial TAAR1 agonists (*e.g.* RO5073012, RO5203648 and RO5263397) (Fig. 4 (14-16)), showing high selectivity for TAAR1 and against the adrenergic α2 receptor [151,153–155]. The 'RO compounds' have been widely applied to study neural effects of selective TAAR1 activation, as reviewed by [156]. Alternative approaches for the identification of novel potent TAAR1 (ant-)agonists used molecular docking screening against a homology model of TAAR1 [157,158]. For the identification of selective TAAR1 antagonists, a Roche library of more than 7 $x10^5$ compounds was screened. Compounds were selected based on their capacity to reduce cAMP levels, following *β*-PEA-mediated stimulation of cells that expressed a chimeric human/rat variant of the TAAR1 receptor [134,159]. Based on its high affinity for rodent TAAR1 and selectivity, RO5212773

(EPPTB, Fig. 4 (13)) was selected [134,159], which is currently the only commercially available TAAR1 antagonist [156]. However, TAAR1 antagonists are high in demand, as cellular responses to EPPTB should be verified by various antagonists of different molecular structures [156]. Also, *in vivo* application of EPPTB is limited by its high clearance [159,160]. Based on homology modelling, Tan *et al.* predicted lead antagonist properties for rat TAAR1 to develop the potent antagonist ET-92 (IC_{50} of ~3 µM (rat) [161].

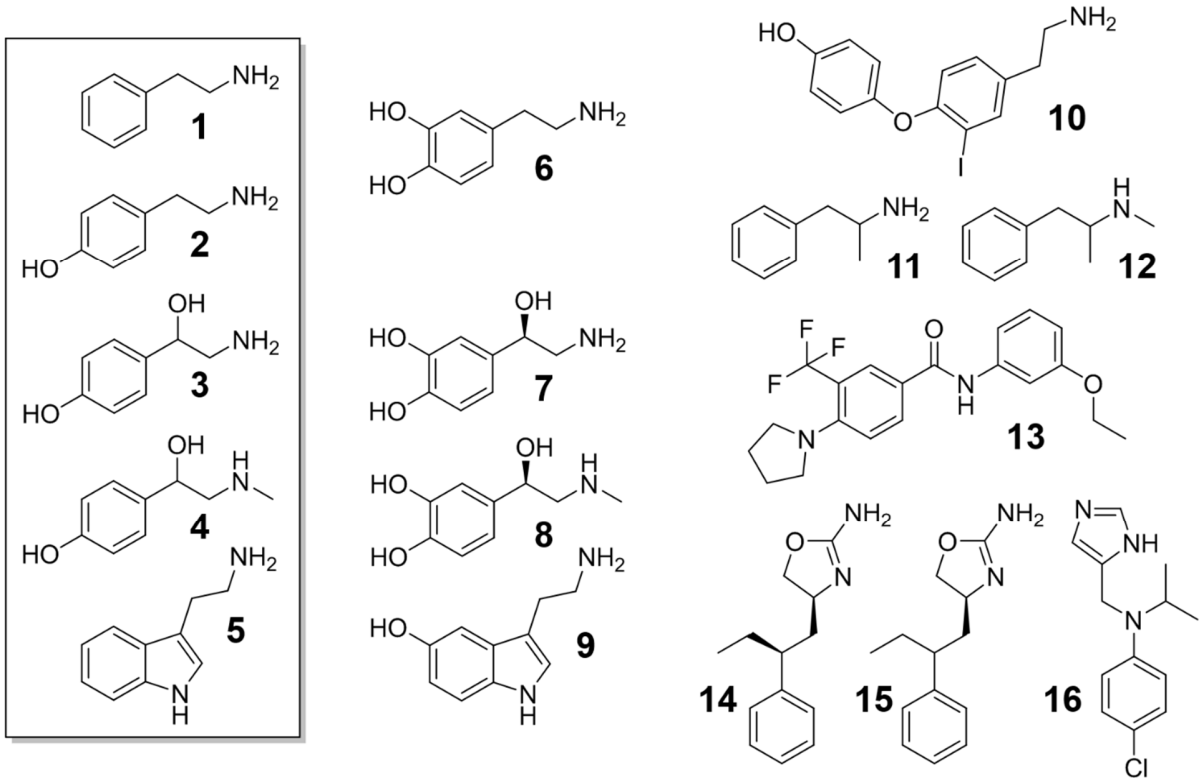

Figure 4. Overview of biogenic amines, TAs and TAAR1 (ant-)agonists. TAs (1-5): **(1)** *β*-PEA, **(2)** *p*-tyramine, **(3)** *p*-octopamine, **(4)** synephrine, **(5)** tryptamine. **Biogenic amines (6-9)**: **(6)** dopamine, **(7)** noradrenaline, **(8)** adrenaline, **(9)** serotonin. **(Synthetic) TAAR1 (ant-)agonists (10-16)**: **(10)** T1AM, **(11)** amphetamine, **(12)** methamphetamine, **(14)** RO5073012, **(15)** RO5166017, **(16)** RO5256390.

1.3.2. Biochemistry of TAs

TAs are generated from respective precursor aromatic amino acids in a single decarboxylation step, catalyzed by aromatic L-amino acid decarboxylase (AADC). That way, *β*-PEA is directly generated from L-phenylalanine, tryptamine from L-tryptophan and *p*-tyramine from L-tyrosine (Fig. 5) [127,162]. *p*-Tyramine is converted by dopamine *β*-hydroxylase (DBH) to generate *p*-octopamine (Fig. 5). *β*-PEA, *p*-tyramine and *p*-octopamine are substrates of phenylethanolamine *N*-

methyltransferase (PNMT) [163] and nonspecific N-methyltransferase (NMT) [164] for the biosynthesis of corresponding secondary amines, *i.e.* synephrine [133], *N*-methyltyramine [165] and *N*-methylphenylethylamine (Fig. 5) [166]. TAs are rapidly inactivated in a single enzymatic oxidation step by monoamine oxidases (MAO), described to reside at outer mitochondrial membranes [167]. MAO-A and MAO-B are the two isoforms of MAO for TA oxidation and inactivation (Fig. 5). While all TAs are metabolized by both MAO isoforms, *β*-PEA is primarily converted by MAO-B [168–171]. MAOs show high turnover rates, leaving TAs with half-life periods in the range of ~30 s [170]. As MAO-B also metabolizes dopamine, inhibitors of MAOs are applied for the treatment of depression and Parkinson's disease in the clinics [172].

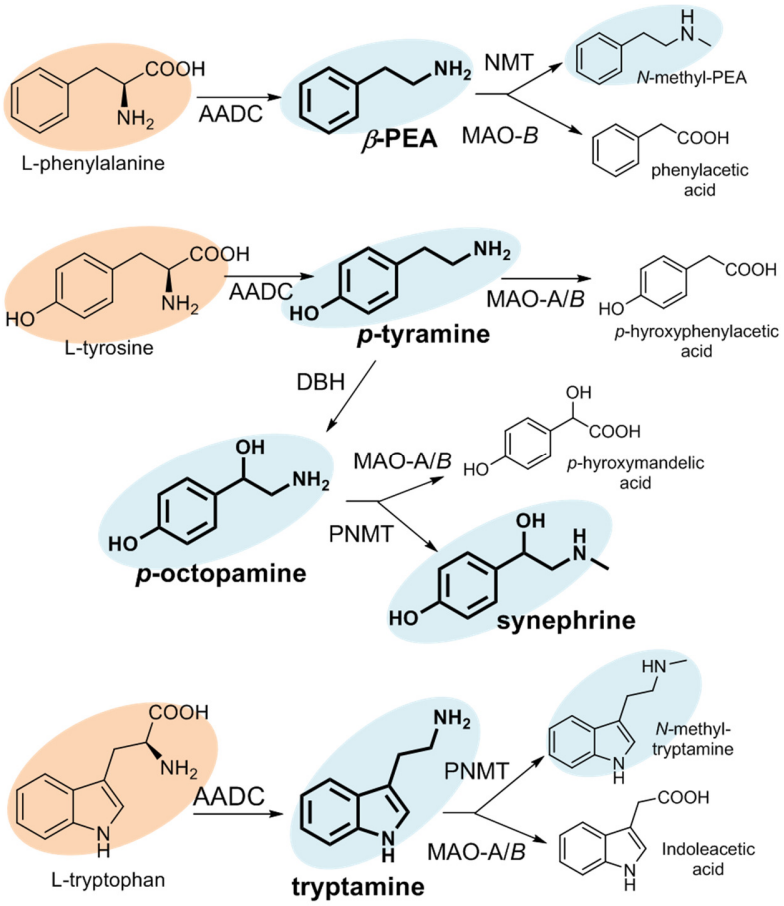

Figure 5. Schematic overview of the main biosynthetic routes for TA generation and degradation in vertebrates. Decarboxylation of the amino acids L-phenylalanine, L-tyrosine and L-tryptophan by aromatic L-amino acid decarboxylase (AADC) yields *β*-PEA, *p*-tyramine and tryptamine. *p*-Tyramine is metabolized to synephrine via *p*-octopamine (dopamine *β*-hydroxylase (DBH), phenylethanolamine *N*-methyltransferase (PNMT)) or directly to *N*-methyltyramine by PNMT. *β*-PEA is converted to *N*-methylpenylethylamine by NMT. *N*-methyltryptamine is generated from tryptamine by PNMT action. TAs are rapidly inactivated by monoamine oxidase (MAO-A/-B) action and have relatively short half-lives in the range of 30 s. TAs are highlighted in blue, amino acids in red [166].

1.3.3. The role of TAAR1 in glucose homeostasis and energy metabolism

So far, research has mainly focused on the neuromodulatory functions of TAAR1 in the CNS, while its role in peripheral tissue has been far less studied. Notably, TAAR1 was found expressed in organs involved in gastric function and nutrient absorption. In rats, TAAR1 mRNA was detected at low to moderate levels in stomach [173,174], duodenum [174,175] and in trace amounts in human as well as mouse islets of Langerhans [132,133]. Here, TAAR1 expression was detected in β-cells but not in α-cells [154,174].

The involvement of TAAR1 in the regulation of energy metabolism was first shown in 2013. Pre-clinical testing of the TAAR1 partial agonist RO5263397 as a treatment for schizophrenia prevented rats from drug-induced weight gain and fat accumulation [154]. Also, TAAR1 mRNA was detected in the murine β-cell line MIN6, rat INS-1, mouse pancreatic β-cells and in human islets [174,176]. Selective TAAR1 agonism by RO5166017 significantly potentiated GSIS from INS-1 cells, from isolated human islets (*in vitro*) and C57BL/6 mice (*in vivo*), along with significantly lowered blood glucose levels [174]. Also, overnight fasted C57BL/6 mice showed reduced appetite, after treatment with TAAR1 agonists [174]. A recent preliminary study in overweight/obese patients with impaired insulin secretion connected single-nucleotide variants in TAAR1 with disturbed glucose homeostasis [177]. All this makes TAAR1 an attractive therapeutic target for the pharmacological modulation of β-cell activity and insulin secretion. Despite of data supporting TAAR1 expression in pancreatic islets, the effect of selective TAAR1 (ant-)agonism on single β-cell activity as well as the role of the presence or selective reduction of endogenous TA levels for $[Ca^{2+}]_i$ oscillations and insulin secretion has not been unraveled yet.

1.4. Fatty acids modulate insulin secretion via GPR40

It has long been described that elevated levels of FAs augment GSIS in isolated rodent islets and pancreata [178–181], in dogs [182], patients [183] and random subjects [184]. Pre-exposure of islet β-cells to FAs renders them hypersensitive to glucose [185]. The insulinotropic potency of FA was described to depend on the degree of saturation and the chain length [186–188]. Long-chain unsaturated FAs are most potent for the stimulation of $[Ca^{2+}]_i$ and insulin release [189,190], such as arachidonic [191–194], oleic [195], linoleic [196] and palmitic acid [197–200]. Interestingly, reductions of blood FA levels correlated with decreased levels of insulin [201,202]. This indicates

that certain FA levels are necessary for efficient GSIS and further that FAs play a role for glucose homeostasis that lies beyond basic modulatory actions.

In 2003, GPR40, an orphan GPCR that was found abundantly expressed in brain and pancreatic tissue, was identified as a receptor for medium and long-chain FAs [203–205]. Overexpression of GPR40 in pancreatic β-cells was reported to augment GSIS [206]. Opposite effects emerged after deletion of GPR40 in β-cells [207,208]. Notably, genetic polymorphisms of GPR40 were connected to alterations in the insulin secretion capacity of healthy subjects [209]. Therefore, GPR40 was suggested as a major player of the potentiating effects that FAs cause on $[Ca^{2+}]_i$ signaling and GSIS [210–213]. It has recently been shown that the photolysis of caged arachidonic acid at the PM of MIN6 cells modulates $[Ca^{2+}]_i$ signaling via GPR40 [214]. FA-mediated stimulation of GPR40 - mainly coupled to $G_{\alpha q}$ - activates PLC, which induces PIP_2 hydrolysis to IP_3 and DAG. IP_3 leads to Ca^{2+} liberation from ER stores and thereby to the elevation of $[Ca^{2+}]_i$. DAG also activates PKD1, along with de-polymerization of F-actin and potentiation of insulin release (Fig. 2 A, C) [195,211,212,215]. Alternative pathways for the FA-mediated modulation of GSIS include the intracellular conversion of FAs to lipid signaling species via long-chain acyl-CoA that potentiate cellular metabolism and GSIS [196,216]. GPR40 stimulation and intracellular metabolism were suspected to each account for 50 % of the effect of FAs on insulin release [217]. The overall pancreatic lipolytic activity enhances extracellular levels of FAs [218,219], indicating their possible role as autocrine signaling factors for insulin secretion. Phospholipase A_2 (PLA_2) liberates FAs from membrane lipids by the hydrolysis of zwitterionic glycerophospholipids [220]. Interestingly, selective inhibition, reduced expression or knock-down of PLA_2 in β-cells correlated with reduced $[Ca^{2+}]_i$ oscillations and decreased GSIS. These effects were reversed by the addition of arachidonic acid [221–224]. Also, lipoprotein lipase, localized within islet capillaries, provides FAs from triglycerides that are transported by lipoproteins to pancreatic islets [225,226]. Notably, inhibition of lipolysis in rat pancreatic islets by a broad lipase inhibitor was connected to reduced insulin secretion in a dose-dependent manner [227]. As previous studies showed that exogenous FAs stimulate insulin secretion, FAs were suspected to play a pivotal role for the coalescence of nutrient segretagogue signals and the modulation of β-cell activity for the secretion of adequate amounts of insulin [228–230]. Even though FAs have been discussed as insulin secretagogues for decades, the role of endogenous FAs levels for single β-cell activity, intercellular and inter-islet signaling has not been investigated so far.

2. Aims of this work

Within the last decade, small molecule insulin secretagogues, such as NO, CO, ATP and glutamate, as well as ions and peptides have gained increasing attention as autocrine signaling factors for intra- or inter-islet communication and β-cell synchronization. Despite of data demonstrating GPR40 and TAAR1 expression in the pancreas, the role of receptor stimulation by endogenous signaling factors for individual β-cell activity and insulin secretion is yet to be determined. This would make autocrine signaling, mediated by TAAR1 and GPR40, as well as respective pathways for the biosynthesis of receptor agonists, attractive therapeutic targets for the pharmacological modulation of β-cell activity and insulin secretion. However, rational drug development, targeting pancreatic autocrine signaling has strongly been limited by our lack of knowledge of 1) the general role of autocrine signaling factors for β-cell activity and insulin secretion, 2) the identity and origin of endogenous pancreatic TAAR1 and GPR40 agonists, 3) the role of endogenous GRP40 and TAAR1 agonists for the maintenance of β-cell activity and insulin secretion 4) relative and absolute abundances of TA- and FA-species in β-cells, 5) the potency of (synthetic) TAAR1 and GPR40 (ant-)agonists for the modulation of β-cell activity and insulin secretion, 6) TAAR1-coupled downstream signaling network(s) relevant to insulin secretion and 7) the location of TAAR1 activation and signaling in β-cells.

In this study, we therefore aimed at 1) investigating the general role of autocrine signaling factors for β-cell activity and insulin secretion and 2) examining whether β-cell activity can be modulated by the selective reduction or replenishment of TA- and FA levels. Also, we were interested in 3) whether $[Ca^{2+}]_i$ oscillations and insulin secretion can be modulated by (synthetic) TAAR1 or GPR40 (ant-)agonists. In addition, we wanted to 4) monitor absolute abundances as well as changes of cellular TA and FA levels in the presence of selective inhibitors for biosynthetic pathways via mass spectrometry. 5) Alterations of TA and FA levels should then be correlated with changes in $[Ca^{2+}]_i$ oscillations, cAMP levels and insulin secretion. TAAR1 has been described as a major player in neural diseases. Therefore, various drugs have been brought to the market for the modulation of brain biogenic amine levels via inhibition of key biosynthetic enzymes or for the direct activation of TAAR1, with yet unknown consequences for overall glucose homeostasis. Therefore, we were also interested in 6) understanding whether β-cell activity and insulin secretion can be modulated by the drug-mediated lowering or increase of endogenous TA levels or direct pharmacological modulation of TAAR1 in the pancreas.

3. Results

3.1. Extracellular signaling factors are essential for *β*-cell activity and insulin secretion

In this work, we exploited the well documented correlation between $[Ca^{2+}]_i$ oscillations and insulin secretion (Figs. 2 B and A1 (appendix), [49,50,231]). Spatiotemporal changes in $[Ca^{2+}]_i$ were followed in real time using the Ca^{2+} sensitive cell-permeant fluorescent indicator Fluo-4 [52]. To quantitatively describe cellular $[Ca^{2+}]_i$ events, traces of representative cells were averaged. Also, numbers of detected 'high-intensity $[Ca^{2+}]_i$ events' per 60 s interval are presented. For this, the height of each $[Ca^{2+}]_i$ event was determined relative to the highest detected peak per trace as a criterion to identify $[Ca^{2+}]_i$ transients as high-intensity events ($\geq$ 60 % of highest peak intensity).

Static incubation of MIN6 cells in the presence of 11 mM glucose is characterized by periodic transients of the cytosolic Ca^{2+} concentration ($[Ca^{2+}]_i$ oscillations, Fig. 6 A+B i). According to literature reports on MIN6 cells and isolated pancreatic islets [74], we observed that MIN6 cells respond to increasing concentrations of external glucose with enhanced GSIS, along with differential levels of $[Ca^{2+}]_i$ oscillations (Fig. A1 (appendix)). Extensive perfusion of glucose-stimulated MIN6 cells with buffer in a perfusion system transiently stopped $[Ca^{2+}]_i$ oscillations (1.5 mL/min for 1 min, 11 mM glucose. The perfusion system is shown in Fig. A2 (appendix)). Oscillations gradually recovered only after stopping the perfusion (Figs. 6 A+B i, D), as reported by Hauke *et al.* [232]. Comparable effects were observed upon washing of MIN6 and mouse primary *β*-cells in the microscopy dish in advance of imaging (Figs. 6 A+B ii, iii, v). Static incubation of MIN6 cells yielded significantly higher insulin levels, compared to constant perfusion (0.15 mL/min, Fig. 6 C), as reported by Hauke *et al.* [232]. This suggested that stringent washing of MIN6 cells removed components from the extracellular space of *β*-cells that are essential for $[Ca^{2+}]_i$ oscillations and GSIS and that can be replenished by *β*-cells after perfusion.

In order to investigate whether $[Ca^{2+}]_i$ oscillations and GSIS can be modulated by endogenous signaling factors, which are secreted by MIN6 cells, a population of 2 x10^6 MIN6 cells was incubated for 30 min with buffer (*i.e.* supernatant, SN). This SN was transferred to an imaging dish containing freshly washed MIN6 cells. Buffer transfer fully recovered $[Ca^{2+}]_i$ oscillations in the entire population of MIN6 cells (Fig. 6 A+B ii, E) and stimulated insulin secretion (Fig. 6 I, MIN6+SN MIN6) [232]. This effect was observed for SNs at different glucose concentrations (Fig. A3 (appendix)). Here, the frequency of the recovered $[Ca^{2+}]_i$ oscillations, as well as counts of high-intensity $[Ca^{2+}]_i$ spikes correlated well with applied buffer glucose levels.

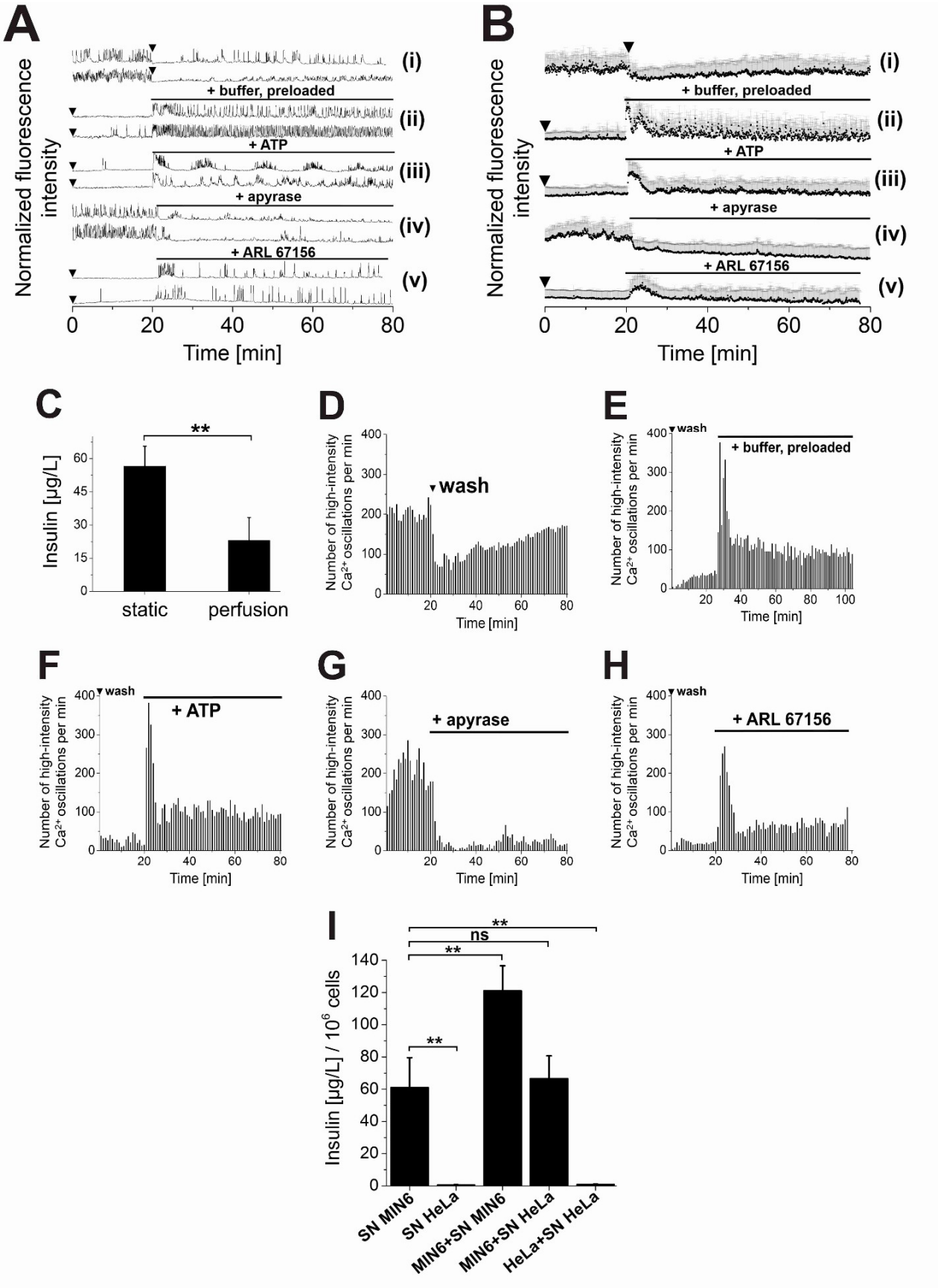
A
Normalized fluorescence intensity
(i)
+ buffer, preloaded
(ii)
+ ATP
(iii)
+ apyrase
(iv)
+ ARL 67156
(v)
0
20
40
60
80
Time [min]
B
Normalized fluorescence intensity
(i)
+ buffer, preloaded
(ii)
+ ATP
(iii)
+ apyrase
(iv)
+ ARL 67156
(v)
0
20
40
60
80
Time [min]
C
Insulin [µg/L]
**
0
15
30
45
60
static
perfusion
D
Number of high-intensity Ca2+ oscillations per min
wash
0
100
200
300
400
20
40
60
80
Time [min]
E
Number of high-intensity Ca2+ oscillations per min
wash
+ buffer, preloaded
0
100
200
300
400
20
40
60
80
100
Time [min]
F
Number of high-intensity Ca2+ oscillations per min
wash
+ ATP
0
100
200
300
400
20
40
60
80
Time [min]
G
Number of high-intensity Ca2+ oscillations per min
+ apyrase
0
100
200
300
400
20
40
60
80
Time [min]
H
Number of high-intensity Ca2+ oscillations per min
wash
+ ARL 67156
0
100
200
300
400
20
40
60
80
Time [min]
I
Insulin [µg/L] / 10^6 cells
**
ns
**
**
0
20
40
60
80
100
120
140
SN MIN6
SN HeLa
MIN6+SN MIN6
MIN6+SN HeLa
HeLa+SN HeLa

Figure 6. Endogenous (autocrine) signaling factors are essential for MIN6 and primary *β*-cell activity and insulin secretion. (A+B) Representative single **(A)** and averaged **(B)** Ca^{2+} traces from MIN6 and mouse primary *β*-cells, stained with the Ca^{2+} indicator Fluo-4. **(D-H)** Number of high-intensity $[Ca^{2+}]_i$ events per 60 s interval. **(A+B i**, **D)** Stringent washing in a perfusion system (1.5 mL/min, indicated by ▼) reduced $[Ca^{2+}]_i$ oscillations in MIN6 cells, which gradually recovered during subsequent static incubation. **(C)** Static incubation of MIN6 cells yielded ~60 % more insulin, compared to constant perfusion. **(A+B ii**, **E)** $[Ca^{2+}]_i$ oscillations of washed MIN6 cells immediately recovered upon addition of buffer that was pre-loaded on 2 x10^6 MIN6 cells. **(A+B iii**, **F)** Addition of ATP (25 µM) to pre-washed MIN6 cells immediately started intermittent $[Ca^{2+}]_i$ oscillations. **(A+B iv**, **G)** Addition of apyrase (0.5 U) reduced $[Ca^{2+}]_i$ oscillations in MIN6 cells. **(A+B v**, **H)** $[Ca^{2+}]_i$ oscillations in pre-washed MIN6 cells started upon addition of ARL 67156 (50 µM), a selective inhibitor of ecto-ATPases. Shown are averages of n = 30 MIN6 cells. **(I)** Transfer of pre-loaded buffer (SN) from a population of MIN6 cells to pre-washed MIN6 cells significantly enhanced insulin secretion (MIN6+SN MIN6). SN from HeLa cells served as a control (MIN6+SN HeLa). Data was corrected for the transferred amount of insulin (as determined from HeLa+SN MIN6: 23.5 ± 12 µg/L). Error bars present SD. Insulin experiments were performed in the presence of 11 mM glucose in quadruplicate (**P<0.01, ANOVA, ns = not significant = P>0.05, with repeated measures as necessary). Washes are indicated by ▼. The figure was adapted, extended and partly modified from Hauke *et al.* [232].

Transfer of pre-loaded SN to washed MIN6 cells presumably recovered the extracellular 'secretome' that was removed from MIN6 cells in the washing step. SN that was harvested from HeLa cells under identical conditions served as a control. Addition of this HeLa SN on top of freshly washed MIN6 cells restarted $[Ca^{2+}]_i$ oscillations only in 3 % of the MIN6 cell population and had no significant effect on insulin secretion (Fig. 6 I, MIN6+SN HeLa). This indicated that extracellular signaling is far less pronounced in the cancer cell line HeLa, compared to *β*-cells.

ATP-mediated synchronization of the *β*-cell secretory machinery is a prime example for the effects that autocrine signaling factors have on insulin secretion [108,109,112]. Previous work described ATP to be amongst para- and autocrine signaling factors within rodent and human pancreatic islets, acting on P2 purinergic receptors in an autocrine feedback loop [106,233]. In line with that, we found that addition of ATP (25 µM) to pre-washed MIN6 cells instantaneously induced intermittent $[Ca^{2+}]_i$ oscillations (Fig. 6 A+B iii and F). Notably, responses in $[Ca^{2+}]_i$ oscillations that were induced by the addition of ATP to pre-washed MIN6 cells were less pronounced compared to effects from pre-loaded buffer transfer (Fig. 6 A+B ii and iii). Therefore, we suspect that the full activity of pre-washed MIN6 cells can only be reconstituted in the presence of the entire spectrum of extracellular factors - herein called the 'cellular secretome'. Endogenous extracellular ATP is degraded to AMP via ADP by membrane-localized ecto-ATPases (*e.g.* adenosine 5´-triphosphatase) [234]. Ecto-ATPases were reported to act as essential determinants for the duration

and extent of purinergic signaling [235]. In line with this, addition of a recombinant ATP-diphosphohydrolase (apyrase (0.5 U)) to oscillating MIN6 cells gradually reduced $[Ca^{2+}]_i$ oscillations (Fig. 6 A+B iv and G). As recombinant apyrase does not penetrate cellular PMs, we suspected that only extracellular ATP levels were selectively reduced. Instead, application of the specific ecto-ATPase inhibitor ARL 67156 (50 µM, [236–238]) to pre-washed MIN6 cells immediately started $[Ca^{2+}]_i$ oscillations (Fig. 6 A+B v, H). All this already identified ATP as an extracellular endogenous (autocrine) signaling factor that is essential for *β*-cell activity.

3.2. TAs are essential signaling factors for the autocrine regulation of *β*-cell activity and insulin secretion

3.2.1. TAs, (synthetic) TAAR1 agonists and antagonists modulate $[Ca^{2+}]_i$ oscillations and insulin secretion

Identified in the CNS as a target for TAs and psychoactive stimulants, TAAR1 has been implicated to play a significant role in the regulation of the limbic network, mood states, in rewarding circuits of addictive drugs as well as cognitive processes [127] and thereby also in the development of psychiatric diseases [152,239]. Much effort has been invested in elucidating the role of TAAR1 activation on dopaminergic signaling in schizophrenia, depression and Parkinson's disease, as reviewed by Berry *et al.* [160]. The detection of TAAR1 mRNA in peripheral tissue, in particular in mouse and human pancreatic *β*-cells as well as in the cell lines INS-1 and MIN6 [174,176] marked a turning point. Recently, TAAR1-mediated signaling was connected to the regulation of peripheral processes, such as insulin secretion [174,176]. Raab *et al.* showed the potentiating effect of the selective TAAR1 agonist RO5166017 on GSIS in pancreatic human islets, INS-1E cells and in live C57BL/6J mice [174]. These studies were the first to describe TAAR1 as an integrator of metabolic control over insulin secretion.

Based on these preliminary findings, we tested selective TAAR1 agonists for their stimulating potencies on pre-washed MIN6 cells that were stained with the Ca^{2+} indicator Fluo-4. Addition of full (RO5166017 and RO5256390 [151,154]), partial (RO5073012 [153]) or endogenous (*β*-PEA, T1AM [161]) TAAR1 agonists (all 25 µM) to pre-washed MIN6 potently induced $[Ca^{2+}]_i$ oscillations, peaking at the time point of addition to gradually decrease over observation time (Fig 7 A+B). According to our hypothesis, these results already showed that the activity of glucose-stimulated MIN6 cells can be modulated in the presence of selective TAAR1 agonists.

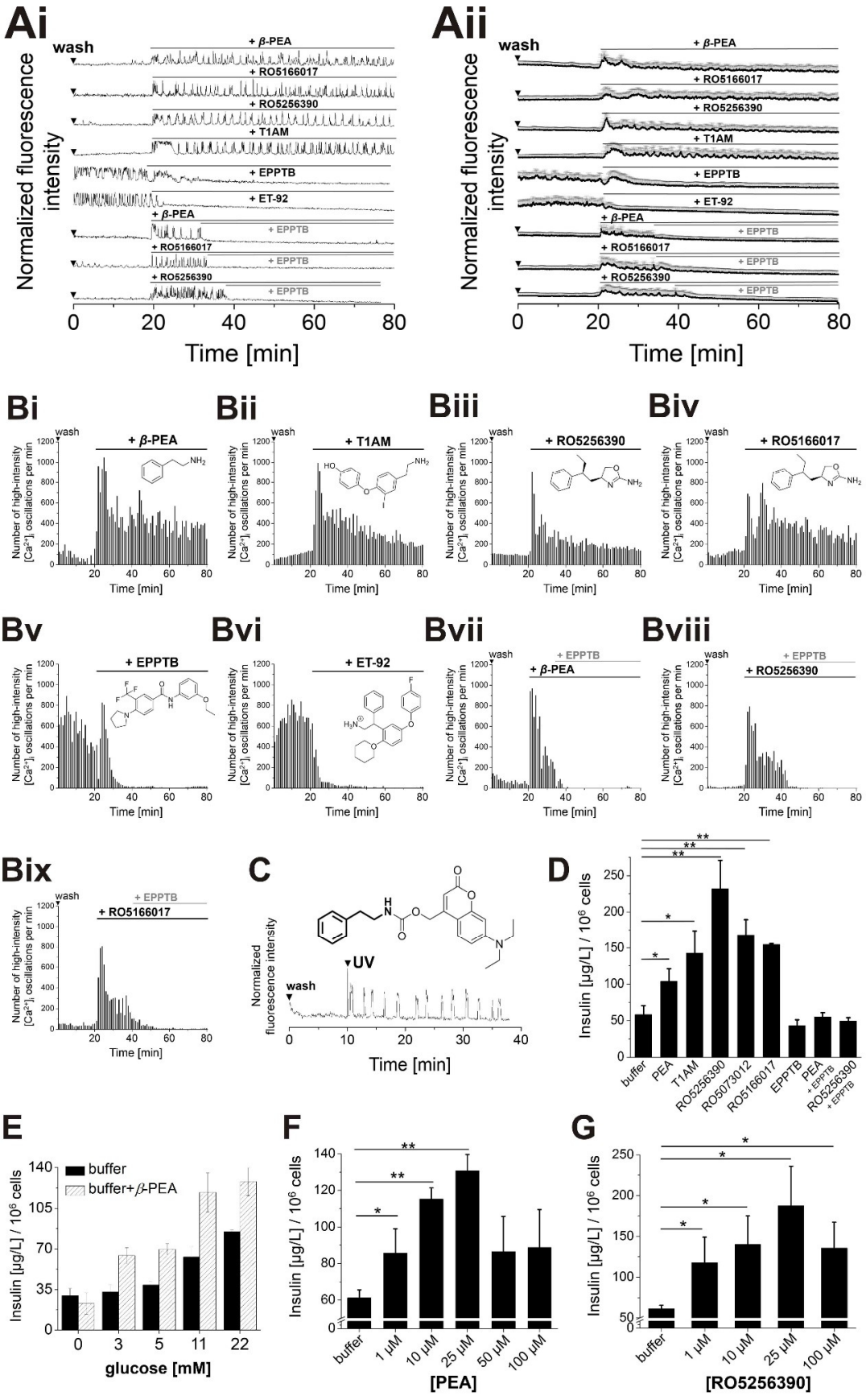
Ai
Aii
wash
+ β-PEA
+ RO5166017
+ RO5256390
+ T1AM
+ EPPTB
+ ET-92
Normalized fluorescence intensity
Time [min]
Bi
Bii
Biii
Biv
Bv
Bvi
Bvii
Bviii
Bix
Number of high-intensity [Ca2+]i oscillations per min
C
UV
Normalized fluorescence intensity
D
Insulin [µg/L] / 10^6 cells
buffer
PEA
T1AM
RO5256390
RO5073012
RO5166017
EPPTB
PEA + EPPTB
RO5256390 + EPPTB
E
buffer
buffer+β-PEA
glucose [mM]
F
[PEA]
G
[RO5256390]

Figure 7. TAAR1 (ant-)agonists modulate $[Ca^{2+}]_i$ oscillations and insulin secretion of MIN6 cells. Representative **(Ai)** single and **(Aii)** averaged Ca^{2+} traces from MIN6 cells. **(Bi–Bix)** Counts of detected high-intensity $[Ca^{2+}]_i$ events per 60 s interval. **(A+B i-iv)** Addition of TAAR1 agonists *β*-PEA, RO5166017, RO5256390 and T1AM to pre-washed MIN6 cells stimulated $[Ca^{2+}]_i$ oscillations. **(A+B v-ix)** The selective TAAR1 antagonists EPPTB and ET-92 decreased $[Ca^{2+}]_i$ oscillations of glucose- or TAAR1-stimulated MIN6 cells. **(C)** Photolysis of caged *β*-PEA by a short UV pulse ($\lambda = 375$ nm) instantaneously started $[Ca^{2+}]_i$ oscillations in pre-washed MIN6 cells. **(D)** Levels of insulin, as determined by insulin ELISA. *β*-PEA, RO5166017, RO5256390 (all 25 µM) and the endogenous agonist T1AM (10 µM) stimulated GSIS ~1.8-, ~2.9-, ~4- and ~2.6-fold. EPPTB reduced GSIS and TAAR1 agonists-mediated effects in MIN6 cells. **(E)** *β*-PEA (25 µM) stimulated insulin secretion from MIN6 cells in the presence of different glucose concentrations, as indicated. **(F+G)** Concentration dependent stimulation of GSIS from MIN6 cells by *β*-PEA or RO5256390. Insulin experiments were performed in the presence of 11 mM glucose in quadruplicate (*P<0.05 and **P<0.01. All unmarked events in D, F and G were not statistically significant = P>0.05. ANOVA, with repeated measures as necessary). Ca^{2+} traces were recorded from cells that were stained with the Ca^{2+} indicator Fluo-4. Shown are averages of 100 MIN6 cells. Washes are indicated by ▼. If not indicated otherwise, experiments were performed in the presence of 11 mM glucose. Caged *β*-PEA was provided by A. Laguerre.

Counts of high-intensity $[Ca^{2+}]_i$ spikes were in comparable ranges for *β*-PEA, T1AM and the synthetic TAAR1 agonist RO5166017 (400 - 500 counts/min from 100 MIN6 cells, Fig. 7 Bi, ii, iv). Slightly lower stimulation was observed for the full agonist RO5256390 (300 - 400 counts/min from 100 MIN6 cells, Fig 7 Biii) and for the partial agonist RO5073012 (300 - 400 counts/min from 100 MIN6 cells, Fig A4 (appendix)). However, based on cAMP measurements, Revel *et al.* reported TAAR1 activation potencies of RO5256390 and RO5166017 that were in comparable ranges to those of *β*-PEA [151,154]. Stimulation of $[Ca^{2+}]_i$ oscillations translated well into increased insulin levels, as determined by insulin ELISA. *β*-PEA stimulation of MIN6 cells potentiated GSIS ~1.8-fold, RO5166017, RO5256390 and RO5073012 ~2.6-, ~4-, and ~2.9-fold (agonist concentration: 25 µM, Fig 7 D). Notably, RO5256390 most potently stimulated insulin secretion. The endogenous TAAR1 agonist T1AM potentiated GSIS ~2.4-fold already at 10 µM (Fig 7 D).

To trigger TAAR1 activation with high spatio-temporal control, we synthesized a photo-caged *β*-PEA (Fig 7 C). For this, the photoactivatable group (‘cage’) 7-diethylamino-4-methylene-coumarin was attached to the primary amino group of *β*-PEA via carbamate formation. The photo-labile coumarin cage masks *β*-PEA and prevents oxidation by MAO. MIN6 cells were loaded with caged *β*-PEA and washed. Caged *β*-PEA started $[Ca^{2+}]_i$ oscillations in pre-washed MIN6 cells only upon application of a short UV-pulse (Fig 7 C). Thereby, *β*-PEA was presumably liberated inside

MIN6 cells. The immediate recovery of $[Ca^{2+}]_i$ oscillations upon light-mediated liberation of *β*-PEA indicates the presence of an intracellular TAAR1 pool that was available for activation.

β-PEA (25 µM) potentiated GSIS from MIN6 cells in the presence of different glucose levels, but not in the absence of glucose (Fig. 7 E). Stimulation of MIN6 cells by *β*-PEA yielded significantly higher levels of insulin at stimulatory glucose concentrations (11 mM and 22 mM: ~119 µg/L and ~128 µg/L), as compared to sub-stimulatory glucose levels (3 mM and 5 mM: ~64 µg/L and ~70 µg/L) (Fig. 7 E). To check whether TAAR1-mediated potentiation of GSIS was dose-dependent, MIN6 cells were stimulated with increasing concentrations of *β*-PEA and RO5256390 in the presence of 11 mM glucose. Insulin secretion increased from 1 µM (agonist) to reach the maximum levels at 25 µM (agonist), approximately 2.2-fold (*β*-PEA) or 4-fold (RO5256390), compared to buffer levels. At higher concentrations, insulin secretion dropped (Fig. 7 F+G).

To examine the general role of TAAR1 stimulation for the maintenance of $[Ca^{2+}]_i$ oscillations and for GSIS, we applied the specific TAAR1 antagonists EPPTB (RO5212773 [134]) and ET-92 [161] to glucose-stimulated MIN6 cells. Notably, EPPTB and ET-92 significantly reduced $[Ca^{2+}]_i$ oscillations and GSIS of MIN6 cells (Fig 7 A+B v, vi, D). This suggested that TAAR1 is either constitutively active or activated by endogenous agonists and that both EPPTB and ET-92 may antagonize this effect. Therefore, EPPTB was previously suggested to act as an inverse agonist [156]. EPPTB and ET-92 decreased $[Ca^{2+}]_i$ oscillations in MIN6 cells, even after preceding stimulation by TAs or TAAR1 agonists (Fig. 7 A+B vii-ix). In fact, reversal of agonist-mediated effects by the selective antagonist EPPTB has been defined as a criterion to identify effects that are mediated by TAAR1 stimulation [134]. Even *β*-PEA and RO5256390-mediated effects on insulin secretion were overruled down to buffer levels by EPPTB (Fig. 7 D). Notably, this showed that selectively targeting TAAR1 was sufficient to modulate $[Ca^{2+}]_i$ oscillations and insulin secretion.

Apart from MIN6 cells, we found that TAAR1 (ant-)agonists also modulated $[Ca^{2+}]_i$ oscillations and insulin secretion of INS-1 and mouse primary *β*-cells. Effects on $[Ca^{2+}]_i$ oscillations were concentration dependent, as shown for the endogenous TAAR1 agonist T1AM (Fig. 8 A). INS-1 cells showed clear $[Ca^{2+}]_i$ responses to the potent TAAR1 agonists T1AM (Fig. 8 A) and RO5256390 at 50 µM (Fig. 8 B). Addition of *β*-PEA, tyramine and RO5166017 to pre-washed INS-1 cells only induced transient $[Ca^{2+}]_i$ oscillations at higher concentrations (100 µM, Fig. 8 B). This might be explained by overall low TAAR1 expression levels within this rat cell line [174] or species-specific differences in TAAR1 activation profiles [241]. Insulin levels that were obtained from INS-1 cells were significantly lower, compared to those of MIN6 cells (Fig. 8 C).

Also, mouse primary β-cells responded well to the TAAR1 agonists β-PEA, tyramine, T1AM and RO5256390 by increased $[Ca^{2+}]_i$ oscillations (25 µM, Fig. 8 D). In line with findings from MIN6 cells, the antagonists EPPTB and ET-92 potently reduced $[Ca^{2+}]_i$ oscillations in mouse primary β-cells (25 µM, Fig. 8 D).

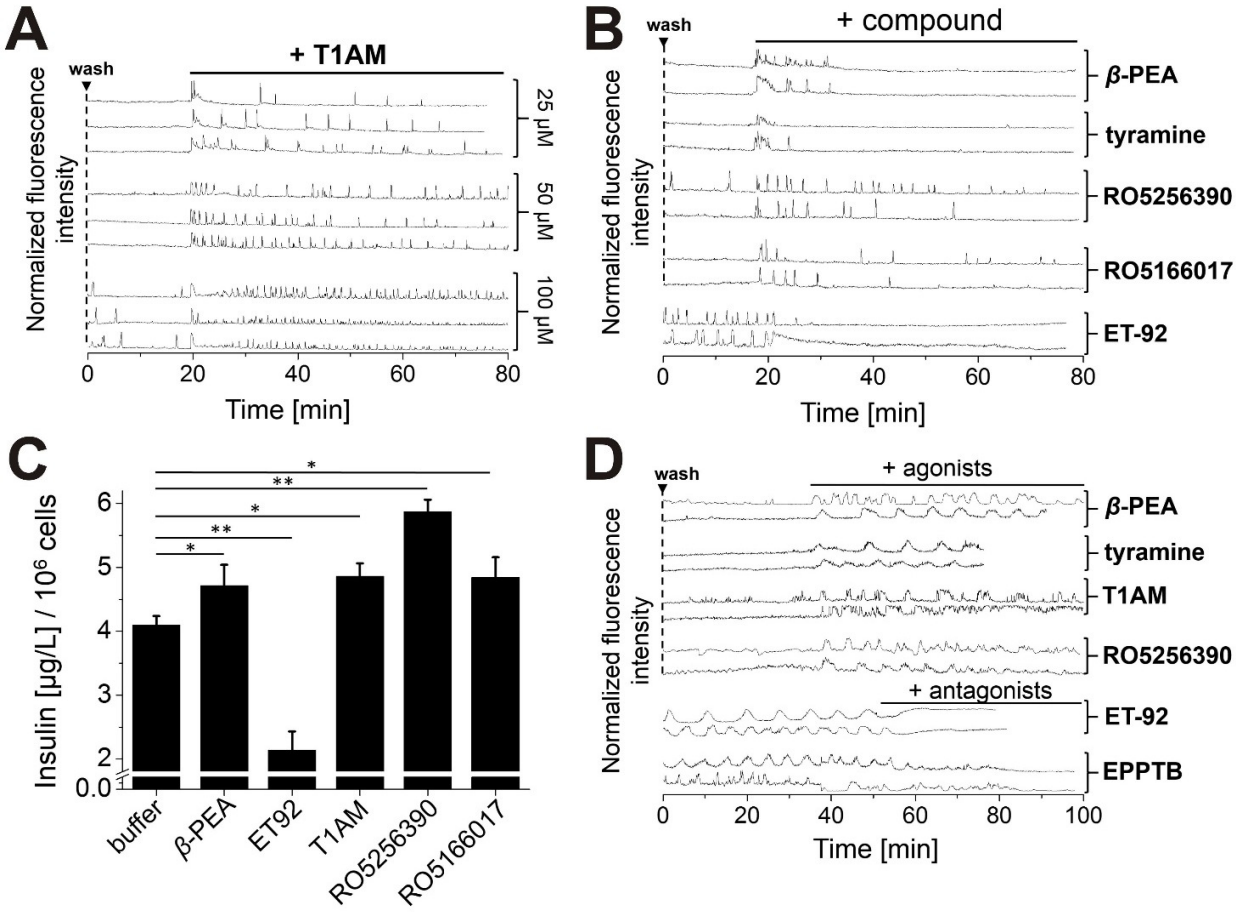

Figure 8. TAAR1 (ant-)agonists modulate $[Ca^{2+}]_i$ oscillations and insulin secretion of INS-1 and mouse primary β-cells. Representative Ca^{2+} traces from **(A+B)** INS-1 and **(D)** mouse primary β-cells. **(A)** Effects of T1AM on $[Ca^{2+}]_i$ oscillations in pre-washed INS-1 cells were concentration dependent. **(B)** β-PEA, tyramine and RO5166017 evoked intermittent $[Ca^{2+}]_i$ oscillations at 100 µM, whereas RO5256390 potently stimulated $[Ca^{2+}]_i$ oscillations in pre-washed INS-1 cells already at 50 µM. The antagonist ET-92 (25 µM) reduced $[Ca^{2+}]_i$ oscillations. **(C)** β-PEA, T1AM, RO5256390 and RO5166017 (all 100 µM) potentiated insulin secretion from INS-1 cells. The TAAR1 antagonist ET-92 (100 µM) significantly reduced GSIS from INS-1 cells. Imaging and insulin experiments in INS-1 cells were performed in the presence of 11 mM glucose in quadruplicate (*P<0.05 and **P<0.01, ANOVA, with repeated measures as necessary). Error bars present SD. **(D)** The TAAR1 agonists β-PEA, tyramine, T1AM, RO5166017 and RO5256390 (all 25 µM) showed potent effects on $[Ca^{2+}]_i$ oscillations of mouse primary β-cells in the presence of 5 mM glucose. $[Ca^{2+}]_i$ oscillations were reduced by ET-92 and EPPTB (25 µM). Ca^{2+} traces were recorded from cells, stained with Fluo-4. Imaging experiments and data analysis were performed together with J. Rada.

3. Results

In line with our hypothesis of TAAR1 as a modulator of *β*-cell activity and insulin secretion, we found that pre-washed MIN6 cells immediately responded to the stimulation by different TAs with increased $[Ca^{2+}]_i$ oscillations. Addition of TAs to pre-washed MIN6 cells evoked pronounced $[Ca^{2+}]_i$ transients, followed by continuous $[Ca^{2+}]_i$ oscillations of differential intensity. Here, the primary amines *β*-PEA (~400 - 500 counts/min in 100 MIN6 cells) and *p*-tyramine (~200 - 300 counts/min in 100 MIN6 cells) were identified as the most potent stimuli (Fig. 9 A+B i+ii), followed by tryptamine (~100 - 200 counts/min in 100 MIN6 cells, Fig. 9 A+B iii). Effects were weakened with increasing modification of the aliphatic side chain or amino group, as observed for *p*-octopamine and the secondary amine *p*-synephrine (~100 counts/min in 100 MIN6 cells, Fig. 9 A+B iv+v). Based on $[Ca^{2+}]_i$ responses, a rank order of potency was determined for tested TAs: *β*-PEA > *p*-tyramine > tryptamine >> *p*-synephrine ≈ *p*-octopamine. This is in line with literature reports on the activation potencies of TAs [138,241]. Corresponding amino acids did not stimulate $[Ca^{2+}]_i$ oscillations in pre-washed MIN6 cells (Fig. 9 A+B vi-viii).

Broad ligand tuning of TAAR1 suggested further investigations for the structure-activity-relation of TAAR1 agonists in MIN6 cells. Therefore, we profiled a selection of *β*-PEA-derived compounds for their potencies to stimulate $[Ca^{2+}]_i$ oscillations with regard to specific modifications of the aromatic moiety and ethylene chain (Fig. 10). Secondary amines (*N*-methyl-PEA, ~200 - 300 counts/min in 100 MIN6 cells, Fig. 10 A+B ii) and tertiary aromatic amines (*N,N*-dimethyl-PEA, ~200 counts/min in 100 MIN6 cells, Fig. 10 A+B iii) were less potent in stimulating $[Ca^{2+}]_i$ oscillations, compared to the corresponding primary amine (*β*-PEA, ~400 - 500 counts/min in 100 MIN6 cells, Fig. 10 A+B i), based on counts of high-intensity $[Ca^{2+}]_i$ spikes. Notably, the TAAR1 activation potency decreased with increasing modifications on the amino group of *β*-PEA, as also reported previously [136]. Still, *N*-methyl-PEA was significantly more potent than *p*-synephrine (~100 counts/min in 100 MIN6 cells, Fig. 9 A+B v). Therefore, we suspected that the potency for the stimulation of $[Ca^{2+}]_i$ oscillations also decreased with increasing modifications of the aliphatic side chain or the aromatic moiety, which was confirmed herein (*β*-methyl-1-PEA, 2-amino-1-phenylethanol, Fig. 10 A+B iv+v and 3- or 4-methoxy-PEA, Fig. 10 A+B vi+vii). These compounds evoked a prominent $[Ca^{2+}]_i$ transient upon addition that was not followed by enhanced continuous $[Ca^{2+}]_i$ oscillations. In line with literature reports, (bulky) residues on the phenyl ring or amino group reduced the TAAR1 activation potency of *β*-PEA-derived compounds [136,242]. Amines with shortened aliphatic chains or non-aromatic amines did not evoke $[Ca^{2+}]_i$ oscillations (1-methyl-1-PEA, benzylamine, cadaverine, Fig. 10 A+B viii-x).

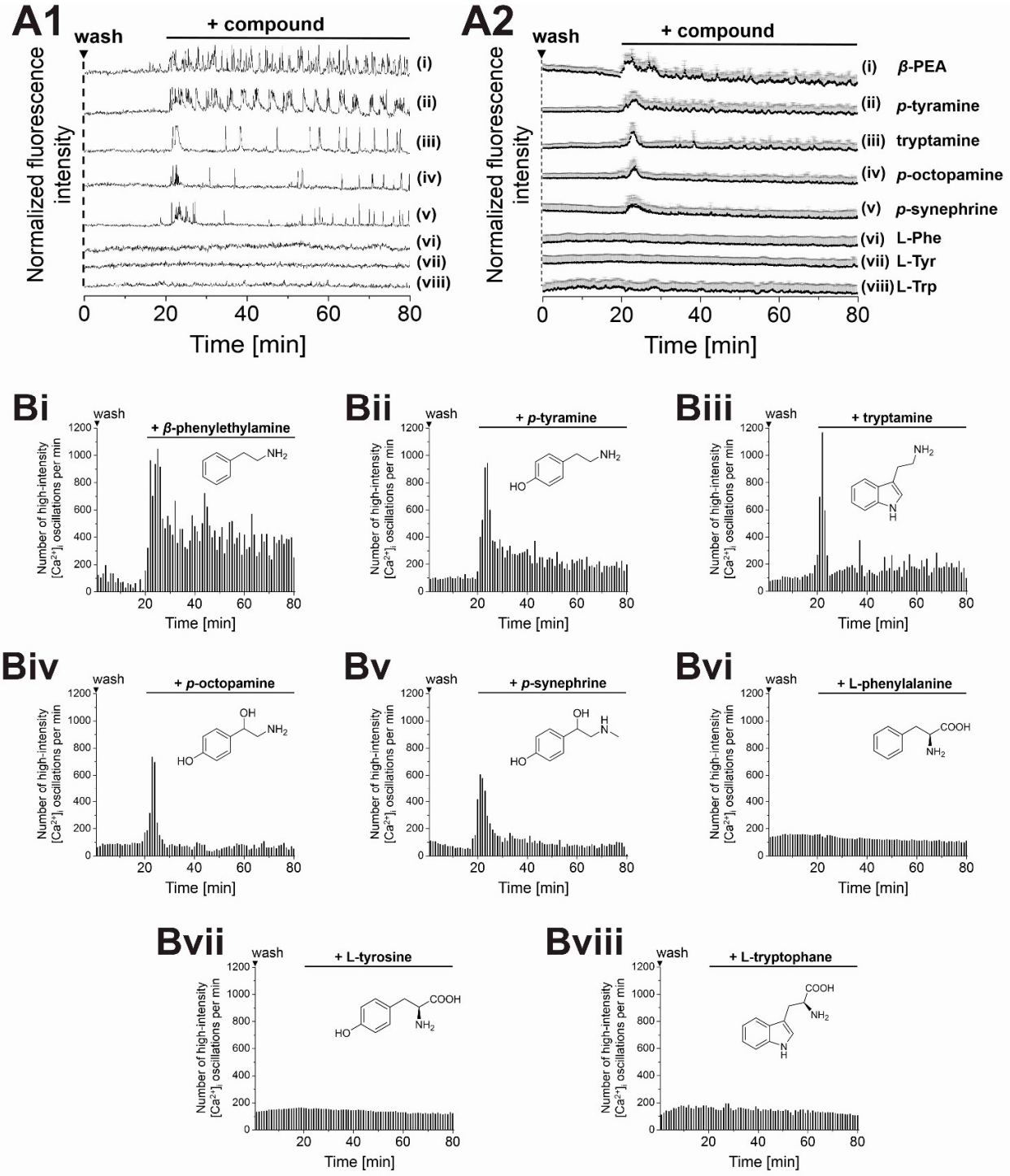

Figure 9. TAs stimulate $[Ca^{2+}]_i$ oscillations in pre-washed MIN6 cells. Representative single **(A1)** and averaged **(A2)** Ca^{2+} traces from MIN6 cells, recorded with the Ca^{2+} indicator Fluo-4. **(B)** Number of high-intensity $[Ca^{2+}]_i$ events per 60 s interval. Effects of amines on $[Ca^{2+}]_i$ oscillations decreased with increasing modifications of the aliphatic side chain or amino group. Based on $[Ca^{2+}]_i$-responses, a rank order of potency was determined for TAs: *β*-PEA > *p*-tyramine > tryptamine >> *p*-synephrine ≈ *p*-octopamine **(A+B i-v)**. **(A+B vi-viii)** Corresponding amino acids served as controls. Compounds were applied at 25 µM final concentration in the presence of 11 mM glucose. Shown are averaged traces from 100 MIN6 cells.

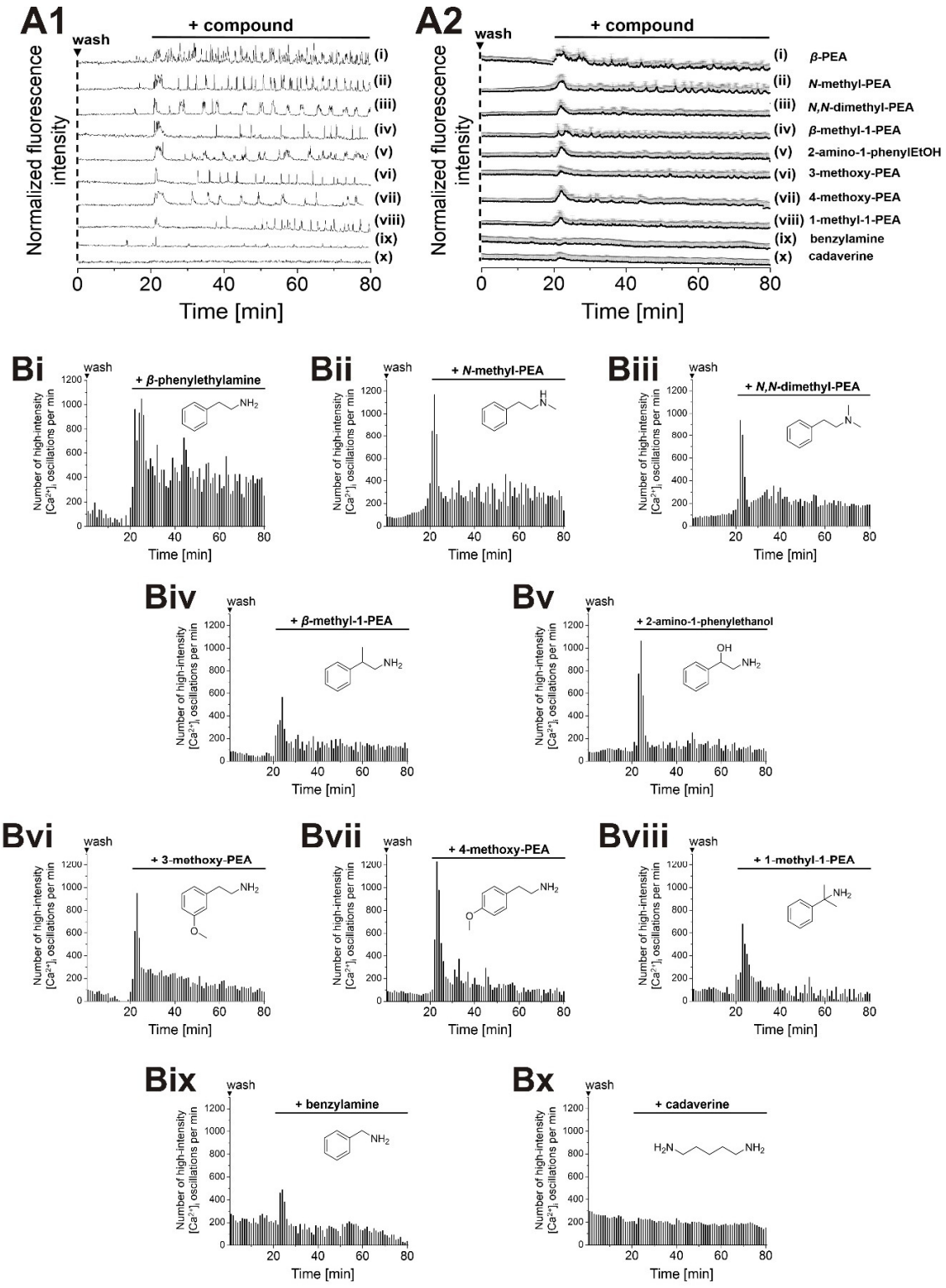

Figure 10. Differential stimulation of $[Ca^{2+}]_i$ oscillations in MIN6 cells by small amines. Representative single **(A1)** and averaged **(A2)** Ca^{2+} traces from MIN6 cells, recorded with the Ca^{2+} indicator Fluo-4. **(B)** Number of high-intensity $[Ca^{2+}]_i$ events per 60 s interval. A selection of (partly *β*-PEA-related) amines was profiled for their potency to stimulate $[Ca^{2+}]_i$ oscillations. Compounds were applied at 25 µM final concentration in the presence of 11 mM glucose. Shown are averaged traces from 100 MIN6 cells.

3.2.2. Psychotropic drugs stimulate $[Ca^{2+}]_i$ oscillations and insulin secretion via TAAR1

TAAR1 has been described to act as a major player in the development of psychiatric disorders, such as schizophrenia, Parkinson's disease, depression and drug addiction [146,152,160,239]. Therefore, the 'RO-compounds', EPPTB and ET-92 were developed as selective synthetic TAAR1 (ant-)agonists for the treatment of psychiatric diseases [134,151,153–155].

In the present work, we demonstrate the potential of these compounds to modulate $[Ca^{2+}]_i$ oscillations and insulin secretion of pancreatic cell lines and primary β-cells (Figs. 7 and 8). Notably, several other psychoactive drugs, such as antidepressants or antiparkinsonian agents have been described as agonists of TAAR1 in the CNS, as reviewed in [156]. Given the structural similarity of several commonly prescribed psychoactive drugs to β-PEA, we expected the stimulation of β-cells via TAAR1 also by these compounds. Therefore, we tested several psychotropic drugs, partly described to act as TAAR1 agonists, for their effects on $[Ca^{2+}]_i$ oscillations and insulin secretion. Tested drugs included dibenzepin, idazoxan and nomifensine (antidepressants), flurazepam (benzodiazepine), diphenylhydramine (antiparkinsonian/insomnia agent), as well as ergoline derivatives lisuride (antiparkinsonian agent) and methysergide (for migraine treatment) [156,243], partly structurally resembling β-PEA. Addition of these compounds to pre-washed MIN6 cells instantaneously evoked $[Ca^{2+}]_i$ oscillations, peaking at the time point of addition to slowly decrease over observation time (Fig. 11 A+B). Based on counts of high intensity $[Ca^{2+}]_i$ oscillations, dibenzepin, idazoxan, nomifensine and flurazepam evoked the strongest responses in pre-washed MIN6 cells. Here, ~400 counts/min in 100 MIN6 cells were determined (Fig. 11 B i, iii, v, vii), comparable to β-PEA stimulation of MIN6 cells. Weaker effects were evoked by lisuride, methysergide and diphenylhydramine, increasing $[Ca^{2+}]_i$ oscillations just above buffer levels (~200 counts/min in 100 MIN6, Fig. 11 B ix, xi, xiii). In line with our observations on $[Ca^{2+}]_i$ oscillations, we found that psychoactive drugs potentiated insulin secretion from glucose-stimulated MIN6 cells ~1.1 – 1.4-fold (Fig. 12 A).

In turn, addition of EPPTB to pre-stimulated MIN6 cells reversed effects of psychoactive drugs on $[Ca^{2+}]_i$ oscillations and insulin secretion down to or even below buffer levels (Fig. 11 and Fig. 12 B). Therefore, the modulation of $[Ca^{2+}]_i$ oscillations and insulin secretion by the tested psychoactive drugs was attributed to TAAR1 stimulation. Equally, the TAAR1 antagonist ET-92 significantly reduced $[Ca^{2+}]_i$ oscillations that were evoked by the addition of dibenzepin to pre-washed MIN6 cells (Fig. A5 (appendix)), thereby also confirming herein observed effects of EPPTB.

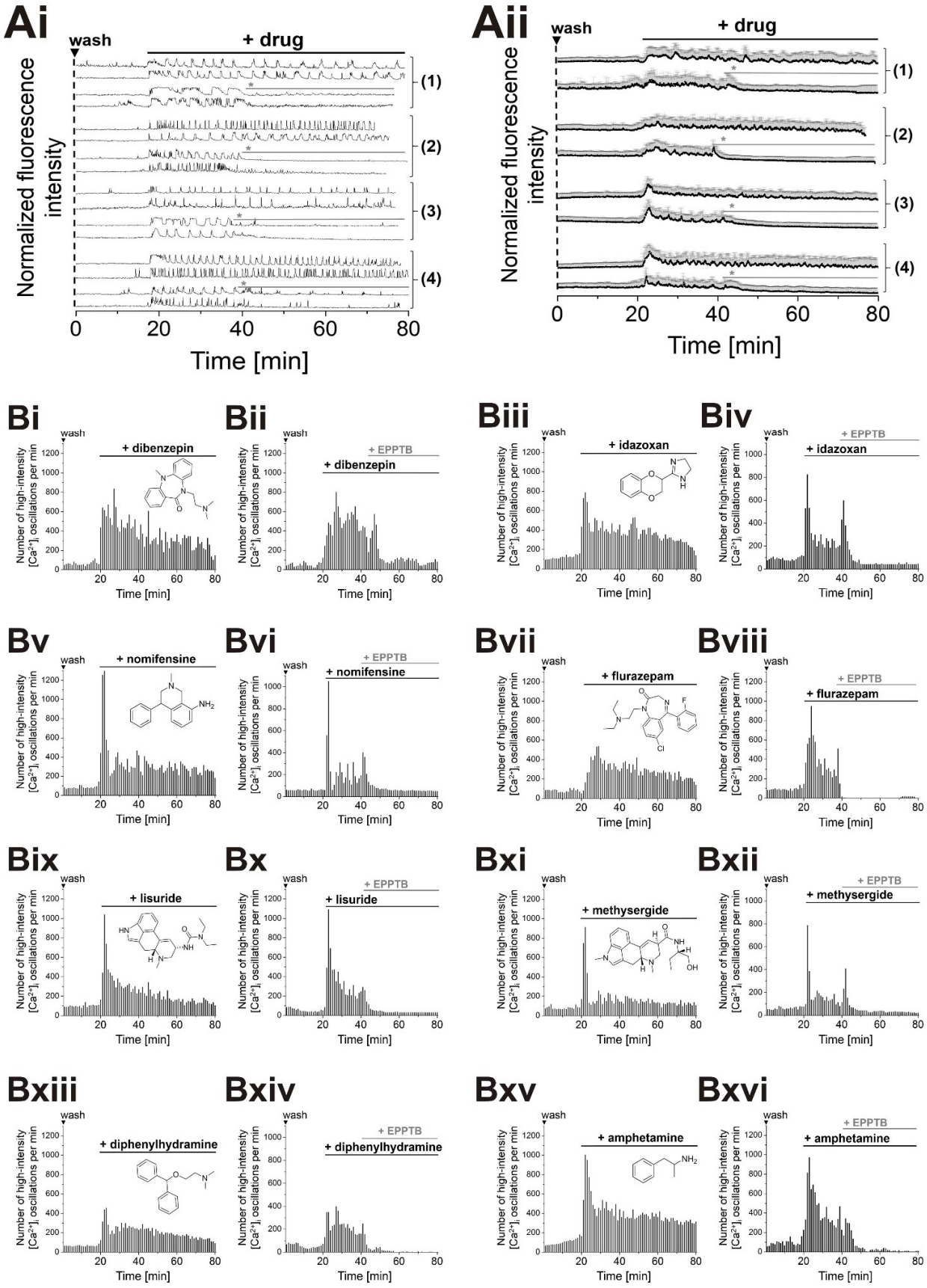
Ai
wash
+ drug
Normalized fluorescence intensity
(1)
(2)
(3)
(4)
0
20
40
60
80
Time [min]
Aii
wash
+ drug
Normalized fluorescence intensity
(1)
(2)
(3)
(4)
0
20
40
60
80
Time [min]
Bi
wash
+ dibenzepin
Number of high-intensity [Ca2+]i oscillations per min
Time [min]
Bii
wash
+ EPPTB
+ dibenzepin
Number of high-intensity [Ca2+]i oscillations per min
Time [min]
Biii
wash
+ idazoxan
Number of high-intensity [Ca2+]i oscillations per min
Time [min]
Biv
wash
+ EPPTB
+ idazoxan
Number of high-intensity [Ca2+]i oscillations per min
Time [min]
Bv
wash
+ nomifensine
Number of high-intensity [Ca2+]i oscillations per min
Time [min]
Bvi
wash
+ EPPTB
+ nomifensine
Number of high-intensity [Ca2+]i oscillations per min
Time [min]
Bvii
wash
+ flurazepam
Number of high-intensity [Ca2+]i oscillations per min
Time [min]
Bviii
wash
+ EPPTB
+ flurazepam
Number of high-intensity [Ca2+]i oscillations per min
Time [min]
Bix
wash
+ lisuride
Number of high-intensity [Ca2+]i oscillations per min
Time [min]
Bx
wash
+ EPPTB
+ lisuride
Number of high-intensity [Ca2+]i oscillations per min
Time [min]
Bxi
wash
+ methysergide
Number of high-intensity [Ca2+]i oscillations per min
Time [min]
Bxii
wash
+ EPPTB
+ methysergide
Number of high-intensity [Ca2+]i oscillations per min
Time [min]
Bxiii
wash
+ diphenylhydramine
Number of high-intensity [Ca2+]i oscillations per min
Time [min]
Bxiv
wash
+ EPPTB
+ diphenylhydramine
Number of high-intensity [Ca2+]i oscillations per min
Time [min]
Bxv
wash
+ amphetamine
Number of high-intensity [Ca2+]i oscillations per min
Time [min]
Bxvi
wash
+ EPPTB
+ amphetamine
Number of high-intensity [Ca2+]i oscillations per min
Time [min]

Figure 11. Psychotropic drugs modulate $[Ca^{2+}]_i$ oscillations in MIN6 cells via TAAR1. Representative single **(Ai)** and averaged **(Aii)** Ca^{2+} traces from MIN6 cells, recorded with the Ca^{2+} indicator Fluo-4. **(Bi – Bxvi)** Counts of detected high-intensity $[Ca^{2+}]_i$ events per 60 s interval. Differential stimulation of $[Ca^{2+}]_i$ oscillations in pre-washed MIN6 cells was observed upon addition of the antidepressants **(Ai+ii (1)**, **Bi)** dibenzepin, **(Biii)** idazoxan and **(Bv)** nomifensine, the benzodiazepine **(Ai+ii (2)**, **Bvii)** flurazepam, the antiparkinsonian agents **(Ai+ii (3)**, **Bix)** lisuride and **(Bxiii)** diphenylhydramine, **(Bxi)** methysergide for migraine treatment as well as **(Ai+ii (4)**, **Bxv)** amphetamine. Compounds were applied at 25 µM in the presence of 11 mM glucose. Drug-induced stimulation of $[Ca^{2+}]_i$ oscillations was reduced by the addition of the TAAR1 antagonist EPPTB (50 µM). Shown are averages of 100 MIN6 cells.

Based on our observations on $[Ca^{2+}]_i$ oscillations and insulin secretion of MIN6 cells, we suspect implications of tested psychotropic compounds even on systemic glucose homeostasis, apart from described CNS effects.

Expecting even more psychoactive drugs to act as modulators of $[Ca^{2+}]_i$ oscillations via TAAR1, we expanded the spectrum of compounds to be screened on MIN6 cells. We tested the livestock feed additive ractopamine that was previously described to act as a TAAR1 agonist [244] and to reduce feed consumption, while promoting muscle mass development [245], indicating effects on both CNS and glucose homeostasis. In fact, addition of ractopamine (25 µM) to pre-washed MIN6 cells potently induced $[Ca^{2+}]_i$ oscillations (~300 - 400 counts/min in 100 MIN6, Fig. A6 (appendix)) that were reduced by the addition of ET-92 (25 µM, Fig. A6 (appendix)).

Also, ergoline (lysergic acid) derivatives are described to act as agonists of TAAR1 [156,241], which was already confirmed herein for lisuride and methysergide on MIN6 cells (Fig. 11 Ai+ii(3), B ix+xi). Based on this, we were also interested in monitoring other ergoline (lysergic acid) derivatives, such as methyergometrine, lysergic acid methylpropylamide (LAMPA) and lysergic acid diethylamide (LSD) for their potencies to stimulate $[Ca^{2+}]_i$ oscillations in MIN6 cells. Even though showing only minor structural differences, tested derivatives were significantly distinct in their potencies to stimulate $[Ca^{2+}]_i$ oscillations (Fig. A7 (appendix)). Whereas LSD and methyergometrine did not show effects on $[Ca^{2+}]_i$ oscillations in the majority of MIN6 cells, addition of LAMPA to pre-washed MIN6 cells induced a prominent $[Ca^{2+}]_i$ transient that was followed by continuous $[Ca^{2+}]_i$ oscillations (Fig. A7 (appendix)). In fact, a low receptor activation potency of LSD on TAAR1 was described (EC_{50}(LSD): 9.7 µM (physiologically relevant TAAR1 activation: EC_{50} < 5 µM), [241]). In line with previous observations, these findings also show that minor structural differences amongst psychoactive drugs might significantly impact the activation potencies of compounds on TAAR1.

Already Bunzow *et al.* connected the structural similarities between *β*-PEA and (meth-)amphetamine with their stimulatory potential on TAAR1 [133]. We found that addition of amphetamine to pre-washed MIN6 cells immediately evoked pronounced $[Ca^{2+}]_i$ oscillations (Fig. 11 Ai+ii(4), Bxv). The potency of amphetamine to stimulate high-intensity $[Ca^{2+}]_i$ oscillations was comparable to that of *β*-PEA and of the antidepressants dibenzepin and idazoxan (~400 counts/min in 100 MIN6 cells) (Fig. 11 Bi, iii and Fig. 10 Bi). This is in line with literature reports on the TAAR1 activation potencies of amphetamine and *β*-PEA [241]. Amphetamine increased insulin levels ~1.4-fold from MIN6 cells (Fig. 12 A). Notably, it was reported that administration of amphetamine results in a rapid increase of immunoassayable plasma insulin in mice and rats, even though the mechanisms have been unclear, so far [246]. Interestingly, early studies on rodents hypothesized that methamphetamine stimulates insulin release by a neural mechanism within the pancreas [246]. Based on our data on $[Ca^{2+}]_i$ oscillations and insulin secretion, we propose amphetamine-mediated stimulation of TAAR1 within *β*-cells as a mechanism for reported effects on blood insulin levels [133].

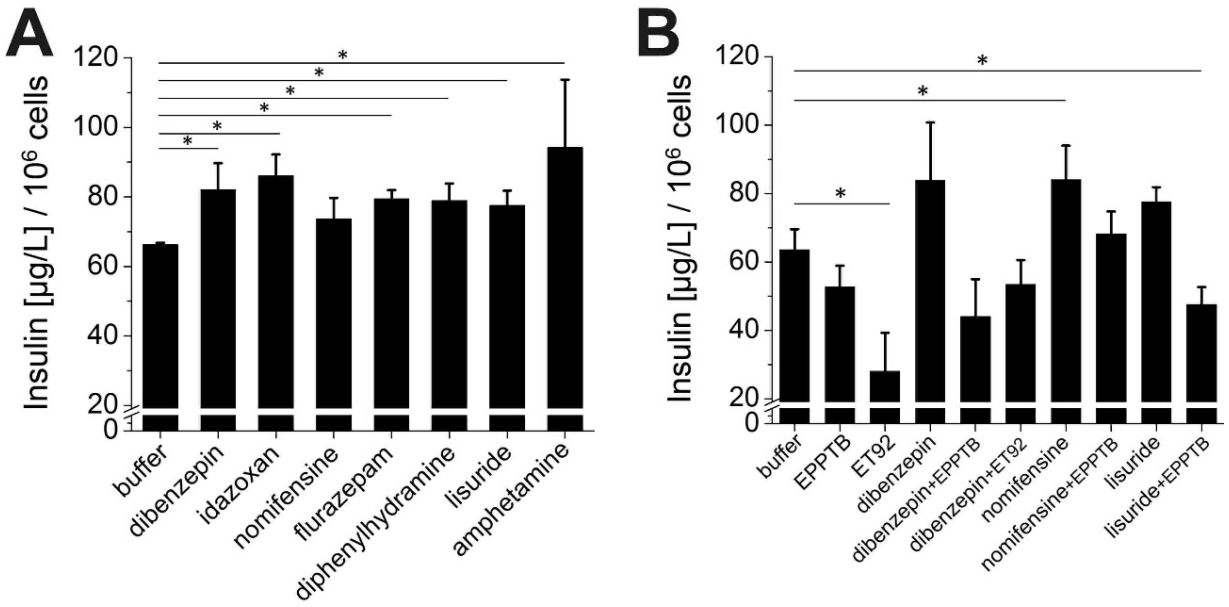

Figure 12. Psychotropic drugs stimulate insulin secretion from MIN6 cells via TAAR1. **(A)** Psychotropic drugs, applied in 25 µM final concentrations, increased insulin secretion from MIN6 cells ~1.1 to 1.4-fold, compared to buffer levels. **(B)** The selective TAAR1 antagonists EPPTB and ET-92 suppressed insulin secretion from glucose-stimulated MIN6 cells below buffer levels. Also, insulin secretion from MIN6 cells that were pre-stimulated by psychotropic drugs was reduced by the addition of TAAR1 antagonists partly even below buffer levels. Insulin experiments were performed in the presence of 11 mM glucose in quadruplicate (*P<0.05 and **P<0.01, all unmarked events were not statistically significant = P>0.05. ANOVA, with repeated measures as necessary). Error bars present SD.

Based on structural similarities with tryptamine, we even expected the psychoactive alkaloid psilocin to stimulate $[Ca^{2+}]_i$ oscillations in pre-washed MIN6 cells via TAAR1. In fact, psilocin has been described to show agonistic activity on TAAR1 [156,241]. Addition of psilocin (25 µM) to pre-washed MIN6 cells instantaneously evoked $[Ca^{2+}]_i$ oscillations that were reduced by the addition of EPPTB (Fig. A8 (appendix)). However, addition of the structural isomer bufotenin (25 µM) to pre-washed MIN6 cells induced a single prominent $[Ca^{2+}]_i$ transient that was not followed by continuous $[Ca^{2+}]_i$ oscillations (Fig. A8, D i+ii (appendix)).

Upon addition to pre-washed mouse primary *β*-cells, dibenzepin, flurazepam and nomifensine (10 µM) evoked strong $[Ca^{2+}]_i$ oscillations in the presence of 5 mM glucose (Fig. 13 A). Also, addition of dibenzepin increased insulin secretion from mouse primary *β*-cells (Fig. 13 B, 25 µM dibenzepin, 5 mM glucose) or INS-1 cells (Fig. 13 C, 100 µM dibenzepin, 11 mM glucose). Addition of ET-92, following stimulation by dibenzepin (25 µM, each) suppressed insulin secretion from mouse primary *β*-cells below buffer levels (Fig. 13 B), thereby confirming our findings from MIN6 cells experiments.

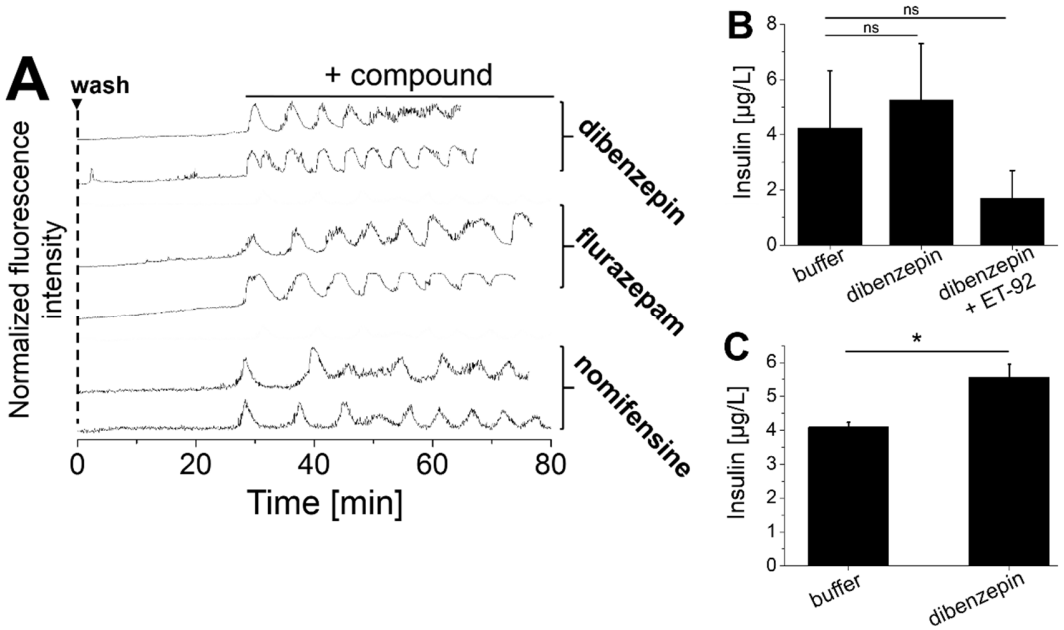

Figure 13. Psychotropic drugs stimulate $[Ca^{2+}]_i$ oscillations and insulin secretion of mouse primary *β*-cells and INS-1 cells. (A) Representative Ca^{2+} traces from single mouse primary *β*-cells, recorded with the Ca^{2+} indicator Fluo-4. Addition of psychotropic drugs (10 µM) to pre-washed mouse primary *β*-cells induced $[Ca^{2+}]_i$ oscillations in the presence of 5 mM glucose. **(B)** Dibenzepin (25 µM) non-significantly increased insulin secretion from mouse primary *β*-cells. ET-92 (25 µM), suppressed dibenzepin-stimulated insulin secretion even below buffer levels. **(C)** Dibenzepin (100 µM) stimulated insulin secretion from INS-1 cells. Experiments on mouse primary *β*-cells (INS-1 cells) were performed at 5 mM (11 mM) glucose in triplicate (quadruplicate) (ns = not significant = P>0.05. *P<0.05, ANOVA, with repeated measures as necessary). Error bars present SD. Experiments were performed together with J. Rada.

3.2.3. Manipulation of TA biochemical pathways modulates endogenous TA levels, $[Ca^{2+}]_i$ oscillations and insulin secretion

TA biosynthetic pathways have been described in neuronal tissue, where β-PEA, tyramine and tryptamine are generated by AADC from precursor amino acids in a rate-limiting decarboxylation step [247]. Whereas all TAs are metabolized by both isoforms of MAO(-A/-B), β-PEA is primarily converted by MAO-B [126,168,169].

We turned to mass spectrometry (MS) to identify and (absolutely) quantify TA levels in MIN6 cells. For this, the SN of MIN6 cells was harvested, dried and combined with scraped MIN6 cells for MeOH / HCl-based extraction in the presence of stable heavy isotope-labeled internal standards (hISDs, Fig. A9 (appendix), for details on the extraction protocol see chapter 6.6. Extraction and MS analysis of TAs). This would reveal TAs as endogenous (autocrine) agonists of TAAR1 in MIN6 cells.

MS analysis of SNs identified a variety of primary amines, including the main TAs β-PEA, tyramine, tryptamine and synephrine (Fig. 14 A). TAs were detected in nanogram amounts, based on hISDs that were spiked to SNs in defined amounts before extraction (Fig. 14 A and A9 (appendix)). Tyramine and β-PEA were detected in highest amounts, followed by tryptamine and synephrine (Fig. 14 A). Thereby, MS revealed that TAAR1 within MIN6 cells is stimulated by a cocktail of endogenous TAs rather than by a single amine. Notably, tyramine and β-PEA – the most abundant TAs identified in our MS screen – most potently evoked $[Ca^{2+}]_i$ oscillations, when added to pre-washed MIN6 cells (Fig. 9 B i+ii). Octopamine was not detected in this screen.

In order to retrace TA biosynthetic pathways via MS, MIN6 cells were subcultured in the presence of stable isotope-labeled canonical amino acids ^{15}N-phenylalanine, -tyrosine and -tryptophan (Fig. A10 (appendix)). Remarkably, we detected heavy isotope-labeled TAs from cells (scraped MIN6 cells and SN combined), which were likely generated in an AADC-mediated decarboxylation step from heavy labeled amino acids (Fig. 14 Bi+ii). Thereby, we identified TAs as endogenous (autocrine) ligands of TAAR1 that are produced within MIN6 cells.

In order to understand the biosynthetic pathways of TAs in MIN6 cells, as well as the role of endogenous TAs for the regulation of MIN6 cell activity, we inhibited key metabolic enzymes of cellular TA biosynthesis and degradation pathways to manipulate endogenous TA levels. For this, we applied selective inhibitors of endogenous MAO-A/-B and AADC to MIN6 cells that were cultured in the presence of ^{15}N-phenylalanine, while monitoring the levels of ^{15}N-β-PEA via MS.

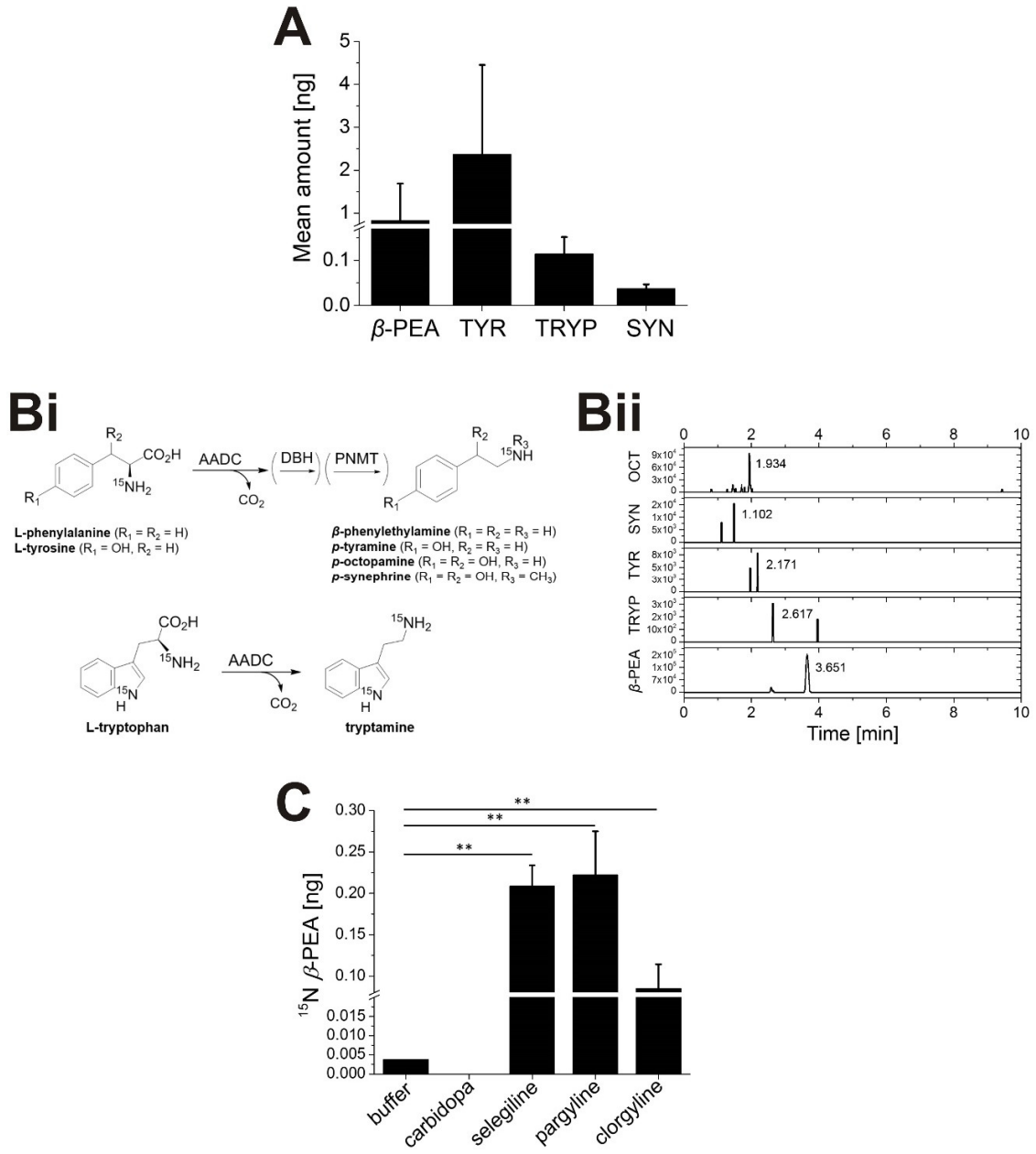

Figure 14. MS-based quantification of TA levels in MIN6 cells. (A) Absolute amounts of TAs, as determined by MS. **(Bi)** Detection of heavy-labeled TAs from MIN6 cells, cultured in medium that was supplemented with ^{15}N-phenylalanine, ^{15}N-tyrosine or ^{15}N-tryptophan **(Bii)**. **(C)** Mean absolute amounts of ^{15}N-β-PEA in MIN6 cells (scraped cells + SN) significantly increased in the presence of MAO inhibitors (selegiline, pargyline, clorgyline). Inhibition of AADC reduced levels of ^{15}N-β-PEA below the detection limit. Experiments were performed in quadruplicate. Error bars represent SD. *p<0.05 and **p<0.01, ANOVA all unmarked events were not statistically significant. LC-MS analysis was performed on a ThermoFisher Q-exactive MS, Waters UPLC (EVO C18 (100x2.1 mm; 2.6 µm) column). For experimental details see chapter 6.6. Extraction and MS analysis of TAs. Amines were detected in separate ion scans. TYR: tyramine, TRYP: tryptamine, SYN: synephrine, OCT: octopamine, DBH: Dopamine β-hydroxylase, PNMT: Phenylethanolamine *N*-methyltransferase. Extractions, MS experiments and data analysis were planned and performed together with K. Keutler.

We applied selective inhibitors of MAO-B (selegiline, pargyline, rasagiline, Ro 16-6491) and MAO-A (clorgyline) or non-selective inhibitors for both MAO isoforms (tranylcypromine, phenelzine) [248]. AACD was inhibited by S-(-)-carbidopa and benserazide [249]. Herein tested inhibitors are partly commonly prescribed drugs for the modulation of brain biogenic amine levels of patients suffering from neurological disorders. MS showed that levels of ^{15}N-β-PEA significantly increased in the presence of the MAO-inhibitors. Notably, selective inhibitors of MAO-B yielded significantly higher levels of ^{15}N-β-PEA (selegiline (~55-fold), pargyline (~59-fold)), compared to either MAO-A inhibition (clorgyline (~22-fold)) or to non-treated MIN6 cells (Fig. 14 C). This is in line with literature, reporting that β-PEA is primarily converted by the MAO-B isoform [126,168,169]. Inhibition of AADC by S-(-)-carbidopa reduced ^{15}N-β-PEA levels below the detection limit of MS (Fig. 14 C).

To investigate the role of endogenous TAs as potential autocrine signaling factors for $[Ca^{2+}]_i$ oscillations and insulin secretion, recombinant MAO-B was added to glucose-stimulated MIN6 cells. Not penetrating the PM of live cells, recombinant MAO-B was supposed to inactivate TAs in the extracellular space of MIN6 cells. In the presence of MAO-B, $[Ca^{2+}]_i$ oscillations gradually decreased (Fig. 15 A+B i), indicating that enzymatic inactivation of extracellular TA-pools directly affected cellular activity. From this we inferred that endogenous TAs are essential (autocrine) signaling factors for the maintenance of $[Ca^{2+}]_i$ oscillations within MIN6 cells, which is also in line with our initial hypothesis.

In a next step, it should be investigated whether the pharmacological modulation of endogenous TA levels translated into $[Ca^{2+}]_i$ oscillations and insulin secretion. Addition of MAO inhibitors to pre-washed MIN6 cells started $[Ca^{2+}]_i$ oscillations and significantly increased insulin secretion, compared to buffer levels, regardless of their mechanism of action or specificity towards MAO-A or -B. Evoking high-intensity $[Ca^{2+}]_i$ oscillations, the MAO inhibitors selegiline, tranylcypromine, Ro 16-6491, phenelzine and clorgyline (~400 - 600 counts/min in 100 MIN6, Fig. 15 B ii, iii, v, viii) were even more potent than β-PEA or the selective synthetic TAAR1 agonists RO5256390 and RO5166017 (Fig. 7). Pargyline and rasagiline (~200 - 300 counts/min in 100 MIN6, Fig. 15 B vi, vii) were less potent than tested TAAR1 agonists. Compared to buffer levels, insulin secretion increased ~3 to 4-fold in the presence of selegiline, tranylcypromine, phenelzine and clorgyline. Pargyline and rasagiline potentiated insulin secretion ~1.5-fold (25 µM, Fig. 15 C). The potentiation of $[Ca^{2+}]_i$ oscillations and insulin secretion following inhibition of key metabolic enzymes is in line with increased levels of TAs that were detected in MS screens.

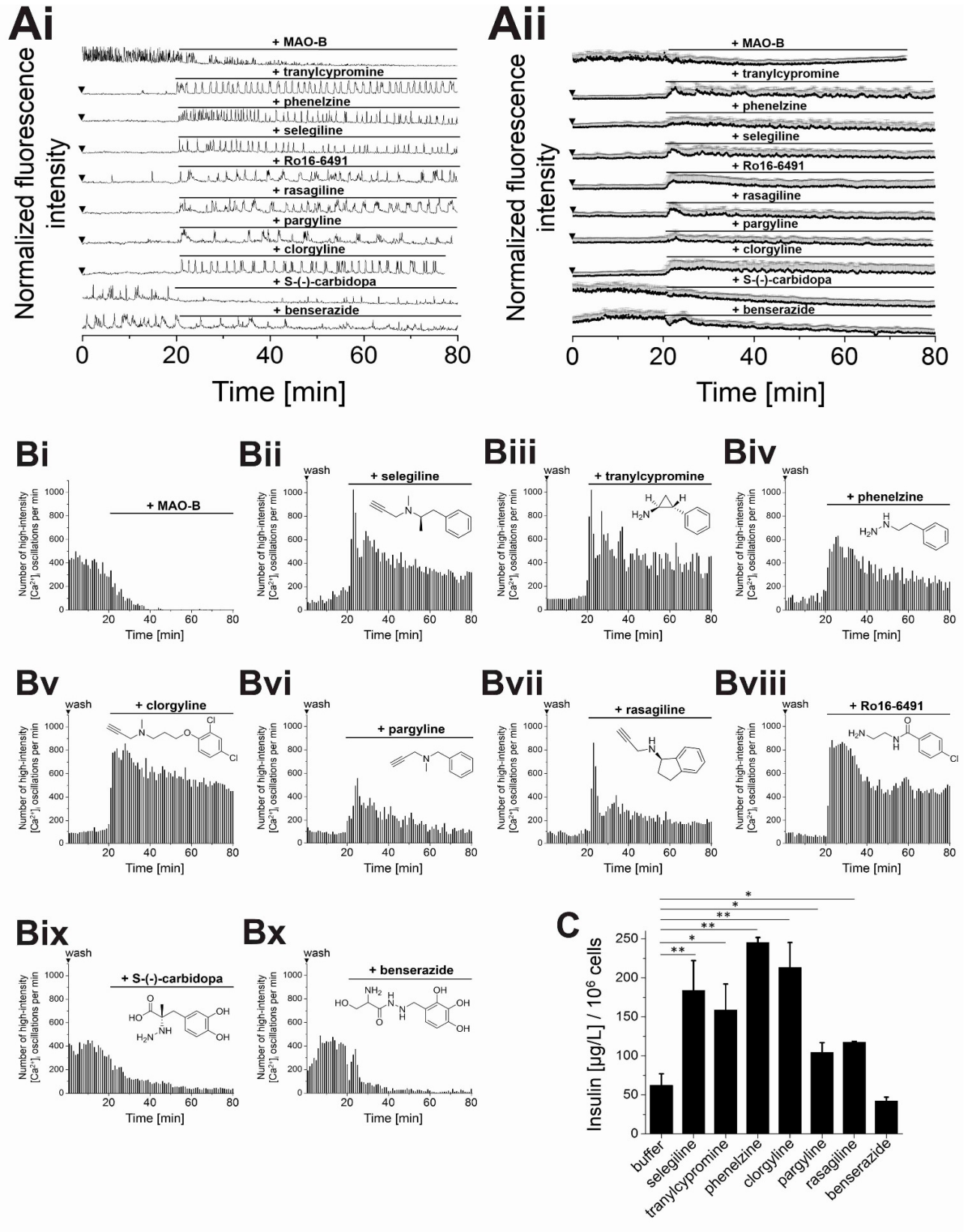
Ai
Normalized fluorescence intensity
+ MAO-B
+ tranylcypromine
+ phenelzine
+ selegiline
+ Ro16-6491
+ rasagiline
+ pargyline
+ clorgyline
+ S-(-)-carbidopa
+ benserazide
Time [min]
Aii
Bi
Bii
Biii
Biv
Bv
Bvi
Bvii
Bviii
Bix
Bx
wash
Number of high-intensity [Ca2+]i oscillations per min
C
Insulin [µg/L] / 10^6 cells
buffer
selegiline
tranylcypromine
phenelzine
clorgyline
pargyline
rasagiline
benserazide

Figure 15. Inhibition of TA biochemical pathways modulates $[Ca^{2+}]_i$ oscillations and insulin secretion of MIN6 cells. (**A**) Representative single **(Ai)** and averaged **(Aii)** Ca^{2+} traces from MIN6 cells, recorded with the Ca^{2+} indicator Fluo-4. (**B**) Counts of high-intensity $[Ca^{2+}]_i$ events per 60 s interval. **(A**, **Bi)** $[Ca^{2+}]_i$ oscillations in glucose stimulated MIN6 cells gradually decreased in the presence of recombinant MAO-B (0.3 U). **(A**, **Bii-viii**, **C)** Inhibition of MAO by selective MAO-A/B inhibitors potentiated $[Ca^{2+}]_i$ oscillations and insulin secretion of pre-washed MIN6 cells. **(A**, **Bix+x**, **C)** AADC inhibitors reduced $[Ca^{2+}]_i$ oscillations and insulin secretion of glucose-stimulated MIN6 cells. MAO-inhibitors were applied at 25 µM, AADC inhibitors at 50 µM in the presence of 11 mM glucose. Shown are averages of 100 MIN6 cells. Insulin experiments were performed in quadruplicate (*P<0.05 and **P<0.01. All unmarked events were not statistically significant = P>0.05. ANOVA, with repeated measures as necessary). Error bars present SD. Washes are indicated by ▼. Imaging and insulin experiments were performed in the presence of 11 mM glucose.

Inhibition of AADC activity by the decarboxylase inhibitor S-(-)-carbidopa has been shown to reduce cellular TA levels (Fig. 14 C and [127]). In line with that, $[Ca^{2+}]_i$ oscillations of glucose-stimulated MIN6 cells decreased after addition of S-(-)-carbidopa or benserazide (50 µM, Fig. 15 A, B ix, x). Benserazide (50 µM) reduced insulin levels ~1.5-fold (Fig. 15 C).

As the modulation of biochemical pathways for the synthesis and degradation of TAs immediately translated into changes of $[Ca^{2+}]_i$ oscillations and insulin secretion, we inferred high metabolic turnover rates of TAs and autocrine feedback. In fact, MAOs have been reported to have high turnover rates, leaving *β*-PEA and tyramine with half-lives of approximately 30 s [126,250–252]. Due to the rapid turnover rate of TAs, extracellular levels of TAs in the nanogram-range were reported [127,166], which is in line with our findings from MS.

Even pre-washed mouse primary *β*-cells responded well to the inhibition of MAO by clorgyline and selegiline (25 µM, 5 mM glucose) with increased $[Ca^{2+}]_i$ oscillations (Fig. 16), confirming our findings from MIN6 cells. Instead, the AADC inhibitor benserazide (10 µM) decreased $[Ca^{2+}]_i$ oscillations in glucose-stimulated mouse primary *β*-cells (Fig. 16). Based on MS and imaging data, we inferred that TAs function as essential autocrine signaling factors of *β*-cells.

In a next step, we aimed at selectively withdrawing TAs from MIN6 cells, while monitoring $[Ca^{2+}]_i$ oscillations. For this, cyclodextrins (CDs) were applied to glucose-stimulated MIN6 cells. CDs are cyclic oligosaccharides with a hydrophilic outside and a hydrophobic interior. They are commonly used to increase the solubility of hydrophobic small molecules, trapping them within their non-polar cavity [253].

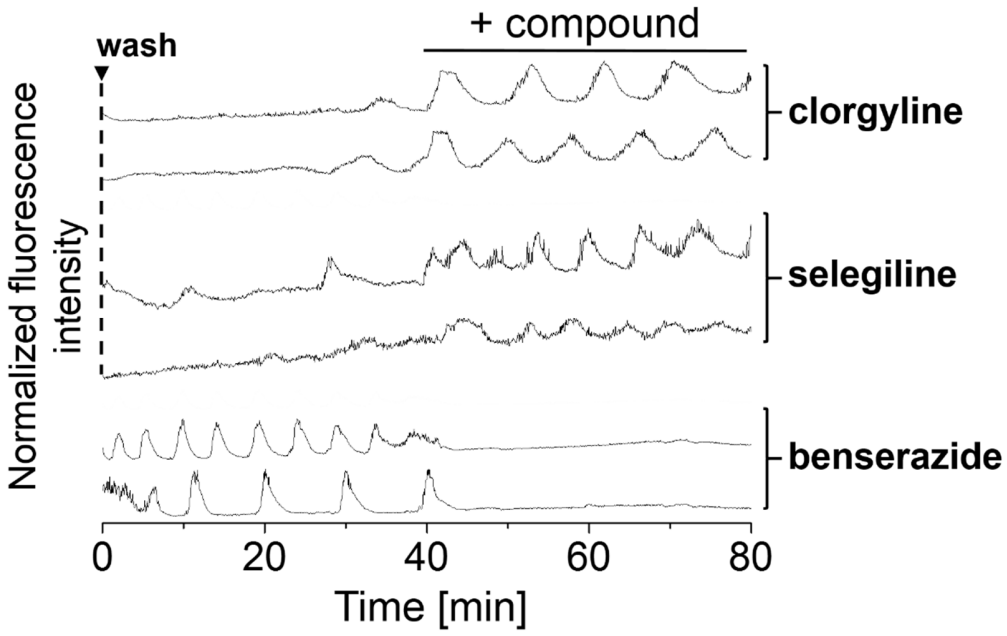

Figure 16. Manipulation of TA biochemical pathways modulates $[Ca^{2+}]_i$ oscillations in mouse primary *β*-cells. Representative Ca^{2+} traces from isolated mouse primary *β*-cells, recorded with the Ca^{2+} indicator Fluo-4. Addition of the MAO-inhibitors clorgyline and selegiline (25 µM) induced $[Ca^{2+}]_i$ oscillations in pre-washed isolated mouse primary *β*-cells. The AADC inhibitor benserazide (10 µM) reduced $[Ca^{2+}]_i$ oscillations in glucose-stimulated isolated mouse primary *β*-cells. Experiments were performed in the presence of 5 mM glucose together with J. Rada.

A *β*-CD-based approach for the removal of aromatic amines from aqueous solutions was previously described [254], suggesting *β*-CD ideal for capturing TAs from MIN6 cells. Derivatization of CDs (*e.g.* with hydroxyl groups) improves the overall water solubility of *β*-CD [253]. Therefore, we applied hydroxypropyl *β*-CD (hp*β*-CD) to MIN6 cells and observed transient reduction of $[Ca^{2+}]_i$ oscillations.

$[Ca^{2+}]_i$ oscillations spontaneously recovered (Fig. 17), presumably after saturation of hp*β*-CD with TAs that were replenished by cellular biosynthesis. Based on the time point of recovery following the addition of hp*β*-CD, MIN6 cells were grouped into three populations: Late (~20 min), intermediate (~10 min) and early (~5 min) restarters (Fig. 17 Ai+ii(1-3)). Hydroxylpropyl *α*-CD (hp*α*-CD), bearing a hydrophobic cavity too small to bind aromatic amines [253], did not show effects on $[Ca^{2+}]_i$ oscillations and served as a control (Fig. 17 Ai+ii(4), C).

In line with our observations of recombinant MAO action on MIN6 cells, this indicated that the presence of aromatic amines is essential for the maintenance of $[Ca^{2+}]_i$ oscillations. However, as

CDs significantly interfered with insulin ELISA measurements, their effects on insulin secretion could not be determined.

β-CDs and derivatives thereof are described to remove cholesterol from plasma membranes at concentrations of 5 - 20 mM, which is ~2 - 3 orders of magnitude higher compared to the herein applied concentrations [255,256]. Therefore, we assume that the cholesterol content of PMs was not affected.

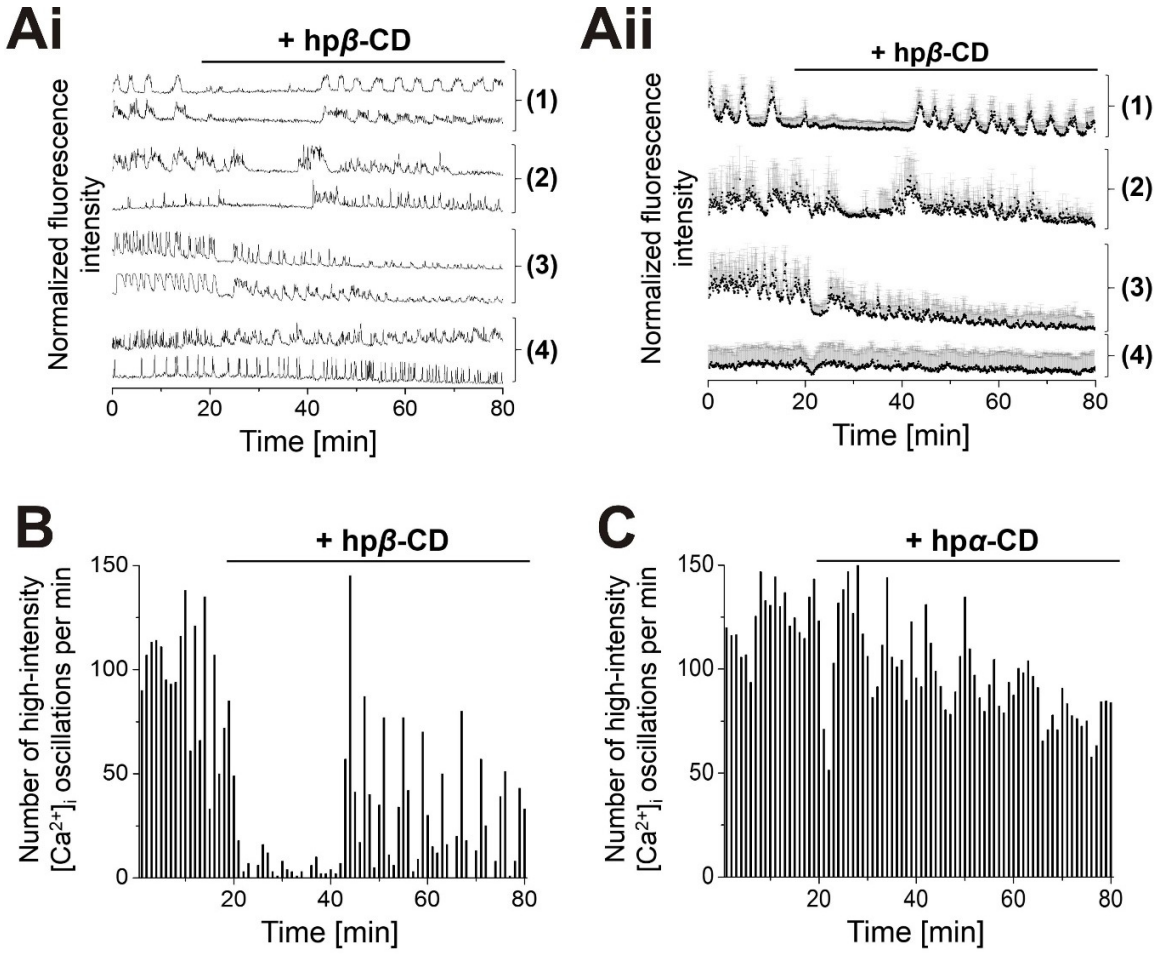

Figure 17. Addition of hp*β*-CD to MIN6 cells transiently reduces $[Ca^{2+}]_i$ oscillations. Representative single **(Ai)** and averaged **(Aii)** Ca^{2+} traces from MIN6 cells, recorded with the Ca^{2+} indicator Fluo-4. (**B+C**) Counts of detected high-intensity $[Ca^{2+}]_i$ events per 60 s interval. (**A(1-3)**) Addition of hp*β*-CD (200 µM) to MIN6 cells transiently reduced $[Ca^{2+}]_i$ oscillations. MIN6 cells were grouped into three populations, depending on the time of recovery after addition of hp*β*-CD: late **(A(1), B)**, intermediate **(A(2))** and early **(A(3))** restarters. **(A(4), C)** hpα-CD, 200 µM served as a control. Shown are averages of 100 MIN6 cells.

3.2.4. TAAR1 (ant-)agonists modulate intracellular cAMP levels

TAAR1 couples to a $G_{\alpha s}$ protein that modulates adenylate cyclase activity [132,133]. Therefore, (ant-)agonism of TAAR1 directly translates into changes of intracellular cAMP levels, which has been exploited as a sensitive read-out in drug screens [136,159,161]. For the determination of cellular cAMP levels after TAAR1 stimulation, several techniques, such as a modified β-lactamase reporter assay [138] or a bioluminescence resonance energy transfer cAMP biosensor [135] have been reported. To monitor downstream signaling of TAAR1 in MIN6 cells, we applied a genetically encoded cytoplasmic cAMP sensor of the 'Epac series', sensing changes of [cAMP] in physiological ranges. Activated by cAMP, the endogenous cellular protein Epac1 acts as a guanine nucleotide exchange factor for Rap1 [257]. The herein applied sensor consists of a truncated version of Epac1, equipped with two Venus fluorescent proteins at the N-terminus (acceptor) and one mTurquoise fluorescent protein at the C-terminus (donor) (Epac, 3rd generation, [258]). Binding of cAMP induces a conformational change that increases the distance between the donor and acceptor fluorophore, leading to a robust decrease of the FRET ratio (Fig. 18 N). FRET values are presented as ratios between acceptor and donor intensities. Presented FRET ratios were set to 1 at the time point immediately before addition of the stimulus. At the end of each experiment, a mix of the adenylate cyclase activator forskolin [259] and the phosphodiesterase inhibitor 3-isobutyl-1-methylxanthine (IBMX) [260] (50 µM, each) was added to MIN6 cells to generate maximum cAMP responses and to confirm that measurements were performed within the dynamic range of the sensor.

For testing cAMP responses, (synthetic) TAAR1 agonists, psychoactive drugs and MAO inhibitors (antiparkinsonian drugs) were applied at 25 µM, as this concentration was found to induce stable $[Ca^{2+}]_i$ responses in MIN6 cells. Addition of β-PEA to Epac^{3rd}-transfected MIN6 cells significantly potentiated cAMP production, as indicated by a significant shift of the normalized FRET ratio (acceptor/donor intensity, Fig. 18 A). Remarkably, this shift could be reversed by the addition of the TAAR1 antagonist EPPTB (Fig. 18 B), which confirms our observations from $[Ca^{2+}]_i$ imaging. Effects of β-PEA on cAMP levels were approximately 1.5 - 2x stronger than those of tyramine (Fig. 18 C), which is in line with literature reports, comparing the receptor activation potencies (EC_{50}s) of TAs. [241]. Even selective synthetic TAAR1 agonists stimulated cAMP production to different extents. However, the partial agonist RO5073012 only transiently stimulated cAMP production that spontaneously declined again (Fig. 18 D).

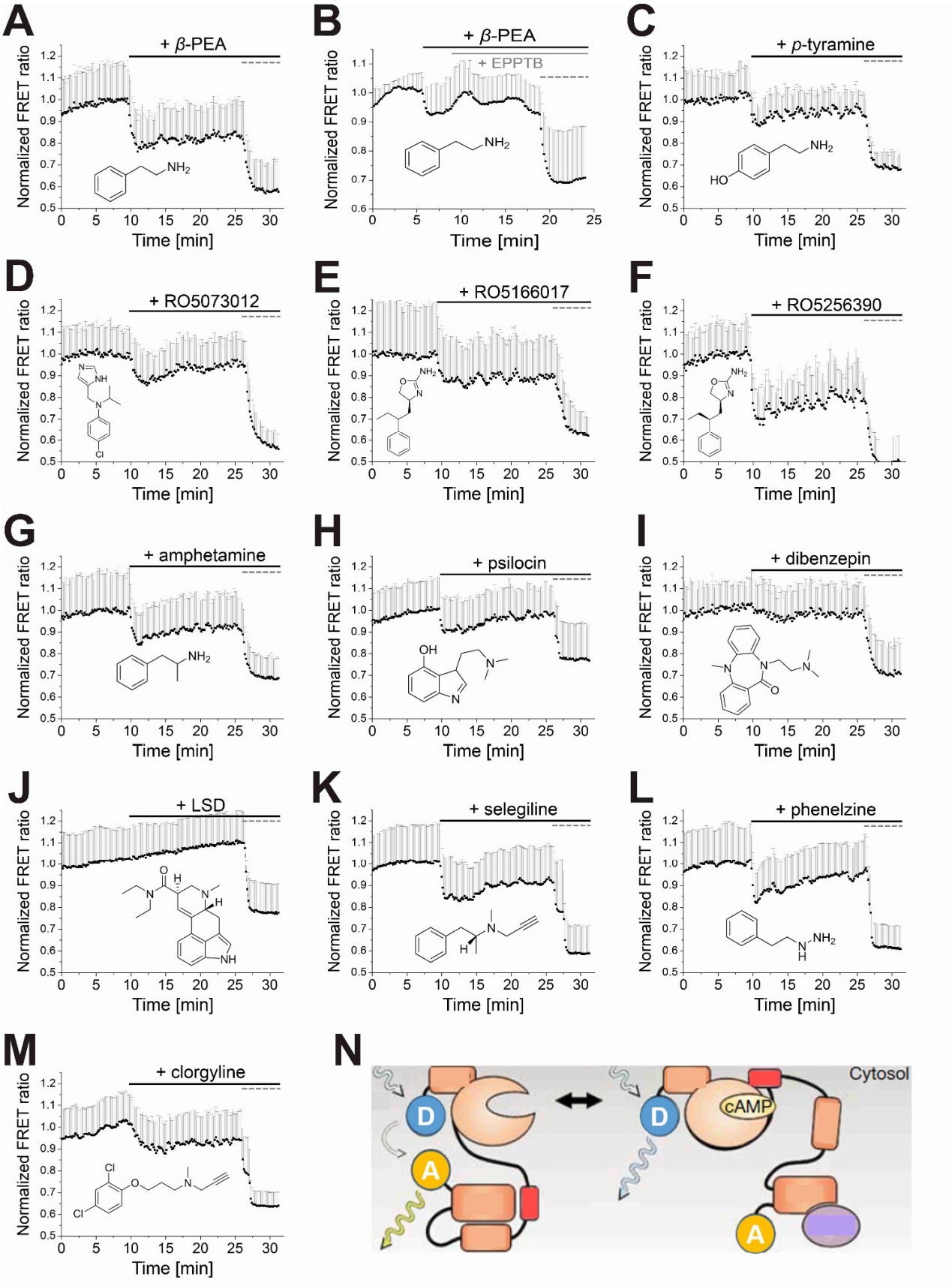
A
+ β-PEA
B
+ β-PEA
+ EPPTB
C
+ p-tyramine
D
+ RO5073012
E
+ RO5166017
F
+ RO5256390
G
+ amphetamine
H
+ psilocin
I
+ dibenzepin
J
+ LSD
K
+ selegiline
L
+ phenelzine
M
+ clorgyline
Normalized FRET ratio
Time [min]
N
Cytosol
D
A
cAMP

Figure 18. TAAR1 agonists modulate intracellular cAMP levels in MIN6 cells. Shown are normalized FRET ratios (acceptor/donor intensity) of the Epac sensor [258]. Tested compounds included **(A-C)** TAs, **(D-F)** synthetic TAAR1 agonists, **(G-J)** psychotropic drugs and **(K-M)** MAO inhibitors (antiparkinsonian drugs). *β*-PEA **(A)** and RO5256390 **(F)** evoked the strongest effects. **(N)** Epac^{3rd}-based sensor for the determination of cAMP levels. A truncated version of Epac1 was equipped with two Venus fluorescent proteins at the N-terminus (acceptor, A) and one mTurquoise at the C-terminus (donor, D). Binding of cAMP induces a conformational change that increases the distance between donor and acceptor, leading to a robust decrease of the FRET ratio. Adapted and modified from [261]. All compounds were applied at 25 µM in the presence of 11 mM glucose. A mix of forskolin and IBMX (50 µM, each) was added to cells at the end of each experiment to induce maximum cAMP responses (dashed grey line). Shown are averages of 20 - 30 MIN6 cells. Experiments and data analysis were planned and performed with J. Rada and M. Andreu.

RO5073012 was found significantly less potent, compared to the full agonists RO5166017 and RO5256390 that permanently increased cAMP levels even to greater extents (Fig. 18 E, F). Effects of RO5256390 were ~2 - 3 times stronger than those of RO5166017 or tyramine. From all TAAR1 agonists tested, RO5256390 showed the strongest effects on cAMP production (Fig. 18 F), directly followed by *β*-PEA (Fig. 18 A). This rank order of potency of artificial (synthetic) TAAR1 agonists is in line with our findings from $[Ca^{2+}]_i$ measurements and literature reports, as compiled in a review by Berry *et al.* [160]. In line with reports by Revel *et al.*, effects of RO5256390 and RO5166017 on cellular cAMP levels were comparable to that evoked by *β*-PEA [151,154]. Amphetamine and psilocin showed potencies for the stimulation of cAMP production that were comparable to those of *p*-tyramine or RO5166017 (Fig. 18 G, H).

Only weak or no effects on cAMP levels were evoked by dibenzepin and LSD (Fig. 18 I, J). In fact, LSD did not show significant effects on $[Ca^{2+}]_i$ oscillations (Fig. A7 (appendix)), in line with literature reports, describing its comparatively low receptor activation potency (EC_{50} (LSD): 9.7 µM) [241].

We hypothesized that inhibition of endogenous MAO would induce cAMP production via TAAR1 stimulation by increased levels of endogenous TAs. In fact, addition of the selective MAO-B inhibitors (and antiparkinsonian agents) selegiline and phenelzine to MIN6 cells potently increased cAMP levels in ranges that were comparable to *β*-PEA stimulation (Fig. 18 K, L). Notably, *β*-PEA is primarily inactivated by MAO-B [126,168,169]. Effects of the selective MAO-A inhibitor clorgyline were significantly weaker (Fig. 18 M). Interestingly, addition of some TAAR1 agonists even induced oscillations of cAMP levels (Fig. 18 C, E, F, G).

Remarkably, application of the phosphodiesterase inhibitor IBMX to glucose-stimulated MIN6 cells in lower doses (25 µM) was found to increase intracellular cAMP levels (Fig. A11 (appendix)). From this we infer that cAMP is produced even under basal stimulatory conditions within MIN6 cells by endogenous agonists. This is in line with our findings from MS, demonstrating the presence of endogenous TAs even under basal stimulatory conditions.

Apart from ATP and TAs, we suspected even other small diffusible cellular metabolites to function as extracellular endogenous (metabolite) signaling factors that are essential for the maintenance of *β*-cell activity and insulin secretion.

3.3. Endogenous FAs are essential signaling factors of pancreatic *β*-cells and insulin secretion

3.3.1. Albumin-mediated buffering of FA levels modulates $[Ca^{2+}]_i$ oscillations and insulin secretion

Preliminary work described the effects of UV-mediated liberation of photo-caged arachidonic acid at different subcellular compartments within MIN6 cells on $[Ca^{2+}]_i$ oscillations and insulin secretion [214]. In a complementary approach, we investigated the role of endogenous FAs for $[Ca^{2+}]_i$ oscillations and insulin secretion of MIN6 and mouse primary *β*-cells. For the selective withdrawal of FAs from *β*-cells, delipidated fatty acid-free bovine serum albumin (FAF-BSA) was applied due to its strong capacity to bind FAs. Albumin has been described to bind long-chain FAs (C16 - C24) at about 2 - 6 sites, depending on the FA chain length [262].

We found that addition of FAF-BSA in 1 % and 0.1 % final concentrations to glucose-stimulated MIN6 and mouse primary *β*-cells immediately terminated $[Ca^{2+}]_i$ oscillations (Fig. 19 A+B i+ii, C+D; for FAF-BSA (1 %) see Fig. A12, (appendix) and movie sections in Fig. A13). Insulin secretion decreased more than 80 % in the presence of 0.1 % FAF-BSA (Fig. 20 H). The impact of FAF-BSA (0.01 %) on $[Ca^{2+}]_i$ oscillations in MIN6 cells was comparatively weak (Fig. A14 (appendix)), indicating a concentration dependent effect of FAF-BSA on $[Ca^{2+}]_i$ oscillations, as described by Hauke *et al.* [232]. Based on these observations, we suspected FAs to be amongst those endogenous signaling factors that are essential for $[Ca^{2+}]_i$ oscillations and insulin secretion.

As the reduction of $[Ca^{2+}]_i$ oscillations was readily reproduced by the addition of fatty acid-free human serum albumin (1 %, FAF-HSA, Fig. A15 (appendix)) or at different glucose concentrations (Fig. A16 (appendix)), we inferred that observed effects neither depended on the source of albumin nor on the applied glucose concentration [232].

Transfer of FAF-BSA (0.1 %), incubated on a population of 2 x10^6 MIN6 cells to pre-washed MIN6 cells, transiently recovered $[Ca^{2+}]_i$ oscillations (Fig. 19 A+B iii, E), as described by Hauke *et al.* [232]. This indicated that the cargo, presumably FAs, that was taken up by FAF-BSA during pre-loading was readily off-loaded again. Accordingly, the intensity of recovered $[Ca^{2+}]_i$ oscillations correlated with the pre-loading time of FAF-BSA on a separate population of MIN6 cells, as well as with applied concentrations of albumin and therefore with the total amount of transferred FAs (Fig. A17 (appendix)) [232].

Replacement of FAF-BSA (0.1 % and 0.01 %) by albumin-free buffer in the perfusion system readily recovered $[Ca^{2+}]_i$ oscillations (Fig. 20 A+B i, C and Fig. A14 (appendix)), whereas slow recovery of $[Ca^{2+}]_i$ oscillations (~20 - 30 min) was observed following the exchange of FAF-BSA (1 %) by buffer (Fig. A12 (appendix)), as described by Hauke *et al.* [232]. Conventional BSA (conv. BSA, *i.e.* BSA saturated by natural FA cargo, see mass spectrometric screen Fig. 22 C), applied to MIN6 and mouse primary β-cells showed significantly milder effects on $[Ca^{2+}]_i$ oscillations, when applied at 1 % and 0.1 % final concentrations (Fig. 20 A+B ii+iii, D+E and Fig. A12 (appendix)) [232].

Pre-saturation of FAF-BSA (0.1 % and 1 %) with the albumin-binders ibuprofen (Ibu) [263] or L-tryptophan (L-Trp) [264] moderated its effects on $[Ca^{2+}]_i$ oscillations of MIN6 and mouse primary β-cells (Fig. 20 A+B iv-vi, F+G and Fig. A12). All this indicated that pre-saturation of BSA lowered its binding capacity for endogenous FAs and thereby weakened its effects on $[Ca^{2+}]_i$ oscillations. Addition of Ibu or L-Trp (400 µM) to MIN6 cells in the presence of FAF-BSA that was pre-loaded on MIN6 cells induced transient $[Ca^{2+}]_i$ spikes (Fig. A18 (appendix)), as shown by Hauke *et al.* [232]. This transient stimulation was interpreted as out-competition of BSA-loaded FAs by albumin binders.

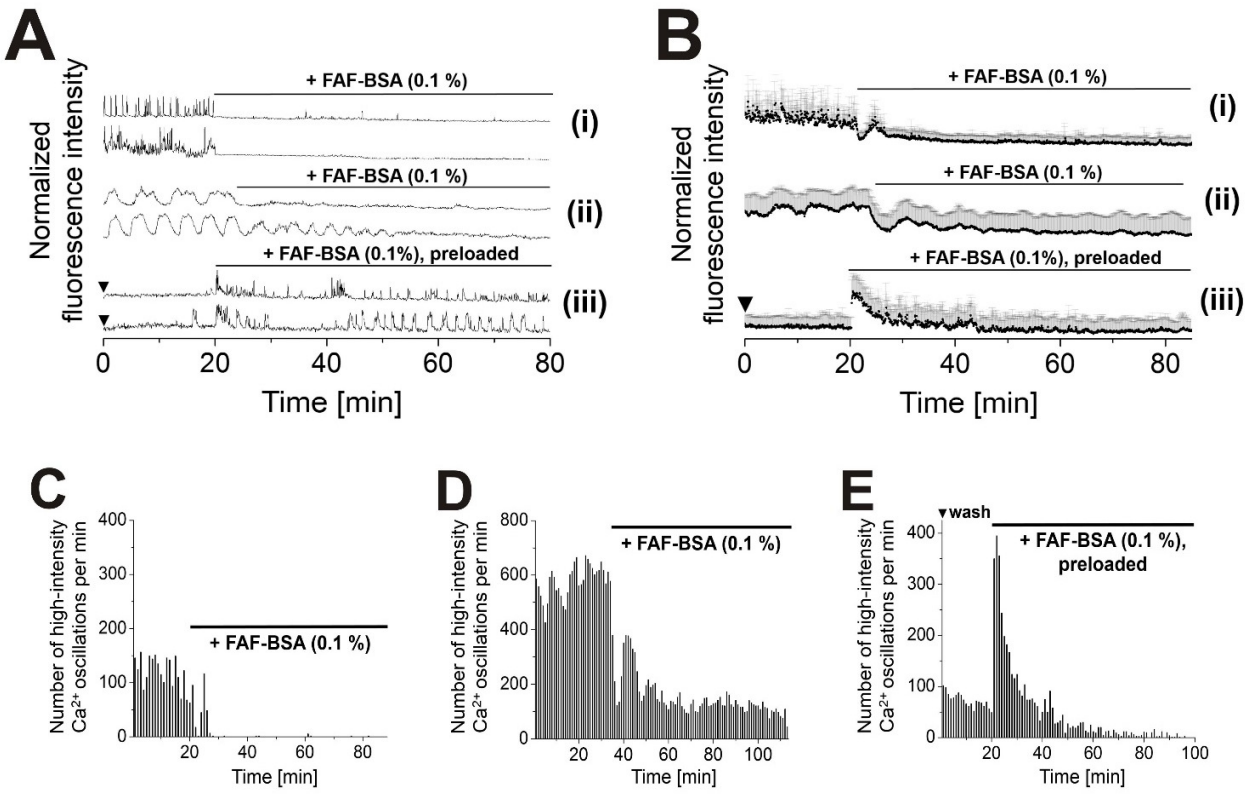

Figure 19. BSA reduces or starts $[Ca^{2+}]_i$ oscillations in MIN6 and mouse primary *β*-cells depending on its FA loading state. (A+B) Representative single **(A)** and averaged **(B)** Ca^{2+} traces from MIN6 and mouse primary *β*-cells, stained with the Ca^{2+} indicator Fluo-4. **(C-E)** Number of high-intensity $[Ca^{2+}]_i$ events per 60 s interval. Addition of FAF-BSA (0.1 %) to MIN6 **(A+B i**, **C)** or mouse primary *β*-cells **(A+B ii**, **D)** immediately reduced $[Ca^{2+}]_i$ oscillations. Transfer of BSA (0.1 %) that was pre-loaded on 2 x10^6 MIN6 cells (pre-loading time: 30 min) to pre-washed MIN6 cells transiently started $[Ca^{2+}]_i$ oscillations **(A+B iii, E)**. Shown are averages of n = 60 mouse primary *β*-cells and n = 30 MIN6 cells. Experiments were performed in the presence of 11 mM glucose. The figure was adapted and modified from Hauke *et al*. [232].

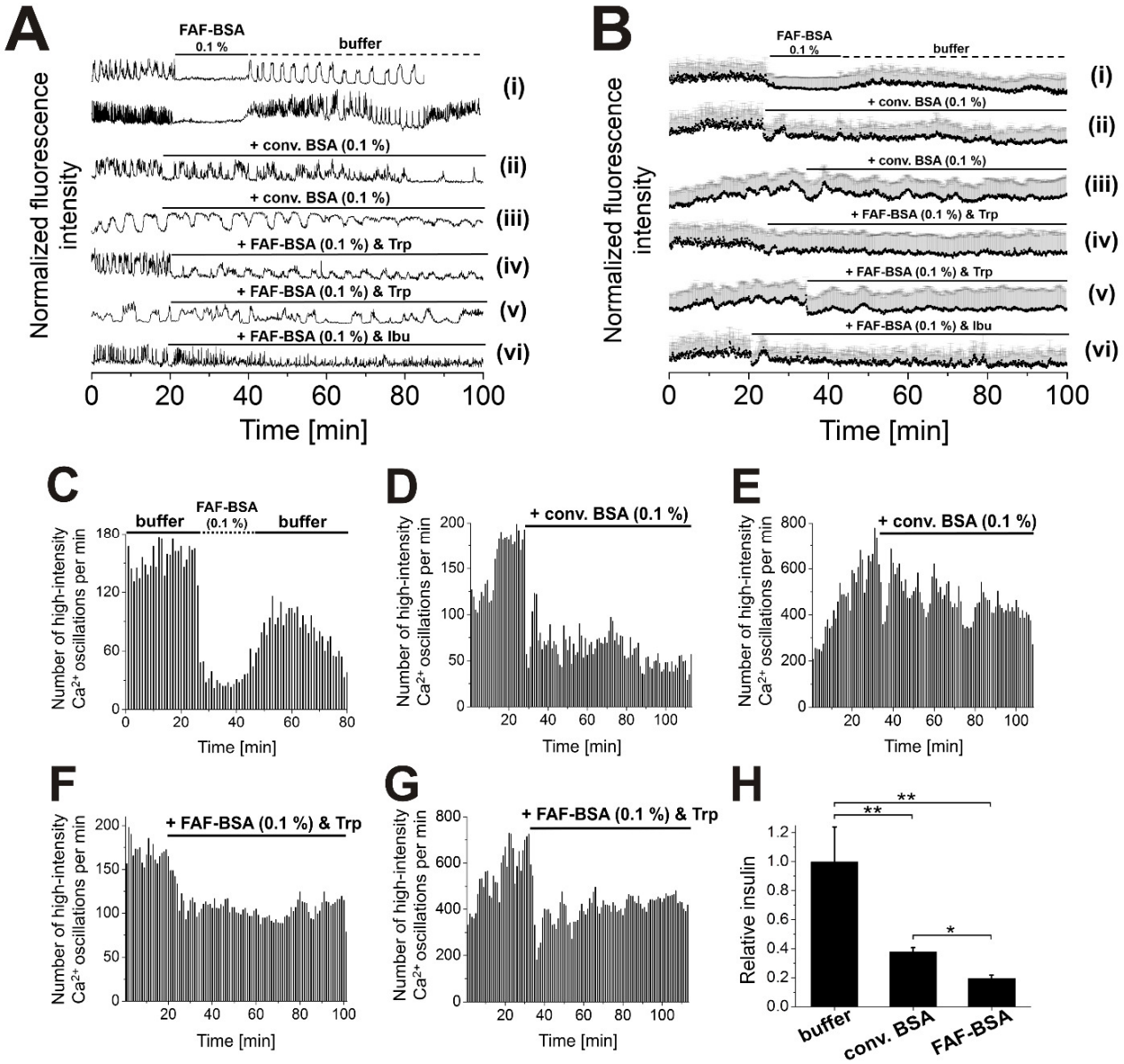

Figure 20. BSA modulates $[Ca^{2+}]_i$ oscillations in MIN6 and mouse primary *β*-cells. (A+B) Representative single **(A)** and averaged **(B)** Ca^{2+} traces from MIN6 and mouse primary *β*-cells, stained with the Ca^{2+} indicator Fluo-4. **(C-G)** Number of high-intensity $[Ca^{2+}]_i$ events per 60 s interval. **(A+B i, C)** MIN6 $[Ca^{2+}]_i$ oscillations immediately stopped upon addition of FAF-BSA (0.1 %) to recover upon exchange of FAF-BSA by buffer. Conv. BSA (0.1 %) or FAF-BSA (0.1 %), pre-saturated with L-Trp or Ibu, reduced, but did not terminate $[Ca^{2+}]_i$ oscillations in **(A+B ii + iv + vi, F)** MIN6 and **(A+B iii + v, G)** mouse primary *β*-cells. **(H)** FAF-BSA (0.1 %, 20 min incubation time) reduced insulin secretion from glucose-stimulated MIN6 cells by more than 80 %, compared to incubation in BSA-free buffer. Shown are averages of n = 60 mouse primary *β*-cells and n = 30 MIN6 cells. Insulin experiments were performed in the presence of 11 mM glucose in quadruplicate (**P<0.01, *P<0.05, ANOVA, ns = not significant = P>0.05, with repeated measures as necessary). Error bars present SD. The set-up of the perfusion system is shown in Fig. A2 (appendix). The figure was adapted from Hauke *et al.* [232].

In order to investigate whether FAs are the major cargo in BSA transfer experiments, the GPR40 antagonist GW1100 (10 µM, [265]) was spiked to FAF-BSA (1 %, pre-loaded on MIN6 cells) and added to pre-washed MIN6 cells. This induces a prominent $[Ca^{2+}]_i$ spike, which was, however, not followed by $[Ca^{2+}]_i$ oscillations (Fig. 21 A+B i, C), as described by Hauke *et al*. [232]. Treating MIN6 cells with GW1100 significantly reduced (10 µM) or terminated (25 µM) $[Ca^{2+}]_i$ oscillations, presumably out-competing endogenous FAs at GPR40 (Fig. 21 A+B iii, E+F and Fig. A19 (appendix)) [232]. All this is in line with reports from Schnell *et al.*, according to which GPR40 activation is essential for the induction and maintenance of $[Ca^{2+}]_i$ oscillations in the presence of glucose [208].

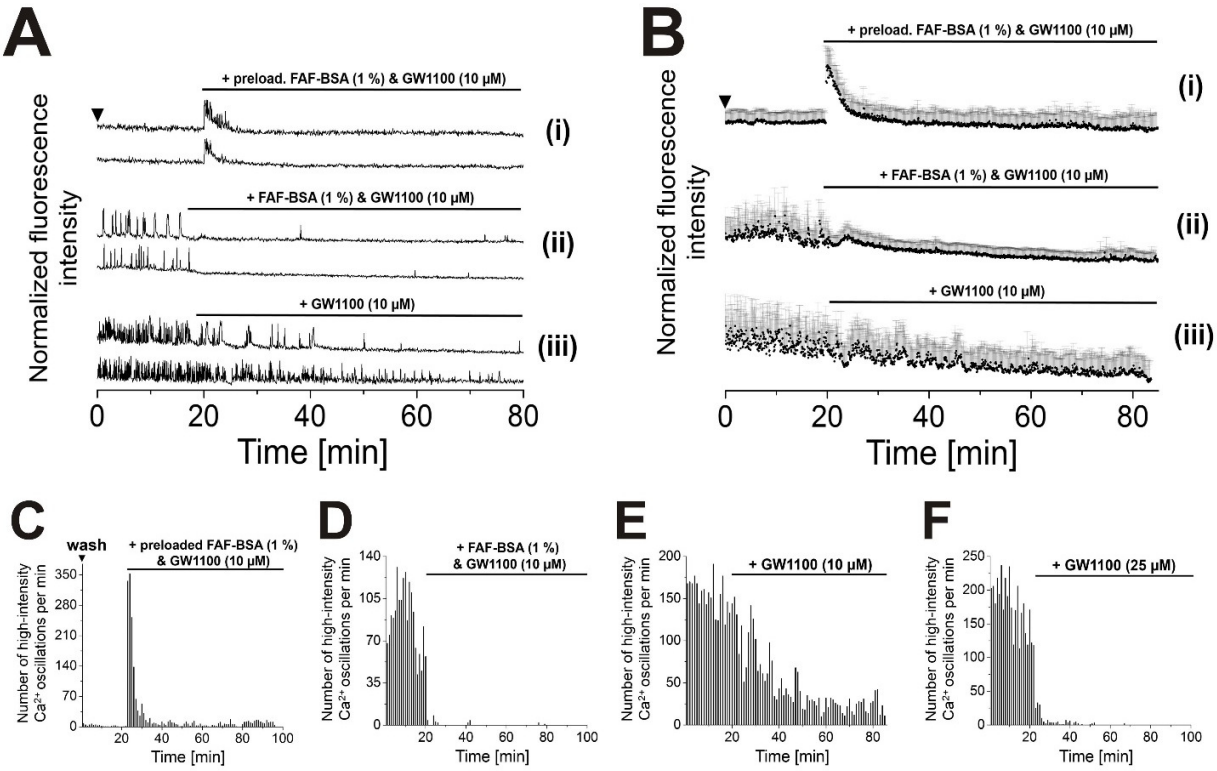

Figure 21. $[Ca^{2+}]_i$ oscillations are stimulated via GPR40 in transfer experiments. Representative single **(A)** and averaged **(B)** Ca^{2+} traces from MIN6 cells, stained with the Ca^{2+} indicator Fluo-4. **(C - F)** Number of high-intensity $[Ca^{2+}]_i$ events per 60 s interval. **(A+B i, C)** FAF-BSA (1 %, pre-loaded on 2 x10^6 MIN6 cells for 30 min) was supplemented with the GPR40 antagonist GW1100 (10 µM). Addition to pre-washed MIN6 cells induced individual prominent $[Ca^{2+}]_i$ transients. **(A+B ii, D)** $[Ca^{2+}]_i$ oscillations immediately stopped after addition of FAF-BSA, spiked with GW1100 (1 %, no pre-loading, GW1100 (10 µM)). **(A+B iii, E)** Addition of GW1100 (10 µM) gradually reduced $[Ca^{2+}]_i$ oscillations. **(F)** Higher concentrations of GW1100 (25 µM) enhanced this effect. Shown are averages of n = 30 MIN6 and n = 60 primary β-cells. See Fig. A19 (appendix) for GW1100 (25 µM) data and for exemplary single Ca^{2+} traces. Experiments were performed in the presence of glucose (11 mM). The figure was adapted from Hauke *et al.* [232].

3.3.2. Monitoring BSA-mediated buffering of FAs from MIN6 cells by mass spectrometry

Following reports on the FA-binding capacity of albumins [266], we traced back FAF-BSA-mediated reduction of $[Ca^{2+}]_i$ oscillations to the withdrawal of FAs from MIN6 cells by BSA. Therefore, mass spectrometry (MS) was applied to monitor the enrichment of FAs by FAF-BSA, following incubation on MIN6 cells. Here, FAF-BSA was applied in 0.1 % final concentration, which was shown to potently reduce $[Ca^{2+}]_i$ oscillations of MIN6 and primary mouse β-cells (Fig. 19). To avoid contamination with palmitic acid, which had previously been reported to cause competing background signal in MS-based detection of FAs, all applied materials were pre-treated with methanol in several steps, according to [267]. FAF-BSA (0.1 %)-supplemented as well as albumin-free SNs were collected after 20 min of incubation on MIN6 cells. The SNs were concentrated more than 10-fold for subsequent chloroform/methanol extraction in advance of MS analysis (see 6. Research design and methods). Palmitic and stearic acid were detected as the most prominent FAs in aqueous SNs (Fig. 22 A) [232].

This is in line with the initial hypothesis of FAs as autocrine signaling factors that β-cells secrete into the extracellular space. FAF-BSA (0.1 %)-containing SNs enriched levels of stearic-, palmitic-, oleic- and elaidic acid 2.7-, 1.2-, 27.3- and 30.6-fold (Fig. 22 A), as described by Hauke *et al.* [232]. Interestingly, the spectrum and relative abundances of FAs, as obtained from FAF-BSA-mediated enrichment, were similar to those of MIN6 cell extracts, where stearic, palmitic, arachidonic, oleic and elaidic acid were most abundant (Fig. 22 B). This confirms the hypothesis that FAF-BSA effectively withdraws FA from MIN6 cells. MS analysis revealed that commercial conv. BSA carried considerable amounts of FAs (Fig. 22 C). The pre-saturation of conv. BSA with FAs explains the weak effects of conv. BSA on $[Ca^{2+}]_i$ oscillations, as observed in imaging experiments (Fig. 20 A+B ii+iii, D, E).

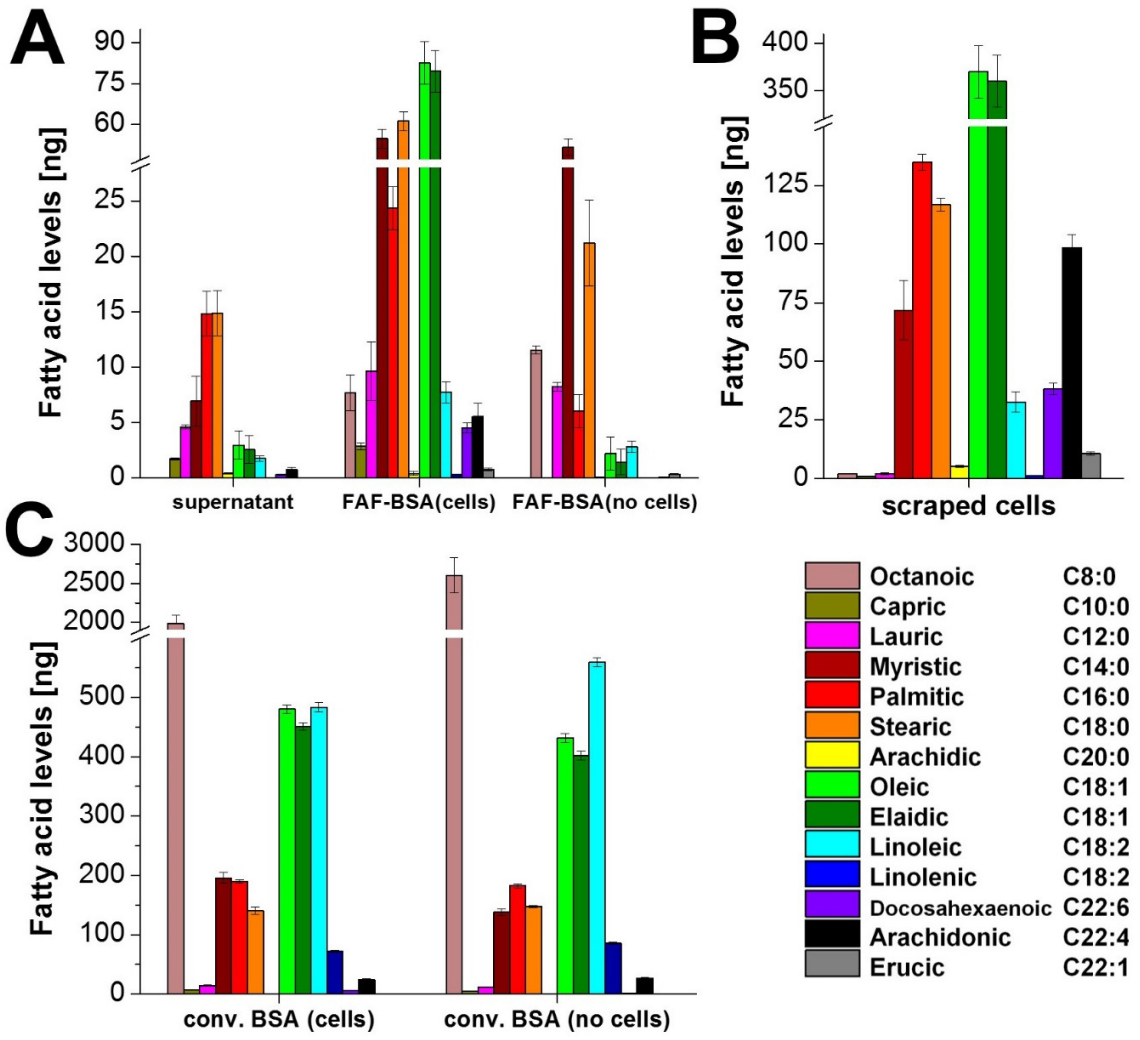

Figure 22. Monitoring FAF-BSA-mediated withdrawal of FAs from MIN6 cells by mass spectromentry. (A) FA levels, detected in the SN of MIN6 cells (**supernatant**), in FAF-BSA (0.1 %), after incubation on MIN6 cells (**FAF-BSA**, **cells**) or in FAF-BSA (0.1 %) without cell contact (**FAF-BSA**, **no cells**). Stearic and palmitic acid were identified as the most abundant FAs in the SN of MIN6 cells (**supernatant**). Oleic, elaidic, stearic and palmitic acid were the most prominent FAs that were enriched by FAF-BSA (0.1 %) from MIN6 cells (**FAF-BSA**, **cells**). **(B)** Levels of FAs, as obtained from MIN6 cell extracts. Oleic, elaidic, arachidonic, palmitic, stearic and myristic acid were detected as the most prominent FAs. **(C)** Conv. BSA contained considerable amounts of FAs, independent of incubation on cells. Experiments were performed on 2 x10^6 MIN6 cells, with 20 min of incubation on cells in the presence of 11 mM glucose. Measurements were done in quadruplicate. Error bars present SD. The figure was adapted from Hauke *et al.* [232].

3.3.3. Fluorescence displacement assay for the detection of secreted FAs

A fluorescence displacement assay was performed for the relative quantification of FA-secretion into aqueous SN of MIN6 cells over incubation time. The assay was based on the environmentally sensitive probe Nile red 2-*O*-butyric acid (NRBA, Fig. 23 A), which preferentially binds hydrophobic protein domains, along with a turn on of fluorescence emission [268]. NRBA fluorescence was detected in the presence of BSA and EtOH, but was quenched in aqueous buffer (Fig. 23 A), as reported by Hauke *et al.* [232]. The emission maximum of NRBA was described to shift to shorter wavelengths with increasing hydrophobicity of its environment [269,270]. Accordingly, the emission maximum, as determined in a solution of EtOH (Fig. 23 A, grey curve), shifted to shorter wavelengths in the presence of BSA (Fig. 23 A) [232]. Various FAF-BSA-to-NRBA ratios were tested – from 1:1 to 4:1 in aqueous buffer. The detected fluorescence intensity decreased with increasing FAF-BSA-to-NRBA ratios (Fig. 23 A) [232].

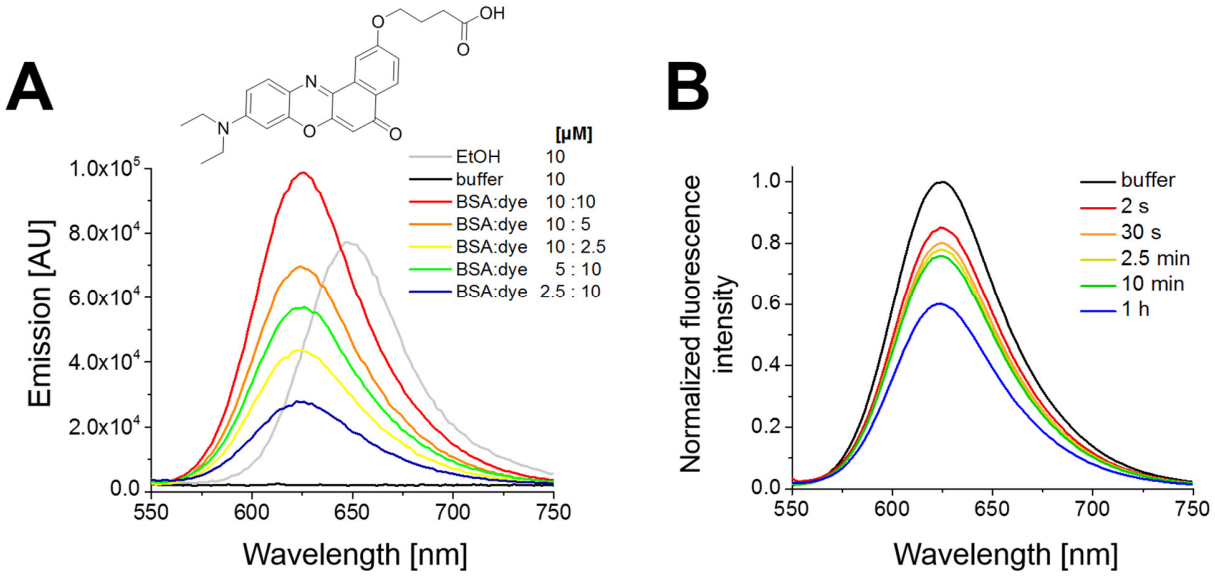

Figure 23. NRBA-based fluorescent displacement assay for the relative quantification of secreted FAs within the SN of MIN6 cells. (A) The NRBA emission maximum as obtained in EtOH (grey trace) shifted to shorter wavelengths in the presence of FAF-BSA (red trace). NRBA fluorescence emission decreased with increasing FAF-BSA-to-NRBA ratios. NRBA fluorescence was quenched in aqueous buffer (black trace). **(B)** FA-containing SN, harvested from MIN6 cells, was added to NRBA-pre-loaded FAF-BSA (10 µM FAF-BSA, NRBA, each) for the competition of NRBA from the BSA binding pocket in a FA-concentration dependent manner. The SN was loaded on 2 x10^6 MIN6 cells for the indicated periods. Buffer (*i.e.* no incubation on cells) served as a reference for normalization (black trace). Assays were performed on a quantamaster QM4/2000SE Photon Technology International spectrofluorometer in a 150 µl quartz cuvette. NRBA was excited at λ = 540 nm. Full emission scans were recorded from λ = 550 – 750 nm with 2 nm step intervals and 0.2 s integration time. Averaged curves of three measurements are shown. The figure was adapted and modified from Hauke *et al.* [232].

The fluorescence emission of BSA-bound NRBA dropped following addition of SN from MIN6 cells. Emission of BSA-bound NRBA further decreased with increasing incubation times of SN on MIN6 cells (Fig. 23 B). Notably, already 2 s of incubation (*i.e.* washing cells) significantly decreased the detected signal (Fig. 23 B, red trace) to further drop within the course of 1 h of incubation, as described by Hauke *et al.* [232]. The buffer value (*i.e.* buffer, no incubation on MIN6 cells) served as a reference for the relative quantification of the detected fluorescence intensity (Fig. 23 B, black trace) [232].

3.3.4. Monitoring FAF-BSA-mediated removal of FAs from cellular plasma membranes using sulfo-caged FAs

Our preliminary MS screen revealed stearic acid (SA) and oleic acid (OA) amongst the most abundant FAs that were enriched by FAF-BSA from MIN6 cells (Fig. 22). Based on these findings and on previous results [214], we employed sulfo-caged (Scg-) SA and OA (Fig. 24 A), bearing negatively charged sulfo-coumarin cages to quantitatively deliver Scg-FAs to PMs of live MIN6 cells. The negative charges of the head group prevent cell entry [214], which was confirmed herein on MIN6 cells (Fig. 24 D).

Even though structurally not identical with FAs, the negatively charged head group and the hydrophobic tail presented essential requirements for the binding of Scg-FAs by BSA [262,271].

The fluorescent properties of the coumarin cage allowed for monitoring of the cellular localization of Scg-FAs and for a quantitative estimation of FAF-BSA-mediated extraction of FAs from MIN6 cells by fluorescence microscopy (Fig. 24 B+C). The fluorescence at the PM rapidly decreased upon addition of FAF-BSA to MIN6 cells that were pre-loaded with Scg-SA (200 µM). Efficiency and dynamics of fluorescence decrease correlated with the applied FAF-BSA concentrations (Fig. 24 B+D) [232]. Accordingly, applied FAF-BSA concentrations inversely correlated with the residual fluorescence intensity on PMs after 500 s of incubation on MIN6 cells (Fig. 24 C), as reported by Hauke *et al.* [232]. This indicated that FAF-BSA efficiently extracted Scg-SA (and therefore also FAs) from PMs of MIN6 cells.

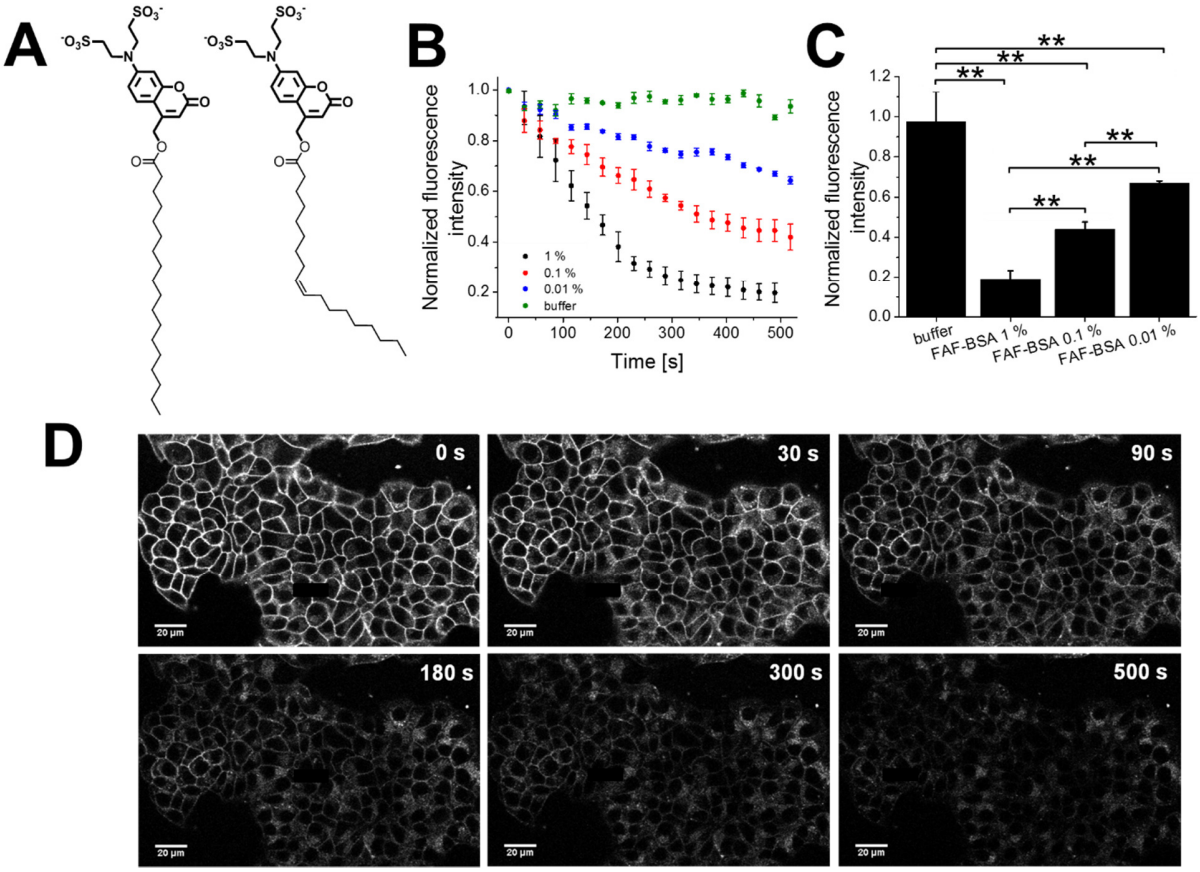

Figure 24. Visualization and quantification of FAF-BSA-mediated extraction of Scg-SA from MIN6 cells. (A) Structures of sulfo-caged stearic (Scg-SA) and oleic acid (Scg-OA). **(B+C)** Quantification of the extraction of Scg-SA (200 µM, pre-incubation) by FAF-BSA from MIN6 cells, based on coumarin fluorescence. **(B)** Time course of coumarin fluorescence of Scg-SA in the presence of FAF-BSA at different concentrations and **(C)** detected fluorescence intensities after 500 s of incubation with FAF-BSA. The fluorescence intensity was normalized to the detected signal prior to addition of FAF-BSA (buffer control). **(D)** Shown MIN6 cells were pre-incubated with Scg-SA (200 µM). FAF-BSA (1 %) was added to Scg-SA-loaded MIN6 cells and incubated for the indicated periods. Experiments were performed at 11 mM glucose. Shown are averages of 100-150 MIN6 cells. **P<0.01, ANOVA. Error bars present SD. Scale bars, 20 µm. Scg-SA was provided by R. Müller. The figure was adapted and modified from Hauke *et al.* [232].

3.3.5. Photolysis of sulfo-caged FAs restarts $[Ca^{2+}]_i$ oscillations following FAF-BSA treatment

Our preliminary findings indicate that FAF-BSA-mediated withdrawal of endogenous FAs reduces $[Ca^{2+}]_i$ oscillations and insulin secretion of MIN6 and mouse primary β-cells (Fig. 19). Accordingly, we suspected that replenishing FA pools at the PM of MIN6 and mouse primary β-cells might reverse FAF-BSA-mediated effects and recover $[Ca^{2+}]_i$ oscillations.

Treatment of glucose-stimulated MIN6 cells with FAF-BSA (0.1 %) reduced $[Ca^{2+}]_i$ oscillations. Scg-SA and Scg-OA were added in 200 µM final concentrations, followed by UV-irradiation. Photolysis of Scg-FAs at MIN6 plasma membranes was supposed to release FAs with good spatiotemporal control, according to preliminary work [214]. Silenced $[Ca^{2+}]_i$ oscillations within FAF-BSA (0.1 %)-treated MIN6 and mouse primary *β*-cells immediately resumed by the photolysis of Scg-SA (200 µM, Fig. 25 A+B i+ii, C+D). Photolysis of Scg-OA and Scg-SA yielded comparable results (Fig A20 and A21 (appendix)), as reported by Hauke *et al.* [232].

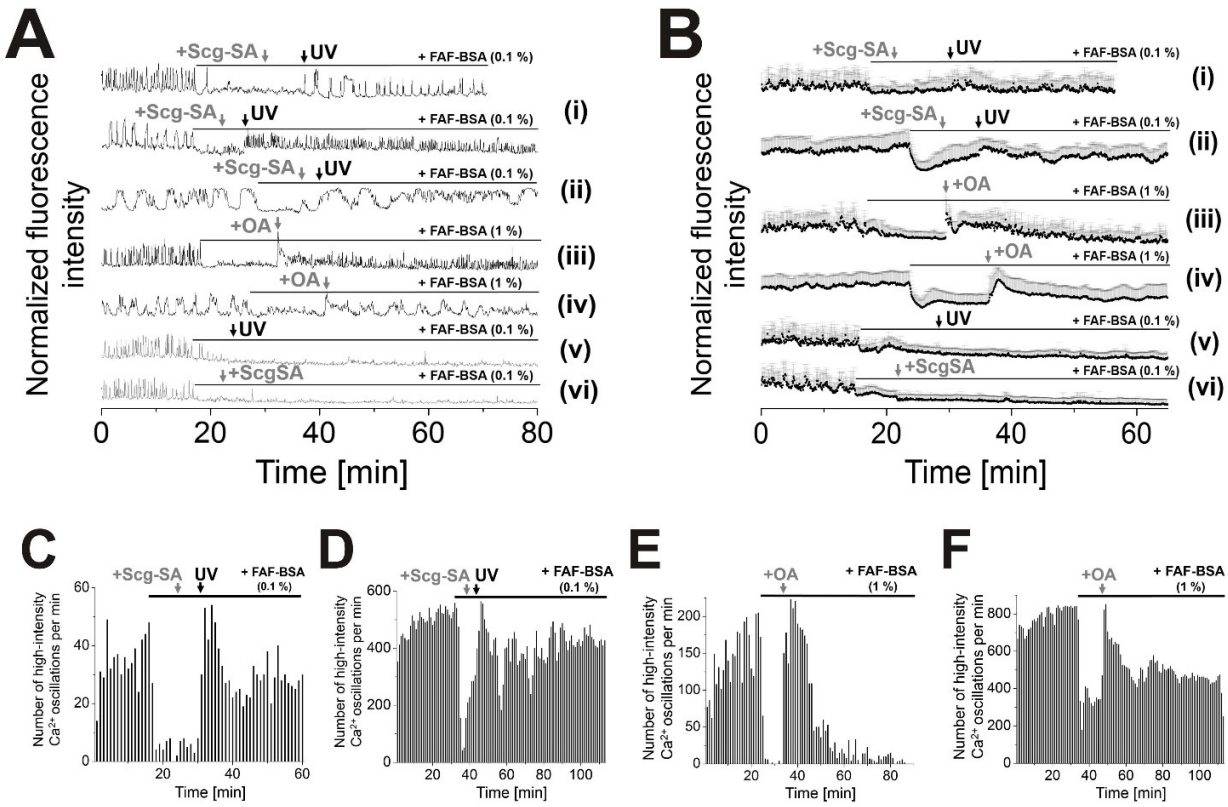

Figure 25. Photolysis of Scg-SA restarts $[Ca^{2+}]_i$ oscillations within MIN6 cells following the addition of FAF-BSA. Representative single **(A)** and averaged **(B)** Ca^{2+} traces from MIN6 and mouse primary *β*-cells, stained with the Ca^{2+} indicator Fluo-4. Following FAF-BSA (0.1 %)-mediated termination, $[Ca^{2+}]_i$ oscillations immediately resumed by the UV-mediated liberation (λ = 375 nm) of Scg-SA (200 µM) or by the addition of OA (200 µM) in **(i+iii)** MIN6 and **(ii+iv)** primary *β*-cells. **(v)** In absence of Scg-SA or **(vi)** without the UV-pulse, FAF-BSA-silenced $[Ca^{2+}]_i$ oscillations did not restart. **(C-F)** Number of high-intensity $[Ca^{2+}]_i$ events per 60 s interval. Restart of $[Ca^{2+}]_i$ oscillations following the photolysis of Scg-SA or by the addition of OA (200 µM, each) in **(C+E)** MIN6 and **(D+F)** mouse primary *β*-cells. Presented are averages of n = 14 MIN6 cells for Bi, C and n = 30 MIN6, 60 primary *β*-cells for the other experiments. Error bars present SD. Exemplary single Ca^{2+} traces for Scg-SA and Scg-OA are shown in Figs. A20 and A21 (appendix). Experiments were performed in the presence of 11 mM glucose. The figure was adapted from Hauke *et al.* [232].

Also, replenishing FA levels after FAF-BSA (0.1 %) treatment by the addition of OA (200 µM) instantaneously recovered $[Ca^{2+}]_i$ oscillations in MIN6 and mouse primary *β*-cells (Fig. 25 A+B iii+iv, E+F). From this we concluded that the presence of endogenous FA levels is not only essential, but sufficient for the induction and maintenance of $[Ca^{2+}]_i$ oscillations in glucose-stimulated *β*-cells [232].

3.3.6. Modulation of $[Ca^{2+}]_i$ oscillations by lipase-mediated FA liberation and FAF-BSA-mediated FA-depletion

Also, it was investigated whether $[Ca^{2+}]_i$ oscillations in MIN6 and mouse primary *β*-cells can be modulated by lipase-mediated artificial elevation of FA levels, followed by FAF-BSA-mediated depletion. For this, recombinant phospholipase A_2 (PLA_2) was applied, which reportedly liberates FAs by the hydrolysis of membrane zwitterionic glycerophospholipids [220].

Addition of recombinant PLA_2 (10 U) to (pre-washed) MIN6 or mouse primary *β*-cells started or enhanced $[Ca^{2+}]_i$ oscillations. Addition of FAF-BSA (1 %) terminated induced $[Ca^{2+}]_i$ oscillations (Fig. 26 A+B i-iii, D+E), thereby reversing PLA_2 action. $[Ca^{2+}]_i$ oscillations that were induced by PLA_2 action decreased after washing of MIN6 cells in a buffer exchange step (Fig. 26 A ii), as reported by Hauke *et al.* [232]. As even recombinant lipoprotein lipase (500 U), described to liberate FAs by the hydrolysis of triglycerides [272], induced $[Ca^{2+}]_i$ oscillations in pre-washed MIN6 cells (Fig. 26 A+B iv, F) [232], we concluded that observed effects were independent of the applied lipase. Insulin secretion increased more than seven-fold in the presence of recombinant PLA_2 (Fig. 26 C)), as reported by Hauke *et al.* [232]. The inhibitors of endogenous PLA_2 bromoenol lactone (BEL, 10 µM) or methyl arachidonyl fluorophosphate (MAF, 10 µM) reduced and eventually stopped $[Ca^{2+}]_i$ oscillations in MIN6 and mouse primary *β*-cells (Fig. 26 A+B v-vii, G+H and Fig. A22 (appendix)). Also, insulin secretion was significantly reduced upon inhibition of endogenous PLA_2 (Fig. 26 C) [232]. Presented results show that $[Ca^{2+}]_i$ oscillations and insulin secretion can be stimulated by elevated FA levels, independent of their origin. The buffering capacity of FAF-BSA was able to reverse these effects.

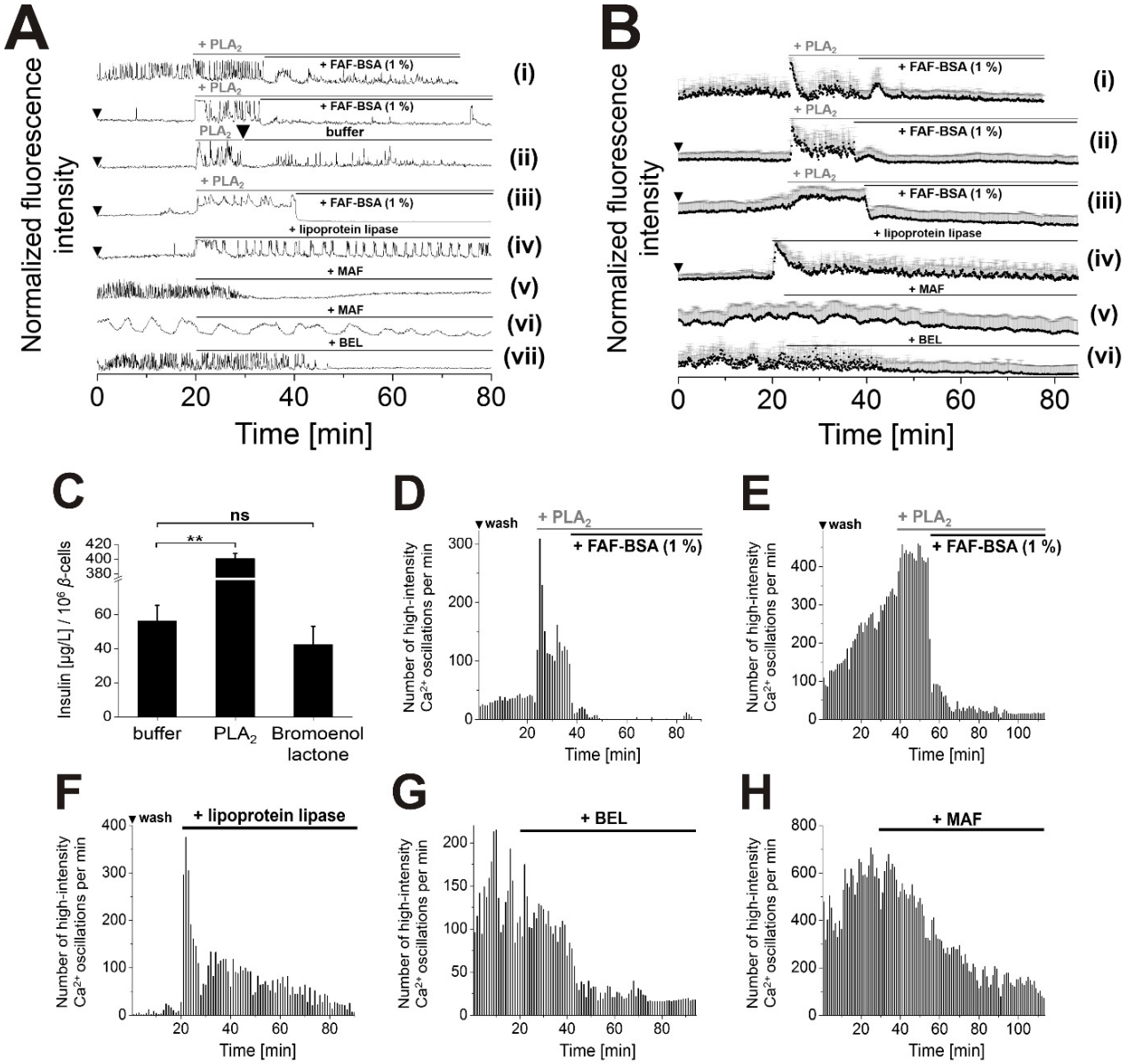

Figure 26. Liberation and depletion of FAs by PLA_2 and FAF-BSA modulate $[Ca^{2+}]_i$ oscillations in MIN6 and mouse primary *β*-cells. Representative single **(A)** and averaged **(B)** Ca^{2+} traces from MIN6 and mouse primary *β*-cells, stained with the Ca^{2+} indicator Fluo-4. **(D-H)** Counts of high-intensity $[Ca^{2+}]_i$ events per 60 s interval. Addition of PLA_2 (10 U) to **(A+B i)** oscillating or **(A+B i**, **D)** pre-washed MIN6 cells or **(A+B iii**, **E)** mouse primary *β*-cells stimulated $[Ca^{2+}]_i$ oscillations (wash indicated by ▼). Addition of FAF-BSA (1 %) to **(A+B i**, **D)** MIN6 and **(A+B iii**, **E)** mouse primary *β*-cells in the presence of PLA_2 terminated $[Ca^{2+}]_i$ oscillations. **(A+B ii)** Exchange of PLA_2 by buffer reduced the stimulation (1.5 mL/min, MIN6 cells). **(A+B iv**, **F)** Addition of lipoprotein lipase (500 U) to pre-washed MIN6 cells induced $[Ca^{2+}]_i$ oscillations. $[Ca^{2+}]_i$ oscillations in glucose-stimulated **(A+B v+vii**, **G)** MIN6 and **(A+B vi**, **H)** primary mouse *β*-cells were reduced and eventually stopped by the addition of PLA_2 inhibitors methylarachidonyl fluorophosphate (MAF) and bromoenol lactone (BEL) (10 µM). **(C)** Insulin secretion from MIN6 cells increased more than 7-fold over baseline in the presence of recombinant PLA_2 (10 U). The PLA_2-inhibitor BEL (10 µM) reduced insulin secretion. Averages of n = 30 MIN6 and n = 60 primary mouse *β*-cells are

presented. Insulin experiments were performed in quadruplicate (ns = not significant = P>0.05. **P<0.01, ANOVA, with repeated measures as necessary). Error bars present SD. Exemplary single Ca^{2+} traces are presented in Fig. A22 (appendix). All experiments were conducted in the presence of 11 mM glucose. The figure was adapted and modified from Hauke *et al.* [232].

4. Discussion

4.1. Extracellular endogenous (autocrine) signaling factors are essential for *β*-cell activity and insulin secretion

Within the last decade, soluble autocrine signaling factors have come more and more into focus as mediators of *β*-cell synchronization and pulsatile insulin secretion, in addition to direct electrical coupling via gap junctions. Expressing several receptors for neurotransmitters that were initially described in the CNS, the secretory activity of pancreatic endocrine cells was manipulated by (ant-)agonists of these receptors [273,274]. In fact, molecules that have long been implicated as neuronal signals within the pancreas are currently coming into focus as auto- or paracrine signals, produced in local endocrine cells of the pancreas [3]. So far, research has mainly focused on small diffusive molecules or neurotransmitters, such as CO, NO, ATP and γ-butyric acid as autocrine signaling factors within the pancreas [48,123].

The objectives of the presented work were to investigate the role of endogenous (autocrine) signaling factors for basal *β*-cell activity and insulin secretion. Here, we aimed at manipulating the levels of extracellular signaling factors, in particular ATP, TAs and FAs, while monitoring $[Ca^{2+}]_i$ oscillations, cAMP levels and insulin secretion as read-outs for cellular activity. Changes in TA and FA levels correlated with alterations in $[Ca^{2+}]_i$ oscillations, cAMP levels and insulin secretion. For this, we selected the murine insulinoma cell line MIN6 as a generally accepted, widespread and appropriate model system of pancreatic *β*-cells. According to previous reports, important signaling pathways for the regulation of insulin secretion in mouse primary *β*-cells were also found in MIN6 cells [74,275]. Herein applied MIN6 cells responded well to various glucose concentrations by differential levels of $[Ca^{2+}]_i$ oscillations and insulin secretion, comparable to the behavior of pancreatic islets [71,73,74]. Stimulation experiments on MIN6 cells were performed in the presence of 11 mM glucose, which lies within the steepest part of the sigmoidal dose-response curve of GSIS and therefore in the dynamic range of MIN6 cells [74]. Therefore, we considered MIN6 cells as being particularly sensitive to external stimuli in the presence of 11 mM glucose. Experiments on primary mouse *β*-cells were performed at 5 mM glucose, which reflects physiological blood glucose concentrations in mice [276]. Apart from insulin, even glucagon, ghrelin and somatostatin secretion was reported in MIN6 cells [75]. This identifies MIN6 cells as a mixed cell line consisting of different pancreatic endocrine cell types, which makes it ideally suited for studies on para- and autocrine signaling [75]. Observed differential oscillatory $[Ca^{2+}]_i$

patterns amongst individual MIN6 cells might be explained by heterogeneous environments of *β*-cells within clusters of α-, δ- and ε-cells or by variable access to stimuli or nutrients.

Studies on pancreatic islet function and regulation have mainly been conducted using animal models. Even in the present work, key findings from experiments on MIN6 cells were validated on mouse primary *β*-cells. However, recent studies have shown significant interspecies variances of overall islet anatomy, structure and paracrine interconnections, making it difficult to generalize findings, as reviewed in [3]. Even significant differences in binding affinities and receptor activation potencies were described not only amongst rodent and human, but also within mouse and rat pancreatic receptors, as shown for TAAR1 by Simmler *et al.* [241]. Whereas most *β*-cells within murine islets directly appose other *β*-cells, human islets show complex paracrine interactions within intermixed α-, δ- and ε-cells [6,21]. In particular, *β*-cells are so tightly intertwined with α-cells in human pancreatic islet that clusters of *β*-/ *α*-cells might remain even after dispersion of islets [277]. Paracrine input from *α*-cells was described to foster insulin secretion from neighboring *β*-cells [278]. As MIN6 cells present a mix of different endocrine cell types [75], they might even resemble the heterogeneous conditions that were described for human islets. However, key findings from MIN6 and mouse primary *β*-cells should still be confirmed in experiments on human primary *β*-cells.

Monitoring $[Ca^{2+}]_i$ oscillations provided a direct, sensitive read-out of rapid, transient individual *β*-cell responses that would have been difficult to detect using insulin ELISA bulk assays. For this, the sensitive and photo-stable Ca^{2+} indicator Fluo-4 was applied [279]. However, synthetic fluorescent Ca^{2+} indicators, such as Fluo-4, Rhod-2 and Fura-2 were recently described to also show side effects, such as suppression of Na,K-ATPase activity, reduction of cell viability and alteration of cell metabolism [280]. Therefore, key experiments of this study should be validated on MIN6 cells that (stably) express genetically encoded Ca^{2+} indicators, such as GCaMP3, described to cause minimal adverse effects on cells [280]. Imaging was performed on a confocal fluorescence microscope that could be set up with a perfusion system. Settings from imaging were transferred to dish experiments for the monitoring of bulk changes in insulin secretion via ELISA. Insulin measurements allowed for the quantitative estimation of cell responses in scales of ~2 $x10^6$ MIN6 or INS-1 cells.

In this work, we showed that the presence of autocrine signaling factors is essential for *β*-cell activity and insulin secretion. Non-selective removal of extracellular (autocrine) factors by stringent washing of *β*-cells in a perfusion system reduced $[Ca^{2+}]_i$ oscillations and insulin secretion.

After stopping the perfusion, $[Ca^{2+}]_i$ oscillations slowly recovered during static incubation, presumably due to replenishment of extracellular (para- or autocrine) signaling factor levels. In a complementary approach, SN that was pre-loaded on a population of MIN6 cells was transferred to another dish, containing pre-washed, non-oscillating MIN6 cells. Upon transfer of pre-loaded buffer amongst different cell populations, $[Ca^{2+}]_i$ oscillations in pre-washed cells immediately fully recovered. As glucose and salt concentrations remained unchanged in transfer experiments, we suspected secreted factors within the SNs - the cellular 'secretome' - to be responsible for the potentiation of $[Ca^{2+}]_i$ oscillations and insulin secretion. Compared to buffer transfer experiments, addition of individual factors to pre-washed cells did not stimulate $[Ca^{2+}]_i$ oscillations to comparable extents. This was shown by the stimulation of pre-washed MIN6 cells with ATP or BSA that was pre-loaded with FAs from another cell population. From this we infer that the presence of the entire spectrum of endogenous signaling factors is necessary to recover the full oscillatory potential of pre-washed *β*-cells. In contrast, selective depletion of individual extracellular factors was sufficient to significantly reduce $[Ca^{2+}]_i$ oscillations and insulin secretion of MIN6 and mouse primary *β*-cells. This was herein demonstrated by the reduction of FA levels in the presence of FAF-BSA, of TA levels by *β*-CD / MAO action or of ATP levels in the presence of apyrase.

Notably, electron micrographs show very narrow extracellular clefts between *β*-cells that are just a few nanometers wide [5]. In line with that, Braun *et al.* calculated the volume of the extracellular space of *β*-cells within pancreatic islets to ~5 pL per *β*-cell, considering the average volume of an individual *β*-cell and of an entire pancreatic islet [123]. Secretion or enzymatic turnover of relatively small amounts of endogenous (autocrine) signaling factors within the extracellular space probably results in significant concentration changes in micromolar ranges [123]. Therefore, the confined extracellular space within pancreatic islets might guarantee effective endogenous signaling and makes the autocrine signaling network highly dynamic so that it can rapidly react and adapt to changes of external stimuli. However, the size of clusters of synchronized *β*-cells within the pancreas is a subject under debate. Estimates vary from individual clusters of *β*-cells up to syncytia, involving the entire *β*-cell population [281].

4.2. TAAR1 integrates effects of aromatic amines into β-cell activity and insulin secretion

Buffer exchange by stringent washing significantly reduced β-cell activity, presumably by the removal of small diffusive extracellular autocrine signaling factors. Following reports of TAAR1 expression in the pancreas, we suspected even TAs to be amongst extracellular factors that contribute to the maintenance of β-cell $[Ca^{2+}]_i$ oscillations and insulin secretion.

In the present work, we show that selective agonists (or antagonists) of TAAR1 have profound and immediate effects on $[Ca^{2+}]_i$ oscillations in β-cells, suggesting implications of TAAR1-mediated signaling on glucose homeostasis. We found that addition of TAs, the endogenous TAAR1 agonist T1AM or synthetic TAAR1 agonists potentiated $[Ca^{2+}]_i$ oscillations in pre-washed MIN6, INS-1 and mouse primary β-cells in the presence of glucose. In line with literature reports, we found that β-PEA and tyramine are - from all TAs - amongst the most potent agonists of TAAR1. However, significant interspecies differences have been reported for the activation potencies of agonists on TAAR1 [241]. β-PEA is more potent than tyramine on mouse and human TAAR1, whereas the opposite applies for rat TAAR1 [133,136]. Rodent, but not human TAAR1 is activated by tryptamine [132,165,282]. Interspecies differences in the activation potencies of some TAAR1 agonists lie within more than one order of magnitude [241], which needs to be taken into consideration when transferring our findings from one to another model system. Therefore, herein presented experiments on TAAR1 stimulation need to be confirmed on a human cell line or human primary β-cells. Effects on $[Ca^{2+}]_i$ oscillations translated well into increased insulin levels. Even though RO5256390 did not show the strongest effects on high-intensity $[Ca^{2+}]_i$ oscillations, it most potently stimulated insulin secretion. This indicated that insulin secretion probably depends less on high-intensity, rather than on continuously enhanced $[Ca^{2+}]_i$ oscillations. β-PEA potentiated insulin secretion in the presence of different glucose concentrations, but not in the absence of glucose. Screening β-PEA and RO5256390 at different concentrations, we found that insulin secretion increased progressively from 1 µM β-PEA (or RO5256390) to maximum levels at 25 µM β-PEA (or RO5256390) final concentrations. Exposure with higher concentrations of TAAR1 agonists (50 and 100 µM) yielded significantly lower insulin levels, possibly indicating receptor desensitization at these concentrations.

Compared to herein applied micromolar concentrations of TAs, we assume that under endogenous conditions within the enclosed islets of Langerhans of the pancreas, β-cell activity might be modulated even by significantly lower levels of TAs in the nano-molar range, as previously

reported [126,127]. Herein performed stimulation experiments were conducted on MIN6 cells, following removal of the entire spectrum of extracellular autocrine signaling factors in preliminary stringent washing steps. Therefore, we assume that higher levels of TAs in micromolar ranges were necessary to overcompensate the missing extracellular stimulatory input from other endogenous (autocrine) signaling factors.

A coumarin-based photo-caging strategy allowed us to liberate *β*-PEA within MIN6 cells with high spatio-temporal control. Stringent washing of MIN6 cells following loading with caged *β*-PEA removed residual external compound, so that the utmost fraction of *β*-PEA was presumably liberated inside MIN6 cells upon UV irradiation. Remarkably, $[Ca^{2+}]_i$ oscillations instantaneously started upon light-mediated release of *β*-PEA in pre-defined spots within MIN6 cells. This suggests the presence of an intracellular TAAR1-pool that was readily accessed by the released *β*-PEA.

In the presence of the selective TAAR1-antagonists EPPTB and ET-92, $[Ca^{2+}]_i$ oscillations and insulin secretion of *β*-cells, pre-stimulated by TAAR1 agonists, were significantly reduced. From this we inferred that observed effects mainly originated from TAAR1 stimulation. Notably, application of the antagonists EPPTB or ET-92 to glucose-stimulated MIN6, INS-1 and mouse primary *β*-cells decreased $[Ca^{2+}]_i$ oscillations and insulin secretion. This indicated that *β*-cells constantly receive stimulatory input from TAAR1 that is either constitutively active or activated by endogenous agonists, presumably endogenous TAs that were identified via MS. Cellular responses to EPPTB – currently the only commercially available selective TAAR1 antagonist – were confirmed by the application of the selective TAAR1 antagonist ET-92, as requested by Rutigliano *et al.* [156]. Our findings are in line with earlier reports on the effects of EPPTB on the firing activity of dopaminergic neurons [283].

In contrast to MIN6 and mouse primary *β*-cells, INS-1 cells show comparatively low endogenous expression levels of TAAR1 [174]. Therefore, stimuli were applied in 4- to 10-fold higher concentrations on INS-1 cells, compared to experiments with MIN6 and mouse primary *β*-cells, to evoke comparable effects on $[Ca^{2+}]_i$ oscillations and insulin secretion. In general, low TAAR1 expression levels – at least under basal conditions – reportedly present one of the major challenges in the TAAR1 field [160].

Based on counts of high-intensity $[Ca^{2+}]_i$ spikes in MIN6 cells, we were able to set up a rank order of potency for TAs: *β*-PEA > *p*-tyramine > tryptamine >> *p*-synephrine ≈ *p*-octopamine, which is in line with literature reports on the activation potencies of TAs [138,160,241]. Based on these results, we suspected that structural modifications of the *β*-PEA skeleton directly determined the

activation potencies of amines on TAAR1. Therefore, we profiled a selection of *β*-PEA-related compounds for their potencies to evoke $[Ca^{2+}]_i$ oscillations in MIN6 cells, with regard to specific modifications of the amino group, the aromatic moiety and the ethylene chain. We found primary amines more potent over secondary and tertiary amines. Also, modifications of the aliphatic side chain (-CH_3, -OH) or aromatic moiety (-OH, -OCH_2) significantly reduced the activation potency. Amines with shorter side chains, as well as non-aromatic amines did not stimulate $[Ca^{2+}]_i$ oscillations in MIN6 cells. This is in line with reports from Lewin *et al.* [242] and Wainscott *et al.* [136], reporting that TAAR1 activation potencies, as described by EC_{50} values, decreased amongst *β*-PEA derivatives with increasing complexity of modifications at the primary amine or aromatic moiety. Similar effects were observed, comparing the potencies of ergoline (lisuride) derivatives on $[Ca^{2+}]_i$ oscillations in pre-washed glucose-stimulated MIN6 cells. Whereas LAMPA and lisuride induced potent effects on $[Ca^{2+}]_i$, no stimulation was induced by LSD or methyergometrine, which is in line with reports from Simmler *et al.* [241].

In addition to $[Ca^{2+}]_i$ imaging and insulin ELISA, the potency of compounds for TAAR1 stimulation was also tested in measurements of the intracellular cAMP concentration, using the FRET-based sensor Epac. As expected from our observations from $[Ca^{2+}]_i$ imaging, we found that *β*-PEA was more potent than *p*-tyramine and that EPPTB reversed *β*-PEA-induced effects. Our findings are in accordance with earlier reports on the effects of EPPTB on basal cAMP levels [134]. We found that *β*-PEA and RO5256390 most potently induced cAMP formation. Here, cAMP levels perfectly reflect determined levels of insulin secretion. In line with findings from $[Ca^{2+}]_i$ imaging and with literature reports, the full TAAR1 agonists RO5256390 and RO5166017 induced significantly stronger cAMP responses, compared to the partial TAAR1 agonists RO5073012 that showed only transient effects on cAMP levels [151,154,155]. Despite of that, RO5073012 significantly stimulated insulin secretion to the same extents as *β*-PEA and RO5166017. This indicates that for a full characterization of compound activity on *β*-cells, $[Ca^{2+}]_i$ oscillations, cAMP levels and insulin secretion need to be determined and compared.

In line with literature reports, cAMP levels evoked by *β*-PEA stimulation were in comparable ranges to that generated by RO5166017 or RO5256390 stimulation [151,154]. Stimulation of cAMP production was not observed for LSD, according to our findings from $[Ca^{2+}]_i$ oscillations. However, the effects of dibenzepin on cAMP levels were significantly lower compared to observed dibenzepin-mediated stimulation of $[Ca^{2+}]_i$ oscillations. Notably, addition of low doses of the phosphodiesterase inhibitor IBMX to glucose-stimulated MIN6 cells increased intracellular cAMP

levels. This indicated that cAMP is produced even under basal stimulatory conditions within MIN6 cells, presumably due to $G_{\alpha s}$ stimulation by endogenous agonists.

There are several problems associated with a direct comparison of the activation potencies of TAAR1 agonists from literature reports with our experimental data. First, different biological test systems were applied as read-outs for receptor activation. Whereas heterologous cell lines (*e.g.* COS-7 or HEK293 cells) that stably express TAAR1 were mostly applied in literature screens [132,151,154,155,282], we herein used β-cell lines with endogenous TAAR1 expression. Therefore, overall receptor expression levels vary amongst different biological test systems. To improve the overall PM localization of TAAR1 in model cell systems for pharmacological characterizations, fusion constructs of TAAR1 were applied in literature screens. Here, the N-terminus of TAAR1 was fused to the first 9 amino acids of the β-adrenergic receptor, which presents an asparagine-linked glycosylation site to increase the glycosylation state and therefore stabilization of TAAR1 at PMs [135]. However, our preliminary data indicate predominant intracellular localization of TAAR1 in MIN6 cells. Therefore, even the intracellular availability of herein tested ligands might also significantly determine their TAAR1 activation potential. In fact, some psychoactive drugs, such as amphetamines, are cargo of monoaminergic transporters and are actively and rapidly shuffled into cells [284]. Therefore, these compounds are better available to intracellular TAAR1 than others, passively overcoming PMs.

However, using racemic mixtures in our presented screens, the stereoselectivity of TAAR1 was not considered. Due to the presence of a stereoselective binding site in TAAR1 [242], screening racemates instead of isolated stereoisomers could have underestimated the activity of more active pure isomers. This presents a limitation of the present study. Also, some TAAR1 agonists are described to act on adrenoreceptors, thereby modulating cAMP production via β- (or α_2-) adrenoreceptors which are positively (or negatively) coupled to adenylyl cyclase. To exclude multiple pharmacologies, TAAR1 agonists should be screened in the presence of selective antagonists of β- / α- adrenoreceptors in future studies, as presented by [136].

Our MS screen detected ^{15}N-labelled TAs in MIN6 cells that were grown in the presence of heavy isotope labelled amino acids ^{15}N-L-phenylalanine, ^{15}N-L-tyrosine and ^{15}N-L-tryptophan. This confirmed the role of TAs as endogenous signaling molecules that are produced within MIN6 cells by the decarboxylation of precursor amino acids. Thereby, TAs meet the definition as autocrine signaling factors, stimulating TAAR1 on the same cell from which they have been released, or neighboring cells of the same type. We interpreted this as evidence that TAAR1 in the pancreas is

activated in an autocrine fashion. In the intact pancreas, TAs might easily reach TAAR1 at the surface of β-cells within the confined extracellular space of the enclosed islet of Langerhans.

MS confirmed the accumulation of ^{15}N-β-PEA upon inhibition of MAO in MIN6 cells that were cultured in the presence of stable isotope-labeled amino acids. As expected, addition of MAO inhibitors to MIN6 cells in the presence of glucose also increased intracellular cAMP concentrations, along with $[Ca^{2+}]_i$ oscillations and insulin secretion due to TAAR1 stimulation by increased levels of endogenous TAs. β-PEA is primarily inactivated by MAO-B [126,168,169]. Notably, selective inhibitors of MAO-B yielded significantly higher ^{15}N-β-PEA levels, compared to MAO-A inhibition within MIN6 cells that were grown in the presence of ^{15}N-labeled L-phenylalanine. Selective MAO-B inhibitors showed stronger effects on cellular cAMP levels than inhibitors of MAO-A, which was, however, not reproduced on $[Ca^{2+}]_i$ oscillations and insulin secretion. The MAO-A inhibitor clorgyline showed effects on $[Ca^{2+}]_i$ oscillations that were comparable to that of MAO-B inhibitors selegiline and tranylcypromine. Counts of high-intensity $[Ca^{2+}]_i$ oscillations correlated well with determined levels of insulin secretion. Inhibition of AADC decreased levels of endogenous TAs below the detection limit in MS screens. Lowering of TA levels directly translated into reduced $[Ca^{2+}]_i$ oscillations and insulin secretion [166]. Equally, addition of recombinant MAO-B to glucose-stimulated MIN6 cells gradually reduced and finally stopped $[Ca^{2+}]_i$ oscillations. Unable to penetrate the PMs of living cells, MAO-B was supposed to degrade only the extracellular fraction of TAs. Reduced levels of external TAs presumably lead to decreased TAAR1 (auto-)stimulation, along with diminished $[Ca^{2+}]_i$ oscillations.

By MS we detected significantly increased levels of TAs, following inhibition of endogenous MAO in MIN6 cells. The significant accumulation of TAs amongst MIN6 cells following selective inhibition of MAO indicated rapid turnover rates of TAs. The fast metabolism of TAs under endogenous conditions reportedly results in extracellular levels of TAs in the nanogram-range, several hundred-fold below those of the classical biogenic amines [127,166], which is in line with our findings from MS. Comparable concentration ranges of TAs have been determined in peripheral tissue [164,170,285–287]. In line with our findings, the inhibition of MAO is described to increase systemic levels of TAs and is therefore an effective means for the treatment of depression [288]. In fact, increased β-PEA levels were determined in MAO-B knockout mice [289]. Addition of aromatic-amine withdrawing β-CD transiently reduced $[Ca^{2+}]_i$ oscillations in glucose-stimulated MIN6 cells. Oscillations spontaneously recovered, presumably after saturation of β-CD with extracellular amines that were constantly supplied from MIN6 cells. The unequal recovery

times of $[Ca^{2+}]_i$ oscillations might be explained by the differential localization of individual MIN6 cells within islets and relating thereto the accessibility of β-CD to β-cells. From this and from our imaging data on the effects of recombinant MAO, as well as of selective MAO or AADC inhibitors, we infer that basal β-cell activity and insulin secretion rely on the presence of endogenous TAs for TAAR1 stimulation and that TAs are essential extracellular autocrine signaling factors in β-cells.

Generating distinct transients of $[Ca^{2+}]_i$ without sustained elevation of overall $[Ca^{2+}]_i$ levels, we suspect that TAs might function as extracellular coordinators or sensitizers of the cellular secretory activity, and are possibly even involved within a positive autocrine feedback loop, as it was reported for ATP [108]. In rodent islets, ATP was found co-released during exocytosis of insulin from secretory granules, reaching extracellular concentrations of more than 25 µM. Also, exocytotic kiss-and-run mechanisms for the release of smaller amounts of ATP have been proposed [104,290,291]. Thereby, small diffusive factors, such as TAs and ATP might modulate or even increase the responsiveness of β-cells glucose. This would explain how β-cells efficiently respond to relatively modest changes in extracellular glucose levels under physiological conditions. Thereby, intercellular and inter-islet diffusion of TAs might even support the propagation of $[Ca^{2+}]_i$ oscillations amongst cells without direct physical contact. As previously reported for ATP [292], even TAs might participate in the adjustment of second messenger systems for the activation of signaling pathways, thereby helping to define the dynamic range of cellular responses.

Imbalances of TAs levels within the brain have long been implicated to contribute to the development of psychiatric disorders, such as schizophrenia, Parkinson's disease, depression and drug addiction [146,152,160,239]. The discovery of TAAR1 in 2001 yielded a molecular 'drugable' target for the treatment of these diseases. Therefore, the 'RO-compounds', EPPTB and ET-92 were developed as selective synthetic (ant-)agonists for the treatment of psychiatric diseases [134,151,153–155]. Interestingly, mental illnesses are often accompanied by metabolic disorders, along with weight gain, but the mechanisms are mostly unclear [293–295]. Even in early reports on the discovery of TAAR1, substantial expression levels of this receptor were identified within organs that are involved in the regulation of glucose homeostasis and nutrient resorption from food [132,156,282,296]. Therefore, it is even more surprising that side effects of MAO inhibitors, antidepressants or psychoactive drugs on pancreatic β-cell activity and insulin secretion have been overlooked so far. From our findings, we suspect A) either direct effects of drug-TAAR1 interactions on β-cell activity or B) indirect modulation of TA levels by specific inhibitors of TA-biochemical pathways and thereby TAAR1 stimulation within pancreatic islets.

4. Discussion

Early reports on thyronamines already determined the '*β*-PEA skeleton' as an essential requirement for TAAR1 agonistic properties [297]. Therefore, all psychotropic drugs applied herein are based on this structure. Prime examples are dibenzepin or diphenylhydramine, resembling the aliphatic part of *β*-PEA or nomifensine, which entirely comprises the structure of *N,N*-dimethyl-phenylethylamine. Even though these compounds are commonly prescribed to selectively address established molecular targets within the CNS, possible interactions with TAAR1 on *β*-cells might provide an explanation for described side effects such as obesity. Remarkably, regular antidepressant use was found to double the risk for the development of T2D in patients with or without indications for severe depression [298]. Also, gain of overall body weight is described as a common side effect of tricyclic antidepressants, which are herein represented by dibenzepin [299]. In fact, herein tested psychoactive drugs, including dibenzepin, stimulated $[Ca^{2+}]_i$ oscillations and insulin secretion to different extents. In particular, administration of MAO-inhibitors was connected to weight gain, with phenelzine as a prime example [300]. In fact, phenelzine was herein shown to significantly potentiate $[Ca^{2+}]_i$ oscillations, cAMP levels and insulin secretion. In contrast, administration of tranylcypromine is not described to cause weight gain [301], even though positively tested herein for the potentiation of $[Ca^{2+}]_i$ oscillations and insulin secretion. Other drug side effects such as reduced appetite might be prevailing here. This indicates the overall complexity, when drug effects that were determined *in cellulo* are transferred to the physiology of an entire organism. Therefore, our findings from cell experiments still need to be confirmed in the living animal in a next step.

Also, the livestock feed additive ractopamine was found to significantly increase $[Ca^{2+}]_i$ oscillations in MIN6 cells. Even though mostly banned due to severe side effects on animal behavior, ractopamine is still approved in some countries such as the U.S., to promote livestock weight gain, also via muscle mass development [245]. Our finding that psychostimulant and hallucinogenic drugs, such as flurazepame, methysergide, the LSD analogue lisuride, but also (meth-)amphetamine stimulate *β*-cells via TAAR1 opens new perspectives about the potential influence of these commonly applied drugs on overall glucose homeostasis.

Interestingly, *β*-PEA and *p*-tyramine were identified as exogenous amines in processed food, such as cheese, fermented meat, wine and chocolate [302]. After consuming aged cheese, patients treated with MAO-inhibitors tend to show hypertensive crises, so called "cheese reactions" [303]. TAs are also generated by the decarboxylation of dietary amino acids in gut microbiota. Examples are *Clostridium sporogenes* or *Ruminococcus gnavus* that are described to convert Trp to

tryptamine via Trp decarboxylase [304–306]. Considering the herein presented role of TAAR1 for the regulation of *β*-cell activity and insulin secretion, we propose exogenous amines from food or amines that are generated within the gut to also exert effects as modulators of glucose homeostasis. Recently, Mühlhaus *et al.* reported natural genetic variants of TAAR1 in diabetic patients with disturbances in overall body weight regulation and glucose homeostasis [177]. Even though not fully conclusive about the general role of these mutations in TAAR1 on overall pathogenesis, this study marks a starting point for therapeutic implications of TAAR1 in T2D and obesity as well as the growing interest of the scientific community into the topic.

4.3. *β*-Cell activity and insulin secretion essentially rely on the presence of FAs as local endogenous signaling factors

Within the last decade, FAs have gained increasing attention as exogenous agonists for the nutrient-mediated release of sufficient amounts of insulin [228,229]. However, up until now, a possible role of FAs as endogenous (local) signaling factors of *β*-cells has hardly been considered.

In the present study, we applied FA-depleted albumin, well described to bind FAs [307], to MIN6 and mouse primary *β*-cells. As initially observed in washing experiments, even the addition of FAF-BSA to *β*-cells significantly reduced $[Ca^{2+}]_i$ oscillations and insulin secretion [232]. This effect depended on the applied FAF-BSA concentration. Our observations indicated that FAs might be amongst those extracellular endogenous signaling factors that were herein shown to be essential for *β*-cell activity and insulin secretion. Detected effects of FAF-BSA on MIN6 $[Ca^{2+}]_i$ oscillations were independent of applied external glucose concentrations or the origin of albumin. However, our observations of FAF-BSA-mediated reduction of $[Ca^{2+}]_i$ oscillations and insulin secretion contradict earlier reports from Straub and Sharp [308], describing significantly increased insulin secretion from rat islets, following 4 - 6 h incubation in the presence FAF-BSA. As we herein monitored immediate effects of FAF-BSA on $[Ca^{2+}]_i$ oscillations and insulin secretion [232], the different time frames within both studies might explain this discrepancy. More likely, Straub and Sharp measured insulin levels in the presence of BSA in the stimulating buffer, receiving artifacts that were herein also observed and had to be corrected for.

Based on our MS screen, we found that FAF-BSA was significantly depleted of FAs, compared to conventional BSA. This also explains the differences in the FA-buffering capacity of FAF-BSA, compared to conventional BSA along with differential effects on $[Ca^{2+}]_i$ oscillations. Even though

structurally distinct from FAs, sulfo-caged FAs served as a good model system to monitor FAF-BSA-mediated depletion of FAs from PMs of MIN6 cells [232]. Adequate enrichment of FAs, especially of (monoun-) saturated long-chain FAs (C16 – C20/22), such as stearic, palmitic, oleic and elaidic acid from MIN6 cells by FAF-BSA was herein detected by MS [232], in line with literature reports [307,309]. In a recent study, Tunaru *et al.* described that 20-hydroxyeicosatetraenoic acid, a metabolite of arachidonic acid, is released by glucose-stimulated mouse as well as human β-cells and stimulates insulin secretion via GPR40 in an autocrine fashion [310]. This supports our hypothesis of a general autocrine role of FAs within pancreatic β-cell signaling.

However, the exact amounts of FAs within pancreatic islets that are available for GPR40 stimulation are unclear and difficult to estimate. The concentration of circulating FAs within human serum lies in the range of ~1 mM. In fact, these concentrations far exceed the level of solubility of FAs, which is estimated to less than 0.1 nM at pH 7.4 and 37 °C (palmitate) [311]. Due to their low solubility, the utmost portion of FAs in the plasma is associated with albumin [312], with only fractional amounts (< 0.01 %) available unbound in the aqueous phase [313,314]. Stimulation of GPR40 is mediated by the bioactive, non-BSA-associated fraction of FAs [188,315]. Additional sources of FAs, such as the lipoprotein lipase-mediated hydrolysis of chylomicrons within islet capillaries [226], further complicate a realistic estimation of the levels of FAs that are available for GPR40 stimulation.

Effects of BSA on β-cell activity were reversible, as MIN6 cells were found to spontaneously recover $[Ca^{2+}]_i$ oscillations, following exchange of albumin by buffer. Notably, $[Ca^{2+}]_i$ oscillations also recovered upon UV-mediated release of photocaged stearic (oleic) acid at the PMs of MIN6 and mouse primary β-cells, or by the direct addition of oleic acid to FAF-BSA-treated β-cells [232]. This is in line with our MS data, showing that FAF-BSA enriched SA by a factor of ~3 and OA ~27-fold. From this we inferred that $[Ca^{2+}]_i$ oscillations can be induced by various types of long-chain FAs and do not depend on a particular FA species [232]. FAs are loaded as well as off-loaded to and from albumin with amazing dynamics and are rapidly turned over, showing physiological half-lives in the range of ~1 - 2 min [313]. In line with this, we found that $[Ca^{2+}]_i$ oscillations within washed MIN6 cells could be stimulated by BSA that was pre-loaded on a separate population of MIN6 cells [232]. This underlines the physiological relevance of albumin-mediated buffering of FAs for β-cell activity under different nutritional conditions.

4. Discussion

FAs reportedly bind albumin sites I – III, whereas site II exhibits affinity to L-Trp and certain drugs [264,266,316]. Therefore, pre-saturation of FAF-BSA with albumin-binders L-Trp and Ibu was supposed to decrease the binding capacity of albumin. Whereas addition of FAF-BSA to glucose-stimulated MIN6 cells showed clear reductions of $[Ca^{2+}]_i$ oscillations, this effect was weakened for BSA that was pre-loaded with L-Trp or Ibu. Here, we suspected competing effects amongst site II-ligands and FAs for albumin binding. Also, pre-saturation of BSA by FAs, as determined for conventional BSA by MS, was shown to reduce albumin-mediated effects on $[Ca^{2+}]_i$ oscillations. In competition experiments, L-Trp and Ibu were added on top of FAF-BSA that was pre-loaded on a separate population of MIN6 cells. $[Ca^{2+}]_i$ oscillations were stimulated, presumably due to cooperative effects or out-competition of FAs by albumin-binders [232]. Out-competition of FAs from binding sites by albumin-binding drugs or vice versa might also have implications on overall plasma concentrations and pharmacokinetics, especially when it comes to drugs with overall low free plasma fractions. Also, diet-related or drug-induced changes of FA plasma concentrations might directly translate into altered insulin secretion.

Lipases within β-cells are described to release significant amounts of FAs into the extracellular space, also suggesting a role of FAs as autocrine signaling factors [218,219,317,318]. Even in the present work, FA levels were artificially elevated by recombinant PLA_2 or lipoprotein lipase action. The presence of recombinant lipases, along with liberation of FAs, immediately translated into increased $[Ca^{2+}]_i$ oscillations. Notably, addition of PLA_2-inhibitors MAF and BEL to MIN6 as well as mouse primary β-cells decreased $[Ca^{2+}]_i$ oscillations as well as insulin secretion [232]. This indicated that endogenous lipase activity along with constant FA-supply is essential for the maintenance of β-cell activity and GSIS.

For the determination of the molecular target of FAs in β-cells, we applied the selective GPR40 antagonist GW1100. We observed gradual reduction of $[Ca^{2+}]_i$ oscillations upon application of GW1100 to glucose-stimulated MIN6 cells, indicating that GPR40 stimulation is essential for the maintenance of β-cell activity [232]. More importantly, FAF-BSA that was pre-loaded on a population of MIN6 cells did not evoke continuous Ca^{2+} spiking when applied together with GW1100 to pre-washed MIN6 cells [232].

GPR40 stimulation by FAs was also described to directly modulate voltage-gated K^+ currents in β-cells and PKA-activation, leading to increased $[Ca^{2+}]_i$ and insulin secretion [319]. We suspect that the withdrawal of FAs by FAF-BSA prevents lowering of K^+ currents by GPR40, along with diminished overall $[Ca^{2+}]_i$ levels in β-cells, which is in line with findings of Schnell *et al.* [208].

4. Discussion

Effects of FAs on ion channels have been determined and are reviewed in [319,320]. Recently, photoswitchable FAs have been shown to directly modulate ATP-sensitive and voltage-gated K^+ channels, along with effects on glucose-stimulated $[Ca^{2+}]_i$ oscillations [321]. The herein observed rapid termination of $[Ca^{2+}]_i$ oscillations in the presence of FAF-BSA as well as the fast recovery upon replacement by buffer indicate the involvement of ion channels as additional immediate targets of FAs.

5. Conclusion and outlook

Impaired insulin secretion is a hallmark in the development of T2D. Within the last decade, the role of intercellular and inter-islet synchronization has gained increasing attention as a prerequisite for the secretion of sufficient amounts of insulin. In light of the steadily growing number of diabetes incidences worldwide, a better understanding of the multiple parameters that regulate insulin secretion on both cellular and molecular levels is strongly required.

In the present study, we extend the traditional roles of ATP, TAs and FAs from exogenous metabolites to essential endogenous (autocrine) signaling factors and potential drivers of $[Ca^{2+}]_i$ oscillations and insulin secretion. Also, we identify TAAR1 and GPR40 as novel integrators of metabolic control that translate stimulation by local pancreatic signaling factors into glucose homeostasis. Based on our findings and on literature reports, we suggest that disturbed insulin secretion in T2D might not necessarily indicate a reduction of the overall pancreatic β-cell mass, but potentially originates from imbalanced or reduced levels of endogenous (autocrine) signaling factors. This, in turn, might lead to impaired or dysfunctional intercellular or inter-islet synchronization and insufficient insulin secretion. Therefore, we hypothesize that the restoration of functional autocrine signaling within the pancreas might also bring back synchronized pulsatile insulin secretion from islets of Langerhans and prevent β-cell exhaustion by insulin hypersecretion, insulin resistance and the progression of T2D. For this, however, the local concentrations and the interplay of signaling factors within pancreatic islets need to be determined. Also, it is of high interest whether individual factors are able to mutually compensate the loss of others.

Herein presented data suggest pancreatic TAAR1 as a direct molecular target of small aromatic amines for the modulation of glucose homeostasis. In future steps, we will test commonly prescribed aminergic psychoactive drugs for their effects on body weight and blood insulin levels in rodents. Furthermore, it will be investigated whether observed (side-)effects on insulin secretion and body weight can be reversed by a combination therapy of psychoactive drugs with selective TAAR1-antagonists that act in the pancreas, but cannot overcome the blood-brain barrier. This would have general implications for antidepressant-based therapies.

With the present work, we are the first to subordinate insulin secretion to the presence of local, endogenous (autocrine) signaling factors. Thereby, the presented work contributes to a more accurate and comprehensive understanding of fundamental regulatory processes of β-cell activity and insulin secretion.

6. Research design and methods

6.1. Reagents

BSA (fatty acid free: cat# A7030. lot# SLBK9735V; conventional: cat#A7906, lot# SLBR0420V), ^{13}C-oleic, ^{13}C-palmitic and ^{13}C-decanoic acid were provided by Sigma-Aldrich (St. Louis, MO, US). Gradient-grade fetal bovine serum (FBS) (cat# 16000-044) and Dulbecco´s Modified Eagle Medium (DMEM) were obtained from Gibco (Carlsbad, Ca). *β*-Mercaptoethanol (50 mM in PBS) was ordered from PAN Biotech (Aidenbach, Germany). Minimal medium for culturing cells in the presence of isotope-labeled amino acids was delivered by Cell Culture Technologies (Gravesano Ticino, Switzerland). Collagenase (from *Clostridium histolyticum*) was obtained from Nordmark Biochemicals (Uetersen, Germany). Histopague 1083 (density: 1.083 g/mL) and Histopague 1119 (density: 1.119 g/mL) were purchased from Sigma-Aldrich. Stable isotope-labelled amino acids and trace amines were purchased from Sigma Aldrich, CDN Isotopes (Quebec, Canada) and Santa Cruz Biotechnology (Huissen, The Netherlands). Solvents of the highest analytical grade were provided by Biosolve (Valkenswaard, The Netherlands), Honeywell (Morristown, US) and Sigma-Aldrich. All other commercially available chemicals and enzymes were ordered from Sigma-Aldrich. All anesthetics used were purchased and stored in compliance with the German Narcotics Act (BtMG).

6.2. Unit definitions of applied recombinant enzymes

according to the supplier, Sigma Aldrich:

Apyrase (from potato, enzyme commission (EC) number: 3.6.1.5, expressed in *Pichia pastoris*)*:* One unit liberates 1.0 µmole of inorganic phosphate from ATP or ADP per minute at pH 6.5 and 30 °C. *Phospholipase A₂* (from bee venom, EC number: 3.1.1.4): 1 U hydrolyzes 1.0 µmole of soybean L-α-phosphatidylcholine to L-α-lysophosphatidylcholine and a fatty acid per minute at pH 8.9 and 25 °C. *Monoamine oxidase B* (from baculovirus infected insect cells, EC number: 1.4.3.4): One unit deaminates 1.0 nmole of Kynuramine per minute at pH 7.4 and 37 °C. *Lipoprotein lipase* (from *Burkholderia sp.*, EC number: 3.1.1.3): 1 U releases 1 nmole of *p*-nitrophenole per minute at pH 7.2 and 37 °C, using *p*-nitrophenol-butyrate as a substrate.

6.3. Tissue culture and insulin measurements

6.3.1. Culturing MIN6 cells

MIN6 cells [73] were cultured in a humidified atmosphere at 37 °C and 8 % CO_2. The culture medium DMEM contained 4.5 g/L glucose and was supplemented with FBS (15 %) and β-mercaptoethanol (70 µM). The medium was sterile-filtered (Millex GV, 0.22 µm) and used within one week after preparation. For imaging, MIN6 cells were seeded into 8-well LabTek microscope dishes (155411 Thermo Scientific) or 40 mm coverslips (Menzel Gläser, Braunschweig, Germany). For *in vitro* assays, MIN6 cells were seeded into ∅ 60 mm or ∅ 35 mm dishes (Nunc delta surface, cat# 150288 / cat# 153066; Roskilde, Denmark) to form pseudoislets within 5 days after seeding. MIN6 cells were used from passages 26 - 36.

A population of MIN6 cells was cultured in the presence of stable isotope-labeled amino acids. Minimal medium, depleted of L-tyrosine, L-tryptophan and L-phenylalanine (Cell Culture Technologies (Switzerland)) was supplemented with stable isotope-labeled (^{15}N) amino acids L-tyrosine, L-tryptophan and L-phenylalanine (0.4 mM, 0.08 mM and 0.4 mM final concentrations, Fig. A10 (appendix)). The pH was adjusted to 7.0 and the medium was sterile-filtered. Prior to use, the medium was supplemented with FBS (15 %) and β-mercaptoethanol (70 µM).

6.3.2. Isolation of mouse primary β-cells

Female Ctrl : CD1 (ICR, outbred) mice (supplied by Carles River Laboratories, cat# CD1S1FE07W) served as donors for primary β-cells that were isolated as previously described [70]. In short, mice were sacrificed by cervical dislocation. A collagenase solution (1 mg/mL) was injected into the pancreatic duct, followed by extraction of the pancreas from the animal and digestion at 37 °C for 10 min. A Histopague gradient (1.083 and 1.119 g/mL) allowed for the isolation of pancreatic islets via density gradient centrifugation. Islets were incubated in RPMI medium (supplemented with 10 % FCS, 100 U/mL penicillin and 100 mg/mL streptomycin) for 24 h. Trypsin digestion (5 min, 37 °C) dissociated islets into single β-cells that were seeded into LabTeks, pre-coated with poly-L-lysine. Animals were housed in the EMBL animal facilities under veterinarian supervision and the guidelines of the European Commission, revised directive 2010/63/EU and AVMA guidelines 2007.

6.3.3. Mouse insulin ELISA

The quantification of insulin secretion was based on an enzyme-linked immunosorbent assay (ELISA) in 96-well format. For the quantification of insulin release from MIN6 or mouse primary β-cells, a mouse insulin ELISA kit (serial number: 10-1247, Mercodia AB, Uppsala, Sweden) was applied. Insulin release from INS-1 cells was measured using a rat insulin ELISA kit (serial number: 10-1250, Mercodia AB, Uppsala, Sweden). Experiments for the determination of insulin secretion were performed in quadruplicate per condition, following the instructions of the supplier. Insulin levels were normalized to the protein content of MIN6 cells, as determined by a BCA assay (Pierce^{TM} BCA Protein assay kit, Thermo Scientific, Rockford, IL, USA). Artifacts of BSA on insulin measurements were corrected according to Fig. A23 (appendix).

6.4. Fluorescence microscopy and spectrophotometry

6.4.1. Confocal laser scanning microscopy

Live cell imaging was performed on a FluoView1200 (Olympus IX83) confocal laser scanning microscope, equipped up with an environment box (made by EMBL) to allow imaging at 37 °C and 5 % CO_2. Olympus 60x Plan-APON (NA 1.4, oil) or 20x UPLS APO (NA 0.75, air) objectives and FluoView software (version 4.2) were applied. Images were acquired using a Hamamatsu C9100-50 EM CCD camera. A 488 nm laser line (120 mW/cm^2, 2.5 %) in combination with a 525/50 emission mirror was applied to image the green channel. A 559 nm laser line (120 mW/cm^2, 2.0 %) and a 643/50 emission filter were used for red channel recordings. A pulsed UV laser line (375 nm, 10 MHz) was applied for uncaging experiments on live cells. Uncaging was performed in the entire field of view for 8 frames (frame time of uncaging: 3.2 s/fame). A dual-scanner set-up allowed for image acquisition of cellular responses during UV stimulation. For monitoring changes of $[Ca^{2+}]_i$ in response to external stimuli, cells were incubated with the acetoxymethyl ester of the Ca^{2+} indicator Fluo-4 (Life Technologies, Eugene, OR), 5 µM in DMEM (1 g/L glucose) for 25 min at 37 °C and 5 % CO_2. The frame time was set to 3.9 s, with images acquired in 4 s intervals. For imaging, MIN6 cells were grown as pseudoislets of ~70 % confluence. Imaging experiments were performed in HEPES buffer (in mM: 115 NaCl, 1.2 $CaCl_2$, 1.2 $MgCl_2$, 1.2 K_2HPO_4 and 20 HEPES, pH 7.4).

6.4.2. Imaging of intracellular cAMP levels using the EPAC sensor

For monitoring changes of intracellular cAMP levels upon TAAR1 stimulation, MIN6 cells were transiently transfected with Epac^{3rd} [mTurquoise-Epac(CD,delDEP)-^{cp173}Venus-Venus] [258]. For this, we used Lipofectamine 3000, following the guidelines of the supplier. Stimuli were applied to cells in 25 µM final concentrations in the presence of 11 mM glucose. Imaging was performed on an Olympus FV1200 microscope, using an Olympus 60x Plan-APON (NA 1.4, oil) objective in a sealed chamber (EMBL incubation box) at 37 ºC and 5 % CO_2. Settings: Frame time: 5 s with 10.0 µs/pixel (640x640 pixels), laser power 1.5 %, pinhole: 600 µm. Epac^{3rd} was excited at $\lambda = 405$ nm. Optical filters were applied for mTurquoise (λ = 450 - 490 nm) and for Venus ($\lambda = 510 - 560$ nm) emission. FRET values are presented as the ratio between donor and acceptor signals. The FRET ratio was set to 1 at the time point immediately before addition of the stimulus. At the end of each experiment, a mix of the adenylate cyclase activator forskolin and the phosphodiesterase inhibitor 3-isobutyl-1-methylxanthine (IBMX) (50 µM, each) was added to MIN6 cells to evoke maximum cAMP responses.

6.4.3. Buffer transfer experiments amongst cell populations

For buffer-transfer experiments amongst different cell populations, HEPES buffer (1.5 mL, variable glucose concentrations) was pre-loaded for 30 min on 2 x10^6 MIN6 cells that were grown to pseudo-islets of ~80 % confluence in ∅ 60 mm dishes (Nunc, Roskilde, Denmark). 150 µl of this SN was transferred to LabTeks containing pre-washed MIN6 cells, stained with Fluo-4 in the presence of 150 µl buffer of the same glucose concentration (1:1 dilution).

For the determination of changes in insulin secretion in buffer transfer experiments, cells were grown in ∅ 60 mm dishes (Nunc, Roskilde, Denmark). Here, 1.5 mL of SN was transferred from a population of 2 x10^6 MIN6 cells to pre-washed target cells that resided in 1.5 mL buffer. Glucose and salt concentrations were kept constant during all transfer experiments.

6.4.4. Perfusion and static incubation of cells

MIN6 cells were seeded on 40 mm glass coverslips to form pseudo-islets within 5 days after seeding. The cover slips were mounted onto a Bioptechs FCS2 perfusion chamber (chamber volume: 0.53 cm^3, ∅ 30 mm). The perfusion system was connected to a calibrated FCS2 micro-perfusion pump, using Teflon-coated tubing. The flow rate was set to 0.15 mL/min and MIN6 cells were perfused for 30 min in the presence of 11 mM glucose.

Static incubation of MIN6 cells served as control. For this, MIN6 cells were seeded in same densities in ∅ 30 mm dishes to form pseudo-islets 5 days after seeding. MIN6 cells were incubated in buffer for 30 min. The insulin content of the collected samples was tested using insulin ELISA, following dilution of samples to balance differences of volumes.

6.4.5. Analysis of imaging data

The open access software tool Fiji [322] was applied for the extraction of fluorescence intensities from individual cells. Following background subtraction, intensities were calculated relative to the maximum detected fluorescence intensity (F/F_0). Representative traces of cells within a field of view were averaged or numbers of detected high-intensity $[Ca^{2+}]_i$ events per 60 s interval were determined. The height of each $[Ca^{2+}]_i$ event was determined relative to the highest detected peak per trace. This served as a criterion to group $[Ca^{2+}]_i$ oscillations into low-intensity (< 60 % of highest peak) and high-intensity (≥ 60 % of highest peak) events. Per condition or tested stimulus, 4 - 6 independent experiments were performed under identical settings. 30 - 100 individual representative MIN6 or 60 primary *β*-cells were picked per condition and their responses were averaged. OriginLab, version 8.5 was applied for statistical analysis and plotting.

6.4.6. NRBA-based fluorescence displacement assay

FAF-BSA (10 µM) and Nile red 2-*O*-butyric acid (NRBA) were pre-incubated in 1:1 ratio at 37 °C for 20 min. NRBA has a high affinity for hydrophobic protein domains. Protein binding of NRBA induces a turn-on of fluorescence emission, along with a shift to shorter wavelengths [270]. 2 x10^6 MIN6 cells were incubated in buffer (11 mM glucose) to allow for the accumulation of FAs. The FA-containing buffer was concentrated to 10 % of its original volume (Labconco concentrator, cat# 7310032, Fort Scott, USA) and added on top of FAF-BSA that was pre-loaded with NBRA. Measurements were performed on a quantamaster QM4/2000SE Photon Technology International spectrofluorometer in combination with 150 µL quartz cuvettes. The excitation wavelength was set to λ = 540 nm. Full emission scans were recorded (λ = 550 – 750 nm) with 2 nm step intervals and 0.2 s integration time.

6.5. Extraction and MS analysis of FAs

6.5.1. Preparation of biological samples for FA extraction

1 x10^6 MIN6 cells were seeded in ∅ 60 mm dishes to form pseudoislets within 5 days of incubation at 37 °C, 5 % CO_2. MIN6 cells were pre-stimulated with buffer in the presence of 11 mM glucose for 30 min at 37 °C. Buffer (1.6 mL, supplemented with BSA, 11 mM glucose) was incubated on MIN6 cells for 20 min at 37 °C. 1.5 mL of this SN were concentrated to 120 µL (4 °C, Labconco concentrator, cat# 7310032, Fort Scott, US). MIN6 cells were then scraped in 120 µL buffer.

6.5.2. MeOH / $CHCl_3$-based FA extraction

A MeOH / $CHCl_3$-based procedure was applied for the extraction of FAs from SNs of MIN6 cells, according to [323]. The entire procedure was performed at 4 °C. 750 µL of ice-cold mix A (4.48 mL MeOH, 2.42 mL $CHCl_3$ and 0.236 mL HCl (1 N)) were added to biological samples, followed by vortexing (30 s per sample). Stable isotope-labeled internal standards ^{13}C-palmitic acid (100 ng/sample), ^{13}C-oleic acid (50 ng/sample) and ^{13}C-decanoic acid (25 ng/sample) were added in 30 µL MeOH per sample as references for the absolute quantification of FAs. 2 M HCl (170 µL) and $CHCl_3$ (725 µL, ice-cold) were added, followed by vortexing (30 s per sample). A two-phase system was generated upon centrifugation (8,000 x g (10 min, 4 °C)), with an upper aqueous layer and a protein band at the interface. The lower (organic) phase was collected in a fresh tube. 708 µL of ice-cold mix B (7.2 mL $CHCl_3$, 3.6 mL MeOH and 2.7 mL 0.01 M HCl) were added to the lower phase. Following centrifugation, (8,000 x g, 10 min, 4 °C), the upper phase was removed and the samples were dried at 4 °C (Labconco concentrator, cat# 7310032, Fort Scott, US). To avoid contamination with palmitate from applied plastics, all applied materials were pre-rinsed with MeOH, according to [267]. Only solvents of the highest analytical grade were applied for extractions and MS analyses.

6.5.3. Liquid chromatography-mass spectrometry (FAs)

Liquid chromatography-mass spectrometry (LC-MS) analysis was performed on a Q-Exactive plus HRMS in ESI negative mode (Thermo Scientific, MA, USA), coupled to a Vanquish UHPLC system (Thermo Fisher Scientific, MA, USA). For the separation of FAs, an Agilent Poroshell column (3x50 mm; 2.7 µm) was applied with the flow rate set to 0.26 mL/min at 40 °C. The mobile phases consisted of acetonitrile:water (6:4) (mobile phase A) and isopropyl alcohol:acetonitrile (9:1) (mobile phase B), supplemented with 10 mM ammonium acetate as a buffer. The UHPLC

system was run in gradient-mode (Table 1). HRMS full scan detected FAs at the mass resolving power R = 70000 in a mass range of 100 - 1200 *m/z*. Data-dependent tandem (MS/MS) mass scans were obtained along with full scans using higher energy collisional dissociation (HCD) with normalized collision energies of 10, 20 and 30 units at the mass resolving power R = 17500.

6.5.4. MS parameters (FAs)

The MS parameters in the Tune software (Thermo Scientific) were set to: spray voltage 4 kV, sheath gas 30 units and auxiliary gas 5 units, S-Lens 65 eV, capillary temperature 320 °C and vaporization temperature of auxiliary gas 300 °C. Data-dependent tandem mass spectra (MS/MS) were obtained for all precursors from an inclusion list. Only background-corrected data is presented.

6.5.5. MS quality controls and analysis sequence (FAs)

All samples were randomized for the LC-MS analysis sequence. Pooled quality controls were included, which contained combined equal volumes of samples that were processed together with others. At the beginning of each sample analysis sequence and after each 6 samples, multiple QC and blank samples were injected in order to stabilize the LC-MS system and to ensure the stability of instrument and analytical method (%CV < 20) throughout the analysis sequence.

6.5.6. MS data analysis (FAs)

Data analysis, including the generation of extracted ion chromatograms (XIC), peak integration and raw data visualization, was performed using the Xcalibur Quan software (Thermo Scientific). The detected exact mass ($\pm$ 5 ppm) and the retention time were matched with respective internal standards to confirm the identity of each FA peak in deprotonated form [M - H^+]. All data were evaluated for the consistency of peak integration. Manual integration was performed whenever necessary. The peak area of the detected analyte to the peak area of the stable isotope-labeled internal standard was used for absolute quantifications. The collected LC-MS data were evaluated using the Xcalibur software tool (Thermo Fisher).

Table 1. Applied gradient for LC-MS analysis of FA extracts. The mobile phase consisted of acetonitrile:H_2O (6:4) (mobile phase A) and isopropyl alcohol:acetonitrile (9:1) (mobile phase B), buffered with 10 mM ammonium acetate.

Time [min]	% mobile phase B
0	20
1.5	20
4	45
5	52
7	66
8	70
9	75
9.5	97
12	97
13	20
15	20

6.6. Extraction and MS analysis of TAs

6.6.1. Cleaning of plastics in advance of extraction

For the reduction of background signal in MS screens, herein applied 2 mL PCR-grade Eppendorf tubes were cleaned in a MeOH/EtOAc-based procedure. Centrifuge tubes were sonicated in 10 % formic acid (H_2O) for 20 min, followed by washing with double-distilled H_2O and with MeOH. The entire procedure was repeated twice, followed by incubation of tubes in MeOH, o/n. On the next day, the same procedure was repeated with EtOAc, instead of MeOH and with incubation of tubes in EtOAc, o/n. After drying, the tubes were applied for sample collections and extractions. Only solvents of the highest analytical grade were applied for extractions and MS analyses.

6.6.2. Preparation of biological samples for TA extraction

MIN6 cells were grown in ∅ 60 mm dishes (Nuclon Delta Surface, Thermo Scientific) to form pseudo-islets of 70 - 80 % confluence within 5 days after seeding. The growth medium was removed and cells were washed twice with DPBS (1 mL) at RT. MIN6 cells were pre-stimulated with buffer (1.5 mL) for 60 min at 37 °C, 5 % CO_2. For priming of MIN6 cells in advance of application of respective stimuli, identical buffer glucose concentrations were selected in pre-

stimulation and stimulation steps. MIN6 cells were incubated in 1.5 mL buffer (+/- stimulus) for 60 min at 37 °C, 5 % CO_2.

Following stimulation, MIN6 cells were scraped in 150 µl HEPES buffer, using disposable cell lifters (Thermo Fisher). 50 µl of this were collected for BCA-based protein quantification (Pierce™ BCA Protein assay kit, Thermo Scientific, Rockford, IL, USA). The residual 100 µl were transferred to 2 mL tubes. 80 % MeOH (in H_2O), supplemented with 2 % formic acid was added and samples were incubated for 30 min at -80 °C. Samples were concentrated to complete dryness under vacuum at 4 °C, o/n. Isotope-labeled TAs were prepared as stock solutions: *β*-PEA (2-phenyl-d_5-ethylamine, 0.965 mg/mL, EtOH), tryptamine (tryptamine-*α*,*α*,*β*,*β*-d_4, 6.7 mg/mL, EtOH), synephrine (synephrine-$^{13}C_2$, ^{15}N, 100 µg/mL, DMSO), octopamine (octopamine-d_3, 1 mg/mL, EtOH) and tyramine (tyramine-d_4, 1 mg/mL, EtOH), (see Fig. A9 (appendix)). Stocks were combined to generate a heavy internal standard master mix (1 µg/mL in EtOH, in the following: hISDs mix). Heavy-isotope labelled TAs within this master mix were spiked into samples. Stocks of non-labeled TAs were prepared (2 µg/mL in EtOH) which served as references and quality controls in LC-MS measurements.

6.6.3. MeOH-based TA extraction

80 % MeOH in H_2O (375 µL), acidified with HCl (1 % final) and 2 - 4 µL of the hISDs mix (1 µg/mL in EtOH) were added to dried samples (SNs and cell pellets, each). Following vortexing, samples were sonicated for 30 min at 4 °C, followed by centrifugation at 4000 x g for 5 min at 4 °C. SN and scraped cell samples were combined in pre-cleaned 2 mL tubes. To check for background signal, 2 - 4 µl of the hISDs mix (1 µg/mL in EtOH) were extracted from cleaned 2 mL centrifuge tubes. Also, cleaned tubes without hISDs were included for extractions. Combined organic phases were dried under vacuum at 4 °C, o/n. Dry samples were stored under argon at -80 °C.

6.6.4. Liquid chromatography-mass spectrometry (TAs)

Separation of metabolites by liquid chromatography was performed on a Vanquish UHPLC system (Thermo Fisher), equipped with a Luna Omega Polar C18 column (1.6 µm, 100x2.1 mm) at a flow of 0.26 mL/min and at 40 °C. Mobile phase A consisted of 7.5 mM ammonium acetate, supplemented with 0.02 % formic acid (pH 4). Mobile phase B consisted of 7.5 mM ammonium

acetate in acetonitrile : H_2O (95:5). The applied gradient for MeOH/HCl extracted samples is listed in table 2.

Extracted samples were re-suspended in 100 µL mobile phase A. Samples were vortexed (10 s) and centrifuged at maximum speed for 2 min at RT. 100 µL of the clear SN were injected. MS was performed on a Q-Exactive Plus (Thermo Fisher) high resolution mass spectrometer (HRMS), equipped with an advanced hybrid quadrupole-Orbitrap. Ionization was achieved by electronspray ionization (ESI-MS) in positive mode (spray-voltage: 4 kV). Spectra were acquired as a full scan (60 - 900 m/z) with a resolution of 35000 (detailed parameters are listed in table 3). The collected LC-MS data were evaluated using the Xcalibur software tool (Thermo Fisher).

Table 2. Applied gradient for LC-MS analysis of TA extracts. Mobile phase A consisted of 7.5 mM ammonium acetate, supplemented with 0.02 % formic acid (pH 4), mobile phase B of 7.5 mM ammonium acetate in acetonitrile : H_2O (95:5).

Time (min)	% of mobile phase B
0	5
1	5
7	54
8	90
11	90
11.5	5
14	5

Table 3. MS parameters for TA detection.

ESI mode	positive
Scan range	full scan (60 - 900 m/z)
Resolution	35,000
Spray voltage	4 kV
S-lens RF level	65/75
Sheath gas	30
Auxiliary gas	5
Probe heater temperature	300 °C
Capillary temperature	320 °C
Injection volume	20 µL

6.6.5. MS quality controls and analysis sequence

To ensure reproducibility within measurements, three quality controls were implemented:

1) Combination of samples to ‘quality control samples’ that were included into the LC-MS analysis sequence

2) Measurement of the hISDs mix within the LC-MS analysis sequence

3) Extraction out of centrifuge tubes in the presence / absence of the hISDs mix.

7. Acknowledgement

The past 3.5 years of my life were great. EMBL is a wonderful place for science that provides an excellent working (and living) environment. Therefore, I would like to thank my supervisor Prof. Dr. Carsten Schultz for giving me the opportunity to work in his group. Carsten always left me the freedom to follow my scientific interests and to independently approach problems from many different angles. Even though sometimes thousands of miles away, he always provided support whenever it was needed. I am happy that I was given the chance to supervise highly motivated and very talented students. Therefore, I would also like to thank Kaya M. Keutler, Jana Tünnermann, Mireia Andreu, Jona Rada, Lora Nacheva, Max Fernkorn and Monica De Maria. It was always a pleasure to plan projects, to share and discuss ideas about experiments and to see how students evolve in the lab. Especially I want to thank the members of my thesis advisory committee: Dr. Anne-Claude Gavin, Prof. Dr. Andres Jäschke and Dr. Jonas Ries for their constant encouragement and good advices throughout my entire PhD. I am grateful to Prof. Dr. Jäschke for his evaluations that contributed to my admission to the 'Studienstiftung des deutschen Volkes' already during my studies and for his recommendation for the 'DECHEMA student prize' that I was awarded in 2016. On this occasion, I would also like to thank Dr. Richard Wombacher for his constant support during the past years, contributing to the 'Rainer-Rudolf prize' 2016 with his recommendation. During my PhD, I was engaged in many productive collaborations. Particularly, I would like to thank Prof. Dr. Henning J. Jessen for the shared exciting projects. I am also grateful to the EMBL core facility members Prasad Phapale (Metabolomics), Stefan Terjung and Marko Lampe (ALMF) for their constant support in mass spectrometry and microscopy.

The EMBL campus also became the center of my social life and made me meet wonderful people that became new friends. Therefore, I would like to thank the entire Schultz group, especially bigDima, Susanne, Ana, Matteo, Victoria, Mevlüt and, in particular, some 'French guy'. Aurelien, I already miss our coffee breaks and the discussions about science and life.

Scientific enthusiasm and career would be meaningless if there was no healthy fundament in life, formed by a circle of people that are unquestionably supportive and loving and helped me focusing on my interests. I want to thank my parents and my siblings for their support throughout my studies and the entire PhD. I want to thank Melanie for walking this path with me together and always giving me a warm welcome and a home after long days in the lab. Without all this constant and loving encouragement in the last almost 3 decades, I probably would not have reached this step.

8. Appendix

8.1. Publication record

This thesis is partly published in the following articles (mark first author *):

- **Hauke S***, Keutler K, Phapale P, Yushchenko DA, Schultz C. **Endogenous fatty acids are essential signaling factors of pancreatic *β*-cells and insulin secretion.** Diabetes 2018. 67(10):1986–1998.
  commentary: Poitout V. **Fatty acids and insulin secretion: From FFAR and near?** Diabetes 2018. 67(10):1932–1934.
- **Hauke S***, Keutler K, Rada J, Lagurre A, Yushchenko DA, Grandy D, Schultz C. **Trace amines are essential metabolites for the autocrine regulation of *β*-cell activity and insulin secretion.** (in preparation).
- **Hauke S***, Rada J, Schultz C. **ATP is an essential endogenous signaling factor for *β*-cell activity.** (in preparation).

Other previous or collaborative publications that are not further described in this thesis:

- **Hauke S***, Dutta AK*, Eisenbeis V, Bezold D, Bittner T, Wittwer C, Thakor D, Pavlovic I, Schultz C and Jessen HJ. **Photolysis of cell-permeant caged inositol pyrophosphates controls oscillations of cytosolic calcium in a *β*-cell line.** (Chem. Sci., in revision).
- Citir M*, **Hauke S***, Müller R, Traynor-Kaplan A, Schultz C. **Monitoring the cellular metabolism of a photo-caged phosphoinositide species with unnatural fatty acids composition and biodegradable protecting groups.** (in preparation).
- Laguerre A, **Hauke S**, Berry M, Qiu J, Kelly M, Schultz C. **Photo-release of 2-arachidonoylglycerol reveals its role in *β*-cell synchronization.** (in preparation).
- Höglinger D, Nadler A, Haberkant P, Kirkpatrick J, Schifferer M, Stein F, **Hauke S**, Porter FD, Schultz C. (2016) **Trifunctional lipid probes for comprehensive studies of single lipid species in living cells.** PNAS 2017. 114(7):1566-1571.
- Pavlovic I, Thakor DT, Vargas JR, McKinlay CJ, **Hauke S**, Anstaett P, Camuña RC, Bigler L, Gasser G, Schultz C, Wender PA, Jessen HJ. (2016) **Cellular delivery and photochemical release of a caged inositol-pyrophosphate induces PH-domain translocation *in cellulo*.** *Nat. Commun.* 2016. 7:10622.
- **Hauke S***, von Appen A, Quidwai T, Ries J, Wombacher R. **Specific protein labeling with caged fluorophores for dual-color imaging and super-resolution microscopy in living cells.** *Chem Sci* 2016. 8(1):559-566.
- Best M, Porth I, **Hauke S**, Braun F, Herten DP, Wombacher R. **Protein-specific localization of a rhodamine-based calcium-sensor in living cells.** *Org. Biomol. Chem.* 2016. 14(24):5606-5611.
- **Hauke S***, Best M*, Schmidt TT, Baalmann M, Krause A, Wombacher R. **Two-step protein labeling utilizing lipoic acid ligase and Sonogashira cross-coupling.** *Bioconjug. Chem.* 2014. 25(9):1632-1637.

Prizes

- 'DECHEMA student prize'. Aachen, 2016.
- 'Rainer Rudolph prize' for protein biochemistry and biotechnology. Halle a.d. Saale, 2016

8.2. Supplementary data

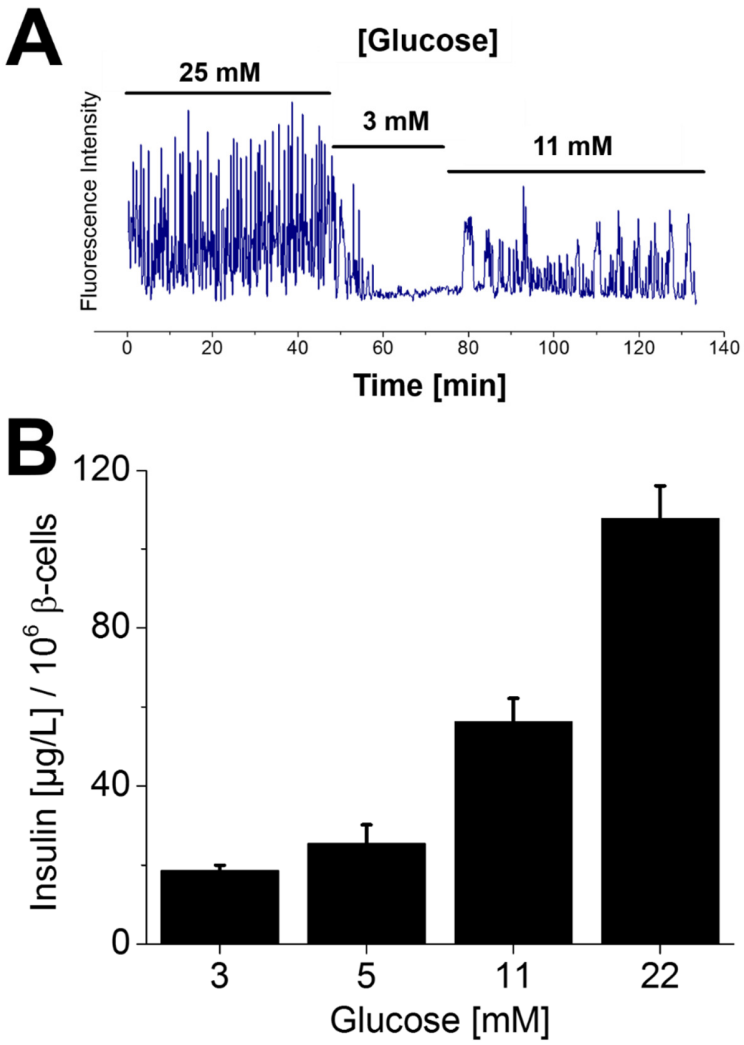

Figure A1. $[Ca^{2+}]_i$ oscillations and insulin secretion correlate with different levels of external glucose. **(A)** MIN6 cells were incubated in the presence of different levels of external glucose to monitor the dynamics of $[Ca^{2+}]_i$ oscillations and insulin secretion. Strong (25 mM glucose), intermediate (11 mM glucose) or no (3 mM glucose) $[Ca^{2+}]_i$ oscillations were detected. $[Ca^{2+}]_i$ was monitored following transient overexpression of the Ca^{2+} sensor R-GECO in MIN6 cells. **(B)** Dynamics of $[Ca^{2+}]_i$ correlated well with insulin secretion at different glucose levels. Stimulatory glucose concentrations (11 and 22 mM) yielded significantly higher insulin levels from MIN6 cells compared to sub-stimulatory glucose concentrations (3 mM and 5 mM). Insulin experiments were performed in quadruplicate. The figure was adapted from Hauke *et al.* [232].

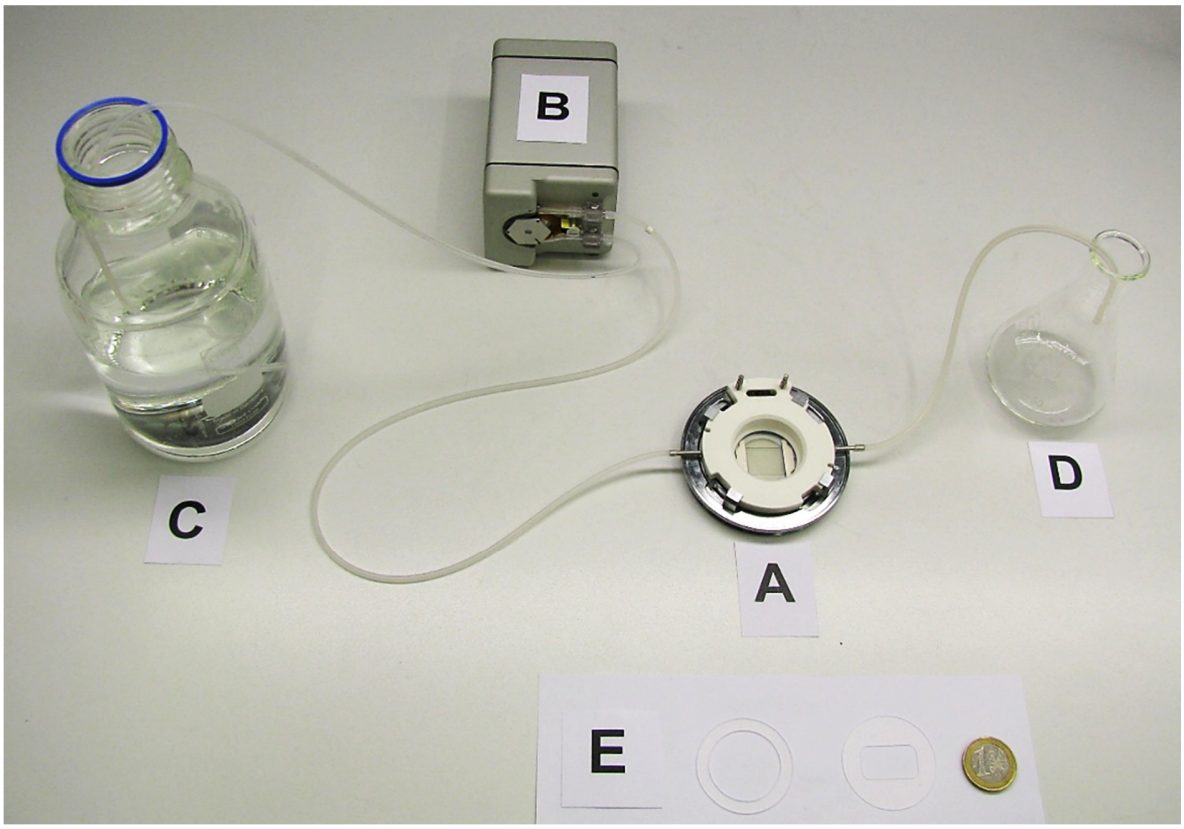

Figure A2. Set-up of the perfusion system. A calibrated pump **(B)** transfers buffer from reservoir **(C)** through the perfusion chamber **(A)** at a pre-defined constant flow rate. The flow through is collected in a reservoir **(D)**. The perfusion chamber can be assembled with gaskets of different sizes and shapes **(E)**, allowing for the adjustment of different chamber volumes and thereby the simulation of different flow conditions. The perfusion system was assembled on the stage of the herein applied Olympus confocal laser scanning microscope within the environment box. This allowed for on-line image acquisition during perfusion or buffer exchange at 37 °C. The figure was adapted from Hauke *et al.* [232].

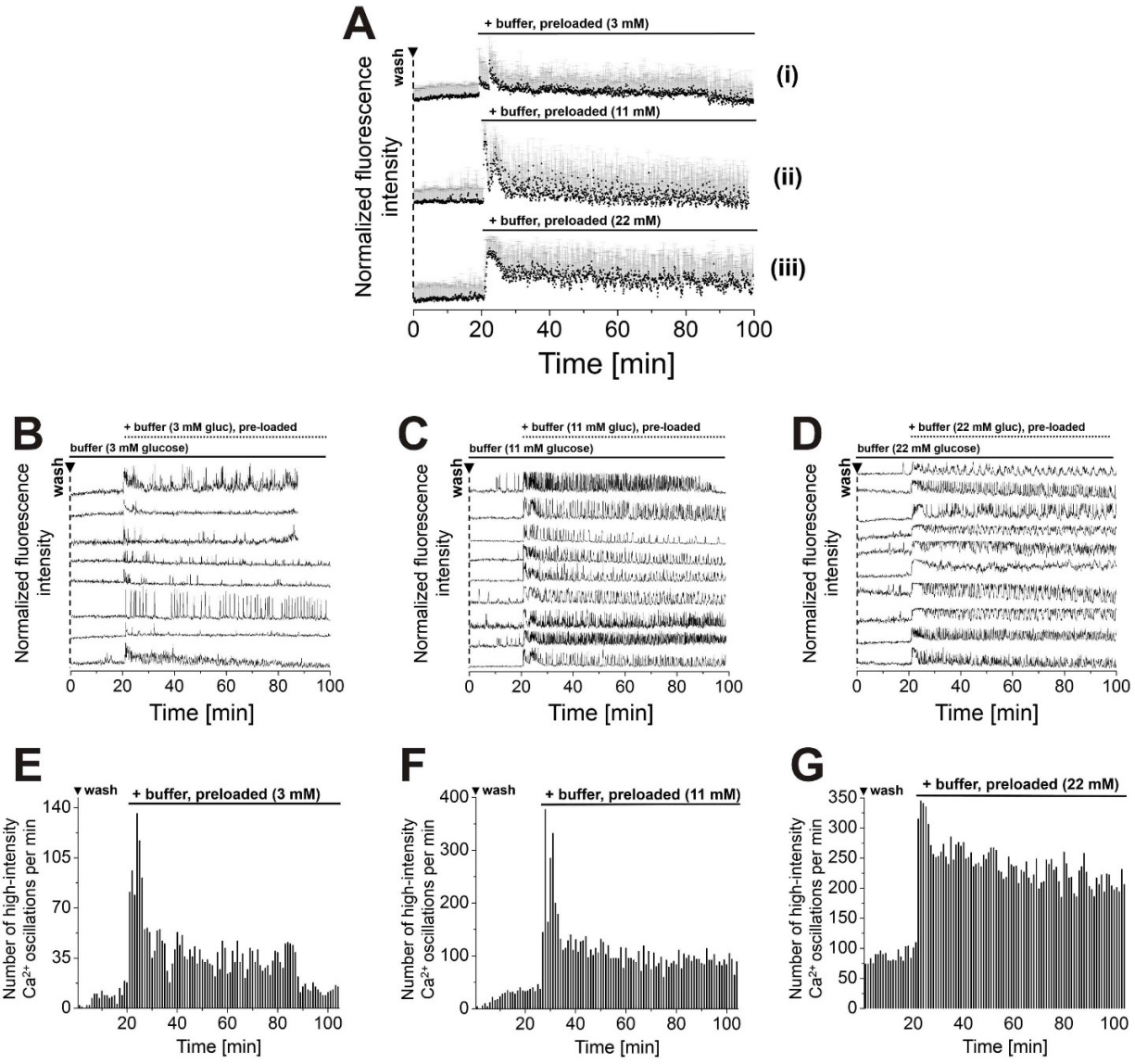

Figure A3. Addition of pre-loaded buffer to washed MIN6 cells recoveres $[Ca^{2+}]_i$ oscillations at different glucose concentrations. (A) Averaged and **(B – D)** representative individual Ca^{2+} traces from MIN6 cells. **(E – G)** Counts of detected high-intensity $[Ca^{2+}]_i$ spikes from MIN6 cells per 60 s interval. Addition of buffer (pre-loaded on a separate population of 2 x10^6 MIN6 cells for 30 min) to pre-washed MIN6 cells instantaneously recovered $[Ca^{2+}]_i$ oscillations. Transfer experiments were performed at different buffer glucose levels (as indicated). Depending on the respective applied glucose concentration, $[Ca^{2+}]_i$ oscillations recovered with different frequencies. Buffer that was pre-loaded on MIN6 cells at 3 mM glucose evoked occasional $[Ca^{2+}]_i$ transients in pre-washed MIN6 cells (**Ai**, **B** and **E**). Buffer, pre-loaded at 11 mM (**Aii**, **C** and **F**) and 22 mM (**Aiii**, **D** and **G**) glucose induced high-frequency oscillations in pre-washed MIN6 cells. Averages of n = 22 MIN6 cells per trace are presented. Ca^{2+} traces were recorded from cells that were stained with the Ca^{2+} indicator Fluo-4. Washes are indicated by ▼. The figure was adapted from Hauke *et al.* [232].

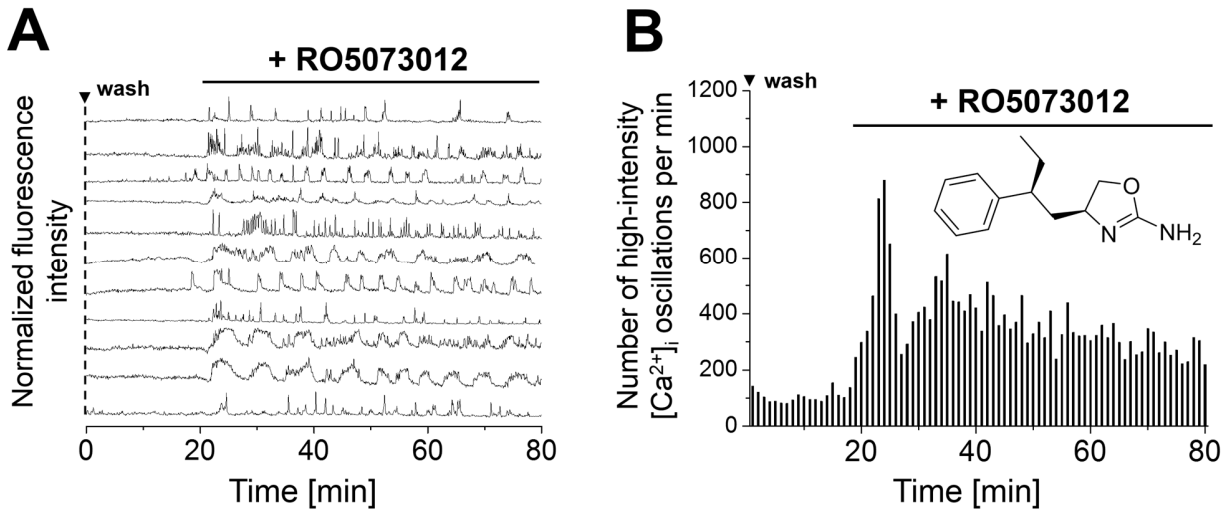

Figure A4. RO5073012 stimulates $[Ca^{2+}]_i$ oscillations in MIN6 cells. (A) Representative single Ca^{2+} traces from MIN6 cells that were stained with the Ca^{2+} indicator Fluo-4. **(B)** Counts of detected high-intensity $[Ca^{2+}]_i$ events per 60 s interval. Addition of the partial TAAR1 agonist RO5073012 (25 µM) to pre-washed MIN6 cells immediately started $[Ca^{2+}]_i$ oscillations. Imaging was performed in the presence of 11 mM glucose. Washes are indicated by ▼. The presented data was obtained from 100 MIN6 cells.

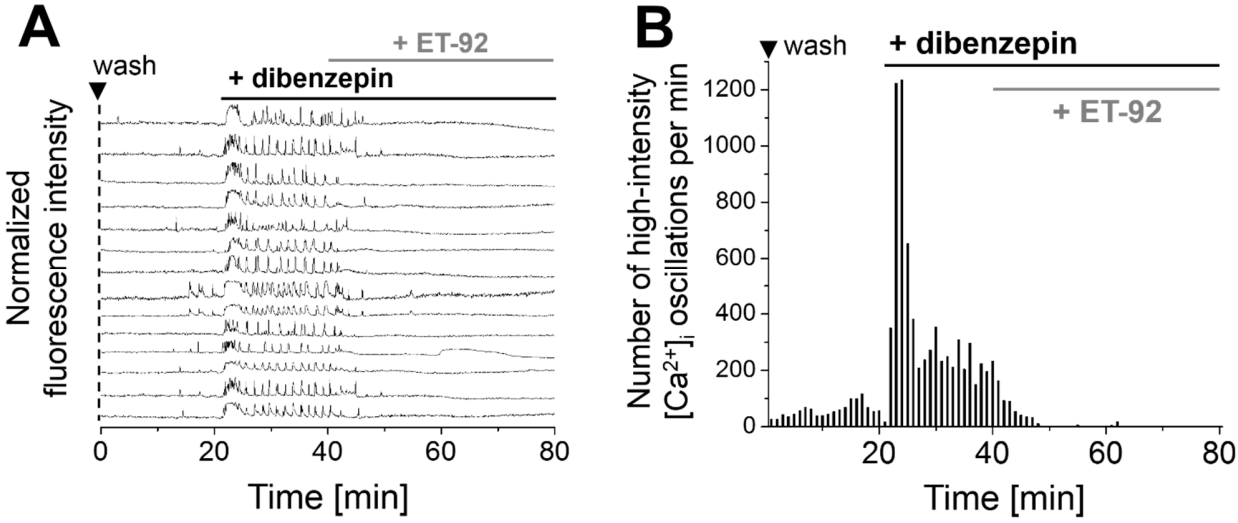

Figure A5. Modulation of $[Ca^{2+}]_i$ oscillations in MIN6 cells by dibenzepin and ET-92. (A) Representative single Ca^{2+} traces from MIN6 cells that were stained with the Ca^{2+} indicator Fluo-4. **(B)** Counts of detected high-intensity $[Ca^{2+}]_i$ events per 60 s interval. Addition of the tricyclic antidepressant dibenzepin (25 µM) to pre-washed MIN6 cells started $[Ca^{2+}]_i$ oscillations. The selective TAAR1 antagonist ET-92 (25 µM) immediately stopped $[Ca^{2+}]_i$ oscillations. Imaging was performed in the presence of 11 mM glucose. Washes are indicated by ▼. The presented data was obtained from 100 MIN6 cells.

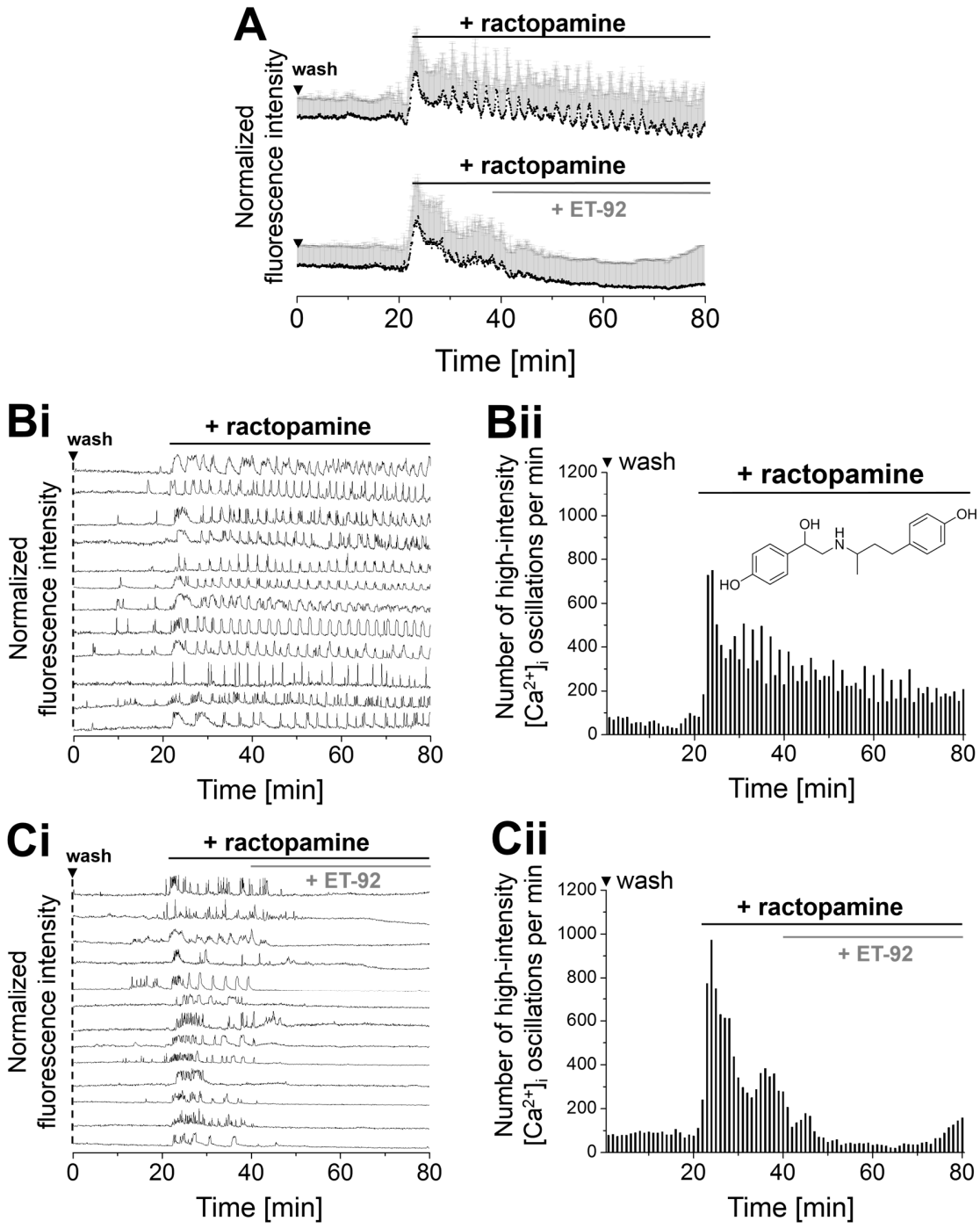

Figure A6. Addition of the feed additive and TAAR1 agonist ractopamine to pre-washed MIN6 cells stimulates $[Ca^{2+}]_i$ oscillations in pre-washed MIN6 cells. (A) Averaged and **(Bi**, **Ci)** representative single Ca^{2+} traces from MIN6 cells that were stained with the Ca^{2+} indicator Fluo-4. (**Bii**, **Cii**) Counts of detected high-intensity $[Ca^{2+}]_i$ events per 60 s interval. Addition of the TAAR1 agonist ractopamine (25 µM) to pre-washed MIN6 cells immediately evoked $[Ca^{2+}]_i$ oscillations, which were reduced upon addition of the TAAR1 antagonist ET-92 (25 µM). Imaging was performed in the presence of 11 mM glucose. Washes are indicated by ▼. The presented data was obtained from 100 MIN6 cells.

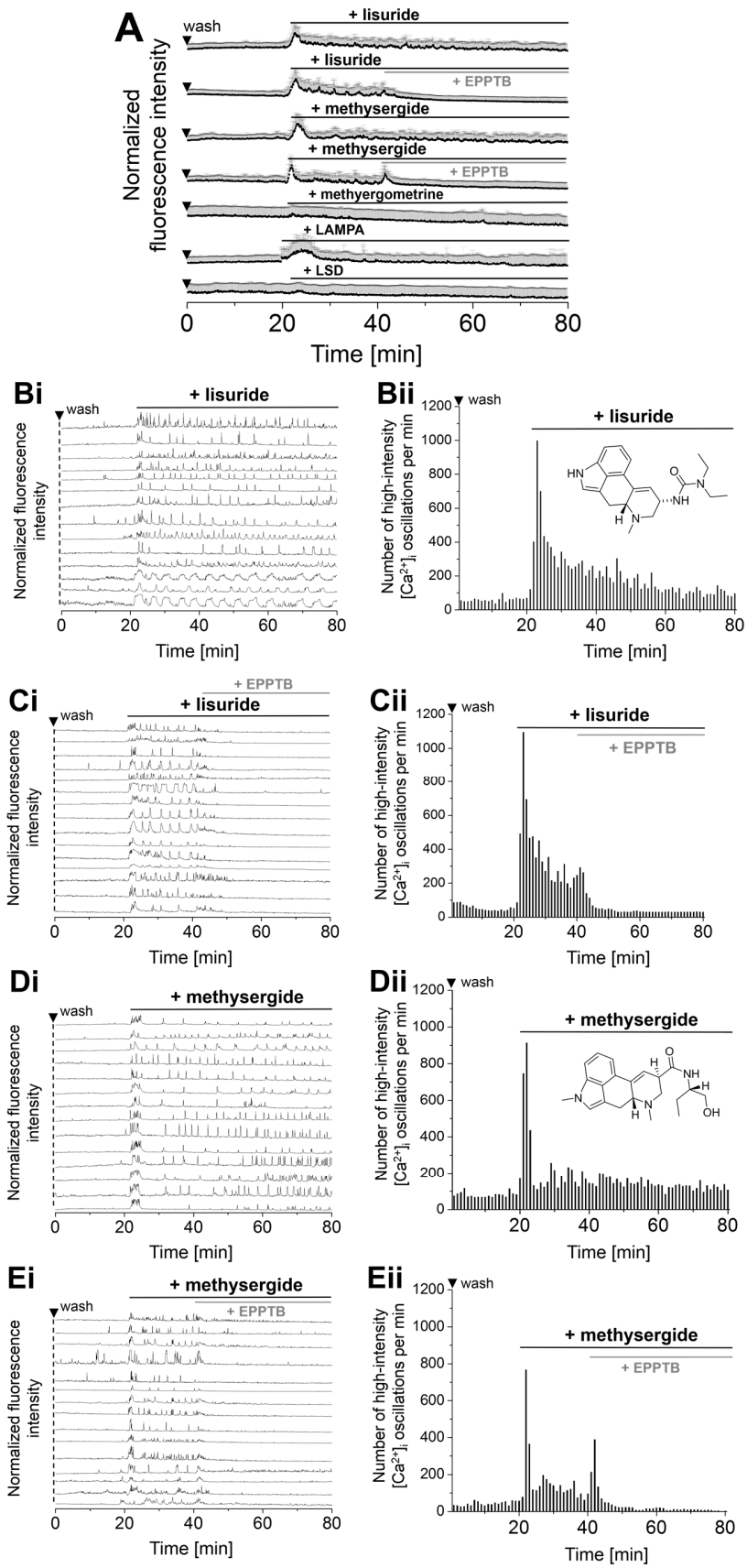
A
wash
+ lisuride
+ lisuride
+ EPPTB
+ methysergide
+ methysergide
+ EPPTB
+ methyergometrine
+ LAMPA
+ LSD
Normalized fluorescence intensity
Time [min]
Bi
Bii
Ci
Cii
Di
Dii
Ei
Eii
Normalized fluorescence intensity
Number of high-intensity [Ca2+]i oscillations per min

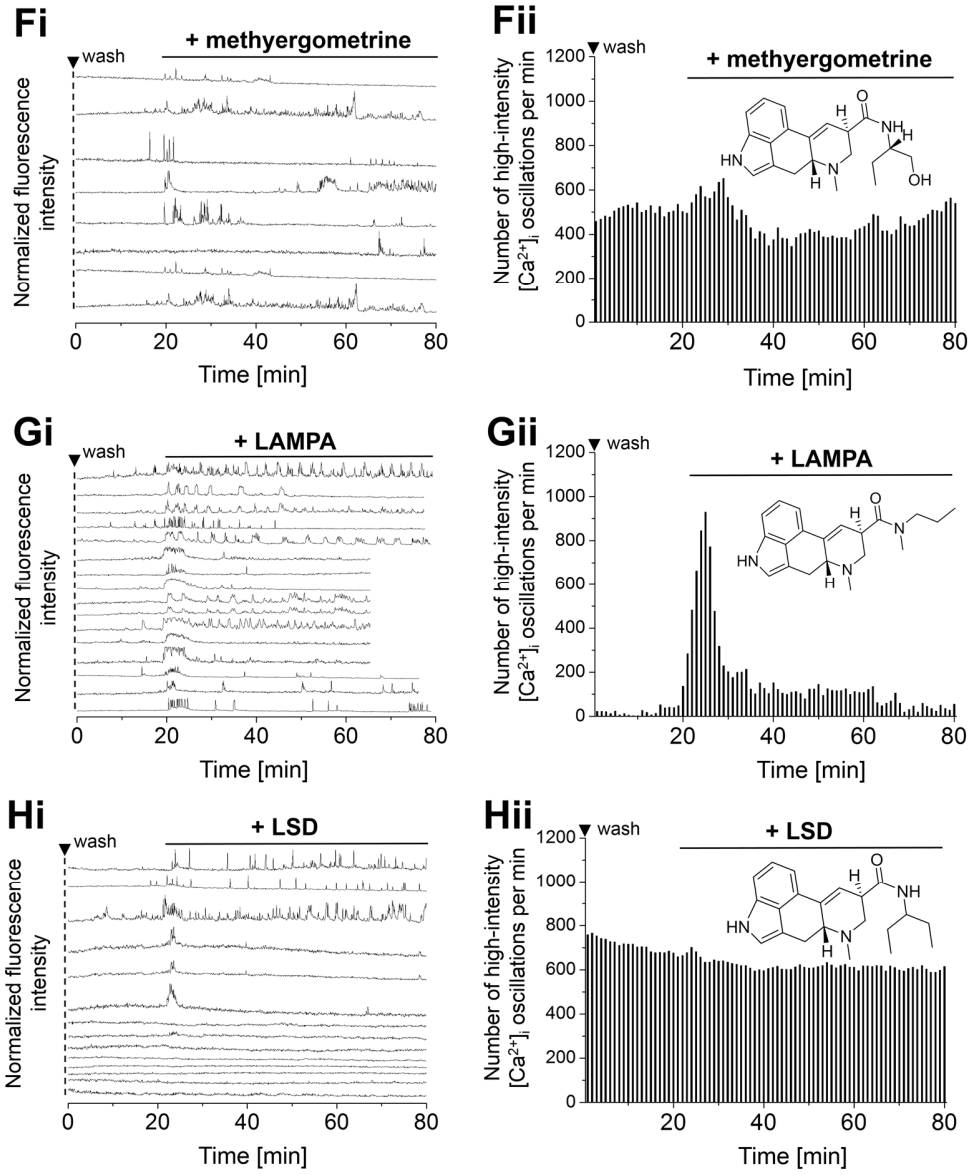

Figure A7. Ergoline (lysergic acid) derivatives show differential stimulatory effects on pre-washed MIN6 cells. **(A)** Averaged and **(Bi**, **Ci**, **Di**, **Ei, Fi**, **Hi)** representative single Ca^{2+} traces from MIN6 cells, recorded with the Ca^{2+} indicator Fluo-4. **(Bii**, **Cii**, **Dii**, **Eii, Fii**, **Hii)** Counts of detected high-intensity $[Ca^{2+}]_i$ events per 60 s interval. **(B)** Addition of the antiparkinson agent and TAAR1 agonist lisuride (25 µM) to pre-washed MIN6 cells instantaneously stimulated $[Ca^{2+}]_i$ oscillations, which were reduced upon additon of EPPTB (50 µM) **(C)**. This confirmed the role of lisuride as a TAAR1 agonist. **(D)** Addition of methysergide (25 µM, migraine treatment) to pre-washed MIN6 cells started $[Ca^{2+}]_i$ oscillations. **(E)** Addition of EPPTB (50 µM) to methysergide-treated cells reduced $[Ca^{2+}]_i$ oscillations. **(F)** The lysergic acid derivative methyergometrine (25 µM, migraine treatment) did not show stimulating effects on $[Ca^{2+}]_i$ oscillations in pre-washed MIN6 cells. **(G)** Addition of lysergic acid methylpropylamide (LAMPA, 25 µM) to pre-washed MIN6 cells induced a pronounced $[Ca^{2+}]_i$-transient that was partly followed by continuous $[Ca^{2+}]_i$ oscillations. **(H)** The lysergic acid derivative LSD induced $[Ca^{2+}]_i$ oscillations only in a minority of MIN6 cells. Imaging was performed at 11 mM glucose. The presented data was obtained from 100 MIN6 cells.

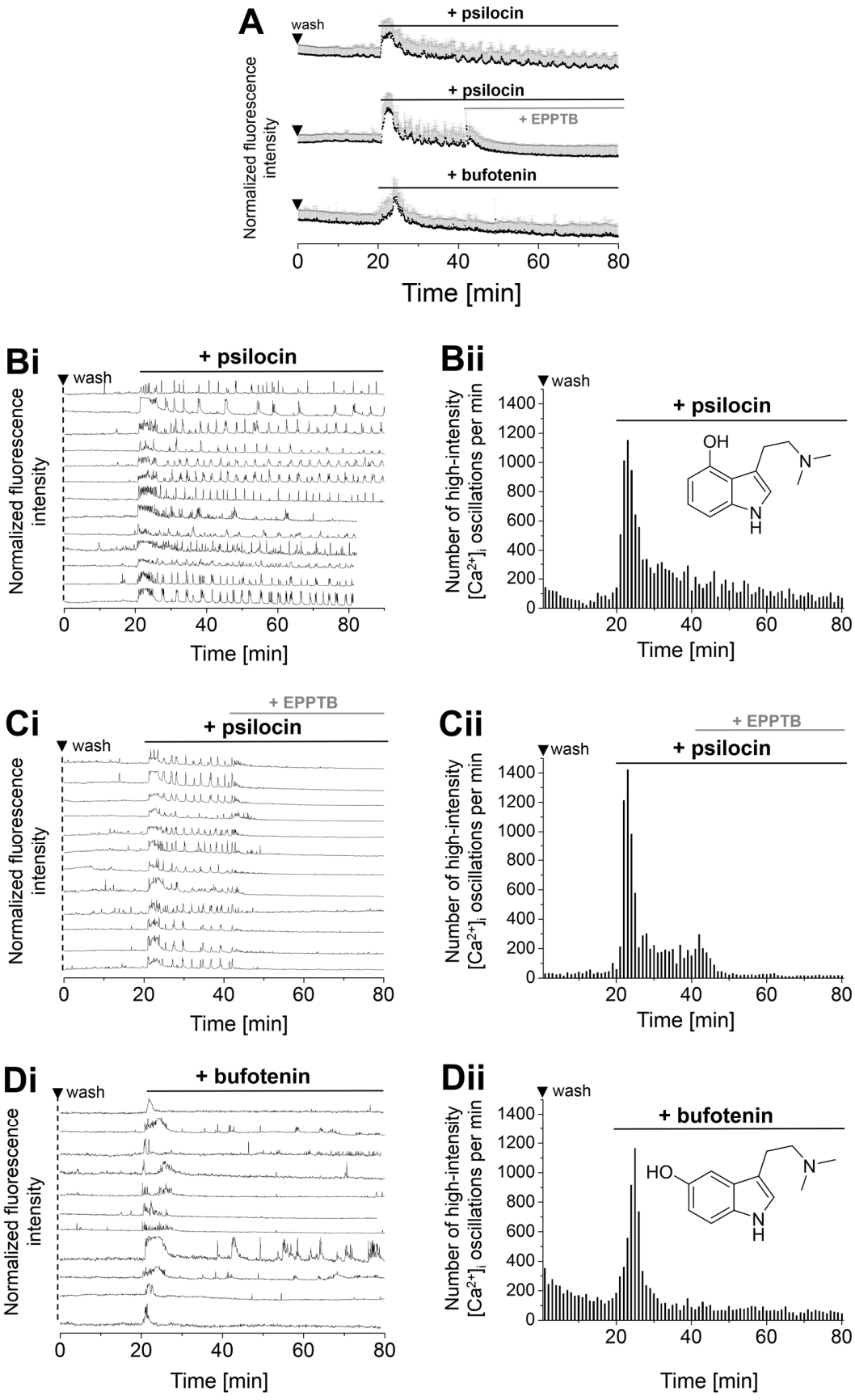
A
wash
+ psilocin
+ psilocin
+ EPPTB
+ bufotenin
Normalized fluorescence intensity
0
20
40
60
80
Time [min]
Bi
wash
+ psilocin
Normalized fluorescence intensity
Time [min]
Bii
wash
+ psilocin
OH
N
N
H
Number of high-intensity [Ca2+]i oscillations per min
0
200
400
600
800
1000
1200
1400
Time [min]
Ci
+ EPPTB
+ psilocin
wash
Normalized fluorescence intensity
Time [min]
Cii
+ EPPTB
wash
+ psilocin
Number of high-intensity [Ca2+]i oscillations per min
Time [min]
Di
wash
+ bufotenin
Normalized fluorescence intensity
Time [min]
Dii
wash
+ bufotenin
HO
N
N
H
Number of high-intensity [Ca2+]i oscillations per min
Time [min]

Figure A8. Differential modulation of $[Ca^{2+}]_i$ oscillations in MIN6 cells by the alkaloids psilocin and bufotenin. (A) Averaged and **(Bi**, **Ci**, **Di)** representative single Ca^{2+} traces from MIN6 cells, recorded with the Ca^{2+} indicator Fluo-4. **(Bii**, **Cii**, **Dii)** Counts of detected high-intensity $[Ca^{2+}]_i$ events per 60 s interval. **(B)** The psychoactive tryptamine analogue psilocin (25 µM) was added to pre-washed MIN6 cells. **(C)** Psilocin-induced stimulation of $[Ca^{2+}]_i$ oscillations was reversed by the addition of the selective TAAR1 antagonist EPPTB (50 µM), attributing psilocin-mediated effects to TAAR1 stimulation. **(D)** Addition of bufotenin (25 µM) to pre-washed MIN6 cells induced a prominent $[Ca^{2+}]_i$ transient that was not followed by continuous $[Ca^{2+}]_i$ oscillations. Washes are indicated by ▼. Imaging was performed in the presence of 11 mM glucose. The presented data was obtained from 100 MIN6 cells.

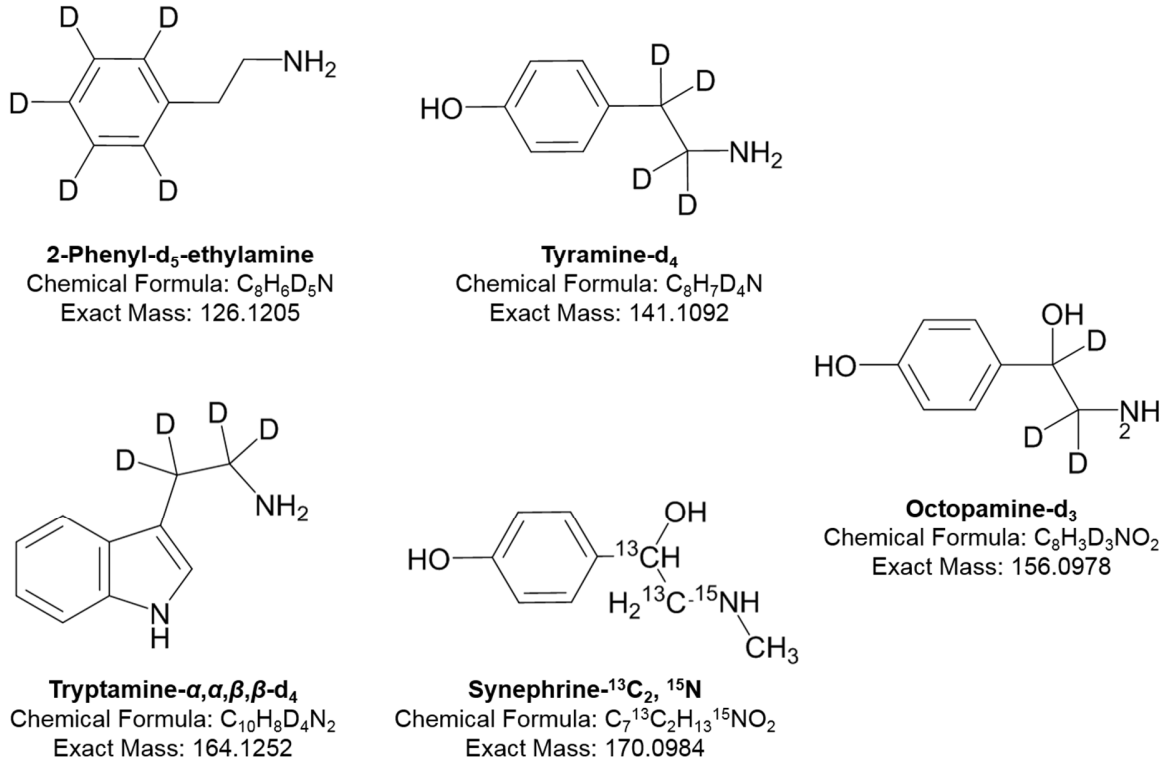

Figure A9. Overview of stable heavy isotope-labelled TAs that were applied as internal standards for the quantification of TA levels in MS screens.

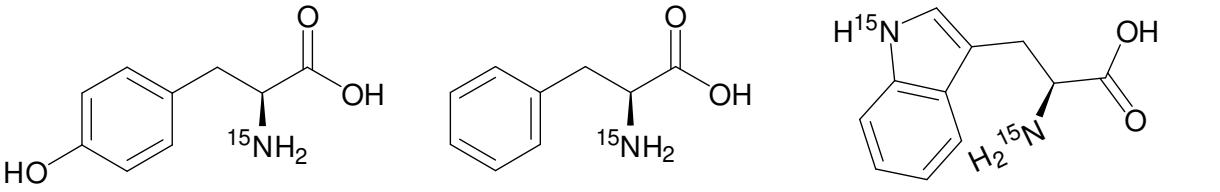

L-Tyrosine-^{15}N
Chemical Formula: $C_9H_{11}{}^{15}NO_3$
Exact Mass: 182,0709

L-Phenylalanine-^{15}N
Chemical Formula: $C_9H_{11}{}^{15}NO_2$
Exact Mass: 166,0760

L-Tryptophan-$^{15}N_2$
Chemical Formula: $C_{11}H_{12}{}^{15}N_2O_2$
Exact Mass: 206,0839

Figure A10. Overview of stable heavy isotope-labelled AAs as metabolic precursors for TAs.

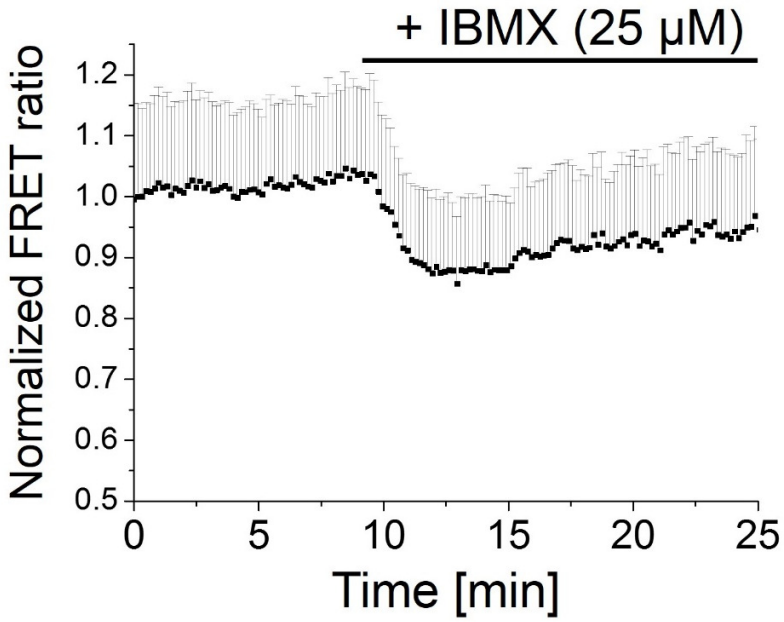

Figure A11. Changes of cAMP levels in MIN6 cells, monitored by the cyctosolic cAMP sensor Epac. Addition of the phosphodiesterase inhibitor 3-isobutyl-1-methylxanthine (IBMX, 25 µM) to glucose-stimulated MIN6 cells increased intracellular cAMP levels, indicated by a drop of the normalized FRET ratio (acceptor/donor intensity) of the EPAC sensor [258]. This indicates that cAMP is produced even under basal activity of MIN6 cells, presumably due to $G_{\alpha s}$ stimulation by endogenous agonists. Experiments and data analysis were planned and performed with J. Rada.

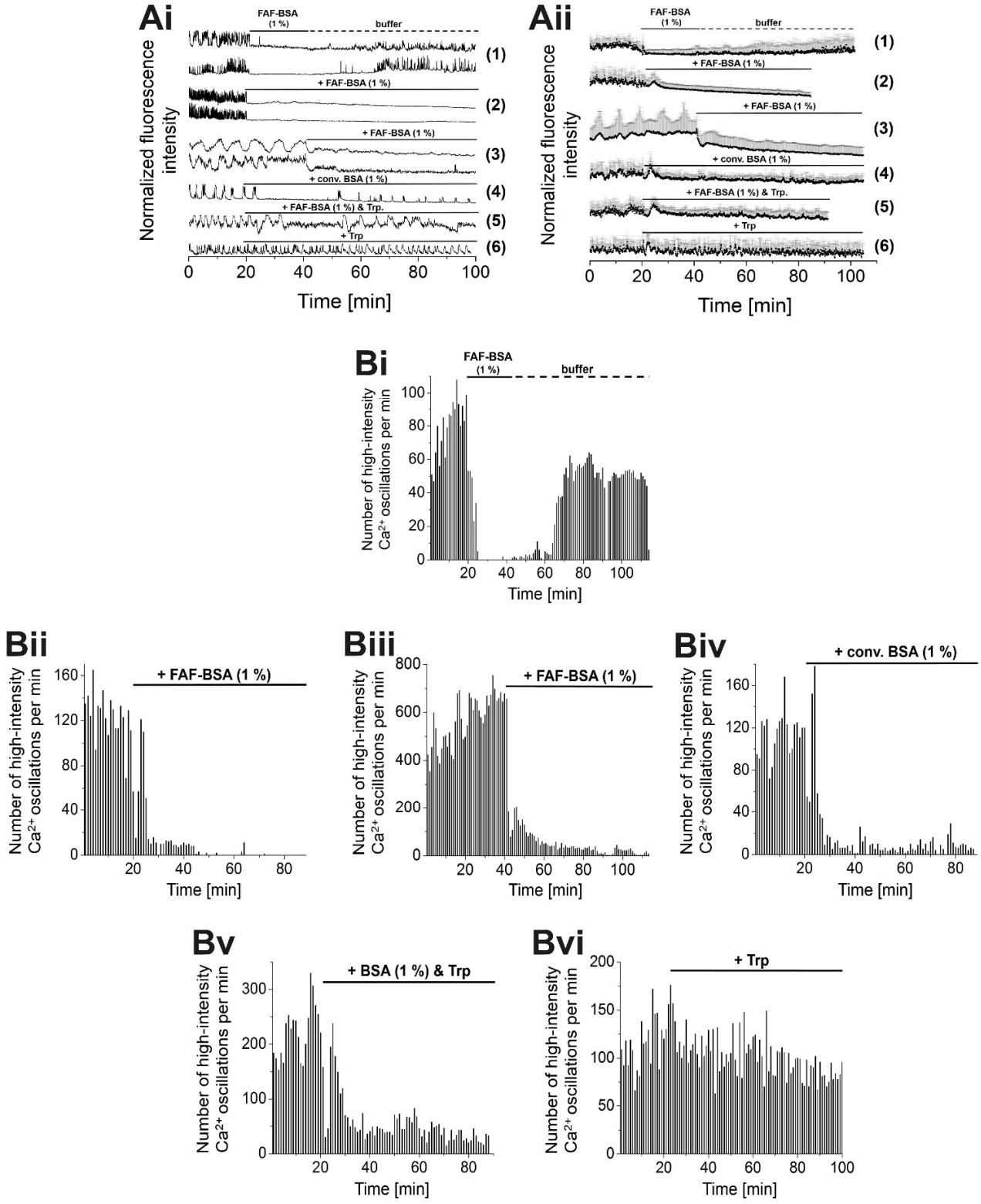
Ai
FAF-BSA (1 %)
buffer
(1)
+ FAF-BSA (1 %)
(2)
+ FAF-BSA (1 %)
(3)
+ conv. BSA (1 %)
(4)
+ FAF-BSA (1 %) & Trp.
(5)
+ Trp
(6)
Normalized fluorescence intensity
0 20 40 60 80 100
Time [min]
Aii
FAF-BSA (1 %)
buffer
(1)
+ FAF-BSA (1 %)
(2)
+ FAF-BSA (1 %)
(3)
+ conv. BSA (1 %)
(4)
+ FAF-BSA (1 %) & Trp.
(5)
+ Trp
(6)
Normalized fluorescence intensity
0 20 40 60 80 100
Time [min]
Bi
FAF-BSA (1 %)
buffer
Number of high-intensity Ca2+ oscillations per min
0 20 40 60 80 100
20 40 60 80 100
Time [min]
Bii
+ FAF-BSA (1 %)
Number of high-intensity Ca2+ oscillations per min
0 40 80 120 160
20 40 60 80
Time [min]
Biii
+ FAF-BSA (1 %)
Number of high-intensity Ca2+ oscillations per min
0 200 400 600 800
20 40 60 80 100
Time [min]
Biv
+ conv. BSA (1 %)
Number of high-intensity Ca2+ oscillations per min
0 40 80 120 160
20 40 60 80
Time [min]
Bv
+ BSA (1 %) & Trp
Number of high-intensity Ca2+ oscillations per min
0 100 200 300
20 40 60 80
Time [min]
Bvi
+ Trp
Number of high-intensity Ca2+ oscillations per min
0 50 100 150 200
20 40 60 80 100
Time [min]

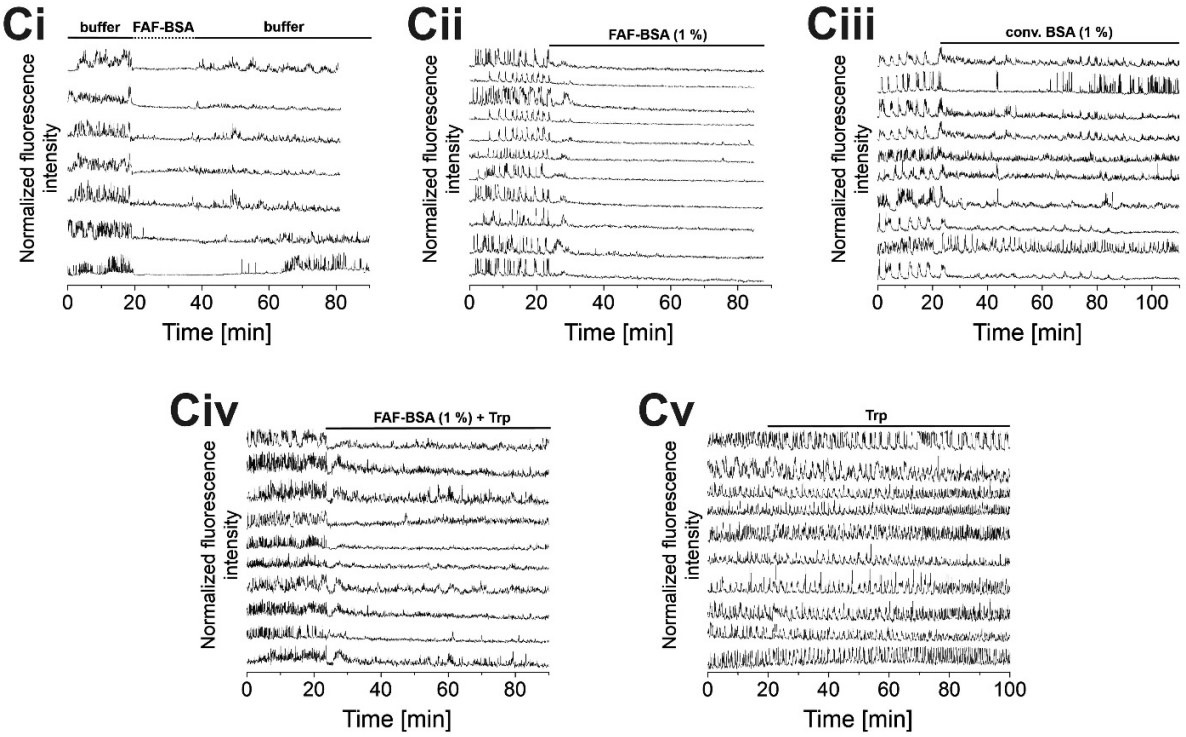

Figure A12. Fatty acid-free (FAF-)BSA (1 %) significantly reduced $[Ca^{2+}]_i$ oscillations in MIN6 and mouse primary *β*-cells. Representative individual **(Ai)** and averaged **(Aii)** Ca^{2+} traces from MIN6 and mouse primary *β*-cells. **(Bi-vi)** Counts of detected high-intensity $[Ca^{2+}]_i$ events per 60 s interval. **(Ci–v)** Individual representative Ca^{2+} traces from MIN6 cells. (**Ai+Aii 1**, **Bi**, **Ci)** $[Ca^{2+}]_i$ oscillations in MIN6 cells immediately stopped upon addition of FAF-BSA (1 %). FAF-BSA was suspected to withdraw endogenous FAs from MIN6 cells. Upon exchange of FAF-BSA by buffer, MIN6 cells slowly resumed $[Ca^{2+}]_i$ oscillations within 20-30 min. **(Ai+Aii 2&3**, **Bii+iii**, **Cii)** Addition of FAF-BSA (1 %) permanently reduced $[Ca^{2+}]_i$ oscillations within MIN6 and primary mouse *β*-cells. **(Ai+Aii 4**, **Biv**, **Ciii)** Conventional BSA (conv. BSA, 1 %) and **(Ai+Aii 5**, **Bv**, **Civ)** FAF-BSA (1 %), pre-saturated with tryptophan (Trp, 400 µM) showed moderate effects on $[Ca^{2+}]_i$ oscillations in MIN6 cells. **(Ai+Aii 6**, **Bvi**, **Cv)** Addition of only Trp (400 µM) to MIN6 cells did not affect $[Ca^{2+}]_i$ oscillations. Shown are averages of n = 13 cells for Ai+Aii 1, Bi and Ci as well as averages of n = 30 MIN6 and n = 60 primary *β*-cells for the rest. Experiments were performed in the presence of 11 mM glucose. Ca^{2+} traces were recorded from cells that were stained with the Ca^{2+} indicator Fluo-4. The figure was adapted from Hauke *et al.* [232].

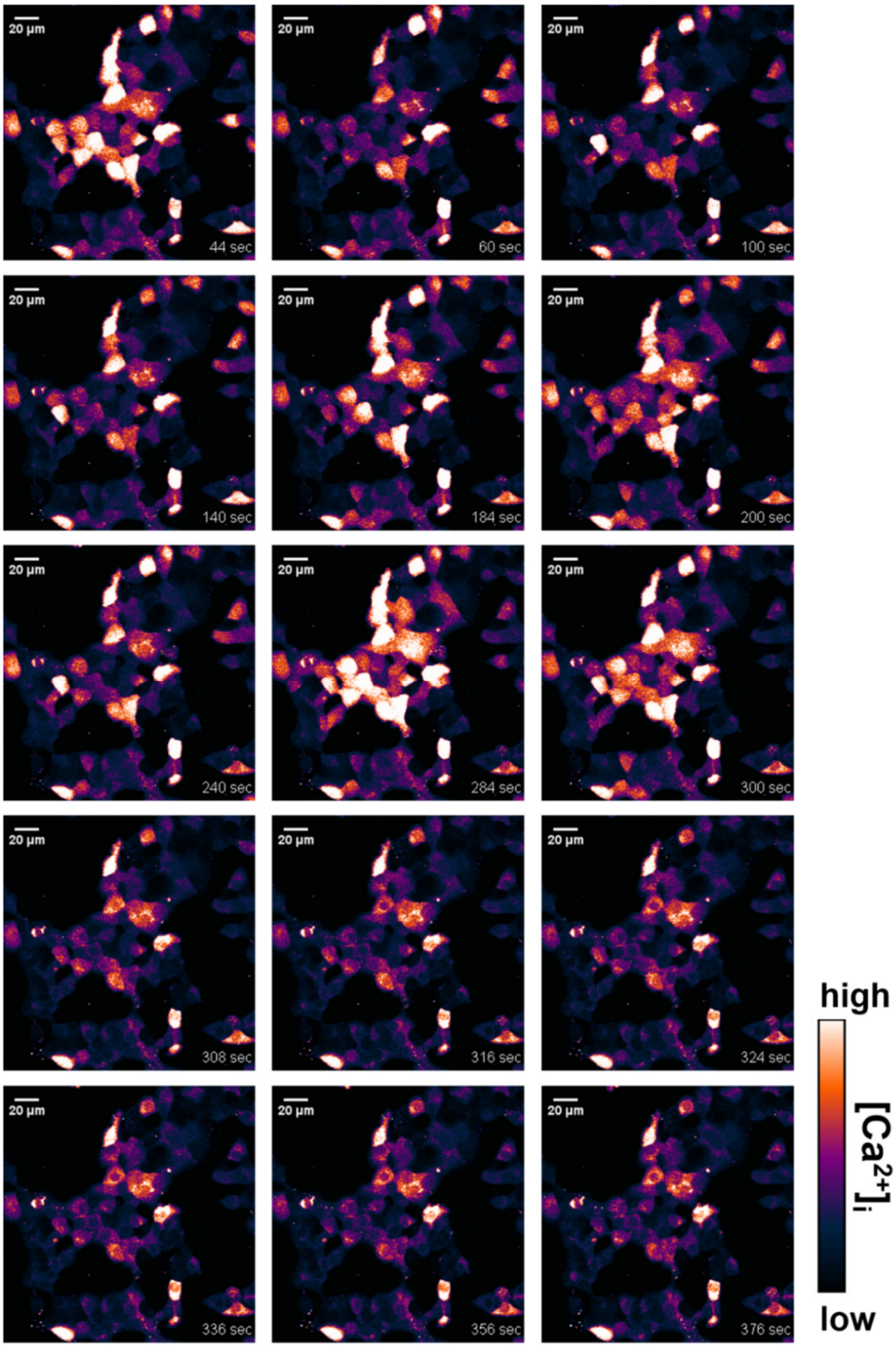

Figure A13. Immediate termination of $[Ca^{2+}]_i$ oscillations in MIN6 cells after addition of fatty acid-free (FAF-) BSA (1 %). Addition of FAF-BSA (1 %) at 300 s immediately terminated $[Ca^{2+}]_i$ oscillations in MIN6 cells that were stained with the Ca^{2+} indicator Fluo-4. Experiments were performed in the presence of 11 mM glucose. Scale bars, 20 µm.

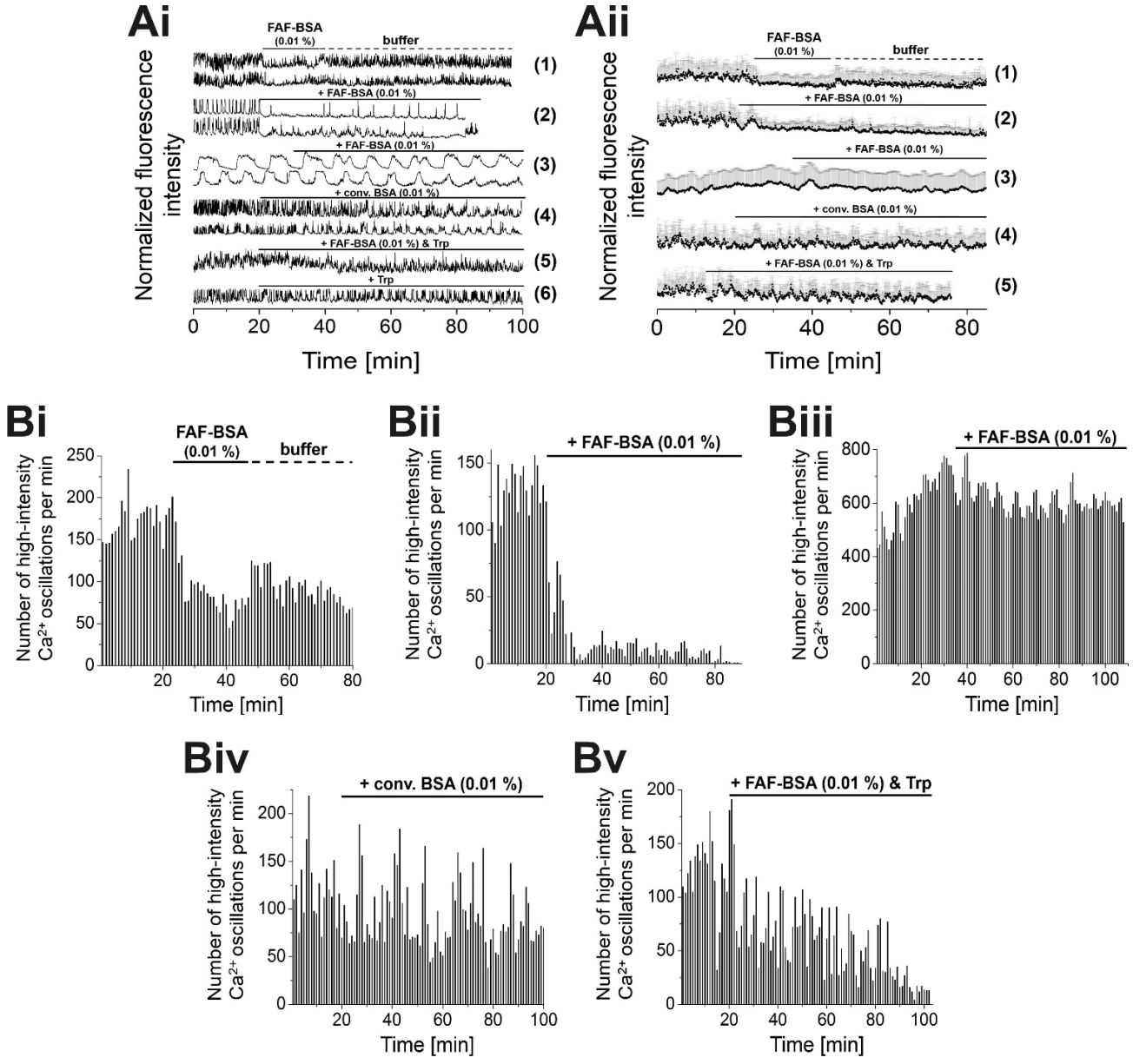
Ai
FAF-BSA
(0.01 %)
buffer
+ FAF-BSA (0.01 %)
+ FAF-BSA (0.01 %)
+ conv. BSA (0.01 %)
+ FAF-BSA (0.01 %) & Trp
+ Trp
(1)
(2)
(3)
(4)
(5)
(6)
Normalized fluorescence intensity
Time [min]
Aii
FAF-BSA
(0.01 %)
buffer
+ FAF-BSA (0.01 %)
+ FAF-BSA (0.01 %)
+ conv. BSA (0.01 %)
+ FAF-BSA (0.01 %) & Trp
(1)
(2)
(3)
(4)
(5)
Normalized fluorescence intensity
Time [min]
Bi
FAF-BSA
(0.01 %)
buffer
Number of high-intensity Ca2+ oscillations per min
Time [min]
Bii
+ FAF-BSA (0.01 %)
Number of high-intensity Ca2+ oscillations per min
Time [min]
Biii
+ FAF-BSA (0.01 %)
Number of high-intensity Ca2+ oscillations per min
Time [min]
Biv
+ conv. BSA (0.01 %)
Number of high-intensity Ca2+ oscillations per min
Time [min]
Bv
+ FAF-BSA (0.01 %) & Trp
Number of high-intensity Ca2+ oscillations per min
Time [min]

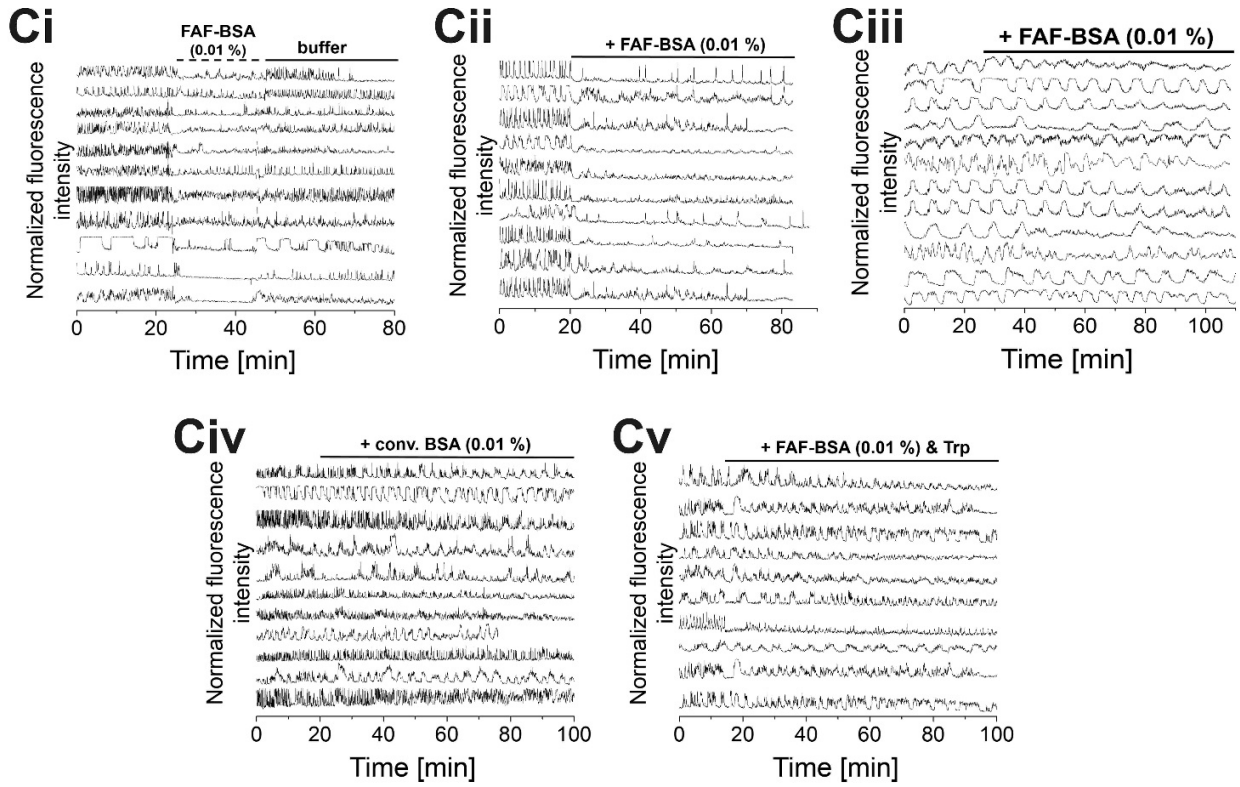

Figure A14. Application of (FAF-)BSA at 0.01 % to glucose-stimulated MIN6 cells showed moderate effects on $[Ca^{2+}]_i$ oscillations. Representative individual **(Ai)** and averaged **(Aii)** Ca^{2+} traces from MIN6 and mouse primary β-cells. **(Bi-v)** Counts of detected high-intensity $[Ca^{2+}]_i$ events per 60 s interval. **(Ci – v)** Individual representative Ca^{2+} traces from MIN6 and mouse primary β-cells. (**Ai+Aii 1**, **Bi**, **Ci)** Addition of FAF-BSA (0.01 %) to glucose-stimulated MIN6 cells showed only minor effects on $[Ca^{2+}]_i$ oscillations. Exchange of FAF-BSA (0.01 %) by buffer immediately resumed $[Ca^{2+}]_i$ oscillations in MIN6 cells. Moderate or missing reduction of $[Ca^{2+}]_i$ oscillations upon addition of FAF-BSA to **(Ai+Aii 2**, **Bii**, **Cii)** MIN6 and **(Ai+Aii 3**, **Biii**, **Ciii)** primary β-cells. **(Ai+Aii 4**, **Biv**, **Civ)** Conventional BSA (conv. BSA, 0.01 %) or **(Ai+Aii 5**, **Bv**, **Cv)** FAF-BSA (0.01 %) that was pre-saturated with tryptophan (Trp, 400 µM) caused moderate effects on $[Ca^{2+}]_i$ oscillations. Averages of n = 30 MIN6 and n = 60 primary β-cells are presented. Experiments were performed in the presence of 11 mM glucose. Ca^{2+} traces were recorded from cells that were stained with the Ca^{2+} indicator Fluo-4. The figure was adapted from Hauke *et al.* [232].

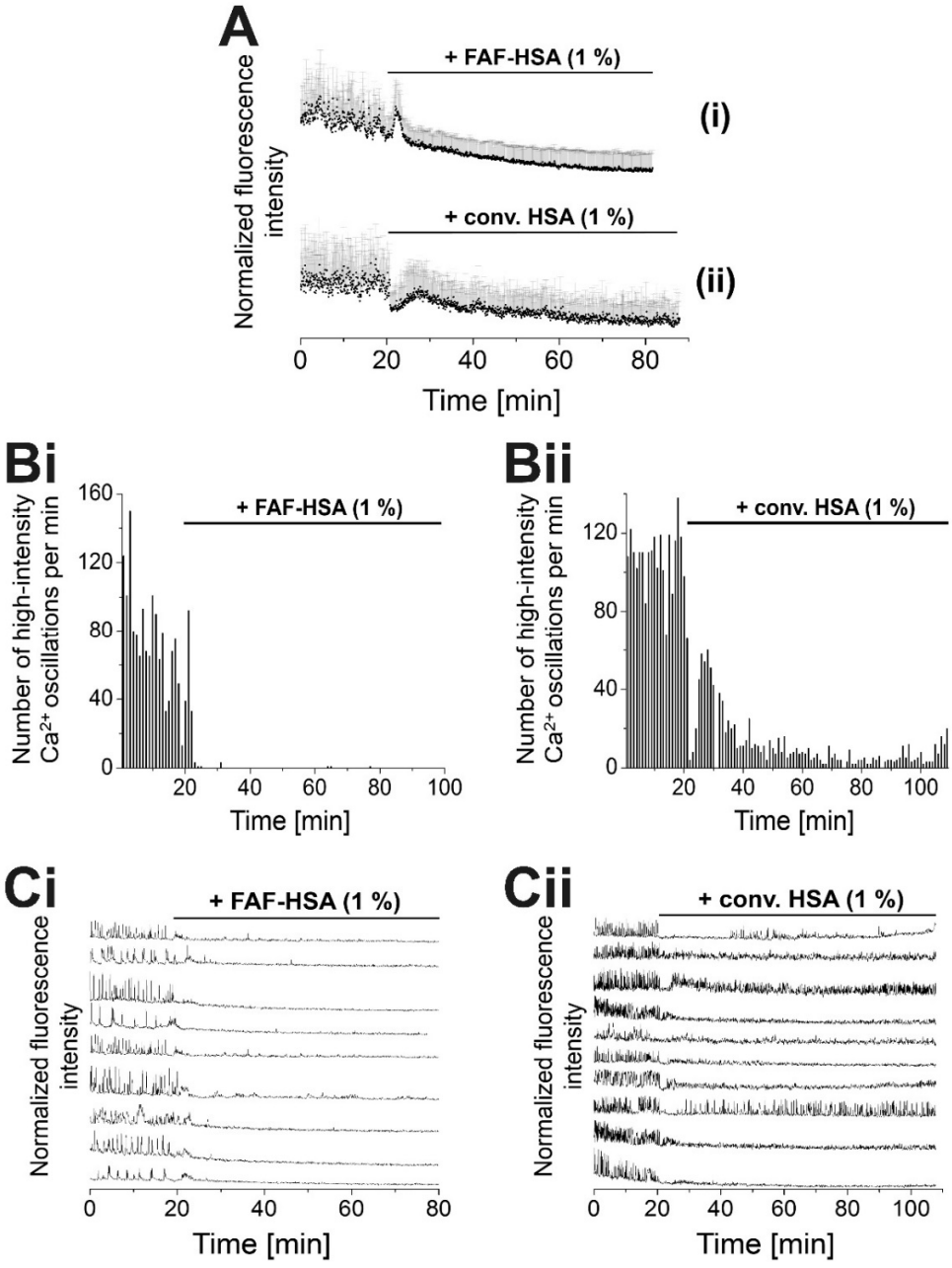

Figure A15. Human serum albumin (HSA) reduced $[Ca^{2+}]_i$ oscillations in glucose-stimulated MIN6 cells. (A) Averaged Ca^{2+} traces, recorded from MIN6 cells. **(Bi + ii)** Counts of detected high-intensity $[Ca^{2+}]_i$ events per 60 s interval. **(Ci+ii)** Representative individual Ca^{2+} traces from MIN6 cells, recorded with the Ca^{2+} indicator Fluo-4. **(Ai**, **Bi** and **Ci)** Fatty acid-free human serum albumin (FAF-HSA, 1 %) potently reduced $[Ca^{2+}]_i$ oscillations in glucose-stimulated MIN6 cells. **(Aii**, **Bii** and **Cii)** $[Ca^{2+}]_i$ oscillations were reduced but not terminated by the addition of conventional human serum albumin (conv. HSA, 1 %). These observations are in line with findings from BSA. Shown are averages of n = 30 MIN6 cells. Experiments were performed in the presence of 11 mM glucose. Ca^{2+} traces were recorded from cells that were stained with the Ca^{2+} indicator Fluo-4. The figure was adapted from Hauke *et al.* [232].

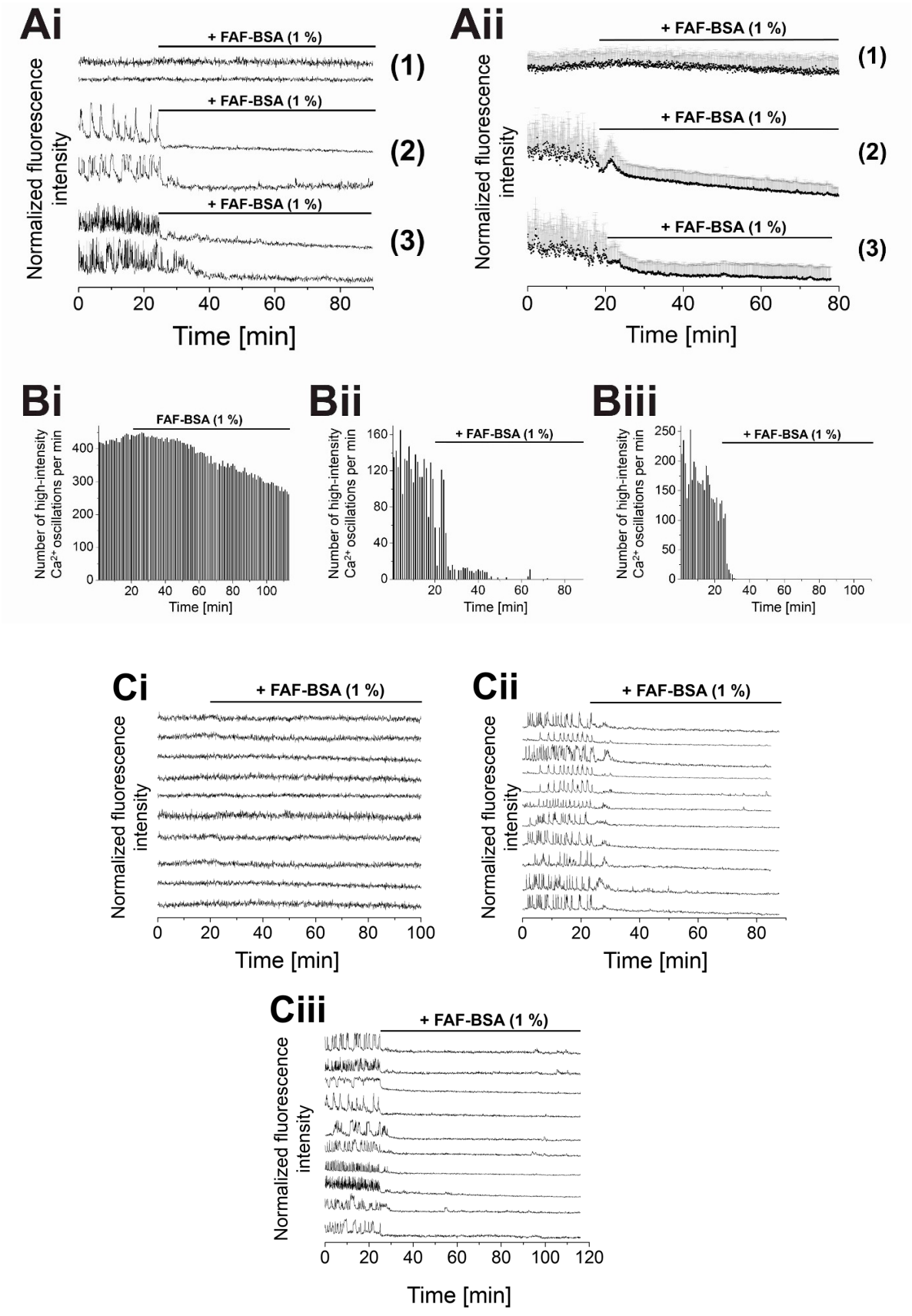
Ai
+ FAF-BSA (1 %)
(1)
+ FAF-BSA (1 %)
(2)
+ FAF-BSA (1 %)
(3)
Normalized fluorescence intensity
0 20 40 60 80
Time [min]
Aii
+ FAF-BSA (1 %)
(1)
+ FAF-BSA (1 %)
(2)
+ FAF-BSA (1 %)
(3)
Normalized fluorescence intensity
0 20 40 60 80
Time [min]
Bi
FAF-BSA (1 %)
Number of high-intensity Ca2+ oscillations per min
0 100 200 300 400
20 40 60 80 100
Time [min]
Bii
+ FAF-BSA (1 %)
Number of high-intensity Ca2+ oscillations per min
0 40 80 120 160
20 40 60 80
Time [min]
Biii
+ FAF-BSA (1 %)
Number of high-intensity Ca2+ oscillations per min
0 50 100 150 200 250
20 40 60 80 100
Time [min]
Ci
+ FAF-BSA (1 %)
Normalized fluorescence intensity
0 20 40 60 80 100
Time [min]
Cii
+ FAF-BSA (1 %)
Normalized fluorescence intensity
0 20 40 60 80
Time [min]
Ciii
+ FAF-BSA (1 %)
Normalized fluorescence intensity
0 20 40 60 80 100 120
Time [min]

Figure A16. FAF-BSA-mediated effects on $[Ca^{2+}]_i$ oscillations are independent of the applied buffer glucose concentration. **(Ai+ii)** Representative individual **(Ai)** and averaged **(Aii)** Ca^{2+} traces from MIN6 cells. **(Bi-iii)** Counts of detected high-intensity $[Ca^{2+}]_i$ events per 60 s interval. **(Ci-iii)** Representative, individual Ca^{2+} traces from MIN6 cells, stained with the Ca^{2+} indicator Fluo-4. FAF-BSA, applied in 1 % final concentrations, immediately stopped $[Ca^{2+}]_i$ oscillations of glucose-stimulated MIN6 cells (11 mM **(Ai+ii 2**, **Bii** and **Cii)** and 22 mM **(Ai+ii 3**, **Biii** and **Ciii)**). **(Ai+ii 1**, **Bi** and **Ci)** Non-oscillating MIN6 cells in the presence of 3 mM glucose were not affected by FAF-BSA (1 %). Shown are averages of n = 30 MIN6 cells. Experiments were performed in the presence of 11 mM glucose. Ca^{2+} traces were recorded from cells that were stained with the Ca^{2+} indicator Fluo-4. The figure was adapted from Hauke *et al.* [232].

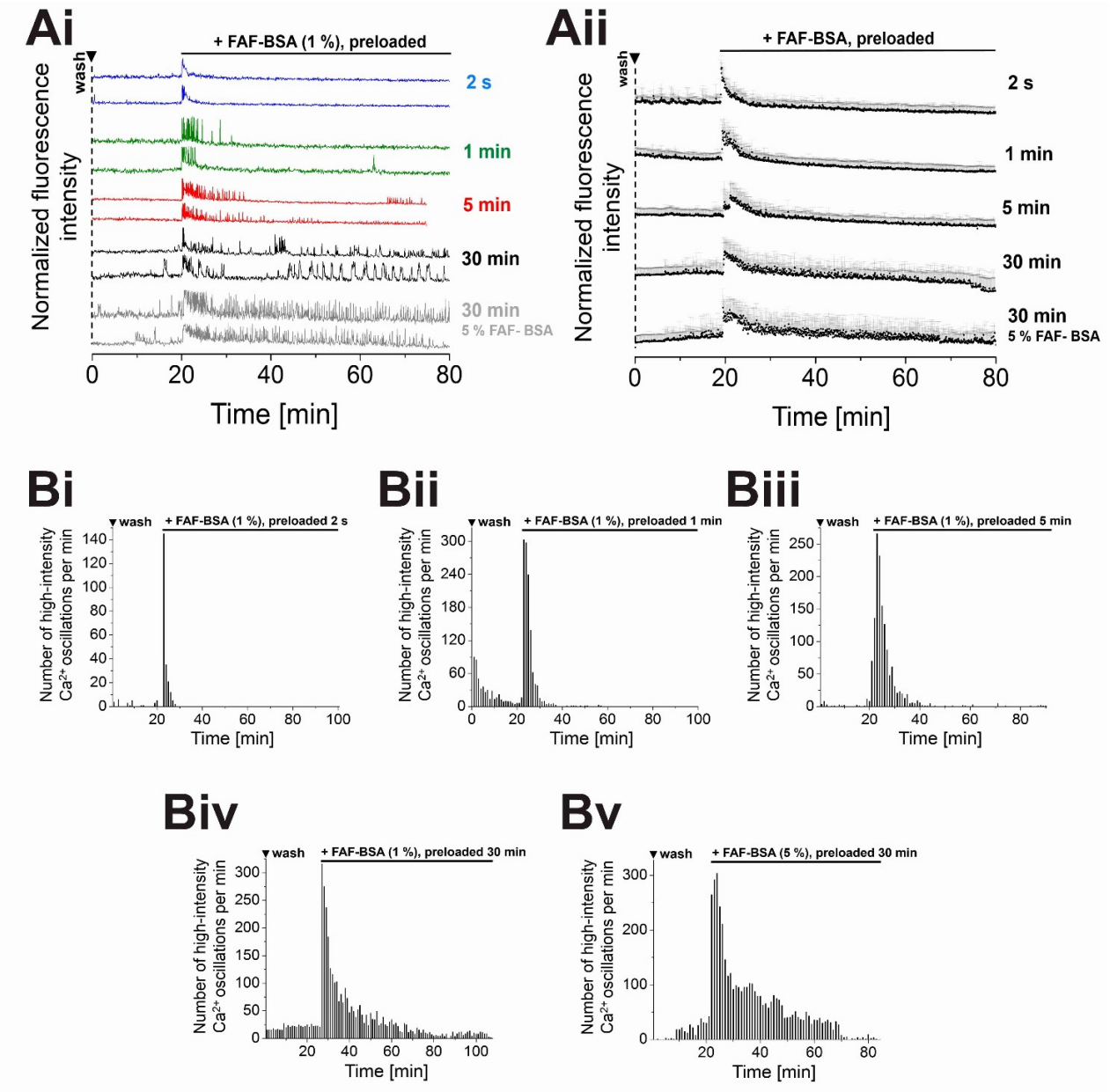

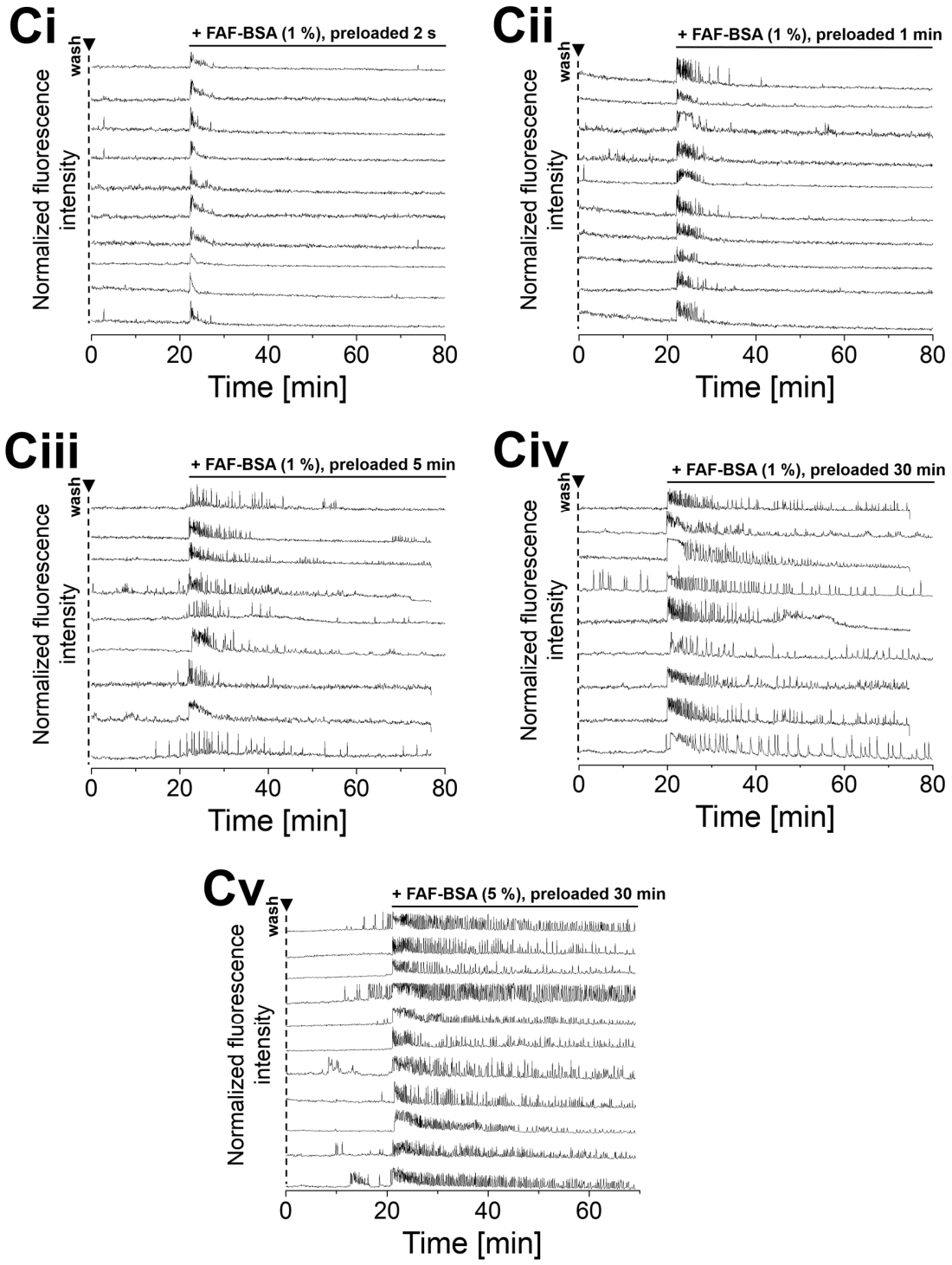

Figure A17. The stimulating effect of pre-loaded FAF-BSA on $[Ca^{2+}]_i$ oscillations upon transfer to pre-washed MIN6 cells is determined by pre-incubation times on another population of MIN6 cells. Representative **(Ai)** individual and **(Aii)** averaged Ca^{2+} traces from MIN6 cells. **(Bi-v)** Counts of detected high-intensity $[Ca^{2+}]_i$ events per 60 s interval. **(Ci-v)** Representative individual Ca^{2+} traces from MIN6 cells, recorded with the Ca^{2+} indicator Fluo-4. (**Ai** + **Aii**) The stimulating effect of FAF-BSA (pre-loaded on 2 x10^6

MIN6 cells) correlates with the pre-loading period and thereby also with the amount of loaded and transferred FAs (from t = 2 s to 30 min (**Bi-iv**, **Ci-iv**)). Pre-incubation times are indicated on the right. In line with that, induced effects were enhanced with increasing concentrations of transferred FAF-BSA (5 %, **Ai** + **Aii**, **Bv** and **Cv**). Stringent washing is indicated by ▼. Averages of n = 30 MIN6 cells are shown. Experiments were performed in the presence of 11 mM glucose. Ca^{2+} traces were recorded from cells that were stained with the Ca^{2+} indicator Fluo-4. The figure was adapted from Hauke *et al.* [232].

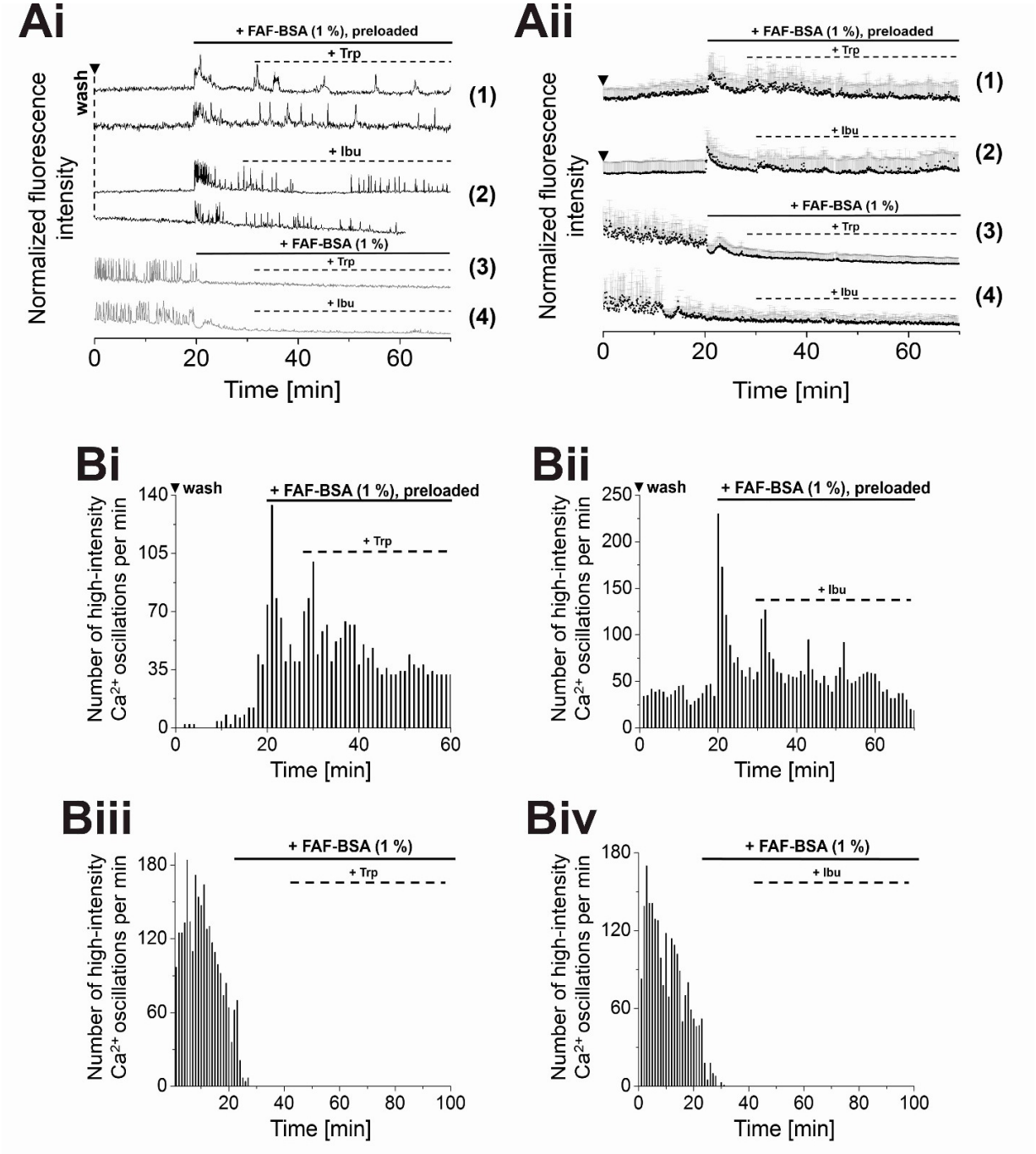

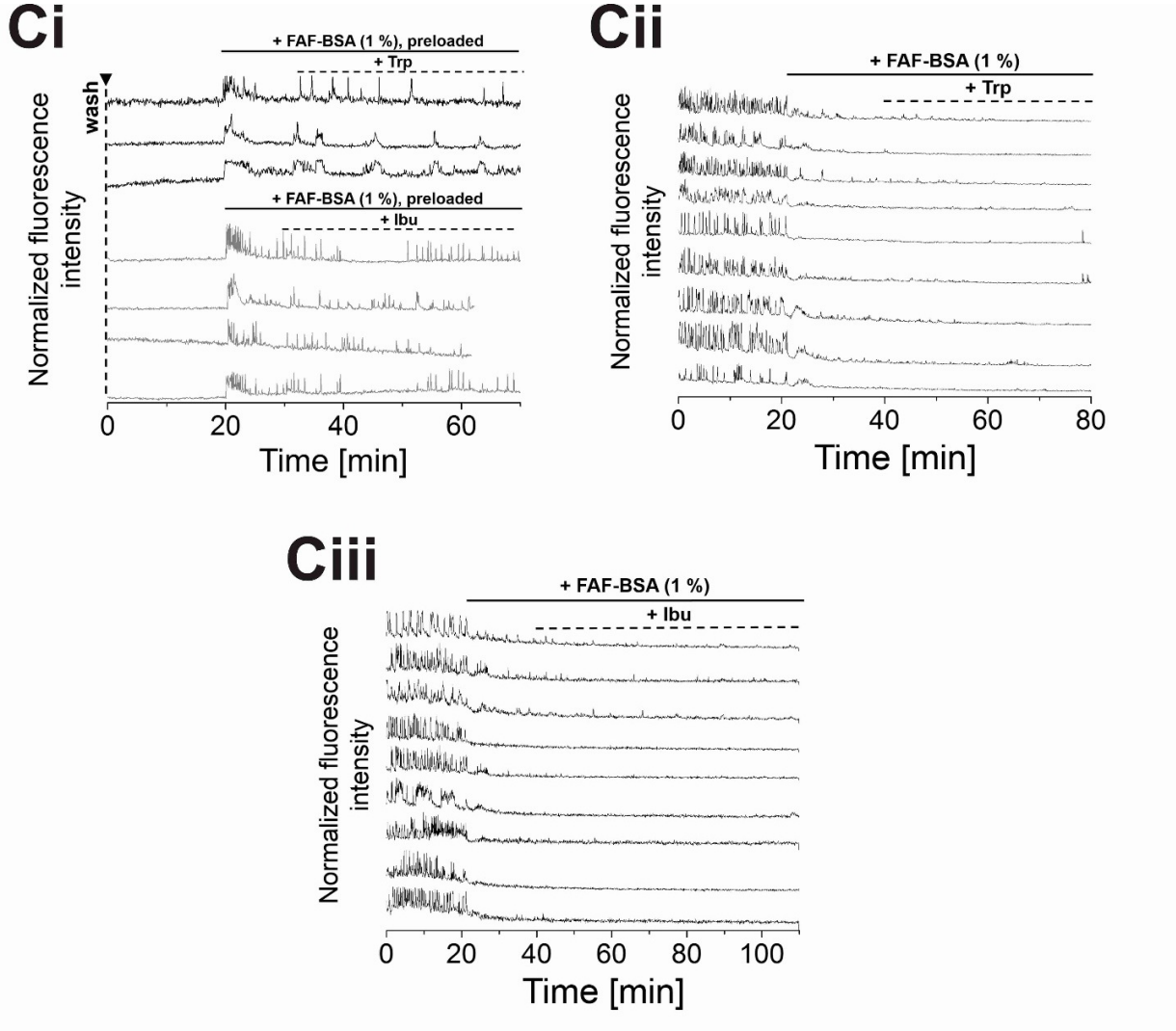

Figure A18. Stimulation of $[Ca^{2+}]_i$ oscillations by the out-competition of FAs from pre-loaded FAF-BSA. (Ai) Representative individual and **(Aii)** averaged Ca^{2+} traces from MIN6 cells. **(Bi-iv)** Counts of detected high-intensity $[Ca^{2+}]_i$ events per 60 s interval. **(Ci-iii)** Representative, individual Ca^{2+} traces from MIN6 cells. Transferred FAF-BSA (1 %) was pre-loaded on a population of on 2 x10^6 MIN6 cells (30 min at 37 °C). (**Ai+Aii 1+2**, **Bi+ii** and **Ci**) Treatment of washed MIN6 cells with pre-loaded FAF-BSA induced prominent $[Ca^{2+}]_i$ transients. Addition of albumin-binders tryptophan (Trp) and ibuprofen (Ibu) (400 µM, each) to MIN6 cells in the presence of pre-loaded FAF-BSA immediately re-enforced $[Ca^{2+}]_i$ oscillations. This indicated that MIN6 cells were stimulated by the out-competed cargo from pre-loaded FAF-BSA. Addition of Trp (**Ai+Aii 3**, **Biii** and **Cii**) or Ibu (**Ai+Aii 4**, **Biv** and **Ciii**) in the presence of FAF-BSA (1 %) did not show comparable effects on $[Ca^{2+}]_i$ oscillations. Shown are averages of n = 30 MIN6 cells. Experiments were performed in the presence of 11 mM glucose. Ca^{2+} traces were recorded from cells that were stained with the Ca^{2+} indicator Fluo-4. The figure was adapted from Hauke *et al.* [232].

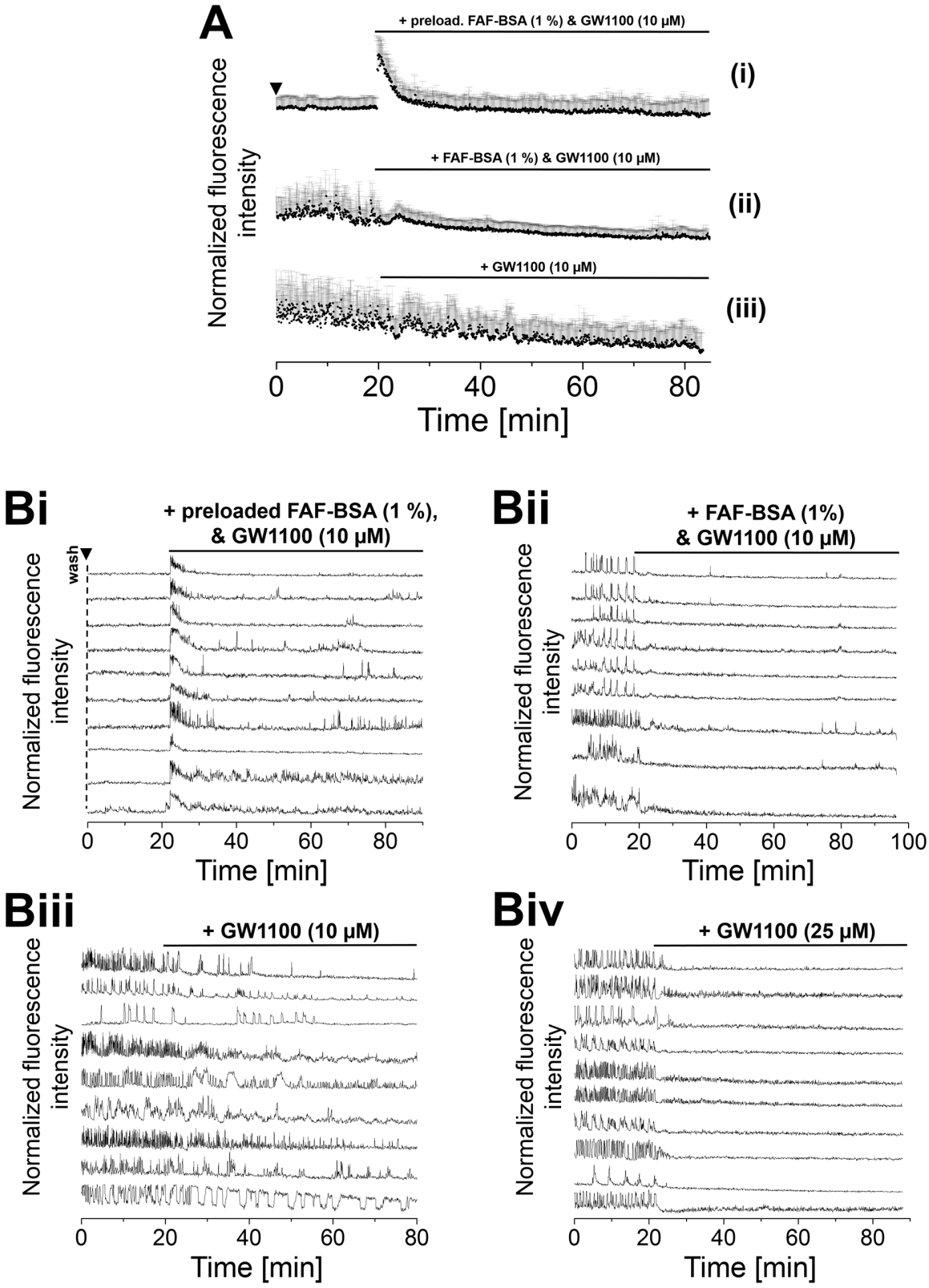
A
+ preload. FAF-BSA (1 %) & GW1100 (10 µM)
(i)
+ FAF-BSA (1 %) & GW1100 (10 µM)
(ii)
+ GW1100 (10 µM)
(iii)
Normalized fluorescence intensity
0
20
40
60
80
Time [min]
Bi
+ preloaded FAF-BSA (1 %), & GW1100 (10 µM)
wash
Normalized fluorescence intensity
0
20
40
60
80
Time [min]
Bii
+ FAF-BSA (1%) & GW1100 (10 µM)
Normalized fluorescence intensity
0
20
40
60
80
100
Time [min]
Biii
+ GW1100 (10 µM)
Normalized fluorescence intensity
0
20
40
60
80
Time [min]
Biv
+ GW1100 (25 µM)
Normalized fluorescence intensity
0
20
40
60
80
Time [min]

Figure A19. Stimulation of MIN6 cells by pre-loaded FAF-BSA is mediated by GPR40. (Ai-iii) Averaged and **(Bi - iv)** representative individual Ca^{2+} traces from MIN6 cells, recorded with the Ca^{2+} indicator Fluo-4. **(Ai+Bi)** FAF-BSA (1 %), pre-loaded on 2 x10^6 MIN6 cells was supplemented with the GPR40 inhibitor GW1100 (10 µM) before transfer to washed MIN6 cells. Even though MIN6 cells showed a prominent $[Ca^{2+}]_i$ transient, continuous $[Ca^{2+}]_i$ oscillations were suppressed. The GPR40 inhibitor GW1100 presumably prevented FA-mediated long-term stimulation of MIN6 cells. **(Aii+Bii)** Addition of FAF-BSA (1 %, no preloading), spiked with GW1100 (10 µM) to glucose-stimulated MIN6 cells shut down $[Ca^{2+}]_i$-oscillations, comparable to the effects that are mediated by FAF-BSA (1 %) alone. **(Aiii+Biii)** GW1100 (10 µM) decreased $[Ca^{2+}]_i$-oscillations. Observed effects were concentration-dependent (25 µM, **(Biv)**). Shown are averages of n = 30 MIN6 cells. Experiments were performed in the presence of 11 mM glucose. Ca^{2+} traces were recorded from MIN6 cells that were stained with the Ca^{2+} indicator Fluo-4. The figure was adapted from Hauke *et al.* [232].

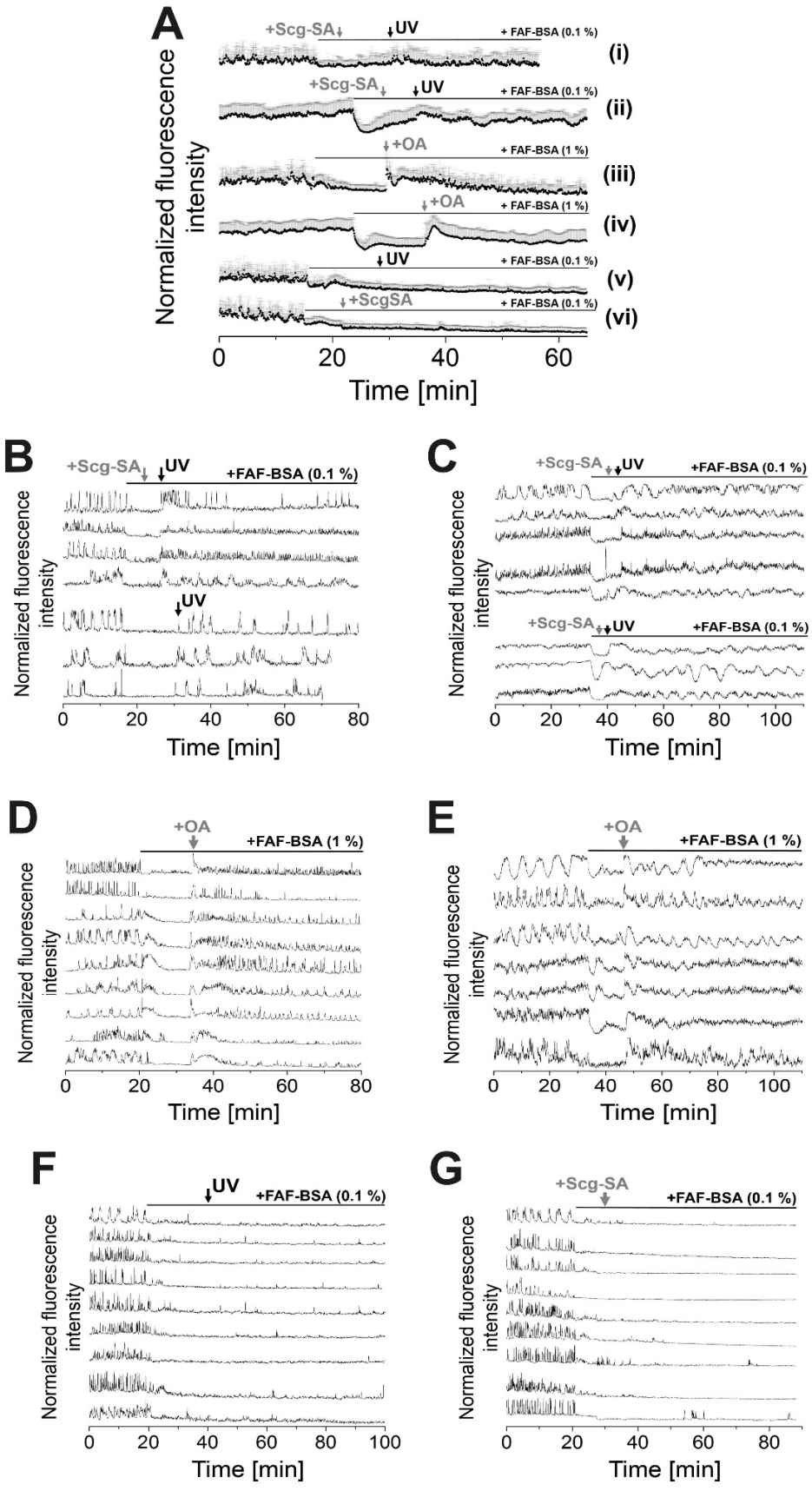
A
+Scg-SA
UV
+ FAF-BSA (0.1 %)
(i)
(ii)
+OA
+ FAF-BSA (1 %)
(iii)
(iv)
(v)
+ScgSA
(vi)
Normalized fluorescence intensity
Time [min]
B
C
D
E
F
G
+FAF-BSA (0.1 %)
+FAF-BSA (1 %)

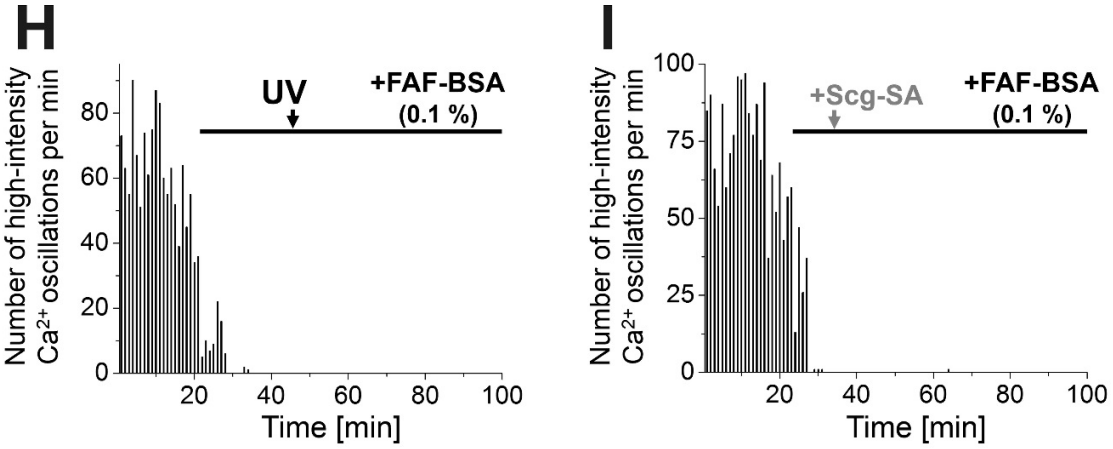

Figure A20. Restart of $[Ca^{2+}]_i$ oscillations in FAF-BSA-treated MIN6 and mouse primary *β*-cells following photolysis of sulfo-coumarin caged stearic acid (Scg-SA) or addition of oleic acid (OA). (A) Averaged and **(B-G)** representative individual Ca^{2+} traces from **(Ai+B, Aiii+D, Av+F, Avi+G)** MIN6 and **(Aii+C**, **Aiv+E)** primary mouse *β*-cells. **(H+I)** Counts of detected high-intensity $[Ca^{2+}]_i$ events per 60 s interval from MIN6 cells. **(Aii+B**, **Aiii+C)** Photolysis of Scg-SA (200 µM, λ = 375 nm) or **(Aiii+D**, **Aiv+E)** addition of OA (200 µM) reconstituted $[Ca^{2+}]_i$ oscillations in FAF-BSA (0.1 %)-treated **(Ai+B**, **Aiii+D)** MIN6 and **(Aii+C**, **Aiv+E)** mouse primary *β*-cells. Replenishment of cellular FA levels following FAF-BSA (0.1 %)-treatment by the photolysis of Scg-SA or addition of OA was suspected to reconstitute $[Ca^{2+}]_i$ oscillations. $[Ca^{2+}]_i$ oscillations did not restart in the absence of **(Av+F**, **H)** Scg-SA or **(Avi+G**, **I)** without the UV pulse. Averages of n = 30 MIN6 and n = 60 primary mouse *β*-cells are shown. Experiments were performed in the presence of 11 mM glucose. Ca^{2+} traces were recorded from MIN6 and primary mouse *β*-cells, stained with the Ca^{2+} indicator Fluo-4. The figure was adapted from Hauke *et al.* [232].

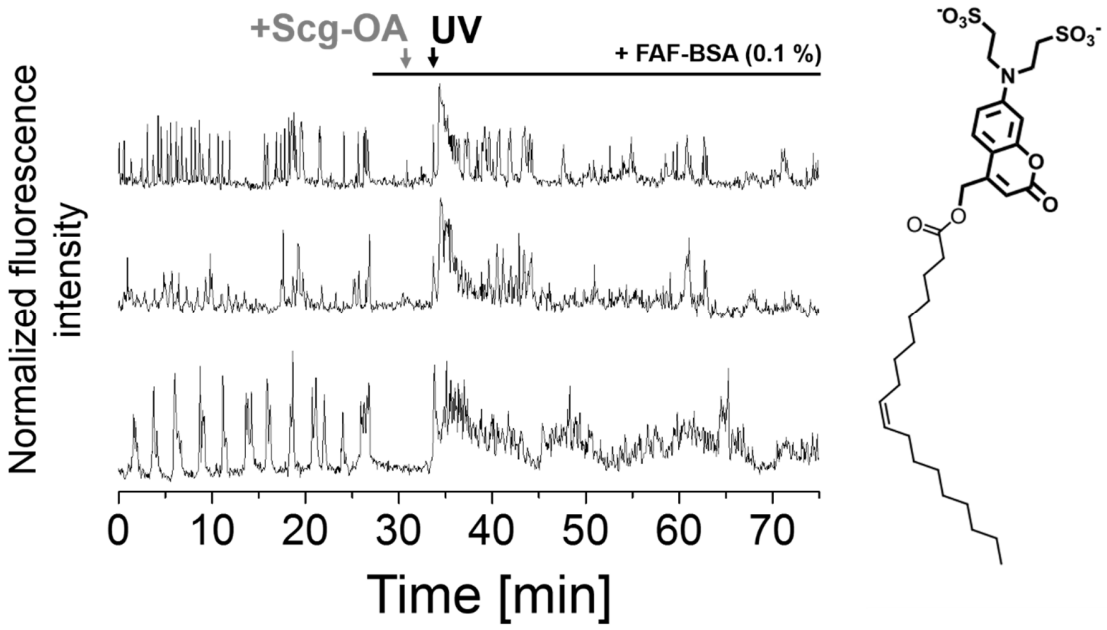

Figure A21. Restart of $[Ca^{2+}]_i$ oscillations in MIN6 cells by the photolysis of sulfo-coumarin caged oleic acid (Scg-OA). Shown are representative individual Ca^{2+} traces from MIN6 cells. Photolysis of Scg-OA (200 µM, λ = 375 nm) in FAF-BSA (0.1 %)-treated MIN6 cells reconstituted $[Ca^{2+}]_i$ oscillations. Experiments were performed in the presence of 11 mM glucose. Ca^{2+} traces were recorded from MIN6 cells, stained with the Ca^{2+} indicator Fluo-4. The figure was adapted from Hauke *et al.* [232].

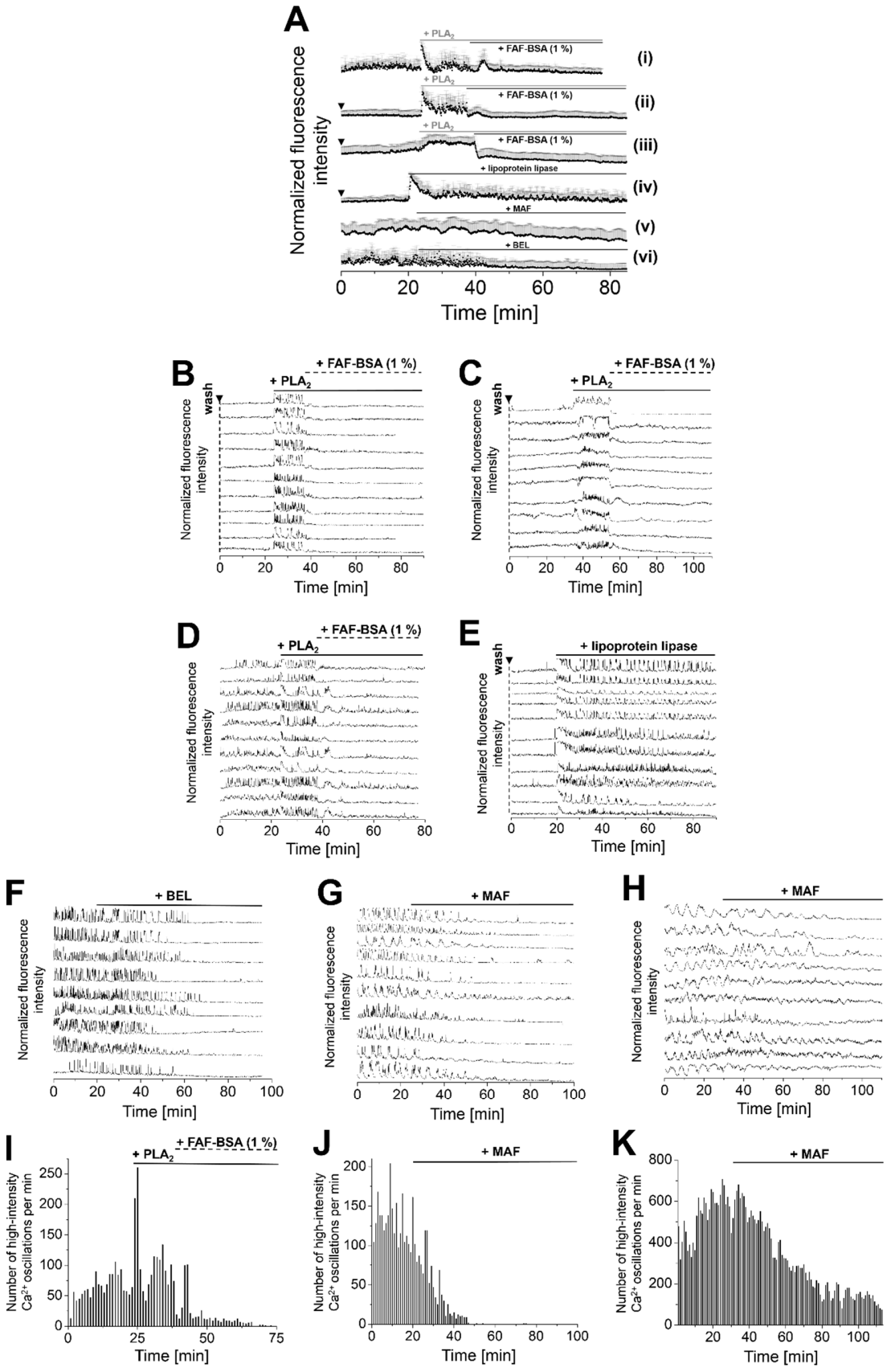
A
+ PLA2
+ FAF-BSA (1 %)
(i)
(ii)
(iii)
+ lipoprotein lipase
(iv)
+ MAF
(v)
+ BEL
(vi)
Normalized fluorescence intensity
Time [min]
B
C
D
E
wash
F
+ BEL
G
+ MAF
H
I
Number of high-intensity Ca2+ oscillations per min
J
K

Figure A22. FA-liberation by PLA_2 and FAF-BSA-mediated FA-depletion modulate $[Ca^{2+}]_i$ oscillations in MIN6 and mouse primary *β*-cells. **(A)** Averaged and **(B–H)** representative individual Ca^{2+} traces from MIN6 cells. **(I-K)** Counts of detected high-intensity $[Ca^{2+}]_i$ events per 60 s interval. $[Ca^{2+}]_i$ oscillations in **(Aii+B**, **Ai+D**, **I)** MIN6 and **(Aiii+C)** mouse primary *β*-cells were stimulated by PLA_2 (10 U) and reduced or terminated by the addition of FAF-BSA (1 %). **(Aiv+E)** Lipoprotein lipase action (500 U) induced $[Ca^{2+}]_i$ oscillations in MIN6 cells. $[Ca^{2+}]_i$ oscillations of **(Avi+F**, **G**, **J)** MIN6 and **(Av+H**, **K)** mouse primary *β*-cells were diminished and finally stopped in the presence of the PLA_2 inhibitors bromoenol lactone (BEL, 10 µM) and methylarachidonyl fluorophosphate (MAF, 10 µM). Averages of n = 30 MIN6 and n = 60 mouse primary *β*-cells are shown. Experiments were performed in the presence of 11 mM. Ca^{2+} traces were recorded from MIN6 and mouse primary *β*-cells, stained with the Ca^{2+} indicator Fluo-4. The figure was adapted from Hauke *et al.* [232].

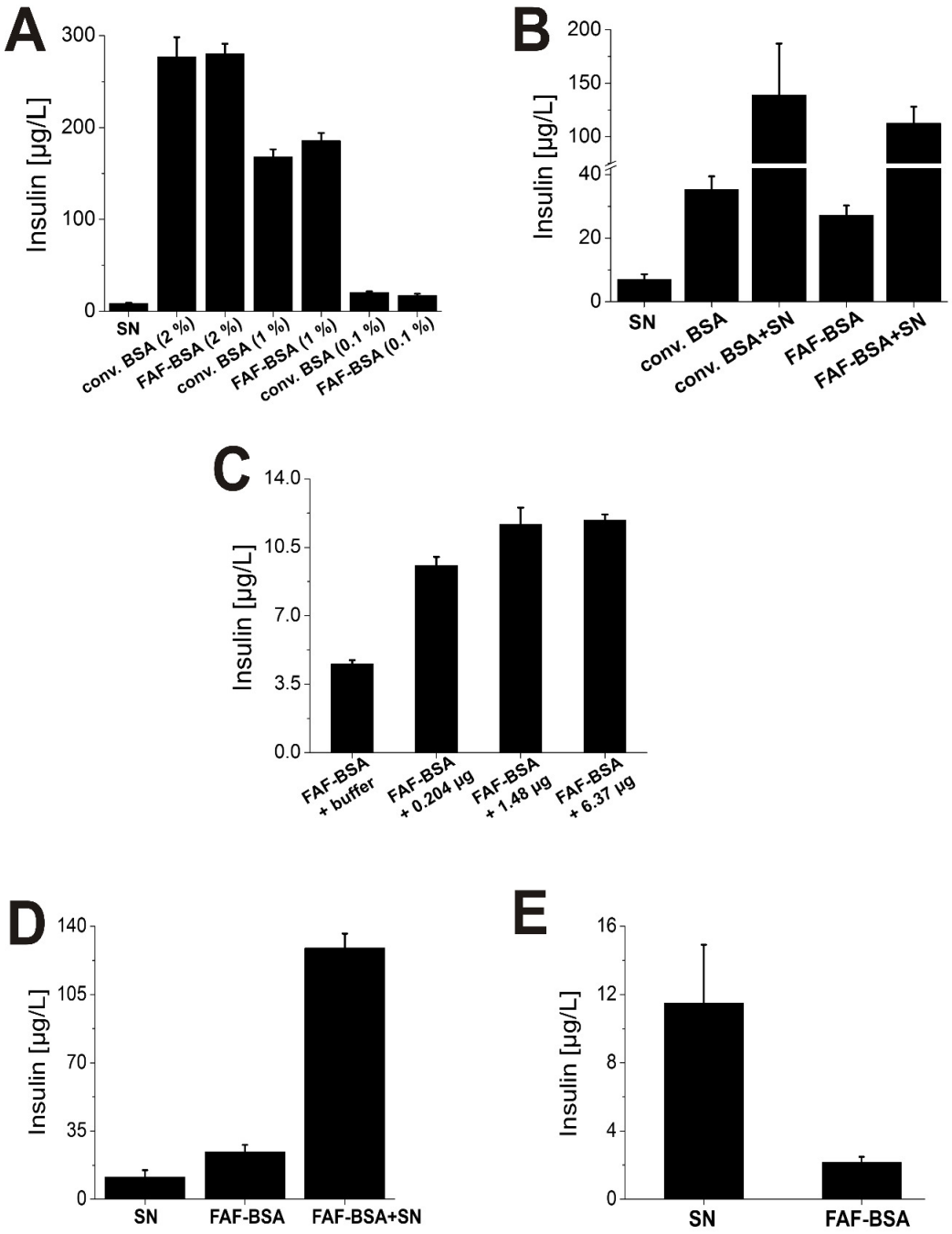

Figure A23. Interference of albumin with the ELISA-based quantification of insulin secretion. (A) Quantification of insulin levels in aqueous supernatant **(SN)**, conv. BSA and FAF-BSA in the presence of 11 mM glucose, following incubation on 2 x10^6 MIN6 cells. Insulin levels were determined in different orders of magnitude, depending on applied BSA concentrations. **(B)** BSA-mediated interference with ELISA measurements was determined by supplementing the supernatant of buffer-stimulated MIN6 cells with BSA (11 mM glucose). Determined insulin levels significantly increased following the addition of 0.1 % (conv. or FAF-) BSA to SNs that were harvested from 2 x10^6 MIN6 cells. We attributed these effects to the unspecific interaction of anti-insulin antibodies with BSA in the presence of insulin. **(C)** 0.1 % FAF-

BSA was supplemented with recombinant human insulin in various concentrations. The determined signal of FAF-BSA in buffer correlated with the spiked amounts of human insulin. **(D + E)** FAF-BSA was spiked into the SNs of MIN6 cells to correct for the interference of albumin in insulin measurements. Division of insulin levels, spiked with BSA [FAF-BSA spike+SN] by insulin levels within MIN6 SN [SN] generated a correction factor (cf) ((cf) = [0.1 % FAF-BSA spike + SN] / [SN]). Insulin levels in albumin-containing SNs [0.1 % FAF-BSA (SN)] were corrected for the albumin effect, using the (cf): corrected value = [0.1 % FAF-BSA (SN)] / (cf). For the determination of insulin levels, a mouse insulin ELISA kit was applied (Mercodia, Mercodia AB, Uppsala, Sweden). Conditions were measured in quadruplicate in the presence of 11 mM glucose.

9. References

1. Röder P V, Wu B, Liu Y, Han W. **Pancreatic regulation of glucose homeostasis.** Exp. Mol. Med. 2016. 48:e219.

2. Virtanen I, Banerjee M, Palgi J, Korsgren O, Lukinius A, Thornell L-E, *et al.* **Blood vessels of human islets of Langerhans are surrounded by a double basement membrane.** Diabetologia 2008. 51:1181–91.

3. Caicedo A. **Paracrine and autocrine interactions in the human islet: More than meets the eye.** Semin. Cell Dev. Biol. 2013. 24:11–21.

4. Hellmann B. **Actual distribution of the number and volume of the islets of Langerhans in different size classes in non-diabetic humans of varying ages.** Nature 1959.184:1498–1499.

5. Longnecker D, Wilson G. **Pancreas. In: Handbook of toxicologic pathology.** San Diego (California, U.S.A.) 1991. pp. 253-278.

6. Brissova M, Fowler MJ, Nicholson WE, Chu A, Hirshberg B, Harlan DM, *et al.* **Assessment of human pancreatic islet architecture and composition by laser scanning confocal microscopy.** J. Histochem. Cytochem. 2005. 53:1087–1097.

7. Elayat AA, el-Naggar MM, Tahir M. **An immunocytochemical and morphometric study of the rat pancreatic islets.** J. Anat. 1995. 186 (Pt 3):629–637.

8. Kahn A. **Insulin regulation of glucose uptake: a complex interplay of intracellular signalling pathways.** Diabetologia 2002. 45:1475–1483.

9. Kohn AD, Summers SA, Birnbaum MJ, Roth RA. **Expression of a constitutively active Akt Ser/Thr kinase in 3T3-L1 adipocytes stimulates glucose uptake and glucose transporter 4 translocation.** J. Biol. Chem. 1996. 271:31372–31378.

10. Zisman A, Peroni OD, Abel ED, Michael MD, Mauvais-Jarvis F, Lowell BB, *et al.* **Targeted disruption of the glucose transporter 4 selectively in muscle causes insulin resistance and glucose intolerance.** Nat. Med. 2000. 6:924–928.

11. Kersten S. **Mechanisms of nutritional and hormonal regulation of lipogenesis.** EMBO Rep. 2001. 2:282–286.

12. Stalmans W, Wulf H, Hue L, Hers H-G. **The sequential inactivation of glycogen phosphorylase and activation of glycogen synthetase in liver after the administration of glucose to mice and rats. The mechanism of the hepatic threshold to glucose.** Eur. J. Biochem. 1974. 41:127–134.

13. Miller TB, Larner J. **Mechanism of control of hepatic glycogenesis by insulin**. J. Biol. Chem. 1973. 248(10):3483-3488.

14. Syed NA, Khandelwal RL. **Reciprocal regulation of glycogen phosphorylase and glycogen synthase by insulin involving phosphatidylinositol-3 kinase and protein phosphatase-1 in HepG2 cells.** Mol. Cell. Biochem. 2000. 211:123–136.

15. Biolo G, Declan Fleming RY, Wolfe RR. **Physiologic hyperinsulinemia stimulates protein synthesis and enhances transport of selected amino acids in human skeletal muscle.** J. Clin. Invest. 1995. 95:811–819.

16. Freychet L, Desplanque N, Zirinis P, Rizkalla SW, Basdevant A, Tchobroutsky G, *et al.* **Effect of intranasal glucagon on blood glucose levels in healthy subjects and hypoglycaemic patients with insulin-depencent diabetes.** Lancet 1988. 331:1364–1366.

17. Göke B. **Islet cell function: α and β cells - partners towards normoglycaemia.** Int. J. Clin. Pract. 2008. 62:2–7.

18. Hauge-Evans AC, King AJ, Carmignac D, Richardson CC, Robinson ICAF, Low MJ, *et al.* **Somatostatin secreted by islet-cells fulfills multiple roles as a paracrine regulator of islet function**. Diabetes 2009. 58:403.

19. Katsuura G, Asakawa A, Inui A. **Roles of pancreatic polypeptide in regulation of food intake.** Peptides 2002. 23:323–329.

20. Kim A, Miller K, Jo J, Kilimnik G, Wojcik P, Hara M. **Islet architecture: A comparative study.** Islets 2009. 1:129–136.

21. Cabrera O, Berman DM, Kenyon NS, Ricordi C, Berggren P-O, Caicedo A. **The unique cytoarchitecture of human pancreatic islets has implications for islet cell function.** Proc. Natl. Acad. Sci. U. S. A. 2006. 103:2334–2339.

22. Betts G, Desaix P, Johnson E, Korol O, Kruse D, Poe B. **Human anatomy and physiology.** Houston (Texas, U.S.A.) 2013. pp. 1123-1128.

23. Henquin J-C, Nenquin M, Stiernet P, Ahren B. **In vivo and in vitro glucose-induced biphasic insulin secretion in the mouse pattern and role of cytoplasmic Ca2+ and amplification signals in β-cells.** Diabetes 2006. 55(2):441-451.

24. Salehi A, Vieira E, Gylfe E, Philippe J. **Paradoxical stimulation of glucagon secretion by high glucose concentrations.** Diabetes 2006. 55(8):2318-2323.

25. Rorsman P, Trube G. **Glucose dependent K+-channels in pancreatic β-cells are regulated by intracellular ATP.** Pflügers Arch. Eur. J. Physiol. 1985. 405:305–309.

26. Henquin JC. **Triggering and amplifying pathways of regulation of insulin secretion by glucose.** Diabetes 2000. 49:1751–1760.

27. MacDonald PE, Rorsman P. **The ins and outs of secretion from pancreatic β-cells: Control of single-vesicle exo- and endocytosis.** Physiology 2007. 22:113–121.

28. Thurmond DC. **Regulation of insulin action and insulin secretion by SNARE-mediated vesicle exocytosis.** Mech. Insul. Action 2007. 52–70.

29. Krippeit-Drews P, Düfer M, Drews G. **Parallel oscillations of intracellular calcium activity and mitochondrial membrane potential in mouse pancreatic β-cells.** Biochem. Biophys. Res. Commun. 2000. 267:179–183.

30. Ainscow EK, Rutter GA. **Glucose-stimulated oscillations in free cytosolic ATP concentration imaged in single islet β-cells: evidence for a Ca2+-dependent mechanism.** Diabetes 2002. 51 Suppl 1:S162-170.

31. Gilon P, Shepherd RM, Henquin JC. **Oscillations of secretion driven by oscillations of cytoplasmic Ca2+ as evidences in single pancreatic islets.** J. Biol. Chem. 1993. 268:22265–22268.

32. Bergsten P, Grapengiesser E, Gylfe E, Tengholm A, Hellman B. **Synchronous oscillations of cytoplasmic Ca2+ and insulin release in glucose-stimulated pancreatic islets.** J. Biol. Chem. 1994. 269:8749–8753.

33. Hellman B, Gylfe E, Grapengiesser E, Lund PE, Berts A. **Cytoplasmic Ca2+ oscillations in pancreatic β-cells.** Biochim. Biophys. Acta 1992. 1113:295–305.

34. Valdeolmillos M, Santos RM, Contreras D, Soria B, Rosario LM. **Glucose-induced oscillations of intracellular Ca2+ concentration resembling bursting electrical activity in single mouse islets of Langerhans.** FEBS Lett. 1989. 259:19–23.

35. Liu Y-J, Tengholm A, Grapengiesser E, Hellman B, Gylfe E. **Origin of slow and fast oscillations of Ca2+ in mouse pancreatic islets.** J. Physiol. 1998. 508:471–481.

36. Gylfe E, Grapengiesser E, Liu YJ, Dryselius S, Tengholm A, Eberhardson M. **Generation of glucose-dependent slow oscillations of cytoplasmic Ca2+ in individual pancreatic β-cells.** Diabetes Metab. 1998. 24:25–29.

37. Longot EA, Tornheimso K, Deeneyt JT, Varnump BA, Tillotsont D, Prentkiii M, *et al.* **Oscillations in cytosolic free Ca2+, oxygen consumption, and insulin secretion in glucose-stimulated rat pancreatic islets.** J. Biol. Chem. 1991. 266:9314-9319.

38. Nilsson T, Schultz V, Berggren PO, Corkey BE, Tornheim K. **Temporal patterns of changes in ATP/ADP ratio, glucose 6-phosphate and cytoplasmic free Ca2+ in glucose-stimulated pancreatic β-cells.** Biochem. J. 1996. 314 (Pt 1):91–4.

39. Jung S-K, Kauri LM, Qian W-J, Kennedy RT. **Correlated oscillations in glucose consumption, oxygen consumption, and intracellular free Ca2+ in single islets of Langerhans.** J. Biol. Chem. 2000. 275:6642-6650.

40. Luciani DS, Misler S, Polonsky KS. **Ca2+ controls slow NAD(P)H oscillations in glucose-stimulated mouse pancreatic islets.** J. Physiol. 2006. 572:379–392.

41. Thore S, Dyachok O, Tengholm A. **Oscillations of phospholipase C activity triggered by depolarization and Ca2+ influx in insulin-secreting cells.** J. Biol. Chem. 2004. 279:19396–19400.

42. Xie B, Nguyen PM, Guček A, Thonig A, Barg S, Idevall-Hagren O. **Plasma membrane phosphatidylinositol 4,5-bisphosphate regulates Ca2+-influx and insulin secretion from pancreatic β-cells.** Cell Chem. Biol. 2016;23:816–826.

43. Wuttke A. **Lipid signalling dynamics at the β-cell plasma membrane.** Basic Clin. Pharmacol. Toxicol. 2015. 116:281–290.

44. Dyachok O, Isakov Y, Sågetorp J, Tengholm A. **Oscillations of cyclic AMP in hormone-stimulated insulin-secreting β-cells.** Nature 2006. 439:349–352.

45. Dyachok O, Idevall-Hagren O, Sågetorp J, Tian G, Wuttke A, Arrieumerlou C, *et al.* **Glucose-induced cyclic AMP oscillations regulate pulsatile insulin secretion.** Cell Metab. 2008. 8:26–37.

46. Tian G, Sandler S, Gylfe E, Tengholm A. **Glucose- and hormone-induced cAMP oscillations in α- and β-cells within intact pancreatic islets.** Diabetes 2011. 60:1535–1543.

47. Tornheim K. **Are metabolic oscillations responsible for normal oscillatory insulin secretion?** Diabetes 1997. 46:1375–1380.

48. Tengholm A, Gylfe E. **Oscillatory control of insulin secretion.** Mol. Cell. Endocrinol. 2009. 297:58–72.

49. Bergsten P. **Slow and fast oscillations of cytoplasmic Ca2+ in pancreatic islets correspond to pulsatile insulin release.** Am. J. Physiol. - Endocrinol. Metab. 1995;268.

50. Jonas J-C, Gilon P, Henquin J-C. **Temporal and quantitative correlations between insulin secretion and stably elevated or oscillatory cytoplasmic Ca2+ in mouse pancreatic β-cells.** Diabetes 1998. 47(8):1266-1273.

51. Gilon P, Henquin JC. **Distinct effects of glucose on the synchronous oscillations of insulin release and cytoplasmic Ca2+ concentration measured simultaneously in single mouse islets.** Endocrinology 1995. 136:5725–5730.

52. Gee KR, Brown KA, Chen W-NU, Bishop-Stewart J, Gray D, Johnson I**. Chemical and physiological characterization of fluo-4 Ca2+-indicator dyes.** Cell Calcium. 2000. 27:97–106.

53. Hellman B, Idahl LA, Lernmark A, Täljedal IB. **The pancreatic beta-cell recognition of insulin secretagogues: does cyclic AMP mediate the effect of glucose?** Proc. Natl. Acad. Sci. U. S. A. 1974. 71:3405–3409.

54. Pipleers DG, Schuit FC, Int Veld PA, Maes E, Hooghe-Peters EL, Winkel M Van De, *et al.* **Interplay of nutrients and hormones in the regulation of insulin release**. Endocrinology 1985. 117:824–833.

55. Prentki M, Matschinsky FM. **Ca2+, cAMP, and phospholipid-derived messengers in coupling mechanisms of insulin secretion.** Physiol. Rev. 1987. 67:1185–1248.

56. Gespach C, Hansen A, Holst J. **Differential regulation of membrane receptors sensitive to histamine (H2-type), isoproterenol (β 2-type) and glucagon-like peptides by the somatostatin analogue Sandostatin in rat gastric glands.** Agents Actions 1989. 27:169–172.

57. Hansen AB, Gespach CP, Rosselin GE, Holst JJ. **Effect of truncated glucagon-like peptide 1 on cAMP in rat gastric glands and HGT-1 human gastric cancer cells.** FEBS Lett. 1988. 236:119–122.

58. Eliasson L, Ma X, Renström E, Barg S, Berggren P-O, Galvanovskis J, *et al.* **SUR1 regulates PKA-independent cAMP-induced granule priming in mouse pancreatic β-cells.** J. Gen. Physiol. 2003. 121:181–197.

59. Seino S, Shibasaki T. **PKA-dependent and PKA-independent pathways for cAMP-regulated exocytosis.** Physiol. Rev. 2005. 85:1303–1342.

60. Bé P, Nagashima K, Nishimura M, Gonoi T, Seino S, Béguin P, *et al.* **PKA-mediated phosphorylation of the human K ATP channel: separate roles of Kir6.2 and SUR1 subunit phosphorylation.** EMBO J. 1999. 18:4722-4732.

61. Ribalet B, Ciani S, Eddlestone GT. **ATP mediates both activation and inhibition of K(ATP) channel activity via cAMP-dependent protein kinase in insulin-secreting cell lines.** J. Gen. Physiol. 1989. 94:693–717.

62. Ämmälä C, Ashcroft FM, Rorsman P. **Calcium-independent potentiation of insulin release by cyclic AMP in single β-cells.** Nature 1993. 363:356–358.

63. Kanno T, Suga S, Wu J, Kimura M, Wakui M. **Intracellular cAMP potentiates voltage-dependent activation of L -type Ca2+ channels in rat islet β-cells.** Pflügers Arch. Eur. J. Physiol. 1998. 435:578–580.

64. Liu Y-J, Grapengiesser E, Gylfe E, Hellman B. **Crosstalk between the cAMP and inositol trisphosphate-signalling pathways in pancreatic β-cells.** Arch. Biochem. Biophys. 1996. 334:295–302.

65. Dyachok O, Gylfe E. **Ca 2+-Induced Ca 2+ Release via Inositol 1,4,5-trisphosphate Receptors is Amplified by Protein Kinase A and Triggers Exocytosis in Pancreatic-Cells.** J. Chem. Biol. 2004. 279(44):45455-45461.

66. Zawalich WS, Zawalich KC, Kelley GG. **Regulation of insulin release by phospholipase C activation in mouse islets: differential effects of glucose and neurohumoral stimulation.** Endocrinology 1995. 136:4903–4909.

67. Montague W, Morgan NG, Rumford GM, Prince CA. **Effect of glucose on polyphosphoinositide metabolism in isolated rat islets of Langerhans.** Biochem. J. 1985. 227:483–489.

68. Miguel JC, Abdel-Wahab YH., Mathias PC., Flatt PR. **Muscarinic receptor subtypes mediate stimulatory and paradoxical inhibitory effects on an insulin-secreting β cell line.** Biochim. Biophys. Acta - Gen. Subj. 2002. 1569:45–50.

69. Wettschureck N, Offermanns S. **Mammalian G proteins and their cell type specific functions.** Physiol. Rev. 2005. 85:1159–1204.

70. Ravier M, Rutter G. **Isolation and culture of mouse pancreatic islets for *ex vivo* imaging studies with trappable or recombinant fluorescent probes.** Mouse cell Cult. Humana Press; 2010. p. 171–184.

71. Skelin M, Rupnik M, Cencic A. **Pancreatic β-cell lines and their applications in diabetes mellitus research.** Altex 2010 27:105–113.

72. Asfari M, Janjic D, Meda P, Li G, Halban PA, Wollheim CB. **Establishment of 2-mercaptoethanol-dependent differentiated insulin-secreting cell lines.** Endocrinology 1992. 130:167–178.

73. Miyazaki JI, Araki K, Yamato E, Ikegami H, Asanto T, Shibasaki Y, *et al.* **Establishment of a pancreatic β-cell line that retains glucose-inducible insulin secretion: special reference to expression of glucose transporter isoforms**. Endocrinology 1990. 127:126–132.

74. Ishihara H, Asano T, Tsukuda K, Katagiri H, Inukai K, Anai M, *et al.* **Pancreatic beta cell line MIN6 exhibits characteristics of glucose metabolism and glucose-stimulated insulin secretion similar to those of normal islets.** Diabetologia 1993. 36:1139–1145.

75. Nakashima K, Kanda Y, Hirokawa Y, Kawasaki F, Matsuki M, Kaku K. **MIN6 is not a pure β-cell line but a mixed cell line with other pancreatic endocrine hormones.** Endocr. J. 2009. 56:45–53.

76. Santos RM, Rosario LM, Nadal A, Garcia-Sancho J, Soria B, Valdeolmillos M. **Widespread synchronous [Ca2+]i oscillations due to bursting electrical activity in single pancreatic islets.** Pflügers Arch. Eur. J. Physiol. 1991. 418:417–422.

77. Goodner C, Walike B, Koerker D, Ensinck J, Brown A, Chideckel E, *et al.* **Insulin, glucagon, and glucose exhibit synchronous, sustained oscillations in fasting monkeys.** Science 1977. 195(4274):177-179.

78. Pørksen N, Hollingdal M, Juhl C, Butler P, Veldhuis JD, Schmitz O. **Pulsatile insulin secretion: Detection, regulation, and role in diabetes.** Diabetes 2002. 51 Suppl 1:S245-254.

79. Shapiro ET, Tillil H, Polonsky KS, Fang VS, Rubenstein HA, Cauter E van. **Oscillations in insulin secretion during constant glucose infusion in normal man: Relationship to changes in plasma glucose.** J. Clin. Endocrinol. Metab. 1988. 67:307–314.

80. Ravier M, Sehlin J, Henquin J. **Disorganization of cytoplasmic Ca2+ oscillations and pulsatile insulin secretion in islets from ob / ob mice.** Diabetologia 2002. 45:1154–1163.

81. Sturis J, Pugh WL, Tang J, Ostrega DM, Polonsky JS, Polonsky KS. **Alterations in pulsatile insulin secretion in the Zucker diabetic fatty rat.** Am. J. Physiol. 1994. 267:E250-259.

82. Lang DA, Matthews DR, Burnett M, Turner RC. **Brief, irregular oscillations of basal plasma insulin and glucose concentrations in diabetic man.** Diabetes 1981. 30:435–439.

83. O'Rahilly S, Turner RC, Matthews DR. **Impaired pulsatile secretion of insulin in relatives of patients with non-insulin-dependent diabetes.** N. Engl. J. Med. 1988. 318:1225–1230.

84. Schmitz O, Pørksen N, Nyholm B, Skjaerbaek C, Butler PC, Veldhuis JD, *et al.* **Disorderly and nonstationary insulin secretion in relatives of patients with NIDDM.** Am. J. Physiol. 1997. 272:E218-226.

85. Matthews DR, Lang DA, Burnett MA, Turner RC. **Control of pulsatile insulin secretion in man.** Diabetologia 1983. 24:231–237.

86. Bratusch-Marrain PR, Komjati M, Waldhäusl WK. **Efficacy of pulsatile versus continuous insulin administration on hepatic glucose production and glucose utilization in type I diabetic humans.** Diabetes. 1986. 35(8):922-926.

87. Paolisso G, Sgambato S, Gentile S, Memoli P, Giugliano D, Varricchio M, *et al.* **Advantageous metabolic effects of pulsatile insulin delivery in noninsulin-dependent diabetic patients.** J. Clin. Endocrinol. Metab. 1988. 67:1005–1010.

88. Paolisso G, Sgambato S, Torella R, Varricchio M, Scheen A, D'onofrio F, *et al.* **Pulsatile insulin delivery is more efficient than continuous infusion in modulating islet cell function in normal subjects and patients with type 1 diabetes.** J. Clin. Endocrinol. Metab. 1988. 66:1220–1226.

89. Paolisso G, Scheen AJ, Giugliano D, Sgambato S, Albert A, Varricchio M, *et al.* **Pulsatile insulin delivery has greater metabolic effects than continuous hormone administration in man: Importance of pulse frequency.** J. Clin. Endocrinol. Metab. 1991. 72:607–615.

90. Ward GM, Walters JM, Aitken PM, Best JD, Alford FP. **Effects of prolonged pulsatile hyperinsulinemia in humans. Enhancement of insulin sensitivity.** Diabetes 1990. 39:501–507.

9. References

91. Orrenius S, Zhivotovsky B, Nicotera P. **Regulation of cell death: the calcium–apoptosis link.** Nat. Rev. Mol. Cell Biol. 2003. 4:552–565.

92. Peiris AN, Stagner JI, Vogel RL, Nakagawa A, Samols E. **Body fat distribution and peripheral insulin sensitivity in healthy men: role of insulin pulsatility.** J. Clin. Endocrinol. Metab. 1992. 75:290–294.

93. Stagner JI, Samols E, Weir GC. **Sustained oscillations of insulin, glucagon, and somatostatin from the isolated canine pancreas during exposure to a constant glucose concentration.** J. Clin. Invest. 1980. 65:939–942.

94. Bergsten P, Hellman B. **Glucose-induced amplitude regulation of pulsatile insulin secretion from individual pancreatic islets.** Diabetes 1993. 42:670–674.

95. Bergsten P, Hellman B. **Glucose-induced cycles of insulin release can be resolved into distinct periods of secretory activity.** Biochem. Biophys. Res. Commun. 1993. 192:1182–1188.

96. Meissner HP. **Electrophysiological evidence for coupling between β-cells of pancreatic islets.** Nature 1976. 262:502–504.

97. Meda P, Perrelet A, Orci L. **Increase of gap junctions between pancreatic β-cells during stimulation of insulin secretion.** J. Cell Biol. 1979. 82:441–448.

98. Orci L, Unger RH, Renold AE. **Structural coupling between pancreatic islet cells.** Experientia 1973. 29:1015–1018.

99. Calabrese A, Zhang M, Serre-Beinier V, Caton D, Mas C, Satin LS, *et al.* **Connexin 36 controls synchronization of Ca2+ oscillations and insulin secretion in MIN6 cells.** Diabetes 2003. 52(2):417-424.

100. Ravier MA, Güldenagel M, Charollais A, Gjinovci A, Caille D, Söhl G, *et al.* **Loss of connexin36 channels alters β-cell coupling, islet synchronization of glucose-induced Ca2+ and insulin oscillations, and basal insulin release.** Diabetes. 2005;54(6):1798-1807.

101. Cunningham BA, Deeney JT, Bliss CR, Corkey BE, Tornheim K. **Glucose-induced oscillatory insulin secretion in perifused rat pancreatic islets and clonal beta-cells (HIT).** Am. J. Physiol. 1996. 271:E702-710.

102. Cao D, Lin G, Westphale EM, Beyer EC, Steinberg TH. **Mechanisms for the coordination of intercellular calcium signaling in insulin-secreting cells.** J. Cell Sci. 1997;110:497-504.

103. Grapengiesser E, Gylfe E, Hellman B. **Synchronization of glucose-induced Ca2+ transients in pancreatic beta-cells by a diffusible factor.** Biochem. Biophys. Res. Commun. 1999. 254:436–439.

104. MacDonald PE, Braun M, Galvanovskis J, Rorsman P. **Release of small transmitters through kiss-and-run fusion pores in rat pancreatic β-cells.** Cell Metab. 2006. 4:283–290.

105. Petit P, Hillaire-Buys D, Manteghetti M, Debrus S, Chapal J, Loubatières-Mariani MM. **Evidence for two different types of P2 receptors stimulating insulin secretion from pancreatic β-cell.** Br. J. Pharmacol. 1998. 125:1368–1374.

106. Jacques-Silva MC, Correa-Medina M, Cabrera O, Rodriguez-Diaz R, Makeeva N, Fachado A, *et al.* **ATP-gated P2X3 receptors constitute a positive autocrine signal for insulin release in the human pancreatic β-cell.** Proc. Natl. Acad. Sci. U. S. A. 2010. 107:6465–6470.

107. Petit P, Lajoix A-D, Gross R. **P2 purinergic signalling in the pancreatic beta-cell: control of insulin secretion and pharmacology.** Eur. J. Pharm. Sci. 2009. 37:67–75.

108. Grapengiesser E, Dansk H, Hellman B. **External ATP triggers Ca2+ signals suited for synchronization of pancreatic β-cells.** J. Endocrinol. 2005. 185:69–79.

109. Grapengiesser E, Dansk H, Hellman B. **Pulses of external ATP aid to the synchronization of pancreatic β-cells by generating premature Ca(2+) oscillations.** Biochem. Pharmacol. 2004. 68:667–674.

110. Hellman B, Dansk H, Grapengiesser E. **Pancreatic β-cells communicate via intermittent release of ATP.** Am. J. Physiol. Endocrinol. Metab. 2004. 286:E759-765.

111. Gylfe E, Tengholm A. Neurotransmitter control of islet hormone pulsatility. Diabetes, Obes. Metab. 2014. 16:102–110.

112. Salehi A, Quader SS, Grapengiesser E, Hellman B. **Inhibition of purinoceptors amplifies glucose-stimulated insulin release with removal of its pulsatility**. 2005. 54(7):2126-2131.

113. Hagren OI, Tengholm A. **Glucose and insulin synergistically activate phosphatidylinositol 3-kinase to trigger oscillations of phosphatidylinositol 3,4,5-trisphosphate in β-cells.** J. Biol. Chem. 2006. 281:39121–39127.

114. Grapengiesser E, Gylfe E, Dansk H, Hellman B. **Nitric oxide induces synchronous Ca2+ transients in pancreatic beta cells lacking contact.** Pancreas 2001. 23:387–392.

115. Lundquist I, Alm P, Salehi A, Henningsson R, Grapengiesser E, Hellman B. **Carbon monoxide stimulates insulin release and propagates Ca2+ signals between pancreatic β-cells.** Am. J. Physiol. - Endocrinol. Metab. 2003. 285(5):E1055-E1063.

116. Richards-Williams C, Contreras JL, Berecek KH, Schwiebert EM. **Extracellular ATP and zinc are co-secreted with insulin and activate multiple P2X purinergic receptor channels expressed by islet beta-cells to potentiate insulin secretion.** Purinergic Signal. 2008. 4:393–405.

117. Li YV. **Zinc and insulin in pancreatic β-cells.** Endocrine 2014. 45:178–189.

118. Wang ZL, Bennet WM, Wang RM, Ghatei MA, Bloom SR. **Evidence of a paracrine role of neuropeptide-Y in the regulation of insulin release from pancreatic islets of normal and dexamethasone-treated rats.** Endocrinology 1994. 135:200–206.

119. Cabrera O, Jacques-Silva MC, Speier S, Yang S-N, Köhler M, Fachado A, *et al.* **Glutamate is a positive autocrine signal for glucagon release.** Cell Metab. 2008. 7:545–554.

120. Braun M, Ramracheya R, Bengtsson M, Clark A, Walker JN, Johnson PR, *et al.* **γ-Aminobutyric acid (GABA) is an autocrine excitatory transmitter in human pancreatic β-cells.** Diabetes. 2010. 59:1694-1701.

121. Franklin IK, Wollheim CB. **GABA in the endocrine pancreas: its putative role as an islet cell paracrine-signalling molecule.** J. Gen. Physiol. 2004. 123:185–190.

122. Leibiger IB, Leibiger B, Berggren P-O. **Insulin feedback action on pancreatic β-cell function.** FEBS Lett. 2002. 532:1–6.

123. Braun M, Ramracheya R, Rorsman P. **Autocrine regulation of insulin secretion.** Diabetes, Obes. Metab. 2012. 14:143–151.

124. Zucchi R, Chiellini G, Scanlan TS, Grandy DK. **Trace amine-associated receptors and their ligands.** Br. J. Pharmacol. 2009. 149:967–978.

125. Kuhar MJ, Couceyro PR, Lambert PD. **Biosynthesis of catecholamines. In: basic biochemistry.** 6th ed. Philadelphia 1999. Chapter 12.

126. Burden DA, Philips SR. **Kinetic measurements of the turnover rates of phenylethylamine and tryptamine *in vivo* in the rat brain.** J. Neurochem. 1980. 34:1725–1732.

127. Berry MD. **Mammalian central nervous system trace amines. Pharmacologic amphetamines, physiologic neuromodulators.** J. Neurochem. 2004. 90:257–271.

128. Pei Y, Asif-Malik A, Canales JJ. **Trace Amines and the Trace Amine-Associated Receptor 1: Pharmacology, Neurochemistry, and Clinical Implications.** Front. Neurosci. 2016. 10:148.

129. Boulton AA, Baker GB, Dewhurst WG, Sandler M. **Neurobiology of the trace amines analytical, physiological, pharmacological, behavioral and clinical aspects.** 1st ed. New York 1984. pp. 13-24.

130. Dyck LE. **Release of Some Endogenous Trace Amines from Rat Striatal Slices in the Presence and Absence of a Monoamine Oxidase Inhibitor.** Trace Amin. Humana Press; 1988p. 223–237.

131. Henry DP, Russell WL, Clemens JA, Plebus LA. **Phenylethlamine and p-tyramine in the extracellular space of the rat brain: Quantification using a new radioenzymatic assay and *in situ* microdialysis.** Trace Amin. Humana Press; 1988. p. 239–50.

132. Borowsky B, Adham N, Jones KA, Raddatz R, Artymyshyn R, Ogozalek KL, *et al.* **Trace amines: identification of a family of mammalian G protein-coupled receptors.** Proc. Natl. Acad. Sci. U. S. A. 2001. 98:8966–8971.

133. Bunzow JR, Sonders MS, Arttamangkul S, Harrison LM, Zhang G, Quigley DI, et al. **Amphetamine, 3,4-methylenedioxymethamphetamine, lysergic acid diethylamide, and metabolites of the catecholamine neurotransmitters are agonists of a rat trace amine receptor.** Mol. Pharmacol. 2001;60(6):1181-1188.

134. Bradaia A, Trube G, Stalder H, Norcross RD, Ozmen L, Wettstein JG, *et al.* **The selective antagonist EPPTB reveals TAAR1-mediated regulatory mechanisms in dopaminergic neurons of the mesolimbic system.** Proc. Natl. Acad. Sci. U. S. A. 2009. 106:20081–20086.

135. Barak LS, Salahpour A, Zhang X, Masri B, Sotnikova TD, Ramsey AJ, *et al.* **Pharmacological characterization of membrane-expressed human trace amine-associated receptor 1 (TAAR1) by a bioluminescence resonance energy transfer cAMP biosensor.** Mol. Pharmacol. 2008. 74:585–594.

136. Wainscott DB, Little SP, Yin T, Tu Y, Rocco VP, He JX, *et al.* **Pharmacologic characterization of the cloned human trace amine-associated receptor1 (TAAR1) and evidence for species differences with the rat TAAR1.** J. Pharmacol. Exp. Ther. 2007. 320:475–485.

137. Tan ES, Naylor JC, Groban ES, Bunzow JR, Jacobson MP, Grandy DK, *et al.* **The molecular basis of sSpecies-specific ligand activation of trace amine-associated receptor 1 (TAAR 1).** ACS Chem. Biol. 2009. 4:209–220.

138. Hu LA, Zhou T, Ahn J, Wang S, Zhou J, Hu Y, *et al.* **Human and mouse trace amine-associated receptor 1 have distinct pharmacology towards endogenous monoamines and imidazoline receptor ligands.** Biochem. J. 2009. 424:39–45.

139. Chiellini G, Bellusci L, Sabatini M, Zucchi R. **Thyronamines and analogues - the route from rediscovery to translational research on thyronergic amines.** Mol. Cell. Endocrinol. 2017. 458:149–155.

140. Hoefig CS, Zucchi R, Köhrle J. **Thyronamines and derivatives: Physiological relevance, pharmacological actions, and future research directions.** Thyroid 2016. 26:1656–1673.

141. Scanlan TS, Suchland KL, Hart ME, Chiellini G, Huang Y, Kruzich PJ, *et al.* **3-Iodothyronamine is an endogenous and rapid-acting derivative of thyroid hormone.** Nat. Med. 2004. 10:638–642.

142. Grandy DK, Miller GM, Li J-X. **"TAARgeting Addiction"—The Alamo Bears Witness to Another Revolution: An Overview of the Plenary Symposium of the 2015 Behavior, Biology and Chemistry Conference.** Drug Alcohol Depend. 2016. 159:9–16.

143. Jing L, Li J-X. **Trace amine-associated receptor 1: A promising target for the treatment of psychostimulant addiction.** Eur. J. Pharmacol. 2015. 761:345–352.

144. Espinoza S, Salahpour A, Masri B, Sotnikova TD, Messa M, Barak LS, *et al.* **Functional interaction between trace amine-associated receptor 1 and dopamine D2 receptor.** Mol. Pharmacol. 2011. 80:416–425.

145. Harmeier A, Obermueller S, Meyer CA, Revel FG, Buchy D, Chaboz S, *et al.* **Trace amine-associated receptor 1 activation silences GSK3β signaling of TAAR1 and D2R heteromers.** Eur. Neuropsychopharmacol. 2015. 25:2049–2061.

146. Espinoza S, Gainetdinov RR. **Neuronal Functions and Emerging Pharmacology of TAAR1.** Taste and Smell 2014. p. 175–194.

147. Miller GM. **The emerging role of trace amine-associated receptor 1 in the functional regulation of monoamine transporters and dopaminergic activity.** J. Neurochem. 2011. 116:164–176.

148. Davis BA, Boulton AA. **The trace amines and their acidic metabolites in depression — an overview.** Prog. Neuro-Psychopharmacology Biol. Psychiatry. 1994. 18:17–45.

149. Sandler M, Ruthven CRJ, Goodwin BL, Coppen A. **Decreased cerebrospinal fluid concentration of free phenylacetic acid in depressive illness.** Clin. Chim. Acta. 1979. 93:169–171.

150. Potkin S, Karoum F, Chuang L, Cannon-Spoor H, Phillips I, Wyatt R. **Phenylethylamine in paranoid chronic schizophrenia.** Science (80-.). 1979. 206(4417):470-471.

151. Revel FG, Moreau J-L, Gainetdinov RR, Bradaia A, Sotnikova TD, Mory R, *et al.* **TAAR1 activation modulates monoaminergic neurotransmission, preventing hyperdopaminergic and hypoglutamatergic activity.** Proc. Natl. Acad. Sci. U. S. A. 2011. 108:8485–8490.

152. Berry M. **The potential of trace amines and their receptors for treating neurological and psychiatric diseases.** Rev. Recent Clin. Trials 2007. 2:3–19.

153. Galley G, Stalder H, Goergler A, Hoener MC, Norcross RD. **Optimisation of imidazole compounds as selective TAAR1 agonists: Discovery of RO5073012.** Bioorg. Med. Chem. Lett. 2012. 22:5244–5248.

154. Revel FG, Moreau J-L, Pouzet B, Mory R, Bradaia A, Buchy D, *et al.* **A new perspective for schizophrenia: TAAR1 agonists reveal antipsychotic- and antidepressant-like activity, improve cognition and control body weight.** Mol. Psychiatry 2013. 18:543–556.

155. Revel FG, Moreau J-L, Gainetdinov RR, Ferragud A, Velázquez-Sánchez C, Sotnikova TD, *et al.* **Trace amine-associated receptor 1 partial agonism reveals novel paradigm for neuropsychiatric therapeutics.** Biol. Psychiatry 2012. 72:934–942.

156. Rutigliano G, Accorroni A, Zucchi R. **The Case for TAAR1 as a Modulator of Central Nervous System Function.** Front. Pharmacol. 2018. 8:987.

157. Cichero E, Espinoza S, Gainetdinov RR, Brasili L, Fossa P. **Insights into the structure and pharmacology of the human trace amine-associated receptor 1 (*h* TAAR1): Homology modelling and docking studies.** Chem. Biol. Drug Des. 2013. 81:509–516.

158. Lam VM, Rodríguez D, Zhang T, Koh EJ, Carlsson J, Salahpour A. **Discovery of trace amine-associated receptor 1 ligands by molecular docking screening against a homology model.** Medchemcomm 2015. 6:2216–2223.

159. Stalder H, Hoener MC, Norcross RD**. Selective antagonists of mouse trace amine-associated receptor 1 (mTAAR1): Discovery of EPPTB (RO5212773).** Bioorg. Med. Chem. Lett. 2011. 21(4):1227-1231.

160. Berry MD, Gainetdinov RR, Hoener MC, Shahid M. **Pharmacology of human trace amine-associated receptors: Therapeutic opportunities and challenges.** Pharmacol. Ther. 2017. 180:161–180.

161. Tan E, Groban ES, Jacobson, Matthew P, Scanlan TS. **Toward Deciphering the Code to Aminergic G Protein-Coupled Receptor Drug Design.** Chem. Biol. 2008. 15:343–353.

162. Dyck LE, Yang CR, Boulton AA. **The biosynthesis ofp-tyramine,m-tyramine, and β-phenylethylamine by rat striatal slices.** J. Neurosci. Res. 1983. 10:211–220.

163. Saavedra JM, Palkovits M, Brownstein MJ, Axelrod J. **Localisation of phenylethanolamine N-methyl transferase in the rat brain nuclei.** Nature 1974. 248:695–696.

164. Saavedra JM, Coyle JT, Axelrod J. **The distribution and properties of the nonspecific N-methyltransferase in brain.** J. Neurochem. 1973. 20:743–752.

165. Lindemann L, Ebeling M, Kratochwil NA, Bunzow JR, Grandy DK, Hoener MC. **Trace amine-associated receptors form structurally and functionally distinct subfamilies of novel G protein-coupled receptors.** Genomics. 2005. 85:372–385.

166. Lindemann L, Hoener MC. **A renaissance in trace amines inspired by a novel GPCR family.** Trends Pharmacol. Sci. 2005. 26:274–281.

167. Green AR, Youdim MBH. **Effects of monoamine oxidase inhibition by clorgyline, deprenyl or tranylcypromine on 5-hydroxytryptamine concentrations in rat brain and hyperactivity following subsequent tryptophan administration.** Br. J. Pharmacol. 1975. 55:415–422.

168. Yang H-YT, Neff NH. **β-Phenylethylamine: A specific substrate for type B monoamine oxidase of brain.** J. Pharmacol. Exp. Ther. 1973;187(2):365-371.

169. Philips SR, Boulton AA. The effect of monoamine oxidase inhibitors on some arylalkylamines in rat striatum. J. Neurochem. 1979. 33:159–167.

170. Durden DA, Philips SR, Boulton AA. **Identification and distribution of β-phenylethylamine in the rat.** Can. J. Biochem. 1973. 51:995–1002.

171. Yang H-YT, Neff NH. **The monoamine oxidases of brain: Selective inhibition with drugs and the consquences for the metabolism of the biogenic amines.** J. Pharmacol. Exp. Ther. 1974. 189(3):733-40.

172. Fiedorowicz JG, Swartz KL. **The role of monoamine oxidase inhibitors in current psychiatric practice.** J. Psychiatr. Pract. 2004. 10:239–248.

173. Adriaenssens A, Lam BYH, Billing L, Skeffington K, Sewing S, Reimann F, *et al.* **A transcriptome-led exploration of molecular mechanisms regulating somatostatin-producing δ-cells in the gastric epithelium.** Endocrinology 2015. 156:3924–3936.

174. Raab S, Wang H, Uhles S, Cole N, Alvarez-Sanchez R, Künnecke B, *et al.* **Incretin-like effects of small molecule trace amine-associated receptor 1 agonists.** Mol. Metab. 2016. 5:47–56.

175. Ito J, Ito M, Nambu H, Fujikawa T, Tanaka K, Iwaasa H, *et al.* **Anatomical and histological profiling of orphan G-protein-coupled receptor expression in gastrointestinal tract of C57BL/6J mice.** Cell Tissue Res. 2009. 338:257–269.

176. Regard JB, Kataoka H, Cano DA, Camerer E, Yin L, Zheng Y-W, *et al.* **Probing cell type-specific functions of Gi in vivo identifies GPCR regulators of insulin secretion.** J. Clin. Invest. 2007. 117:4034–4043.

177. Mühlhaus J, Dinter J, Jyrch S, Teumer A, Jacobi SF, Homuth G, *et al.* **Investigation of naturally occurring single-nucleotide variants in human TAAR1.** Front. Pharmacol. 2017. 8:807.

178. Malaisse WJ, Malaisse-Lagae F, Sener A, Hellerström C. **Participation of endogenous fatty acids in the secretory activity of the pancreatic β-cell.** Biochem. J. 1985;227(3):995-1002.

179. MONTAGUE W, TAYLOR KW. **Regulation of insulin secretion by short chain fatty acids.** Nature 1968. 217:853–853.

180. Mokuda O, Sakamoto Y, Hu H-Y, Kawagoe R, Shimizu N. **Effects of long chain free fatty acids on glucose-induced insulin secretion in the perfused rat pancreas.** 25(11):596-597.

181. Campillo JE, Valdivia MM, Rodriguez E, Osorio C. **Effect of oleic and octanoic acids on glucose-induced insulin release *in vitro*.** Diabete Metab. 1979. 5(3):183–187.

182. Crespin SR, Greenough WB, Steinberg D, Steinberg D. **Stimulation of insulin secretion by infusion of free fatty acids.** J. Clin. Invest. 1969. 48(10):1934–1943.

183. Opara EC, Burch WM, Hubbard VS, Akwari OE**. Enhancement of endocrine pancreatic secretions by essential fatty acids.** J. Surg. Res. Academic Press; 1990. 48(4):329–332.

184. Balasse EO, Ooms HA. **Role of plasma free fatty acids in the control of insulin secretion in man.** Diabetologia 1973. 9(2):145–151.

185. Hosokawa H, Corkey BE, Leahy JL. **β-Cell hypersensitivity to glucose following 24-h exposure of rat islets to fatty acids.** Diabetologia 1997. 40(4):392–397.

186. Opara EC, Garfinkel M, Hubbard VS, Burch WM, Akwari OE. **Effect of fatty acids on insulin release: role of chain length and degree of unsaturation.** Am. J. Physiol. - Endocrinol. Metab. 1994. 266(4):E635-639.

187. Kirsten Kudahl A, Søren G, Heidi Majgaard J, Janus Laust T, Hermansen K. **Differential effects of cis and trans fatty acids on insulin release from isolated mouse islets.** Metabolism. 1999. 48(1):22–29.

188. Warnotte C, Nenquin M, Henquin J-C. **Unbound rather than total concentration and saturation rather than unsaturation determine the potency of fatty acids on insulin secretion.** Mol. Cell. Endocrinol. 1999. 153(1-2):147–53.

189. Gravena C, Mathias PC, Ashcroft SJH. **Acute effects of fatty acids on insulin secretion from rat and human islets of Langerhans.** J. Endocrinol. 2002. 173(1):73–80.

190. Stein DT, Stevenson BE, Chester MW, Basit M, Daniels MB, Turley SD, *et al.* **The insulinotropic potency of fatty acids is influenced profoundly by their chain length and degree of saturation.** J. Clin. Invest. 1997. 100(2):398–403.

191. Yeung-Yam-Wah V, Lee AK, Tse A. **Arachidonic acid mobilizes Ca2+ from the endoplasmic reticulum and an acidic store in rat pancreatic β-cells.** Cell Calcium. 2012;51(2):140–148.

192. Ramanadham S, Gross R, Turk J. **Arachidonic acid induces an increase in the cytosolic calcium concentration in single pancreatic islet β-cells.** Biochem. Biophys. Res. Commun. Academic Press; 1992. 184(2):647–653.

193. Wolf BA, Pasquale SM, Turk J. **Free fatty acid accumulation in secretagogue-stimulated pancreatic islets and effects of arachidonate on depolarization-induced insulin secretion.** Biochemistry 1991. 30(26):6372-6379.

194. Wolf BA, Turk J, Sherman WR, McDaniel ML. **Intracellular Ca2+ mobilization by arachidonic acid. Comparison with myo-inositol 1,4,5-trisphosphate in isolated pancreatic islets.** J. Biol. Chem. 1986. 261(8):3501–3511.

195. Fujiwara K, Maekawa F, Yada T. Oleic acid interacts with GPR40 to induce Ca2+ signaling in rat islet β-cells: mediation by PLC and L-type Ca2+ channel and link to insulin release. Am. J. Physiol. - Endocrinol. Metab. 2005;289.

196. Zhao Y, Wang L, Qiu J, Zha D, Sun Q, Chen C, *et al.* **Linoleic acid stimulates [Ca2+]i increase in rat pancreatic β-cells through both membrane receptor- and intracellular metabolite-mediated pathways.** PLoS One 2013. 8:e60255.

197. Kristinsson H, Smith DM, Bergsten P, Sargsyan E. **FFAR1 is involved in both the acute and chronic effects of palmitate on insulin secretion.** Endocrinology 2013. 154(11):4078–4088.

198. Olofsson CS, Salehi A, Holm C, Rorsman P. **Palmitate increases L-type Ca2+ currents and the size of the readily releasable granule pool in mouse pancreatic β-cells.** J. Physiol. 2004. 557(3):935–948.

199. Remizov O, Jakubov R, Düfer M, Krippeit Drews P, Drews G, Waring M, *et al.* **Palmitate-induced Ca2+-signaling in pancreatic β-cells.** Mol. Cell. Endocrinol. 2003. 212(1-2):1–9.

200. Parker SM, Moore PC, Johnson LM, Poitout V. **Palmitate potentiation of glucose-induced insulin release: a study using 2-bromopalmitate.** Metabolism. 2003. 52(10):1367–1371.

201. Stein DT, Esser V, Stevenson BE, Lane KE, Whiteside JH, Daniels MB, *et al.* **Essentiality of circulating fatty acids for glucose-stimulated insulin secretion in the fasted rat.** J. Clin. Invest. 1996. 97(12):2728–2735.

202. Boden G, Chen X, Iqbal N. **Acute lowering of plasma fatty acids lowers basal insulin secretion in diabetic and nondiabetic subjects.** Diabetes. 1998. 47(10):1609-1612.

203. Itoh Y, Kawamata Y, Harada M, Kobayashi M, Fujii R, Fukusumi S, *et al.* **Free fatty acids regulate insulin secretion from pancreatic β-cells through GPR40.** Nature 2003. 422(6928):173–176.

204. Briscoe CP, Tadayyon M, Andrews JL, Benson WG, Chambers JK, Eilert MM, *et al*. **The orphan G protein-coupled receptor GPR40 is activated by medium and long chain fatty acids.** J. Biol. Chem. 2003. 278:11303–11311.

205. Kotarsky K, Nilsson NE, Flodgren E, Owman C, Olde B. **A human cell surface receptor activated by free fatty acids and thiazolidinedione drugs.** Biochem. Biophys. Res. Commun. 2003. 301(2):406–410.

206. Nagasumi K, Esaki R, Iwachidow K, Yasuhara Y, Ogi K, Tanaka H, *et al.* **Overexpression of GPR40 in pancreatic β-cells augments glucose-stimulated insulin secretion and improves glucose tolerance in normal and diabetic mice.** Diabetes. 2009. 58(5):1067-1076.

207. Alquier T, Peyot M-L, Latour MG, Kebede M, Sorensen CM, Gesta S, *et al.* **Deletion of GPR40 impairs glucose-induced insulin secretion *in vivo* in mice without affecting intracellular fuel metabolism in islets.** Diabetes 2009. 58(11):2607-2615.

208. Schnell S, Schaefer M, Schöfl C. **Free fatty acids increase cytosolic free calcium and stimulate insulin secretion from β-cells through activation of GPR40.** Mol. Cell. Endocrinol. 2007. 263(1-2):173–180.

209. Ogawa T, Hirose H, Miyashita K, Saito I, Saruta T. **GPR40 gene Arg211His polymorphism may contribute to the variation of insulin secretory capacity in Japanese men.** Metabolism. 2005. 54(3):296–299.

210. Steneberg P, Rubins N, Bartoov-Shifman R, Walker MD, Edlund H. **The FFA receptor GPR40 links hyperinsulinemia, hepatic steatosis, and impaired glucose homeostasis in mouse.** Cell Metab. 2005. 1(4):245–258.

211. Salehi A, Flodgren E, Nilsson NE, Jimenez-Feltstrom J, Miyazaki J, Owman C, *et al.* **Free fatty acid receptor 1 (FFA1R/GPR40) and its involvement in fatty-acid-stimulated insulin secretion.** Cell Tissue Res. 2005. 322(2):207–215.

212. Shapiro H, Shachar S, Sekler I, Hershfinkel M, Walker MD. **Role of GPR40 in fatty acid action on the β-cell line INS-1E.** Biochem. Biophys. Res. Commun. 2005. 335(1):97–104.

213. Poitout V. **The ins and outs of fatty acids on the pancreatic β-cell.** Trends Endocrinol. Metab. 2003. 14(5):201–203.

214. Nadler A, Yushchenko DA, Müller R, Stein F, Feng S, Mulle C, *et al.* **Exclusive photorelease of signalling lipids at the plasma membrane.** Nat. Commun. 2015. 6:10056.

215. Ferdaoussi M, Bergeron V, Zarrouki B, Kolic J, Cantley J, Fielitz J, *et al.* **G protein-coupled receptor (GPR)40-dependent potentiation of insulin secretion in mouse islets is mediated by protein kinase D1.** Diabetologia 2012. 55(10):2682–2692.

216. Nolan CJ, Madiraju MSR, Delghingaro-Augusto V, Peyot M-L, Prentki M. **Fatty acid signaling in the β-cell and insulin secretion.** Diabetes. 2006. 55(Supplement 2):S16-S23.

217. Latour MG, Alquier T, Oseid E, Tremblay C, Jetton TL, Luo J, *et al.* **GPR40 is necessary but not sufficient for fatty acid stimulation of insulin secretion *in vivo*.** Diabetes. 2007;56(4):1087-1094.

218. Mugabo Y, Zhao S, Lamontagne J, Al-Mass A, Peyot M-L, Corkey BE, *et al.* **Metabolic fate of glucose and candidate signaling and excess-fuel detoxification pathways in pancreatic β-cells.** J. Biol. Chem. 2017. 292(18):7407–7422.

219. Peyot M-L, Nolan CJ, Soni K, Joly E, Lussier R, Corkey BE, *et al.* **Hormone-sensitive lipase has a role in lipid signaling for insulin secretion but is nonessential for the incretin action of glucagon-like peptide 1.** Diabetes 2004. 53(7):1733–1742.

220. Burke JE, Dennis EA. **Phospholipase A2 structure/function, mechanism, and signaling.** J. Lipid Res. 2009. 50(Supplement):S237-S242.

221. Thams P, Capito K. **Inhibition of glucose-induced insulin secretion by the diacylglycerol lipase inhibitor RHC 80267 and the phospholipase A2 inhibitor ACA through stimulation of K+ permeability without diminution by exogenous arachidonic acid.** Biochem. Pharmacol. 1997;53(8):1077–1086.

222. Larsson-Nyrén G, Grapengiesser E, Hellman B. **Phospholipase A2 is important for glucose induction of rhythmic Ca2+ signals in pancreatic β-cells.** Pancreas 2007. 35(2):173–179.

223. Song K, Zhang X, Zhao C, Ang NT, Ma ZA. **Inhibition of Ca2+ -independent phospholipase A_2 results in insufficient insulin secretion and impaired glucose tolerance.** Mol. Endocrinol. 2005. 19(2):504–515.

224. Persaud SJ, Roderigo-Milne HM, Squires PE, Sugden D, Wheeler-Jones CPD, Marsh PJ, *et al.* **A key role for beta-cell cytosolic phospholipase A(2) in the maintenance of insulin stores but not in the initiation of insulin secretion.** Diabetes 2002. 51(1):98–104.

225. Marshall BA, Tordjman K, Host HH, Ensor NJ, Kwon G, Marshall CA, *et al.* **Relative hypoglycemia and hyperinsulinemia in mice with heterozygous lipoprotein lipase (LPL) deficiency. Islet LPL regulates insulin secretion.** J. Biol. Chem. 1999. 274(39):27426–27432.

226. Cruz WS, Kwon G, Marshall CA, Mcdaniel ML, Semenkovich CF. **Glucose and insulin stimulate heparin-releasable lipoprotein lipase activity in mouse islets and INS-1 cells: a potential link between insulin resistance and β-cell dysfunction.** J. Biol. Chem. 276(15):12162-12168

227. Mulder H, Yang S, Winzell MS, Holm C, Ahrén B. **Inhibition of lipase activity and lipolysis in rat islets reduces insulin secretion.** Diabetes 2004. 53(1):122–128.

228. Newgard CB, McGarry JD. **Metabolic coupling factors in pancreatic β-cell signal transduction.** Annu. Rev. Biochem. 1995. 64:689–719.

229. Torres N, Noriega L, Tovar AR. **Nutrient modulation of insulin secretion.** Vitam. Horm. 2009. 80:217–244.

230. Husted AS, Trauelsen M, Rudenko O, Hjorth SA, Schwartz TW. **GPCR-Mediated Signaling of Metabolites.** Cell Metab. 2017. 25(4):777–796.

231. Gilon P, Shepherd RM, Henquin JC. **Oscillations of secretion driven by oscillations of cytoplasmic Ca2+ as evidences in single pancreatic islets.** J. Biol. Chem. 1993. 268(30):22265–22268.

232. Hauke S, Keutler K, Phapale P, Yushchenko DA, Schultz C. **Endogenous fatty acids are essential signaling factors of pancreatic β-cells and insulin secretion.** Diabetes 2018. 67(10):1986–1998.

233. Tengholm A. **Purinergic P2Y1 receptors take centre stage in autocrine stimulation of human β-cells.** Diabetologia 2014. 57(12):2436–2439.

234. Lavoie EG, Fausther M, Kauffenstein G, Kukulski F, Künzli BM, Friess H, *et al.* **Identification of the ectonucleotidases expressed in mouse, rat, and human Langerhans islets: potential role of NTPDase3 in insulin secretion.** Am. J. Physiol. Metab. 2010. 299(4):E647–656.

235. Bours MJL, Swennen ELR, Di Virgilio F, Cronstein BN, Dagnelie PC. **Adenosine 5′-triphosphate and adenosine as endogenous signaling molecules in immunity and inflammation.** Pharmacol. Ther. 2006. 112(2):358–404.

236. Crack BE, Pollard CE, Beukers MW, Roberts SM, Hunt SF, Ingall AH, *et al.* **Pharmacological and biochemical analysis of FPL 67156, a novel, selective inhibitor of ecto-ATPase.** Br. J. Pharmacol. 1995. 114(2):475–481.

237. Westfall TD, Kennedy C, Sneddon P. **The ecto-ATPase inhibitor ARL 67156 enhances parasympathetic neurotransmission in the guinea-pig urinary bladder.** Eur. J. Pharmacol. 1997. 329(2-3):169–173.

238. Lévesque SA, Lavoie ÉG, Lecka J, Bigonnesse F, Sévigny J. **Specificity of the ecto-ATPase inhibitor ARL 67156 on human and mouse ectonucleotidases.** Br. J. Pharmacol. 2007. 152(1):141–150.

239. Boulton AA. **Trace amines and mental disorders.** Can. J. Neurol. Sci. / J. Can. des Sci. Neurol. 1980. 7(3):261–263.

240. Revel FG, Meyer CA, Bradaia A, Jeanneau K, Calcagno E, André CB, *et al.* **Brain-Specific Overexpression of Trace Amine-Associated Receptor 1 Alters Monoaminergic Neurotransmission and Decreases Sensitivity to Amphetamine.** Neuropsychopharmacology 2012. 37(12):2580–2592.

241. Simmler LD, Buchy D, Chaboz S, Hoener MC, Liechti ME. ***In vitro* characterization of psychoactive substances at rat, mouse, and human trace amine-associated receptor 1.** J. Pharmacol. Exp. Ther. 2016. 357(1):134–144.

242. Lewin AH, Navarro HA, Wayne Mascarella S. **Structure–activity correlations for β-phenethylamines at human trace amine receptor 1.** Bioorg. Med. Chem. 2008. 16(15):7415–7423.

243. Lüllmann H, Mohr K, Wehling M, Hein L. **Pharmakologie und Toxikologie.** 18th ed. Stuttgart 2016. p. 415.

244. Liu X, Grandy DK, Janowsky A. **Ractopamine, a livestock feed additive, is a full agonist at trace amine-associated receptor 1.** J. Pharmacol. Exp. Ther. 2014. 350(1):124–129.

245. Rikard-Bell C, Curtis MA, van Barneveld RJ, Mullan BP, Edwards AC, Gannon NJ, *et al.* **Ractopamine hydrochloride improves growth performance and carcass composition in immunocastrated boars, intact boars, and gilts.** J. Anim. Sci. 2009. 87(11):3536–3543.

246. McMahon EM, Andersen DK, Feldman JM, Schanberg SM. **Methamphetamine-induced insulin release.** Science 1971. 174(4004):66–68.

247. Berry MD, Juorio A V., Li X-M, Boulton AA. **Aromaticl-amino acid decarboxylase: A neglected and misunderstood enzyme.** Neurochem. Res. 1996. 21(9):1075–1087.

248. Volz H-P, Gleiter CH. **Monoamine Oxidase Inhibitors.** Drugs Aging 1998. 13(5):341–355.

249. Jonkers N, Sarre S, Ebinger G, Michotte Y. **Benserazide decreases central AADC activity, extracellular dopamine levels and levodopa decarboxylation in striatum of the rat.** J. Neural Transm. 2001. 108(5):559–570.

250. Wu PH, Boulton AA. **Distribution and Metabolism of Tryptamine in Rat Brain.** Can. J. Biochem. 1973. 51(7):1104–1112.

251. Wu PH, Boulton AA. **Distribution, metabolism, and disappearance of intraventricularly injected *p* -tyramine in the rat.** Can. J. Biochem. 1974. 52(5):374–381.

252. Wu PH, Boulton AA. **Metabolism, distribution, and disappearance of infected β-phenylethylamine in the rat.** Can. J. Biochem. 1975. 53(1):42–50.

253. Del Valle EMM. **Cyclodextrins and their uses: a review.** Process Biochem. 2004. 39(9):1033–1046.

254. Yilmaz E, Memon S, Yilmaz M. **Removal of direct azo dyes and aromatic amines from aqueous solutions using two β-cyclodextrin-based polymers.** J. Hazard. Mater. 2010. 174(1-3):592–597.

255. Zidovetzki R, Levitan I. **Use of cyclodextrins to manipulate plasma membrane cholesterol content: Evidence, misconceptions and control strategies.** Biochim. Biophys. Acta - Biomembr. 2007. 1768(6):1311–1324.

256. Christian AE, Haynes MP, Phillips MC, Rothblat GH. **Use of cyclodextrins for manipulating cellular cholesterol content.** J. Lipid Res. 1997. 38:2264–2272.

257. de Rooij J, Zwartkruis FJT, Verheijen MHG, Cool RH, Nijman SMB, Wittinghofer A, *et al.* **Epac is a Rap1 guanine-nucleotide-exchange factor directly activated by cyclic AMP.** Nature 1998. 396:474–477.

258. Klarenbeek JB, Goedhart J, Hink MA, Gadella TWJ, Jalink K. **A mTurquoise-based cAMP sensor for both FLIM and ratiometric read-out has improved dynamic range.** PLoS One 2011. 6:e19170.

259. Seamon K, Daly JW. **Activation of adenylate cyclase by the diterpene forskolin does not require the guanine nucleotide regulatory protein.** J. Biol. Chem. 1981. 256(19):9799-9801.

260. Lugnier C, Schoeffter P, Le Bec A, Strouthou E, Stoclet JC. **Selective inhibition of cyclic nucleotide phosphodiesterases of human, bovine and rat aorta.** Biochem. Pharmacol. 1986. 35(10):1743–1751.

261. Ponsioen B, Zhao J, Riedl J, Zwartkruis F, van der Krogt G, Zaccolo M, *et al.* **Detecting cAMP-induced Epac activation by fluorescence resonance energy transfer: Epac as a novel cAMP indicator.** EMBO Rep. 2004. 5(12):1176–1180.

262. Choi J-K, Ho J, Curry S, Qin D, Bittman R, Hamilton JA. **Interactions of very long-chain saturated fatty acids with serum albumin.** J. Lipid Res. 2002. 43(7):1000–1010.

263. Whitlam JB, Crooks MJ, Brown KF, Veng Pedrrsen P. **Binding of nonsteroidal anti-inflammatory agents to proteins—I. Ibuprofen-serum albumin interaction.** Biochem. Pharmacol. 1979. 28(5):675–678.

264. McMenamy RH, Oncley JL. **The specific binding of L-tryptophan to serum albumin.** J. Biol. Chem. 1958. 233(6):1436–1447.

265. Briscoe CP, Peat AJ, McKeown SC, Corbett DF, Goetz AS, Littleton TR, *et al.* **Pharmacological regulation of insulin secretion in MIN6 cells through the fatty acid receptor GPR40: identification of agonist and antagonist small molecules.** Br. J. Pharmacol. 2006. 148:619–628.

266. Hamilton JA, Era S, Bhamidipati SP, Reed RG**. Locations of the three primary binding sites for long-chain fatty acids on bovine serum albumin.** Proc. Natl. Acad. Sci. U. S. A. 1991. 88:2051–2054.

267. Yao C-H, Liu G-Y, Yang K, Gross RW, Patti GJ. **Inaccurate quantitation of palmitate in metabolomics and isotope tracer studies due to plastics.** Metabolomics. 2016. 12(9):143–149.

268. Black SL, Stanley WA, Filipp F V., Bhairo M, Verma A, Wichmann O, *et al.* **Probing lipid- and drug-binding domains with fluorescent dyes.** Bioorg. Med. Chem. 2008. 16(3):1162–1173.

269. Sackett DL, Wolff J. **Nile red as a polarity-sensitive fluorescent probe of hydrophobic protein surfaces.** Anal. Biochem. 1987. ;167(2):228–234.

270. Greenspan P, Fowler SD. **Spectrofluorometric studies of the lipid probe, nile red.** J. Lipid Res. 1985. 26(7):781–789.

271. Spector AA. **Fatty acid binding to plasma albumin.** J. Lipid Res. 1975. 16(3):165–179.

272. Mead JR, Irvine SA, Ramji DP. **Lipoprotein lipase: structure, function, regulation, and role in disease.** J. Mol. Med. 2002. 80(12):753–769.

273. Rubí B, Ljubicic S, Pournourmohammadi S, Carobbio S, Armanet M, Bartley C, *et al.* **Dopamine D2-like receptors are expressed in pancreatic beta cells and mediate inhibition of insulin secretion.** J. Biol. Chem. 2005. 280:36824–36832.

274. Cerasi E, Effendic S, Luft R. **Role of adrenergic receptors in glucose-induced insulin secretion in man.** Lancet 1969. 294(7615):301–302.

275. Sacco F, Humphrey SJ, Cox J, Mischnik M, Schulte A, Klabunde T, *et al.* **Glucose-regulated and drug-perturbed phosphoproteome reveals molecular mechanisms controlling insulin secretion.** Nat. Commun. 2016. 7:13250.

276. Rerup C, Lundquist I. **Blood glucose level in mice.** Eur. J. Endocrinol. 1966. 52(4):357–37.

277. Bosco D, Armanet M, Morel P, Niclauss N, Sgroi A, Muller YD, *et al.* **Unique arrangement of alpha- and beta-cells in human islets of Langerhans.** Diabetes 2010. 59(5):1202–1210.

278. Wojtusciszyn A, Armanet M, Morel P, Berney T, Bosco D. **Insulin secretion from human beta cells is heterogeneous and dependent on cell-to-cell contacts.** Diabetologia 2008. 51(10):1843–1852.

279. Gee KR, Brown KA, Chen W-NU, Bishop-Stewart J, Gray D, Johnson I. **Chemical and physiological characterization of fluo-4 Ca2+-indicator dyes.** Cell Calcium 2000. 27(2):97–106.

280. Smith NA, Kress BT, Lu Y, Chandler-Militello D, Benraiss A, Nedergaard M. **Fluorescent Ca2+ indicators directly inhibit the Na,K-ATPase and disrupt cellular functions.** Sci. Signal. 2018. 11:eaal2039.

281. Bavamian S, Klee P, Britan A, Populaire C, Caille D, Cancela J, *et al.* **Islet-cell-to-cell communication as basis for normal insulin secretion.** Diabetes, Obes. Metab. 2007. 9(Supplement 2):118–132.

282. Bunzow, Sonders, Arttamangkul, Harrison, Zhang, Quigley, *et al.* **Amphetamine, 3,4-methylenedioxymethamphetamine, lysergic acid diethylamide, and metabolites of the catecholamine neurotransmitters are agonists of a rat trace amine receptor.** Mol. Pharmacol. 2001. 60(6):1181–1188.

283. Leo D, Mus L, Espinoza S, Hoener MC, Sotnikova TD, Gainetdinov RR. **Taar1-mediated modulation of presynaptic dopaminergic neurotransmission: Role of D2 dopamine autoreceptors.** Neuropharmacology 2014. 81:283–291.

284. Zaczek R, Culp S, De Souza EB. **Interactions of [3H]amphetamine with rat brain synaptosomes. II. Active transport.** J. Pharmacol. Exp. Ther. 1991. 257(2):830-835.

285. Philips SR, Burden DA, Boulton AA. **Identification and Distribution of Tryptamine in the Rat.** Can. J. Biochem. 1974. 52(6):447–451.

286. Kinniburgh DW, Boyd ND. **Determination of plasma octopamine and its level in renal disease.** Clin. Biochem. 1979. 12(1):27–32.

287. Ibrahim KE, Couch MW, Williams CM, Fregly MJ, Midgley JM. **m-Octopamine: Normal occurrence with p-octopamine in mammalian sympathetic nerves.** J. Neurochem. 1985. 44(6):1862–1867.

288. Jarrett RB, Schaffer M, McIntire D, Witt-Browder A, Kraft D, Risser RC. **Treatment of atypical depression with cognitive therapy or phenelzine.** Arch. Gen. Psychiatry 1999. 56(5):431-437.

289. Grimsby J, Toth M, Chen K, Kumazawa T, Klaidman L, Adams JD, *et al.* **Increased stress response and β–phenylethylamine in MAOB–deficient mice.** Nat. Genet. 1997. 17(2):206–210.

290. Detimary P, Jonas JC, Henquin JC. **Stable and diffusible pools of nucleotides in pancreatic islet cells.** Endocrinology 1996. 137(11):4671–4676.

291. Wayne Leitner J, Sussman KE, Vatter AE, Howard Schneider F. **Adenine nucleotides in the secretory granule fraction of rat islets.** Endocrinology 1975(3). 96:662–677.

292. Ostrom RS, Gregorian C, Insel PA. **Cellular release of and response to ATP as key determinants of the set-point of signal transduction pathways.** J. Biol. Chem. 2000. 275(16):11735–11739.

293. Zimmermann U, Kraus T, Himmerich H, Schuld A, Pollmächer T. **Epidemiology, implications and mechanisms underlying drug-induced weight gain in psychiatric patients.** J. Psychiatr. Res. 2003. 37(3):193–220.

294. Patten SB, Williams JVA, Lavorato DH, Khaled S, Bulloch AGM**. Weight gain in relation to major depression and antidepressant medication use.** J. Affect. Disord. 2011. 134(1-3):288–293.

295. Dixon JB, Dixon ME, O'Brien PE. **Depression in Association With Severe Obesity.** Arch. Intern. Med. 2003. 163(17):2058-2065.

296. Raab S, Wang H, Uhles S, Cole N, Alvarez-Sanchez R, Künnecke B, *et al.* **Incretin-like effects of small molecule trace amine-associated receptor 1 agonists.** Mol. Metab. 2016. 5(1):47–56.

297. Scanlan TS, Suchland KL, Hart ME, Chiellini G, Huang Y, Kruzich PJ, *et al.* **3-Iodothyronamine is an endogenous and rapid-acting derivative of thyroid hormone.** Nat. Med. 2004. 10(6):638–642.

298. Kivimäki M, Hamer M, Batty GD, Geddes JR, Tabak AG, Pentti J, *et al.* **Antidepressant medication use, weight gain, and risk of type 2 diabetes: a population-based study.** Diabetes Care 2010. 33(12):2611–2616.

299. Berken GH, Weinstein DO, Stern WC. **Weight gain. A side-effect of tricyclic antidepressants.** J. Affect. Disord. 1984. 7:133–138.

300. Rabkin J, Quitkin F, Harrison W, Tricamo E, McGrath P. **Adverse reactions to monoamine oxidase inhibitors. Part I. A comparative study.** J. Clin. Psychopharmacol. 1984. 4:270–278.

301. Cantú TG, Korek JS. **Monoamine oxidase inhibitors and weight gain.** Drug Intell. Clin. Pharm. 1988. 22(10):755–759.

302. Stratton JE, Hutkins RW, Taylor SL SL. **Biogenic amines in cheese and other fermented foods: A review.** J. Food Prot. 1991. 54(6):460–470.

303. Blackwell B, Mabbitt LA. **Tyramine in cheese related to hypertensive crises after monoamine-oxidase inhibition.** Lancet 1965. 285(7392):938–940.

304. Williams BB, Van Benschoten AH, Cimermancic P, Donia MS, Zimmermann M, Taketani M, *et al.* **Discovery and characterization of gut microbiota decarboxylases that can produce the neurotransmitter tryptamine.** Cell Host Microbe 2014. 16(4):495–503.

305. Mazzoli R, Pessione E. **The neuro-endocrinological role of microbial glutamate and GABA signaling.** Front. Microbiol. 2016. 7:1934.

306. Mu C, Yang Y, Zhu W. **Gut microbiota: The brain peacekeeper.** Front. Microbiol. 2016. 7:345.

307. Ashbrook DJ, Spector AA, Santos EC, Fletcher JE. **Long chain fatty acid binding to human plasma albumin.** J. Biol. Chem. 1975. 250(6):2333–2338.

308. Straub SG, Sharp GWG. **Massive Augmentation of Stimulated Insulin Secretion Induced by Fatty Acid–Free BSA in Rat Pancreatic Islets.** Diabetes. 2004. 53(12):3152-3258.

309. Ashbrook DJ, Spector AA, Fletcher JE. **Medium chain fatty acid binding to human plasma albumin.** J. Biol. Chem. 1972. 247(21):7038–7042.

310. Tunaru S, Bonnavion R, Brandenburger I, Preussner J, Thomas D, Scholich K, *et al.* **20-HETE promotes glucose-stimulated insulin secretion in an autocrine manner through FFAR1.** Nat. Commun. 2018. 9:177.

311. Vorum H, Brodersen R, Kragh-Hansen U, Pedersen AO. **Solubility of long-chain fatty acids in phosphate buffer at pH 7.4.** Biochim. Biophys. Acta - Lipids Lipid Metab. 1992. 1126(2):135–142.

312. Richieri G V., Anel A, Kleinfeld AM. **Interactions of long-chain fatty acids and albumin: Determination of free fatty acid levels using the fluorescent probe ADIFAB.** Biochemistry 1993. 32(29):7574–7580.

313. Peters T. **All about Albumin - Biochemistry, Genetics and Medical Applications.** San Diego (California, U.S.A.) 1992. pp. 15-53.

314. Rose H, Conventz M, Fischer Y, Jüngling E, Hennecke T, Kammermeier H. **Long-chain fatty acid-binding to albumin: re-evaluation with directly measured concentrations.** Biochim. Biophys. Acta - Lipids Lipid Metab. 1994. 1215(3):321–326.

315. Poitout V, Amyot J, Semache M, Zarrouki B, Hagman D, Fontés G. **Glucolipotoxicity of the pancreatic beta cell.** Biochim. Biophys. Acta - Mol. Cell Biol. Lipids 2010. 1801(3):289–298.

316. Kober A, Sjöholm I. **The binding sites on human serum albumin for some nonsteroidal antiinflammatory drugs.** Mol. Pharmacol. 1980. 18(3):421-426.

317. Mulder H, Yang S, Winzell MS, Holm C, Ahrén B. **Inhibition of lipase activity and lipolysis in rat islets reduces insulin secretion.** Diabetes. 2003. 53(1):122-128.

318. Poitout V. **Fatty acids and insulin secretion: From FFAR and near?** Diabetes 2018. 67(10):1932–1934.

319. Feng DD, Luo Z, Roh S, Hernandez M, Tawadros N, Keating DJ, *et al.* **Reduction in voltage-gated K $^+$ currents in primary cultured rat pancreatic β-cells by linoleic acids.** Endocrinology 2006. 147(2):674–682.

320. Jacobson DA, Weber CR, Bao S, Turk J, Philipson LH. **Modulation of the pancreatic islet beta-cell-delayed rectifier potassium channel Kv2.1 by the polyunsaturated fatty acid arachidonate.** J. Biol. Chem. 2007. 282(10):7442–7449.

321. Frank JA, Yushchenko D, Fine NHF, Duca M, Citir M, Broichhagen J, *et al.* **Optical control of GPR40 signalling in pancreatic β-cells.** Chem. Sci. 2017. 8(11):7604–7610.

322. Schindelin J, Arganda-Carreras I, Frise E, Kaynig V, Longair M, Pietzsch T, *et al.* **Fiji: an open-source platform for biological-image analysis.** Nat. Methods 2012. 9(7):676–682.

323. Clark J, Anderson KE, Juvin V, Smith TS, Karpe F, Wakelam MJO, *et al.* **Quantification of PtdInsP3 molecular species in cells and tissues by mass spectrometry.** Nat. Methods 2011. 8(3):267–272.